AUTONOMOUS UNDERWATER VEHICLES (AUV) SENSITIVITY OF MOTION RESPONSE TO GEOMETRIC AND HYDRODYNAMIC PARAMETERS AND AUV BEHAVIOURS WITH CONTROL PLANE FAULTS

CENTRE FOR NEWFOUNDLAND STUDIES

TOTAL OF 10 PAGES ONLY MAY BE XEROXED

(Without Author's Permission)

DOUGLAS EDWARD PERRAULT

001311

CENTRE FOR NFLD. STUDIES
MEMORIAL UNIVERSITY
OF NEWFOUNDLAND

INFORMATION TO USERS

This manuscript has been reproduced from the microfilm master. UMI films the text directly from the original or copy submitted. Thus, some thesis and dissertation copies are in typewriter face, while others may be from any type of computer printer.

The quality of this reproduction is dependent upon the quality of the copy submitted. Broken or indistinct print, colored or poor quality illustrations and photographs, print bleedthrough, substandard margins, and improper alignment can adversely affect reproduction.

In the unlikely event that the author did not send UMI a complete manuscript and there are missing pages, these will be noted. Also, if unauthorized copyright material had to be removed, a note will indicate the deletion.

Oversize materials (e.g., maps, drawings, charts) are reproduced by sectioning the original, beginning at the upper left-hand corner and continuing from left to right in equal sections with small overlaps.

ProQuest Information and Learning
300 North Zeeb Road, Ann Arbor, MI 48106-1346 USA
800-521-0600

National Library of Canada
Acquisitions and Bibliographic Services
395 Wellington Street
Ottawa ON K1A 0N4
Canada

Bibliothèque nationale du Canada
Acquisitions et services bibliographiques
395, rue Wellington
Ottawa ON K1A 0N4
Canada

Your file Votre référence

Our file Notre référence

The author has granted a non-exclusive licence allowing the National Library of Canada to reproduce, loan, distribute or sell copies of this thesis in microform, paper or electronic formats.

L'auteur a accordé une licence non exclusive permettant à la Bibliothèque nationale du Canada de reproduire, prêter, distribuer ou vendre des copies de cette thèse sous la forme de microfiche/film, de reproduction sur papier ou sur format électronique.

The author retains ownership of the copyright in this thesis. Neither the thesis nor substantial extracts from it may be printed or otherwise reproduced without the author's permission.

L'auteur conserve la propriété du droit d'auteur qui protège cette thèse. Ni la thèse ni des extraits substantiels de celle-ci ne doivent être imprimés ou autrement reproduits sans son autorisation.

0-612-73560-5

Canada

Autonomous Underwater Vehicles (AUV) Sensitivity of Motion Response to Geometric and Hydrodynamic Parameters and AUV Behaviours with Control Plane Faults

by

©Douglas Edward Perrault

B. Eng., Technical University of Nova Scotia (1996)
M. A. Sc., University of Victoria (1998)

A thesis submitted to the
School of Graduate Studies
in partial fulfillment of the
requirements for the degree of
Doctor of Philosophy

Faculty of Engineering and Applied Science
Memorial University of Newfoundland

June 2002

Autonomous Underwater Vehicles (AUV) Sensitivity of Motion Response to Geometric and Hydrodynamic Parameters and AUV Behaviours with Control Plane Faults

by

Douglas Edward Perrault

Abstract

Autonomous underwater vehicles (AUV) are rapidly emerging as an important tool in ocean exploration and maritime defence systems. Reliability is one of the key issues in making these vehicles viable for scientific, commercial, and military applications. The vehicles must be able to accomplish the mission, or some subset of the mission objectives.

The research herein is concerned with defining vehicle behaviours in the light of design choices that will result in improved vehicle performance under nominal (fault-free) operating conditions and with guarantees of acceptable vehicle behaviour even with control plane faults. Numerical studies were performed using a computer model of the AUV C-SCOUT (Canadian Self-Contained Off-the-shelf Underwater Testbed). Because it is typical of many vehicles active in the world today, the results are qualitatively valid for a large number of vehicles. Quantifying the behaviours provides a foundation for further analysis of behaviours in various planned and unplanned conditions the vehicle will experience over the course of its active lifetime.

First, a numerical study was made of the effect of variations of geometry on added mass coefficients. The results demonstrate that intuitive expectations for the effects of geometry on added mass are valid.

A second numerical study was made of the sensitivity of AUV response measures in turning circles and zigzag maneuvers to variations in hydrodynamic parameters. The results have specific implications for the design of AUV, and provide a baseline of behaviours inherent to the vehicle itself.

Finally, a numerical study was made of vehicle response during holding course, diving, and turning, while the vehicle is experiencing various angles of jam on each of the control planes, and while the vehicle is missing one of the control planes. This information was used to define the vehicle behaviour, to generate conclusions about vehicle controllability, and to suggest safe operation envelopes for guarantees of mission success.

The contributions made in this work include a systematic description of the effects of varying vehicle design parameters and hydrodynamic parameters (which result from certain design choices). Also included is a systematic analysis of the effects of control plane faults on the response of the vehicle.

Thesis Supervisor: Neil Bose. Ph. D.
Title: Chair. Ocean and Naval Architectural Engineering. Faculty of Engineering and Applied Science. Memorial University of Newfoundland

Thesis Supervisor: Christopher D. Williams. Ph. D.
Title: Research Engineer. National Research Council of Canada Institute for Marine Dynamics

Thesis Supervisor: Siu O'Young. Ph. D.
Title: Associate Professor. Instrumentation Control and Automation (INCA) Centre. Faculty of Engineering and Applied Science. Memorial University of Newfoundland

Contents

List of Figures

List of Tables

Who laid the foundations of the earth.
that it should not be removed for ever.
Thou coveredst it with the deep as with a garment:
the waters stood above the mountains.
At thy rebuke they fled:
at the voice of thy thunder they hasted away.
They go up by the mountains:
they go down by the valleys
unto the place which thou hast founded for them.
Thou hast set a bound that they may not pass over;
that they turn not again to cover the earth.
O LORD, how manifold are thy works!
in wisdom hast thou made them all:
the earth is full of thy riches.
So is this great and wide sea,
wherein are things creeping innumerable,
both small and great beasts.

Psalm 104: 5-9, 24-25

O LORD God of hosts,
who is a strong LORD like unto thee?
or to thy faithfulness round about thee?
Thou rulest the raging of the sea:
when the waves thereof arise, thou stillest them.
The heavens are thine, the earth also is thine:
as for the world and the fulness thereof, thou hast founded them.

Psalm 89: 8, 9, 11

Acknowledgments

This work is a direct result of the grace of God through Jesus Christ in allowing me the opportunity and providing the resources in a multitude of ways.

The work would not have been possible without the support and encouragement of my wife Marina (Proverbs 31:10-12), and children, Samuel, Timothy, and the newest blessing, Sarah.

I have been fortunate to have the counsel and support of my supervisors: Dr. Neil Bose, Dr. Siu O'Young, and Dr. Chris D. Williams. (Proverbs 11:14)

There are many, many others who have helped me along the way, to whom I owe much.

Financial support came from an NSERC (Natural Sciences and Engineering Research Council of Canada) PGS (Post-Graduate Studies) B Scholarship, from Memorial University of Newfoundland (MUN) via Graduate Research Assistance, from the Institute for Marine Dynamics (IMD) of the National Research Council (NRC) of Canada, from the Maritime Awards Society of Canada (MASC) in the form of the Maritime Studies Scholarship; and from an NSERC Strategic Project entitled "Ocean Environmental Risk Engineering Using Autonomous Underwater Vehicles."

The C-SCOUT project is part of a collaborative venture partially funded by a five year NSERC Strategic Grant entitled. "Offshore Environmental Risk Engineering Using Autonomous Underwater Vehicles". This grant. aimed at environmental effects monitoring and assessment of offshore petroleum discharges. involves the following research and industrial partners:

- Ocean Engineering Research Centre (OERC) of Memorial University of Newfoundland (MUN) - OERC objectives are to form a focus for ocean related engineering research from all disciplines in the Faculty of Engineering and Applied Science and to build cross disciplinary links to other parts of the University. institutions and industry. Ocean engineering research at MUN is very strong with one of its main strengths being the diversity of projects and researchers that have been and are associated with the Centre.

- Instrumentation. Control and Automation (INCA) Centre of Memorial University of Newfoundland (MUN) - INCA is an industrial outreach centre of excellence with expertise in the computerized embedded systems. INCA is part of MUN whose response is to the development of the oil and gas industry off the coast of Newfoundland and Labrador. This is an education and research centre adjacent to the oil patch and committed to excellence in instrumentation. control and automation.

- National Research Council (NRC) of Canada. Institute for Marine Dynamics (IMD) - IMD was established in St. John's. Newfoundland. in 1985 as Canada's national centre for ocean technology research and development. It provides innovative solutions and technical expertise in support of Canadian industry. and collaborates with international companies and research agencies to bring new technology to Canada. The Institute's capability is unique to the nation and no other organization offers the combination of knowledge. experience and world-class facilities.

- C-CORE - Since 1975. C-CORE in St. John's. NF activities have grown to include applied research and development. technology transfer and technology demonstration. commercialization of intellectual property and specialized advisory services to a wide range of industries.

- University of Victoria. Space and Subsea Robotics Laboratory - The subsea activities of the Space and Subsea Robotics Laboratory encompass both autonomous and remotely-operated undersea vehicles (AUV and ROV). as well as towed and tethered marine systems. including moored buoys.

- Petro-Canada through the Terra Nova Alliance - A major Canadian oil and gas company who are currently operators of the Terra Nova oil field in the Jeanne d'Arc Basin with a strong reputation for environmental stewardship and corporate responsibility.

- International Submarine Engineering Ltd. (ISE) - International Submarine Engineering Ltd. is a world player in the design and development of autonomous and remotely operated underwater vehicles (AUV and ROV) and robotic systems.

- Geo-Resources Inc. (GRI) - Geo-Resources Inc. is a privately owned Canadian company. which was established in 1986 whose mandate at that time was to provide ocean mapping services for domestic and international customers. In recent years the focus has shifted toward research and development projects with an emphasis on creating commercially viable software based products. GRI has experience in areas such as multibeam sonar mapping. tidal monitoring. GPS positioning. and operation of remotely controlled vehicles for anti-submarine warfare and mine hunting trials.

Researchers:

- Neil Bose - Professor and Chair. Ocean and Naval Architectural Engineering. Faculty of Engineering and Applied Science. MUN
- Mahmoud Haddara - Associate Dean. Graduate Studies and Research. Faculty of Engineering and Applied Science. MUN
- Mike Hinchey - Professor. Mechanical Engineering. Faculty of Engineering and Applied Science. MUN
- Tahir Husain - Professor. Civil Engineering. Faculty of Engineering and Applied Science. MUN
- Meyer Nahon - Associate Professor. Department of Mechanical Engineering. University of Victoria
- Siu O'Young - Associate Professor. Electrical and Computer Engineering. Faculty of Engineering and Applied Science. MUN
- Charles Randell - C-CORE
- Brian Veitch - Junior Chair. Ocean Environmental Risk Engineering: Assistant Professor. Faculty of Engineering and Applied Science. MUN
- Christopher D. Williams - Research Engineer. NRC IMD

Graduate Students:

- Timothy Curtis - Responsible for the design, construction, outfitting, and preliminary testing of the C-SCOUT AUV.
- Mukhtasor - Studied dispersion modeling of undersea plumes discharged from offshore drilling platforms.
- Vanessa Pennell - Studied environmental monitoring using autonomous underwater vehicles.
- Doug Perrault - Dynamics and control of underwater vehicles.
- Doug Pittman - Studied sonar returns and mapping.
- Rehan Sadiq - Studied fates modeling of undersea plumes.
- Aaron Saunders - Investigated a through-body thruster system for the C-SCOUT AUV.
- Lloyd Smith - Completed initial wiring and coding for C-SCOUT; assisted electrical students on a part-time basis.
- Steve Taylor - Developing an autonomous controller for an AUV based on a Distributed Micro-controller Architecture.
- Roy Thomas - Responsible for completing the second phase of in-water experiments with the C-SCOUT AUV.

Work Term Students:

- Hermen Bijleveld - Developed and tested a cyclic-pitch propulsion system for the C-SCOUT AUV.
- Renee Boileau - Worked on the initial design for the C-SCOUT AUV.
- Timothy Curtis - Worked on the initial design for the C-SCOUT AUV.
- Lucas Gray - Machined the majority of the C-SCOUT AUV structural components.
- Erin MacNeil - Machine work on C-SCOUT and testing of the control surfaces.
- Sheila Pomroy Assisted in the rebuilding of the C-SCOUT computer system.
- Rocky Taylor - Responsible for control plane actuator housing redesign and C-SCOUT test frame implementation.
- Steve Taylor - Responsible for rebuilding and ruggedizing the C-SCOUT onboard electronics and software, and some systems integration.
- Meggan Vickerd - Responsible for machining and constructing some parts of C-SCOUT and also fabricated C-SCOUT II.
- Dan Vyselaar - Assisted in development of a mounting system to attach C-SCOUT II to the planar motion mechanism for hydrodynamic testing; assisted in construction of cyclic-pitch propulsor.

Table 1: Abbreviations

Abbreviation	Definition
AUV	Autonomous Underwater Vehicle(s)
BRC	Balance Resolving Center
C-SCOUT	Canadian Self-Contained Off-the-shelf Underwater Testbed
CURV	Cable-controlled Undersea Recovery Vehicle
DATCOM	(USAF) DATa COMpendium
DOF	Degrees of Freedom
DREA	Defence Research Establishment Atlantic
EEM	Environmental Effects Monitoring
ERS	Emergency Response System
ESAM	Estimate Submarine Added Mass
IMD	Institute for Marine Dynamics
LQG	Linear Quadratic Gaussian
MDTF	Marine Dynamics Test Facility
MUN	Memorial University of Newfoundland
NACA	National Advisory Committee on Aeronautics
NRC	National Research Council (Canada)
NRC(US)	National Research Council (United States)
OERC	Ocean Engineering Research Centre
PID	Proportional Integral Derivative
PMM	Planar Motion Mechanism
RCV	Remotely Controlled Vehicle(s)
ROV	Remotely Operated Vehicle(s)
SNAME	Society of Naval Architects and Marine Engineers
SPURV	Self-Propelled Underwater Research Vehicle
WHOI	Woods Hole Oceanographic Institute

Table 2: Operator Notation

Operation	**Example**	**Definition**
˙(dot) over a symbol	$\dot{u} = du/dt$	Derivative with respect to time
′(prime) of a symbol	$m' = m/(1/2)\,\rho l^3$	Non-dimensional form of a symbol
subscript u, v, w, p, q, r, $\dot{u}$, $\dot{v}$, $\dot{w}$, $\dot{p}$, $\dot{q}$, or $\dot{r}$ applied to X, Y, Z, K, M, N	$X_{\dot{u}} = \partial X/\partial \dot{u}$	Partial derivative with respect to subscript
′(prime) of result of previous operation	$Y'_{\dot{p}} = (\partial Y/\partial \dot{p})'$ $= \partial Y'/\partial \dot{p}'$	Non-dimensional form of the partial derivative with respect to the subscript

Table 3: Symbols

Symbol	Definition
$\mathbf{A}$	Dynamics matrix in the standard state-space model
A	Angle of attack of the hull
A	Simulations of vehicle behaviour with active roll compensation via all control planes
A_{CP}	Reference (planform) area for the control planes
A_{Hull}	Reference (wetted surface) area of the hull
A_P	Planform area of the hull
A_{P0}	Planform area of the hull from the nose to the station x_0
A_{ref}	Reference area (general usage)
a_0	(2-D) section lift-curve slope at $\alpha = 0$ for a control plane
a_e	Effective aspect ratio of a control plane
$\mathbf{B}$	Control input matrix in the standard state-space model
$\mathbf{B}$	Buoyant force
B	Body-fixed reference frame, typically used as a subscript
b	Control plane span
b	Subscript denoting center of buoyancy
$\mathbf{C}$	State to output matrix in the standard state-space model
$C_{\mathcal{L}}$, $C_{\mathcal{D}}$	Lift and drag coefficients respectively (general usage)
$C_{\mathcal{D}_0}$	Drag coefficient at zero angle of attack
$C_{\mathcal{D}_C}$	Crossflow drag coefficient (general usage)
$C_{\mathcal{D}_{Hull}}$, $C_{\mathcal{L}_{Hull}}$	Drag and lift coefficients for the hull
$C_{\mathcal{D}_{Fins}}$, $C_{\mathcal{L}_{Fins}}$	Drag and lift coefficients for the control planes
$C_{D,Hull}$, $C_{L,Hull}$	Drag and lift coefficients for the hull (Excel^{TM} plots)
$C_{D,Fins}$, $C_{L,Fins}$	Drag and lift coefficients for the control planes (Excel^{TM} plots)
C_m	Pitching moment coefficient (general usage)
$C_{m_{\overline{c/4}}}$	Pitching moment coefficient about the quarter-chord axis of the control plane

Symbol	Definition
C_N	Normal force coefficient (general usage)
CE	Center of effort (for the hull)
CP	Center of pressure (for the control planes)
CP_C	Location of the center of pressure of the control plane. chord-wise in the control plane reference frame
CP_S	Location of the center of pressure of the control plane. span-wise in the control plane reference frame
c	Control plane chord
c_r	Control plane chord at the root
c_t	Control plane chord at the tip
$\mathbf{D}$	Input to output matrix in the standard state-space model
$\mathcal{D}$	Drag force (general usage)
$\mathcal{D}_{Hull}$	Drag force on the hull
$\mathcal{D}_{HCP}$	Drag force on the horizontal control planes
$\mathcal{D}_{VCP}$	Drag force on the vertical control planes
D	Hull diameter
d	A metric of length representing a moment arm
E	Simulations of vehicle behaviour with active roll compensation via elevators
e	Oswald's efficiency factor for a control plane
$\mathbf{F}$	Force vector. $\mathbf{F} = \begin{bmatrix} \mathbf{X} & \mathbf{Y} & \mathbf{Z} \end{bmatrix}^T$
$\mathbf{F}_C$	Control forces
$\mathbf{F}_E$	Environmental forces - waves, current, etc.
$\mathbf{F}_I$	Ideal fluid forces - "Added Mass"
$\mathbf{F}_R$	Real fluid forces - "Damping"
$\mathbf{F}_S$	Static (hydrostatic) forces - weight and buoyancy
$\mathbf{F}_s$	A 6×2 matrix representing the weight and buoyancy contributions to the equations of motion

Symbol	Definition
$\mathbf{F}_\eta$	Augmented matrix of hydrodynamic derivatives
$\mathbf{F}'_\eta$	Matrix of hydrodynamic derivatives
$\mathbf{F}_{\dot{\eta}}$	Augmented matrix of virtual added mass derivatives
$\mathbf{F}'_{\dot{\eta}}$	Matrix of virtual added mass derivatives
$\mathbf{f}(\phi, \theta)$	Traditional transformation matrix for angular velocities from inertial to body-fixed reference frame
f_N	Normal force on the hull at a particular station along the length
$\mathbf{G}$	Moment vector. $\mathbf{G} = [\ \mathbf{K}\ \ \mathbf{M}\ \ \mathbf{N}\ ]^T$
g	Subscript denoting center of gravity (mass)
$\mathbf{H}$	Angular momentum vector. $\mathbf{H}=\mathbf{I}\boldsymbol{\nu}_2$
$\mathbf{I}$	Matrix of inertial properties
I	Inertial reference frame, typically used as a subscript
I_{xx}, I_{yy}, I_{zz}	Momenta of inertia about the x_B, y_B, and z_B axis respectively
I_{xy}, I_{xz}, I_{yz}	Products of inertia about the x_B-y_B, x_B-z_B, and y_B-z_B planes respectively
$\mathbf{K}$	Moment about the x_B axis, described in the body-fixed reference frame
$\mathbf{K}_{pqr}$	2×6 matrix of kinematic equations for augmenting the linear model
$\mathbf{K}_{\phi\theta}$	2×2 matrix of kinematic equations for augmenting the linear model
$\mathbf{k}$	Unit vector that defines the (equivalent) axis about which frame B is rotated with respect to I
K_p, K_q, K_r	Derivatives of roll moment with respect to angular velocities (rotary moment derivatives)
K'_p, K'_q, K'_r	Nondimensional derivatives of roll moment with respect to angular velocities (rotary moment derivatives)
$K_{\dot{p}}, K_{\dot{q}}, K_{\dot{r}}$	Derivatives of roll moment with respect to angular accelerations (mass-moment of inertia coefficients)
$K'_{\dot{p}}, K'_{\dot{q}}, K'_{\dot{r}}$	Nondimensional derivatives of roll moment with respect to angular accelerations (mass-moment of inertia coefficients)

Symbol	Definition
K_u. K_v. K_w	Derivatives of roll moment with respect to translational velocities (static moment derivatives)
K'_u. K'_v. K'_w	Nondimensional derivatives of roll moment with respect to translational velocities (static moment derivatives)
$K_{\dot{u}}$. $K_{\dot{v}}$. $K_{\dot{w}}$	Derivatives of roll moment with respect to translational accelerations (mass-moment of inertia coefficients)
$K'_{\dot{u}}$. $K'_{\dot{v}}$. $K'_{\dot{w}}$	Nondimensional derivatives of roll moment with respect to translational accelerations (mass-moment of inertia coefficients)
$K_{\delta T}$	Derivative of roll with respect to thruster output. δ_T
$K_{\delta al}$. $K_{\delta ap}$. $K_{\delta as}$. $K_{\delta au}$	Derivatives of roll with respect to control plane deflections. δ_{al}. δ_{ap}. δ_{as}. δ_{au}
k_1	Apparent mass factor in the longitudinal axis
k_2	Apparent mass factor in the transverse axis
k_z	Gain of depth controller
$\mathbf{L}$	Linear momentum vector. $\mathbf{L} = m\boldsymbol{\nu}_1$
L	Hull length
$\mathcal{L}$	Lift force (general usage)
$\mathcal{L}_{Hull}$	Lift force on the hull
$\mathcal{L}_{HCP}$	Lift force on the horizontal control planes
$\mathcal{L}_{VCP}$	Lift force on the vertical control planes
l	Reference length
$\mathbf{M}$	Moment about the y_B axis described in the body-fixed reference frame
$\mathbf{M}_A$	Augmented apparent mass matrix (sum of real and virtual added mass matrices)
$\mathbf{M}'_A$	Apparent mass matrix (sum of real and virtual added mass matrices)
$\mathbf{M}_R$	Real (physical) mass matrix
$\mathbf{M}_V$	Virtual added mass matrix
M_p. M_q. M_r	Derivatives of pitch moment with respect to angular velocities (rotary moment derivatives)
M'_p. M'_q. M'_r	Nondimensional derivatives of pitch moment with respect to angular velocities (rotary moment derivatives)

Symbol	Definition
M_p. M_q. M_r	Derivatives of pitch moment with respect to angular accelerations (mass-moment of inertia coefficients)
M'_p. M'_q. M'_r	Nondimensional derivatives of pitch moment with respect to angular accelerations (mass-moment of inertia coefficients)
M_u. M_v. M_w	Derivatives of pitch moment with respect to translational velocities (static moment derivatives)
M'_u. M'_v. M'_w	Nondimensional derivatives of pitch moment with respect to translational velocities (static moment derivatives)
M_u. M_v. M_w	Derivatives of pitch moment with respect to translational accelerations (mass-moment of inertia coefficients)
M'_u. M'_v. M'_w	Nondimensional derivatives of pitch moment with respect to translational accelerations (mass-moment of inertia coefficients)
$M_{\delta T}$	Derivative of pitch with respect to thruster output. δ_T
$M_{\delta al}$. $M_{\delta ap}$. $M_{\delta as}$. $M_{\delta au}$	Derivatives of pitch with respect to control plane deflections. δ_{al}. δ_{ap}. δ_{as}. δ_{au}
m	Mass of the body
N	Moment about the z_B axis described in the body-fixed reference frame
N	Simulations of vehicle behaviour with no active compensation: i.e. only passive roll stabilization
NR	No range of acceptable behaviour indicated by simulations
N_p. N_q. N_r	Derivatives of yaw moment with respect to angular velocities (rotary moment derivatives)
N'_p. N'_q. N'_r	Nondimensional derivatives of yaw moment with respect to angular velocities (rotary moment derivatives)
N_p. N_q. N_r	Derivatives of yaw moment with respect to angular accelerations (mass-moment of inertia coefficients)
N'_p. N'_q. N'_r	Nondimensional derivatives of yaw moment with respect to angular accelerations (mass-moment of inertia coefficients)

Symbol	Definition
N_u. N_v. N_w	Derivatives of yaw moment with respect to translational velocities (static moment derivatives)
N'_u. N'_v. N'_w	Nondimensional derivatives of yaw moment with respect to translational velocities (static moment derivatives)
$N_{\dot{u}}$. $N_{\dot{v}}$. $N_{\dot{w}}$	Derivatives of yaw moment with respect to translational accelerations (mass-moment of inertia coefficients)
$N'_{\dot{u}}$. $N'_{\dot{v}}$. $N'_{\dot{w}}$	Nondimensional derivatives of yaw moment with respect to translational accelerations (mass-moment of inertia coefficients)
$N_{\delta T}$	Derivative of yaw with respect to thruster output. δ_T
$N_{\delta al}$. $N_{\delta ap}$. $N_{\delta as}$. $N_{\delta au}$	Derivatives of yaw with respect to control plane deflections. δ_{al}. δ_{ap}. δ_{as}. δ_{au}
P	Subscript referring to hull lift-drag plane
P	Generic input parameter
P_{nom}	Nominal value of the generic input parameter
p. q. r	Roll (about x_B). pitch (about y_B). and yaw (about z_B) angular velocities respectively
p_0	Overshoot width of path of the vehicle in a zigzag maneuver
$\mathbf{R}$	Rotation matrix mapping the decomposition of a given vector in B to a decomposition in I
$\mathbf{r}$	An arbitrary vector
$\mathbf{r}_B$	Denotes the vector. $\mathbf{r}$. described (or "decomposed") in the body frame
$\mathbf{r}_I$	Denotes the vector. $\mathbf{r}$. described (or "decomposed") in the inertial frame
$\mathbf{r}_{CE}$	Position vector describing the location of the center of effort of the hull in the body frame
$\mathbf{r}_{CP}$	Position vector describing the location of the center of pressure of a control plane in the body frame
R	Simulations of vehicle behaviour with active roll compensation via rudders
R	Generic output parameter
R_{nom}	Nominal value of the generic output parameter
r_x	Hull radius at station x
r_{x_0}	Hull radius at station x_0

Symbol	Definition
$\mathbf{S}$	Augmented matrix of rigid-body coupling coefficients
$\mathbf{S}'$	Matrix of rigid-body coupling coefficients
$\mathbf{S}(\mathbf{r})$	A skew-symmetric matrix representing the crossproduct $\mathbf{r} \times \cdot$
S	Sensitivity
S_x	Cross-sectional area of the hull at station x
S_{x_0}	Cross-sectional area of the hull at station x_0
$\mathbf{T}$	Traditional transformation matrix from inertial to body-fixed reference frame
T	Superscript denoting the transpose of a vector or matrix
$\mathbf{U}$	Augmented control input matrix
$\mathbf{U}'$	Control input matrix
u, v, w	Surge (along x_B), sway (along y_B), and heave (along z_B) linear velocities respectively
$\boldsymbol{\nu}$	Vector of linear and angular velocities expressed in the body-fixed reference frame. $\boldsymbol{\nu} = \begin{bmatrix} \boldsymbol{\nu}_1^T & \boldsymbol{\nu}_2^T \end{bmatrix}^T = \begin{bmatrix} u & v & w & p & q & r \end{bmatrix}^T$
$\boldsymbol{\nu}_1$	Vector of translational velocities along the body-fixed axes. $\boldsymbol{\nu}_1 = \begin{bmatrix} u & v & w \end{bmatrix}^T$
$\boldsymbol{\nu}_2$	Vector of angular velocities about the body-fixed axes. $\boldsymbol{\nu}_2 = \begin{bmatrix} p & q & r \end{bmatrix}^T$
$\boldsymbol{\nu}_{CE}$	Velocity at the center of effort in body frame. $\boldsymbol{\nu}_{CE} = \begin{bmatrix} v_{CE}(x) & v_{CE}(y) & v_{CE}(z) \end{bmatrix}^T$
$\boldsymbol{\nu}_{CP}$	Velocity at the center of pressure in the body frame. $\boldsymbol{\nu}_{CP} = \begin{bmatrix} v_{CP}(x) & v_{CP}(y) & v_{CP}(z) \end{bmatrix}^T$
V	Velocity (scalar)
V_{CE}	Magnitude of the velocity at the center of effort
V_{CP}	Magnitude of the velocity at the center of pressure
$\mathbf{W}$	Weight force
$\mathbf{X}$	Force along the x_B axis, described in the body-fixed reference frame
$\mathbf{X}_{Hull}$	Force on the hull along the x_B axis, described in the body-fixed reference frame

Symbol	Definition
$\mathbf{X}_{HCP}$	Force on the horizontal control planes along the x_B axis, described in the body-fixed reference frame
$\mathbf{X}_{VCP}$	Force on the vertical control planes along the x_B axis, described in the body-fixed reference frame
$\mathbf{x}$	State vector in the standard state-space model
X_p, X_q, X_r	Derivatives of surge force with respect to angular velocities (rotary force derivatives)
X'_p, X'_q, X'_r	Nondimensional derivatives of surge force with respect to angular velocities (rotary force derivatives)
$X_{\dot{p}}$, $X_{\dot{q}}$, $X_{\dot{r}}$	Derivatives of surge force with respect to angular accelerations (inertia coefficients)
$X'_{\dot{p}}$, $X'_{\dot{q}}$, $X'_{\dot{r}}$	Nondimensional derivatives of surge force with respect to angular accelerations (inertia coefficients)
X_u, X_v, X_w	Derivatives of surge force with respect to translational velocities (static force derivatives)
X'_u, X'_v, X'_w	Nondimensional derivatives of surge force with respect to translational velocities (static force derivatives)
$X_{\dot{u}}$, $X_{\dot{v}}$, $X_{\dot{w}}$	Derivatives of surge force with respect to translational accelerations (inertia coefficients)
$X'_{\dot{u}}$, $X'_{\dot{v}}$, $X'_{\dot{w}}$	Nondimensional derivatives of surge force with respect to translational accelerations (inertia coefficients)
x_0	Hull station that is the limit of integration in Perkins' method for determining the lift coefficient
x_1	Hull station where the rate of change of cross-sectional area first reaches its maximum negative value
x_B, y_B, z_B	Linear coordinates in the body-fixed reference frame
x_{CE}, y_{CE}, z_{CE}	Linear coordinates of the center of effort (hull) in the body-fixed reference frame
x_{CP}, y_{CP}, z_{CP}	Linear coordinates of the center of pressure (fins) in the body-fixed reference frame
x_I, y_I, z_I	Linear coordinates in the inertial reference frame
x_{aqca}	Distance from the nose to the quarter-chord axis of the after control planes
x_b, y_b, z_b	Linear coordinates of the center of buoyancy in the body-fixed reference frame

Symbol	Definition
x_{fqca}	Distance from the nose to the quarter-chord axis of the forward control planes
x_g, y_g, z_g	Linear coordinates of the center of mass (gravity) in the body-fixed reference frame
x_{qca}	Distance from the nose to the quarter-chord axis of the control planes
x_m	Distance to moment center
x_p	Variable of integration
x_{p0}	Distance to limit of integration
$X_{\delta T}$	Derivative of surge force with respect to thruster output, δ_T
$X_{\delta al}$, $X_{\delta ap}$, $X_{\delta as}$, $X_{\delta au}$	Derivatives of surge force with respect to control plane deflections, δ_{al}, δ_{al}, δ_{al}, δ_{al}
Y	Force along the y_B axis, described in the body-fixed reference frame
Y_{Hull}	Force on the hull along the y_B axis, described in the body-fixed reference frame
Y_{HCP}	Force on the horizontal control planes along the y_B axis, described in the body-fixed reference frame
Y_{VCP}	Force on the vertical control planes along the y_B axis, described in the body-fixed reference frame
$\mathbf{y}$	Output vector in the standard state-space model
Y_p, Y_q, Y_r	Derivatives of sway force with respect to angular velocities (rotary force derivatives)
Y'_p, Y'_q, Y'_r	Nondimensional derivatives of sway force with respect to angular velocities (rotary force derivatives)
$Y_{\dot{p}}$, $Y_{\dot{q}}$, $Y_{\dot{r}}$	Derivatives of sway force with respect to angular accelerations (inertia coefficients)
$Y'_{\dot{p}}$, $Y'_{\dot{q}}$, $Y'_{\dot{r}}$	Nondimensional derivatives of sway force with respect to angular accelerations (inertia coefficients)
Y_u, Y_v, Y_w	Derivatives of sway force with respect to translational velocities (static force derivatives)
Y'_u, Y'_v, Y'_w	Nondimensional derivatives of sway force with respect to translational velocities (static force derivatives)

Symbol	Definition
$Y_{\dot{u}}$. $Y_{\dot{v}}$. $Y_{\dot{w}}$	Derivatives of sway force with respect to translational accelerations (inertia coefficients)
$Y'_{\dot{u}}$. $Y'_{\dot{v}}$. $Y'_{\dot{w}}$	Nondimensional derivatives of sway force with respect to translational accelerations (inertia coefficients)
$Y_{\delta T}$	Derivative of sway force with respect to thruster output. δ_T
$Y_{\delta al}$. $Y_{\delta ap}$. $Y_{\delta as}$. $Y_{\delta au}$	Derivatives of sway force with respect to control plane deflections. δ_{al}. δ_{ap}. δ_{as}. δ_{au}
$\mathbf{Z}$	Force along the z_B axis. described in the body-fixed reference frame
$\mathbf{Z}_{Hull}$	Force on the hull along the z_B axis. described in the body-fixed reference frame
$\mathbf{Z}_{HCP}$	Force on the horizontal control planes along the z_B axis. described in the body-fixed reference frame
$\mathbf{Z}_{VCP}$	Force on the vertical control planes along the z_B axis. described in the body-fixed reference frame
Z_p. Z_q. Z_r	Derivatives of heave force with respect to angular velocities (rotary force derivatives)
Z'_p. Z'_q. Z'_r	Nondimensional derivatives of heave force with respect to angular velocities (rotary force derivatives)
$Z_{\dot{p}}$. $Z_{\dot{q}}$. $Z_{\dot{r}}$	Derivatives of heave force with respect to angular accelerations (inertia coefficients)
$Z'_{\dot{p}}$. $Z'_{\dot{q}}$. $Z'_{\dot{r}}$	Nondimensional derivatives of heave force with respect to angular accelerations (inertia coefficients)
Z_u. Z_v. Z_w	Derivatives of heave force with respect to translational velocities (static force derivatives)
Z'_u. Z'_v. Z'_w	Nondimensional derivatives of heave force with respect to translational velocities (static force derivatives)
$Z_{\dot{u}}$. $Z_{\dot{v}}$. $Z_{\dot{w}}$	Derivatives of heave force with respect to translational accelerations (inertia coefficients)
$Z'_{\dot{u}}$. $Z'_{\dot{v}}$. $Z'_{\dot{w}}$	Nondimensional derivatives of heave force with respect to translational accelerations (inertia coefficients)
z_{err}	Depth error
$Z_{\delta T}$	Derivative of heave force with respect to thruster output. δ_T
$Z_{\delta al}$. $Z_{\delta ap}$. $Z_{\delta as}$. $Z_{\delta au}$	Derivatives of heave force with respect to control plane deflections. δ_{al}. δ_{ap}. δ_{as}. δ_{au}

Symbol	Definition
α, α'	Angle of attack in radians unless otherwise specified
β, β'	Angle of sideslip in radians unless otherwise specified
γ_0	Overshoot angle of the vehicle in a zigzag maneuver
Δ	Difference operator
δ	Control input
δ_{al}, δ_{ap}, δ_{as}, δ_{au}	Control plane commands for after lower, after port, after starboard, and after upper fins respectively
δ_{HCP}	Deflection of the horizontal control planes
δ_T	Thrust input command
δ_{VCP}	Deflection of the vertical control planes
ϵ	Small perturbation
$\boldsymbol{\eta}$	Vector of position and orientation expressed in the inertial reference frame. $\boldsymbol{\eta} = \begin{bmatrix} \boldsymbol{\eta}_1^T & \boldsymbol{\eta}_2^T \end{bmatrix}^T = \begin{bmatrix} x & y & z & \phi & \theta & \psi \end{bmatrix}^T$
$\boldsymbol{\eta}_1$	Position in the inertial reference frame. $\boldsymbol{\eta}_1 = \begin{bmatrix} x & y & z \end{bmatrix}^T$
$\boldsymbol{\eta}_2$	Orientation in the inertial reference axes. $\boldsymbol{\eta}_2 = \begin{bmatrix} \phi & \theta & \psi \end{bmatrix}^T$
η	Ratio of finite length to infinite length cylinders
Ξ	Subscript denoting equilibrium condition
ρ	Density of the fluid (sea water - assumed to be 1030 kg / m^3)
τ	Period of the zigzag maneuver
Φ	Hull roll angle
ϕ	Orientation angle about an intermediate reference frame axis x_3
θ	Orientation angle about an intermediate reference frame axis y_2
ψ	Orientation angle about the inertial reference frame axis z_I
ψ_{err}	Heading error
Ω	Sweep angle of control plane
∇	Displacement: the mass of the volume of water displaced by the outer hull of the vehicle

Chapter 1

Introduction

The surface of the earth is two thirds water, yet we know very little about what is contained in vast areas of oceans and seas. In fact, we know more about objects in space millions of kilometers away than we do about the ocean which has a depth of only 11 kilometers at its deepest point. Yet the oceans may hold a wealth of resources we may need in the future. Undersea exploration is the key to tapping these resources. We also know that these huge masses of water play a major role in the earth's weather patterns, but more information must be obtained in order to understand and model their role in the earth's ecosystems. In addition, knowledge of what is happening under the waves is a major concern for defense of any country with a coastline.

1.1 Necessity of Ocean Exploration

In 1991, the Marine Board of the United States National Research Council set out to form a strategy for the development and deployment of underwater vehicles for work and research under the sea. The results of their study were released in 1996 under the title "Undersea Vehicles and National Needs"[1]. One of their conclusions was the following (p. 5):

> Conclusion 1: The nation has vital economic and scientific needs to

> significantly advance its capabilities for working, monitoring, and measuring in the ocean. Those needs involve national security, environmental protection, resource exploitation, and science. Undersea vehicles can contribute strongly to these capabilities by giving human beings access to new kinds of information about little known areas of the ocean and the seabed - information that may have a major impact on the well-being of large populations.

In terms of national security, military applications for underwater vehicles include mine detection and mapping, covert operations in hostile waters, and monitoring the traffic in friendly waters. The military have been, until recently, the only ones with money and inclination to develop the technology (others have had the inclination, but money was hard to come by).

In the scientific realm, applications include profiling icebergs [2], water column and benthic survey and sampling [3]. In addition, underwater vehicles provide views of organisms unavailable by any other means. They also provide a tool for environmental monitoring [4].

Commercially, there are uses for underwater vehicles in many areas. For example, nuclear power plant cooling tunnel inspections could be done with underwater vehicles ([5] suggests using autonomous vehicles because the tether of a remotely operated vehicle would be a handicap in the long tunnels). Further examples in the offshore oil industry include vehicles as underwater "eyes" for riser installation, pipe-laying, etc. [6], under ice surveys, underwater profiling of icebergs, inspection of structures and devices (e.g. Kort nozzles) [7].

It is important that man be able to operate underwater: he needs "eyes" and "hands" to accomplish a wide variety of military, scientific, and commercial tasks.

1.2 Brief History of Underwater Operations

Man has historically been curious as to what goes on under the waves. Legend has it that Alexander the Great (356-323 B.C.) was lowered into the Aegean Sea in a glass diving bell. It was not until 1620. however. that an actual submersible boat was successfully built and tested by Dr. Cornelius Van Drebbel (1572-1634). It was a leather covered rowboat that made several trips under the Thames river. Later. in 1690. Edmund Halley (discoverer of Halley's Comet) patented a diving bell that was capable of submergence to 60 feet (18 m) for 90 minutes. In 1715. Englishman John Lethbridge built the "diving engine". which was used for many years. It was an oak cylinder reinforced with iron hoops. It had a glass view port. and the operator's arms protruded through greased leather cuffs. The diver could stay under for 30 minutes at 60 feet (18 m). These were ancestors of modern submarines. deep submergence rescue vehicles. and one-atmosphere diving suits.

1.2.1 Manned Vehicles

Submarines

The developments in submersible technology in the years that followed were driven by military goals. although the various navies did not necessarily think there was a need for such contraptions. American David Bushnell built the *Turtle* which was used unsuccessfully against the British ship *HMS Eagle* in New York harbour in 1776. In 1800. Robert Fulton of steamship fame (*Clermont* in 1807). built the *Nautilus* for the French government. but was unable to convince them of its usefulness as a military tool. In the 1850s a Prussian corporal. Wilhelm Bauer. built submarines first for the Germans. then for the Russians when the Germans dismissed his work. Submarines were again used with dubious success in the American Civil War - the *CSS Hunley* sank twice on training missions (the second time taking all hands including its backer. cotton broker H. L. Hunley). and finally sank a third time after sinking the *USS*

Housatonic. It was discovered in 1995 and subsequently raised. In 1874, John Phillip Holland submitted a design for a submarine to the US Secretary of the Navy. His efforts, after many discouragements, eventually lead to the first practical submarine (the *Holland VI*, later the *USS Holland* when the US Navy bought it in 1900) that used a gasoline engine for travelling on the surface and charging batteries, and an electric motor for submerged operation. Later submarines (starting with the French submarine *Aigrette* in 1904) used diesel engines rather than gasoline for obvious safety reasons. From there, submarines have developed such that there is a wide variety of military versions up to and including nuclear powered missile delivery systems, as well as many non-military submarines for tourist[1] purposes and private use.

Submersibles

For scientific missions, the work on submersible[2] technology began in earnest only relatively recently. In 1930, William Beebe, a zoologist, descended to 1426 feet (435 m) in a bathysphere ("deep sphere"), a hollow steel sphere with an inside diameter of 54 inches, and 3-inch thick glass viewports. The heavy ball was lowered from a barge to depth with a steel cable. If the cable snapped, the bathysphere would sink to the bottom. Power for telephone and lights was provided from the surface via a second cable, and an air hose was also used. In 1934, Beebe and Otis Barton descended to 3028 feet (923 m). Barton descended to 4500 feet (1372 m) in a modified bathysphere, off California in 1948. Swiss balloonist Auguste Piccard and his son, Jacques, built a bathyscaphe ("deep boat") in 1954. The *FNRS-2*[3] consisted of a steel ball suspended from a metal float filled with gasoline. Buoyancy was adjusted by releasing iron ballast in a controlled manner. In February of that year, Georges Houot and Pierre-Henri Willm descended to 13827 feet (4050 m) in this bathyscaphe. Piccard and his son

[1] Janes Underwater Technology 2000-2001[8] lists 13 types of tourist submarines in operation world wide.

[2] Submersibles, unlike submarines, tend to lack the ability to perform long-range operations. They are typically transported to the site of interest and launched from a support vessel.

[3] *FNRS-1* was a high-altitude balloon.

built the *Trieste* in 1952-3. This bathyscaphe achieved world-wide fame in 1960 when Jacques Piccard and US Navy Lieutenant Don Walsh descended 35,800 feet (10,911 m) to the bottom of the Challenger Deep in the Marianas Trench of the Pacific Ocean, the deepest known part of the ocean's floor. In 1953, Jacques Cousteau designed the *Diving Saucer* for scientific observations in waters up to 1000 feet deep. In 1962 the *ALVIN* (named after Wood's Hole Oceanographic Institute (WHOI) researcher Allyn Vine who had championed the need for it) was funded. It was launched in 1964 and is still in service today, in spite of having sunk in 5500 feet (1676 m) of water in 1968 (it was recovered less than a year later). This famous submersible has been involved in finding a lost H-bomb off the Spanish coast in 1966, discovering the existence of thermal vents in 1977, and exploring the *HMS Titanic* in 1986. Jane's [8] lists 25 types of manned submersibles, including *ALVIN*, currently active.

1.2.2 Unmanned Vehicles

To accomplish the necessary underwater work, manned submarines have traditionally been the tool of choice since they allowed humans to get down there and have a look for themselves. They are, however, expensive and involve risk for the occupants. Several submarines have been lost over the years with accompanying loss of life. There have been some successful rescues. In 1939, the *Squallus* rescue using a new diving bell, the McCann Rescue Chamber, saw 33 men rescued from 243 feet (71 m) [9]. To reduce costs and risks, current technology is concentrating on development of unmanned submersibles. "Any system that will remove man from the water and can do the job with efficiency is preferred." ([6] p. 240) There are several types of unmanned submersibles in use today.

Remotely Operated Vehicles (ROV)

Remotely operated vehicles are unmanned submersibles that are operated from a ship via a tether through which power and communications are available to the vehicle.

In the early 1960s the Cable-controlled Undersea Recovery Vehicle (CURV) was developed by the US Navy (the former Pasadena Annex of the Naval Ordnance Test Station) to retrieve test ordinance lost off San Clemente Island at depths as great as 2000 feet. The vehicle became famous in 1966 with the recovery of an H-bomb off Spain in 2800 feet of water. This success spawned later generations of vehicles designated CURV II. CURV II-B. CURV II-C and CURV III. CURV. now referred to as CURV I. pioneered the concept of undersea teleoperators and is credited as the first practical remotely operated vehicle (ROV). Throughout the 60s. 70s. and 80s. the ROV has matured and become an important tool for the offshore oil industry for inspection and underwater intervention. At present there are about 134 ROV of different type and manufacturer in use world wide for a wide variety of tasks [8].

Autonomous Underwater Vehicles (AUV)

ROV are less expensive than manned submersibles and remove the risk to the operators by allowing them to sit in relative comfort on the surface ship. The major drawback is the tether. There is a high risk of the vehicle getting tangled up in it. Also. at greater depths. these systems tend to run into problems with snap loading. during which large tensions are generated in the tether. It is not uncommon to lose an ROV when the cable snaps.

Autonomous underwater vehicles have no cable and are free swimming devices. In principle they further reduce the operating costs since it should not be necessary to have a surface ship constantly monitoring them – once launched they are left to carry out their mission and return to a pre-programmed pick-up site. The onboard power supply limits this type of vehicle in terms of the duration of mission achievable. They require a compact. lightweight. long-lasting power source.

SPURV (Self-Propelled Underwater Research Vehicle) is the first instance of an autonomous underwater vehicle. though some point to the torpedo. invented in 1867[1].

[1]In 1867. the Englishman. Robert Whitehead developed the "automobile torpedo" (until that

as the true beginnings of AUV technology. Though contemporary with the ROV, the AUV has largely been an experimental vehicle until recent years. To quote Drew Michel [10]:

> "Autonomous underwater vehicles, or AUVs, have slowly progressed for the past twenty-five years, limited by inadequate control logics, processing hardware, energy limitations and, primarily, by lack of perceived need. As with ROVs, AUVs have been pushed mostly for military applications, where the need for standoff or rapid broad area coverage for force multiplication of costly naval vessels overrides other considerations. It is probably safe to say that the dawning of the AUV is upon us and recent developments in energy, advanced algorithms and processors, and such innovations as fibre optic micro cable that can be dispensed over distances in excess of 200 km (without repeaters) to give wide communication bandwidths have given rise to a broader experience base. Additionally, efforts to bring down costs will influence positive future considerations of AUVs as practical scientific and commercial tools."

They have only recently matured to the level of commercial viability, but there is currently a recognition of the need for AUV, and an expectation of increased benefit from using these vehicles.

"There is a clear need for AUV for a broad range of research applications, most of which are linked to what is presently known about the oceans." ([3] p. 222)

"The new perspective provided by AUV will teach a great deal more than what we might anticipate" ([3] p. 222)

Currently there are on the order of 75 AUV of various manufacture in use today as testbed vehicles, as search and survey tools, and for military purposes [8].

---

time stationary mines were called torpedoes).

AUV technology is rapidly becoming a viable tool to accomplish the scientific, commercial, and military needs faced today. Schostak [11] makes a business case for autonomous vehicles in the offshore oil industry. Bjerrum [12] contends that AUV are commercially viable now and offers the example of one of his vehicle's (Maridan 200) search for diamonds off Nambia. Griffiths et al. [13] describe some of their successes with the Autosub-1, as further proof of the maturity of AUV as survey tools. Northcutt et al. [14] make the case for AUV in deeper water to replace deep towed systems. Bob Barton [15] reports:

> "Overall, said Roger Lott, data from AUV surveys will reveal slope instabilities, mud volcanoes and evidence of benthic communities living on and around hydrate seepages. None of this, he says, could be mapped to such quality or resolution - if at all - by conventional deeptow survey systems: 'We're seeing things we just couldn't see before,' he said."

Other Types of Unmanned Underwater Vehicles

There are several other types of vehicles for various purposes, such as trencher/crawlers for pipeline and cable laying operations, and diver delivery vehicles. There are also underwater vehicles that are tetherless but not autonomous: they are called Remotely Controlled Vehicles (RCV), and involve higher-level commands sent to the vehicle from the operator onboard the support vessel via an acoustic modem. Jane's [8] lists 18 such RCV systems.

The focus of this work is on AUV, since they are a maturing technology with immense potential for being man's underwater "eyes", "ears", "hands", "feet", "brain", ...

1.3 Technological Requirements

In order for AUV to be firmly established as a viable, mature technology there are several issues that need to be addressed. Since 1981 (see [16]), there has been a perceived need for improvements in energy systems, navigation, guidance and control. These needs were still relevant in 1987, though communications and systems integration were also identified as concerns [17]. In 1993, Collins [18] raised the issue of cost effectiveness. The raising of this business related issue is a sure sign of a maturing technology. In 1998, Griffiths [19] pointed out the need to address legal issues (e.g. insurance and liabilities), demonstrating the emergence of AUV technology as a viable commercial entity. He also reiterated the need for developments in energy and communications technology, and in software verification.

NRC(US) [1] in 1996 concurred in general (p. 5)

> Conclusion 3: The committee finds the technological advances most critical to these important missions are in the areas of ocean sensors, subsea communications, and mission and task-performing control systems.

The "mission and task-performing control systems" part of this conclusion had to do with implementing reliable, high-level control algorithms, but mission and task performance are dependent on the vehicle behaviour under operating conditions. In the 1981 paper, the issue of reliability or fault-tolerance was also raised as requiring attention, but the issue has since been left off of the list of enabling technologies. Much work has been done on the fault tolerance of electronics and microprocessors, and indeed the issue was raised in the context of artificial intelligence, but there is little work done in the area of actuator fault conditions. It seems that the prevailing thought is that actuator faults should be handled by aborting the mission and recovering the vehicle. This may not be economically or physically possible in some missions. In most cases, it would be better to be able to extend the mission or at least accomplish some subset of the mission objectives.

1.4 Environmental Effects Monitoring (EEM) with AUV

Among the myriad of uses for AUV. is a vital role in environmental effects monitoring (EEM). With the offshore oil and gas industry growing rapidly. it is important that new and innovative methods for EEM be considered. One of the means of accomplishing the task is to use an AUV that is equipped with suitable sensors for detecting the presence of the chemicals in drilling wastes and produced waters. This AUV could be used to monitor and assess chemical content in discharges of offshore installations.

Such an AUV needs to be designed with the ability to (a) hover in place for long periods in cross-currents. and. (b) return to a known (x.y.z) position with accuracy and precision. It also needs to be very reliable. even (and particularly) in a structured environment (i.e.. with fixed obstacles).

The AUV. Canadian Self-Contained Off-the-shelf Underwater Testbed (C-SCOUT). was built at the Institute for Marine Dynamics (IMD) of the National Research Council (NRC) of Canada. and the Ocean Engineering Research Centre (OERC) of Memorial University of Newfoundland (MUN). This AUV is part of the Natural Sciences and Engineering Research Council (NSERC) Strategic Project: "**Offshore Environmental Engineering using Autonomous Underwater Vehicles**" which involves a number of research and industrial partners including MUN. IMD. C-CORE. the University of Victoria. Petro-Canada. International Submarine Engineering (ISE) Ltd.. and Geo-Resources [4]. A prototype vehicle has been built as a platform for (sub)system development and testing. The C-SCOUT was designed to be able to cruise ahead or astern with a high degree of maneuverability. and to be able to hover. even in a crosscurrent. making it suitable for a variety of environmental monitoring missions. It has multiple fins (control surfaces) and multiple through-body thrusters. The fins are used for maneuvering at speeds above approximately three knots while the number and placement of the thrusters provides a high degree of control for posi-

tioning and orienting the vehicle while maneuvering at low speeds or while hovering in-place within a cross-current. The maneuvering capabilities make it possible to place and hold C-SCOUT-mounted equipment such as sensors or samplers at known locations in the water column. This vehicle will be a valuable tool for monitoring and assessing discharges of offshore installations, and for gathering data to validate numerical models (which have also been developed within the scope of the strategic project) that predict the consequences of these discharges.

1.5 Vehicle Behaviours

In order to accomplish the mission objectives or even a specific subset of the mission objectives (a particular task), there must be some knowledge of the dynamics and hydrodynamics involved; i.e. the vehicle behaviour. During the design stage, it is possible to choose parameters that will enhance specific mission-related abilities of the vehicle. Model simulations and scale model testing allow the designer to "optimize" those parameters. Some of the risks to a particular type of mission or task may be reduced or even eliminated by good design choices. It is useful to establish the most sensitive and/or significant parameters in the design process. Further, knowledge about the behaviour of the vehicle under fault conditions may be very useful in extending the vehicle's capabilities so as to "save" the mission or task. Simulations of typical fault conditions provide information about vehicle behaviour that will aid in mission re-evaluation and re-planning. The information may even lead to streamlined fault-detection algorithms. Control plane faults are the most obvious cause of changes in vehicle behaviour. Reliable control requires clear understanding of the physics of the vehicle behaviour, even under fault conditions. This knowledge facilitates achieving the goal of extending the mission beyond nominal capabilities.

The work presented herein is intended to describe the effects of changes in design parameters on vehicle behaviour, and to describe the effects of actuator fault con-

ditions on vehicle behaviour. The primary motivation for the work is to investigate vehicle behaviours in light of controllability, and extending the nominal operating capabilities. Accurate control of AUV is not trivial, and, as in any system, is best accomplished when as many factors as possible are accounted for.

1.6 Modeling and Control of AUV

The problem of nominal control of autonomous underwater vehicles has been well stated by Yuh [20]. The dynamics of AUV are fundamentally multivariable and nonlinear due to rigid body coupling and the hydrodynamic forces on the vehicle. This nonlinear behaviour is similar to that of aircraft except that the high density of water increases the significance of the forces and moments due to fluid motion. The dense fluid also leads to significant effects on the vehicle's motion as a result of accelerating the fluid surrounding the vehicle ("added mass"). In fact, hydrodynamic characteristics of the vehicle are often poorly known and change with operating conditions and payload configurations. Even when tests are conducted to find the parameters, the values obtained are only valid for conditions near those of the test.

Controlling a highly nonlinear system such as an AUV, that has significant uncertainty in the parameters, and is operating in an unpredictable, nonhomogeneous environment is a difficult task. Controlling such a system so as to be able to maintain control even in the event of component failure, has typically been addressed as three separate problems: first - a robust nominal controller that will handle the nonlinearities and parameter uncertainties; second - detection and isolation of component failures (before they become debilitating, if possible); and third - reconfiguring the controller to accomplish the task.

Most nominal control systems found in the literature which are applied to underwater vehicles, are model based. When assumptions are made to linearize the model, some well-established techniques for linear systems can be employed. Jalv-

ing and Storkersen [21] linearized and decoupled an AUV model then applied PID controllers. Healey [22] used the Linear Quadratic Gaussian (LQG) method because it is robust with respect to parameter uncertainties and small disturbances to the vehicle system. Chellabi and Nahon [23] used feedback linearization with an LQG approach to develop a controller. Adaptive control (Fossen and Fjellstad [24], Fossen and Sagatan [25], Goheen and Jefferys [26], and Yuh [27] [20] [28]) has been used to attempt to account for uncertainty of the parameters, but this control method still relies on a linear model. Others have focused on sliding mode control (see e.g., Yoerger and Slotine [29], and Dougherty, et al. [30]). Cristi, et al. [31] have combined sliding mode control with adaptive control. Yuh, et al. [32] have also used neural networks as a vehicle controller. Sordalen [33], et al. use differential geometry to derive a control law based only on a kinematic model. Nakamura and Savant [34] use a Liapunov-like function for a control law.

There is much less information in the literature on fault detection in AUV control systems. Determining when a fault has occurred or will occur is dependent on the values of system parameters. Alekseev et al. [35] use an observer-based approach to identify parameters. Healey proposed methods for identifying parameters using Kalman filters and neural networks [36] and using Kalman filters, batched least squares, and exponentially weighted least squares [37].

There is also relatively little in the literature on fault handling in AUV control systems. Rodríguez and Dobeck [38] use an expert systems approach to keep the vehicle safe by aborting the mission when a fault occurs. Barnett et. al. [39] also use a rule based method for handling faults, but their application is more sophisticated and allows completion of the mission where possible. Payton et al. [40] have a novel approach that uses what is known to be possible rather than trying to determine the problem. Leonard [41] [42] [43] synthesizes controls using differential geometry, and averaging theory, but this method has serious drawbacks for typical AUV because of the separation of the center of buoyancy from the center of gravity [44].

Modeling the vehicle is important for control purposes, and it is important for investigating the sensitivity of AUV to various changes in parameters. The modeling of AUV has been developed from work on submarines, torpedoes, airships and missiles.

Lambert [45] investigated the effect of changing the linear stability derivatives on the behaviour of a torpedo, focusing on the stability margins to determine the accuracy required for the stability derivatives. This study was done without the aid of modern computing facilities, and therefore involved a number of simplifying assumptions unnecessary with the tools available today.

Gertler and Hagen [46] developed the Standard Equations of Motion for Submarines, based on a Taylor Series Expansion of the Newton-Euler equations of motion for a body moving through a fluid, and on much experimental experience. The equations were updated by Feldman [47].

Humphreys and Watkinson [48] used Gertler and Hagen's work to develop linear equations of motion for underwater vehicles. Then they use USAF DATCOM to generate the necessary coefficients. Nahon [49] uses the same idea with an updated DATCOM, and compares the results with data from other sources.

Humphreys [50] developed the equations of motion based on small perturbations (similar to Taylor Series Expansion), then formulates them into linear system transfer functions. He presented an example case to show typical values to be expected.

Fossen [51] uses a quaternion approach for modeling and control of AUV.

The modeling approach used in this work involves standard vector representation of the Newton-Euler equations of motion, where the forcing function is constructed from lift and drag relations. The model was used to examine the sensitivity of AUV to variations in hydrodynamic parameters. It was also used to investigate the behaviour of the vehicle when a control plane fault occurs. Chapter Two provides information about the physical vehicle, C-SCOUT, a streamlined AUV, and also presents the nonlinear and linear models developed based on the base configuration of C-SCOUT.

1.7 Methodology Used

1.7.1 Sensitivity of Added Mass to Changes in Vehicle Geometry

Added mass coefficients can have a significant effect on the transient response of a body, and they are dependent on the geometry of the body and the flow conditions it is experiencing. Part of the concept for C-SCOUT is that modules may be added, or change positions. It is therefore useful to know what effects variations of geometry will have on the added mass. A sensitivity study using a computer program called Estimate Submarine Added Mass (ESAM) provided information about how vehicle added mass characteristics change with variation of vehicle geometry. Several features of the vehicle were systematically varied and the added mass determined for each variation. The data were analyzed for trends. This work reports actual data in support of the conventional thinking. A study of this nature has not been reported before now. The work has been submitted for publication [52], and makes up Chapter Three of this thesis.

1.7.2 Sensitivity of Vehicle Response to Variations in Hydrodynamic Parameters

It is useful to know how accurate the model parameters need to be in order to ensure a reasonable amount of fidelity between the hydrodynamic model and the physical system. It is also important to know how variations in the hydrodynamic properties of a vehicle (which are dependent on design choices) will change the response of the AUV. To investigate these issues, a sensitivity study using a fully nonlinear computer model of the C-SCOUT was made to identify the changes in the behaviours of the vehicle as the hydrodynamic parameters are systematically varied.

Humphreys and Watkinson [53] demonstrated a method of estimating added mass

coefficients from vehicle geometry. They went on to compare the values estimated with those determined from experiments. They also performed a sensitivity analysis on the added mass coefficients in the linear transfer functions, keying in on stability and control issues. The present study looked at other hydrodynamic parameters, as well as added mass, and uses a nonlinear model, looking at vehicle motion response parameters in specific maneuvers to evaluate the sensitivity and importance of the various parameters to the vehicle performance.

Sen [54] investigated the sensitivity of vehicle response to variations in hydrodynamic coefficients. Here, Sen's method for sensitivity analysis was used with a different modeling approach to provide new data. Sen used the standard Taylor Series Expansion approach, while the present model is based on lift and drag equations. The Taylor Series Expansion requires experimental data to supply the values of the coefficients, while the method of lift and drag forces uses empirical values already available.

Several standard maneuvers were simulated for each variation of a set of hydrodynamic parameters such as the lift coefficient for the hull ($C_{L_{Hull}}$). The maneuvers chosen were turning circles for indication of changes in steady state vehicle response; horizontal and vertical zigzags were chosen to highlight variations in the vehicle's transient response. These maneuvers were chosen for the simulations because they are standard maneuvers used in testing real ships and/or submarines.

The results of the sensitivity study are important for making valid design choices, and for understanding the effects of the particular design choices on the controllability, maneuverability, and stability of the vehicle. These results have also been submitted for publication [55], and they constitute Chapter Four herein.

1.7.3 Effects of Control Plane Faults on Vehicle Response

It may be important to be able to operate the vehicle when it has reduced control authority due to a control plane fault, such as a jammed or a missing control plane.

Knowledge of how the vehicle behaves under these conditions will allow the mission planner to make critical decisions about the viability of the mission or of certain specific subtasks. Knowledge of vehicle behaviours under fault conditions can also facilitate the use of operational envelopes in restricted waters: i.e. a healthy AUV may be restricted in the magnitude of control plane deflections, so that it can maintain a safe trajectory even if a control plane fails. A systematic study was made involving simulations of the vehicle under fault conditions to identify the vehicle behaviours typical of such fault conditions. The simulation tool used is a linear model of the C-SCOUT, and the maneuvers used were those most likely to be desired during normal operation: holding course, a controlled dive, and a turn in the horizontal plane. The work on behaviours during faults is new, and is reported in Chapter Five.

1.8 Principle Results and Conclusions

In Chapter Six, the main results for each of the studies are presented, and conclusions are drawn.

The study of the sensitivity of added mass to variations in vehicle geometry has demonstrated that conventional thinking based on the axisymmetric, streamlined, slender body geometry of a typical vehicle is valid. As the length-to-diameter ratio increases, it is the mass-moments of inertia about the axes normal to the length of the hull that are most affected. It is the same mass-moments of inertia that are again most affected by the variation of the location of the control planes along the length of the hull. The size of the control planes affects each of the added mass coefficients approximately equally.

Examination of the effects of changing the hydrodynamic parameters, including the added masses, highlighted several facts that are important to consider for design of the vehicle and its controller. These effects include the following:

- Even though the vehicle is not symmetric about the reference x-y plane (it is

symmetric about the x-z plane), and the weight-buoyancy couple is only relevant in the vertical plane, the response in horizontal zigzags is very similar to the response in vertical zigzags.

- Although changing the roll added mass-moment of inertia does not cause any significant change in the vehicle response, the other principle coefficients must be known with reasonable accuracy to have a good model of the vehicle, since varying the principle added mass derivatives can significantly change the vehicle response in transient maneuvers. Varying the heave-pitch coupling element also results in changing the response of the vehicle, but none of the other coupling coefficients cause the same magnitude of effects. It is useful to design the vehicle so as to reduce the influence of the added mass derivatives as much as possible by streamlining the vehicle and reducing the size of the appendages.

- Increasing the hull lift force causes the vehicle to turn more sharply, but it makes it more difficult to recover from the turn. This is consistent with the destabilizing influence of a side force applied forward of the center of mass. Increasing the hull drag slows the vehicle down, tending to reduce the spatial requirements at the expense of requiring more time, and, consequentially, more energy to complete the maneuver. Some effort must be made in the design of the vehicle to reduce the drag as much as possible. This will also reduce the lift on the hull, and therefore the effort required to initiate or recover from a turn.

- Increasing the drag on the control planes has the same effect as increasing the hull drag: the vehicle is slower and requires more energy to complete the maneuver. Increasing the lift of the after fins increases the stability of the vehicle, reducing the turning ability, but increasing the ability of the vehicle to initiate and recover from turns; i.e. more fin lift translates into more control authority.

- Varying the distance from the center of mass to the center of effort of the hull

illustrates that there are conflicting requirements for the vehicle response in transient conditions as opposed to the vehicle response in steady conditions.

- Variation of the location of the center of pressure of the control plane along the span of the control plane (perpendicular to the hull for C-SCOUT) has virtually no effect on the response of the vehicle in any of the maneuvers studied. Moving the location of the center of pressure causes the vehicle respond consistent with the concept of increased control authority with increased moment arm to the center of pressure.

The combination of the two sensitivity studies shows how the added mass and other hydrodynamic parameters affect vehicle motion. Together, these studies provide valuable data about the design choices available to the vehicle designer. The data can be applied to a given set of constraints, enabling the designer to make informed decisions.

The results of the sensitivity simulations using the nonlinear model confirm the results obtained by others in earlier studies using linear models. Therefore they validate the nonlinear model.

The investigation of vehicle behaviour under control plane actuator faults provides useful operational data, as well as information pertinent to control strategies. In general, the depth controller gain should be kept as high as possible without inducing instability in the vehicle response.

To guarantee adequate performance even with jammed control planes, the port and starboard control planes should be restricted to angles near zero. Since this is too restrictive, especially in maneuvers involving diving, the operational envelope for the horizontal planes can be expanded as required for the mission, but some degradation of performance can be expected if one of the horizontal planes jams at an angle not near zero.

The operational envelope for the upper and lower (vertical) control planes is less restricted, while still providing guarantees of acceptable performance even with jammed

planes. The choice of active roll compensation depends on how important the roll angle is to the task at hand: use all the remaining planes to compensate for the effects of the jammed plane if roll must be limited. otherwise no roll compensation is necessary or of benefit.

The fault condition simulations provide useful information. especially concerning safe operating envelopes for the C-SCOUT for particular mission requirements. The information can also be used to enable the vehicle to perform self-diagnosis procedures under some conditions.

The thesis is completed with a list of recommendations for future work in Chapter Seven.

1.9 Contributions and Relevance

It is to be noted that a portion of the work herein may be a repeat of military AUV research. however. such research has not been reported in the open literature. Therefore. this research presents important "new" information to the underwater vehicle community at large.

This work reports actual data in support of the conventional thinking concerning the effects of changes in geometry of the vehicle on the added mass of the vehicle. The systematic study provides useful information for guiding design choices. as well as operational decisions for modular vehicles.

The results of the systematic study of the sensitivity of the vehicle motion response to variations in hydrodynamic parameters are also important for making valid design choices. and for understanding the effects of the particular design choices on the controllability. maneuverability. and stability of the vehicle. Again. the information presented here is also useful in operation of an AUV such as C-SCOUT for making decisions about control algorithms when the configuration of the vehicle is altered.

Effects of control plane faults on vehicle motion response have been catalogued for

a number of specific instances representing a range of possible control plane faults. Conclusions are drawn about how roll compensation helps or hurts performance during a maneuver with a fault present. In addition, the fault behaviours are used to define safe operation limits for the vehicle (using an arbitrary set of acceptability criteria). This represents new information that is applicable in a qualitative sense across the range of streamlined (axisymmetric) vehicles, and can be used by vehicle operators to make critical decisions about mission viability.

Chapter 2

C-SCOUT: The Real and the Virtual

The Institute for Marine Dynamics (IMD) of the National Research Council (NRC) Canada and the Ocean Engineering Research Centre (OERC) of Memorial University of Newfoundland (MUN) began a collaborative effort in September of 1998 to design a streamlined autonomous underwater vehicle (AUV). This AUV, the Canadian Self-Contained Off-the-shelf Underwater Testbed (C-SCOUT), is intended to serve as a test bed for systems research, and as a general research and development tool for years to come.

One of the key elements in the vehicle's effectiveness as a test bed is a fundamental understanding of its maneuverability and of its sensitivity to changes in hydrodynamic parameters. Knowledge of these characteristics will allow the systems designer to separate inherent vehicle behaviour (i.e. the behaviour of the test bed) from behaviour induced by the system being tested, resulting in a clear measurement of the performance of that system. Knowledge of the behaviour of the vehicle is also important when considering large-scale changes in parameters such as occur when an actuator fault condition is encountered, or when a large payload module is added.

2.1 The Physical Vehicle

The C-SCOUT vehicle was designed and built by graduate students at Memorial University of Newfoundland, by work term students employed by IMD and OERC, and by IMD and MUN technical personnel [56] [57] [58] [59] [60] [61] [62] [63] [64] [65] [66]. The AUV is part of the Natural Sciences and Engineering Research Council (NSERC) Strategic Project: "Offshore Environmental Engineering using Autonomous Underwater Vehicles" which involves a number of research and industrial partners including MUN, IMD, C-CORE, the University of Victoria, Petro-Canada, International Submarine Engineering (ISE) Ltd., and Geo-Resources [4]. Future variations of the AUV can be configured for a wide variety of missions including ocean environmental monitoring, search and survey, under ice operations, iceberg profiling, oceanographic sampling, and mine detection and countermeasures. The prototype vehicle has been built as a platform for (sub)system development and testing.

The C-SCOUT was designed to be able to cruise ahead or astern with a high degree of maneuverability, and to be able to hover, even in a crosscurrent. It was therefore designed to be streamlined in shape, and has an ellipsoid nose, parallel cylindrical mid-body, and a cubic spline tail. The full configuration (see Figure 2-1) will have the four aft control surfaces, as well as four forward control surfaces. The control planes are all-movable surfaces and are tapered ($c_t/c_r = 0.4$) NACA 0015 sections with an aspect ratio of six and zero angle of sweep. In addition, this fully actuated version will be equipped with six through-body thrusters, placed so that, along with the main propulsor, they facilitate motion control in any degree of freedom (DOF).

The construction of the vehicle is being accomplished in stages. The base configuration of the vehicle has four control surfaces aft, and a single thruster aft for propulsion (see Figure 2-2).

To make the vehicle easily amenable to a wide variety of configurations, including upgrade to the full configuration, the AUV was designed and constructed as simply as possible using modular sections, such that reconfiguration can be accomplished with

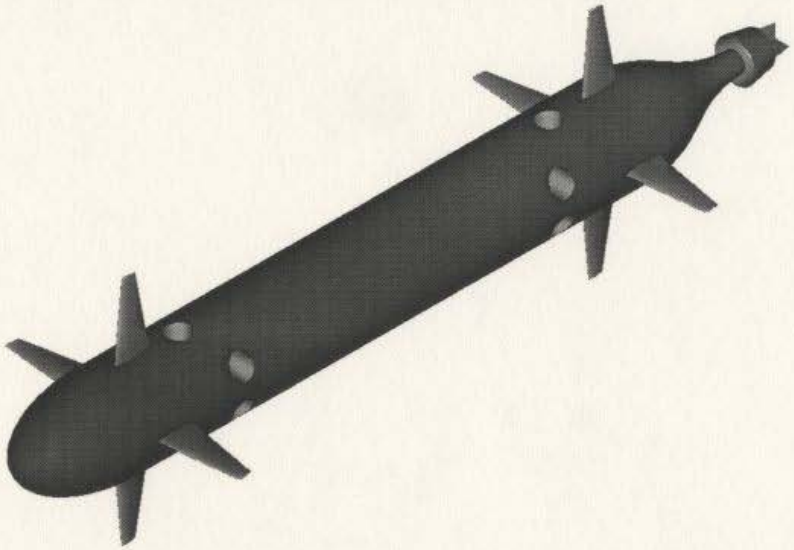

Figure 2-1: Full Configuration C-SCOUT AUV

minimal time delay. It is the modular nature that allows lengthening and shortening of the vehicle to accommodate various payloads and control system configurations.

C-SCOUT is typical of many vehicles active in the world today; it is a hydrodynamically streamlined, axi-symmetric, slender body using control planes for directional control. It is atypical in that the after control planes are mounted on the parallel mid-body rather than on the tail section. This allows greater variation of the configuration of the vehicle, i.e. different tail sections and main propulsors may be used without redesigning the control plane section. The elliptical nose and cubic spline tail section (designed to increase the inflow to the propulsor) are also somewhat distinctive.

To date, the first vehicle (base configuration) has been built and is currently undergoing systems validation. A second hull has been fabricated for full-scale hydro-

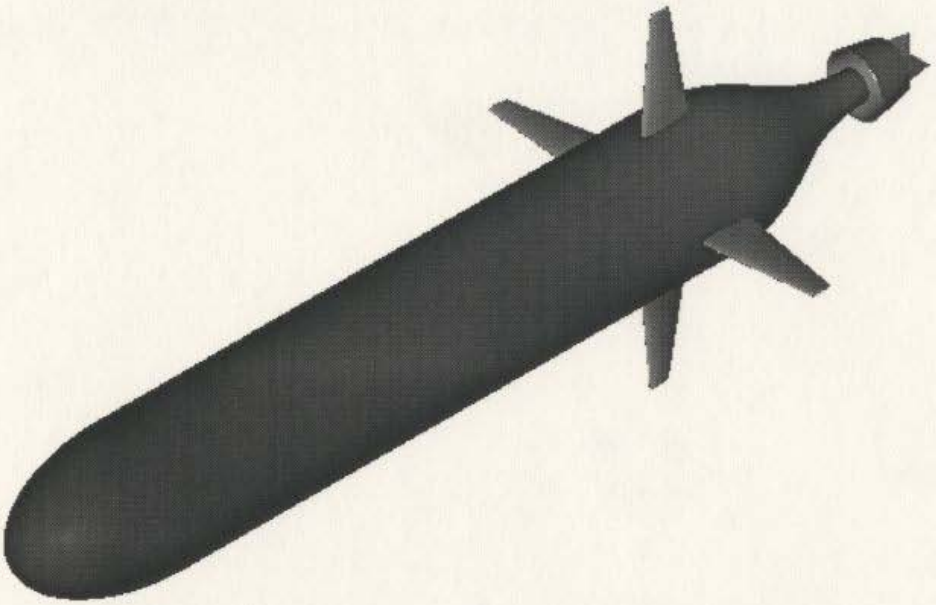

Figure 2-2: Base Configuration C-SCOUT AUV

dynamic experiments. This hull has already been used for testing a novel propulsion scheme (a cyclic-pitch propeller) for low speed directional control without control planes or through-body thrusters. It is also currently being used to test flow conditions for through-body thrusters.

2.2 The Virtual Vehicle

A computer model can be used to determine the value of vehicle design parameters and to validate design choices. It is also useful for designing and testing control algorithms. In addition, the model can be used after the vehicle is built to pre-screen mission scenarios, or to aid in the post mission analysis.

In conjunction with the physical vehicle, a computer model was developed to test ideas and algorithms before committing them to hardware. The nonlinear com-

puter model [67] and the linearized model formulated from it were developed in Matlab^{TM}/Simulink^{TM}.

This fully nonlinear model is based on the physics of rigid-body motion in a fluid. The motion of an autonomous underwater vehicle, like the motion of any body in 3-D space, can be described in terms of the Newton-Euler laws of motion, where the rate of change of momentum of a rigid body is equated to the forces/moments causing the change.

$$\mathbf{F} = \dot{\mathbf{L}}$$

$$\mathbf{G} = \dot{\mathbf{H}}$$

where $\mathbf{F}$ is the force vector and $\mathbf{G}$ is the moment vector. $\mathbf{L}$ and $\mathbf{H}$ are the linear momentum and angular momentum vectors, respectively, and are products of mass, m, and linear velocity, $\boldsymbol{\nu}_1$, and of inertia, $\mathbf{I}$, and angular velocity, $\boldsymbol{\nu}_2$, respectively.

$$\mathbf{L} = m\boldsymbol{\nu}_1$$

$$\mathbf{H} = \mathbf{I}\boldsymbol{\nu}_2$$

The rate of change of momentum of the body is a function of its inertial characteristics, while the forces and moments causing the change are a summation of the external forces and moments acting on the body. For a body such as an AUV, there are motions in six degrees of freedom: surge, sway, heave, roll, pitch, and yaw (see Figure 2-3). There is also significant coupling between the motions in different DOF. On the assumption that the vehicle behaves as a perfectly rigid body, the quantities defining the rate of change of momentum in each DOF can be determined exactly, algebraically. The external forces and moments, however, by their nature are somewhat uncertain. Typically the excitation force terms are a function of the motion variables (see for example equation (2.1) where $\mathbf{X}$ represents the total force in the surge direction), and

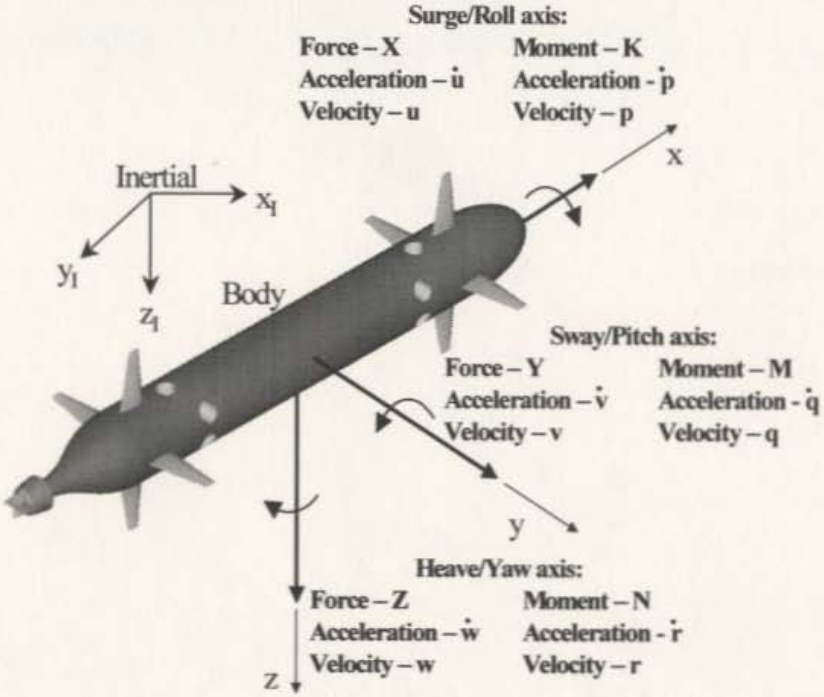

Figure 2-3: Inertial and Body-fixed Reference Frames

can be written as a Taylor Series Expansion.

$$\mathbf{X} = \mathbf{f}\left(\dot{u}, \dot{v}, \dot{w}, \dot{p}, \dot{q}, \dot{r}, u, v, w, p, q, r, \phi, \theta, \delta_j\right) \tag{2.1}$$

For example, equation (2.2) is the Taylor Series Expansion of the excitation forces in the surge direction. Only the linear terms have been retained.

$$\begin{aligned} \mathbf{X} \;=\; & X_{\dot{u}}\dot{u} + X_{\dot{v}}\dot{v} + X_{\dot{w}}\dot{w} + X_{\dot{p}}\dot{p} + X_{\dot{q}}\dot{q} + X_{\dot{r}}\dot{r} \\ & + X_u u + X_v v + X_w w + X_p p + X_q q + X_r r \\ & + X_\phi \phi + X_\theta \theta \\ & + \Sigma X_{\delta_j}\delta_j \\ & + \mathbf{X}_\Xi \end{aligned} \tag{2.2}$$

Note that the subscript notation, $X_{i\cdot}$ denotes the partial derivative of $\mathbf{X}$ with respect to the i^{th} state variable. The first line of the right-hand side of equation (2.2) contains the forces due to acceleration, and the $X_{i\cdot}$ coefficients represent the added masses for the vehicle. The second line contains the forces due to velocity dependent effects. The third line contains the forces due to the orientation of the vehicle: i.e. the gravitational and buoyancy forces[1]. The fourth line contains the forces due to control actuators, where δ_j include the control surface deflections, e.g. δ_{as} for the after starboard control plane, etc. The last line is the force required to maintain the equilibrium state (e.g. straight and level flight at a constant forward speed) about which the Taylor Series Expansion is taken. The terms represent physical effects on the vehicle as a whole, and are not always analytically simple to determine. This method requires physical model testing in order to determine the coefficients (hydrodynamic derivatives) of the terms in the Taylor Series Expansion.

The nonlinear model of the C-SCOUT is also based on the Newton-Euler equations of motion, but the excitation terms are formulated in terms of the lift and drag forces that are applied to each of the components of the vehicle, i.e. to the hull and the control planes. The resulting forces and moments are summed together to provide the forcing function applied to the vehicle. This method is called the body build-up technique [68] or the component build-up method [69]. The advantage here is that these forces can, for the most part, be determined analytically, and therefore provide a quick answer without excessive computational effort. They must, however, be verified by physical model testing to ensure accuracy in the computer model. This testing will also quantify the interactions between the hull and the control planes. A further advantage of the component build-up method is that it is not limited to a region about the nominal operating (equilibrium) state of the vehicle, an assumption inherent in the Taylor Series Expansion method. It does, however, depend on coefficients that have

[1] Note that equation (2.2) does not contain the term $X_{\psi\cdot}\psi$ since the yaw attitude (vehicle heading) does not contribute to the gravitational and buoyancy forces.

some physical constraints (e.g. control plane stall angle) over the range of vehicle motions. These constraints must be accounted for in the computer model or they constitute limits of validity for the model.

The forcing function includes terms from both viscous effects (lift and drag) and from pressure effects ("added mass" and radiation damping), as well as terms for gravity and buoyancy forces. Each set of forces and moments are dependent on the geometry of the vehicle. Changing the geometry of the vehicle is therefore expected to have an effect on the forces experienced by the vehicle.

2.2.1 Assumptions

An autonomous underwater vehicle can be modeled as a rigid body in space. The rigid body assumption means that all flexure of the vehicle body is neglected, and that the vehicle is of fixed dimensions and mass distribution. Even a moderately sized vehicle, however, will flex to some extent when force is applied to it (e.g. forces developed by control plane angles of attack intended to cause the vehicle to rotate will also cause the vehicle to bend slightly). Variations in pressure on the hull will also cause elastic deformations and changes in buoyancy due to compression. All of these effects are relatively minor, and can be ignored or treated as uncertainty in the model.

In addition, some vehicles use variable ballast systems to maintain buoyancy and trim in the face of significant variations of density and temperature of the ocean environment. The obvious penalty (in terms of control) for these systems is that the vehicle no longer has a constant mass or mass distribution. This too can be accounted for in terms of uncertainty in the model, or as a disturbance to the control system.

The computer model for C-SCOUT assumes a rigid body with constant mass and distribution of mass properties. C-SCOUT does not have a variable ballast system (yet), so the mass distribution is essentially constant. The model is limited to small angles of attack on the hull and control planes.

2.3 Dynamics and Hydrodynamics

Describing the motion of a body in 3-D space in terms of the Newton-Euler laws of motion is known as vector mechanics, and is the most intuitive approach for AUV motion. The trajectory of the vehicle is usually one of the important reasons for modeling vehicle dynamics: it involves a position (and often an orientation) in space over an interval of time. The position and orientation of a vehicle are most easily described by vectors. Vectors, by definition, require a reference frame, since they consist of a magnitude and a direction.

2.3.1 Frames of Reference

The vehicle can move freely in all three dimensions, that is, it has six degrees of freedom (DOF) - three translational and three rotational. The description of the vehicle motions, as well as description of the orientation and position of the vehicle, are facilitated by the use of orthogonal reference frames, the two most important of which are the inertial reference frame and the body-fixed reference frame (see Figure 2-3).

The inertial frame is "fixed" to the earth and it is denoted by the subscript I, e.g. $\mathbf{r}_I$ denotes an arbitrary vector, $\mathbf{r}$, described (or "decomposed") in the inertial frame. The SNAME [70] standard inertial reference frame is a right-handed, orthogonal set of axes where the z_I-axis is directed downward towards the center of the earth (i.e. in the direction of the pull of gravity). The direction of the x_I-axis is arbitrary as long as it is in the horizontal plane (orthogonal to the z_I-axis); it is usually taken to be coincident with the forward direction of the vehicle at time zero. Once the direction of the x_I-axis has been chosen, the direction of the y_I-axis is defined in accordance with the right hand rule for right orthogonal frames. The body-fixed frame has its origin at the center of mass of the vehicle[2]. It moves with the vehicle, and is denoted

[2]The body-fixed frame could be attached at any point on (or even off) the vehicle body, but it

by the subscript B, e.g. $\mathbf{r}_B$ denotes the vector, $\mathbf{r}$, described in the body frame. It is to be noted that $\mathbf{r}_I$ and $\mathbf{r}_B$ may describe the same vector, but with respect to the two different reference frames. The x_B-axis of the body frame is pointed towards the nose of the vehicle, the y_B-axis points directly to starboard, and the z_B-axis is directed toward the bottom of the vehicle. The six basic motions are: translation along the x_B-axis (called surge), translation along the y_B-axis (sway), translation along the z_B-axis (heave), rotation about the x_B-axis (roll), rotation about the y_B-axis (pitch), and rotation about the z_B-axis (yaw).

In addition to these two basic frames, it is useful to define other frames for important relationships between the vehicle and the environment. For example, in order to ascertain the body forces on the vehicle, it is necessary to know the velocity of the vehicle relative to the flow of water in which it is immersed (see Figure 2-4). The

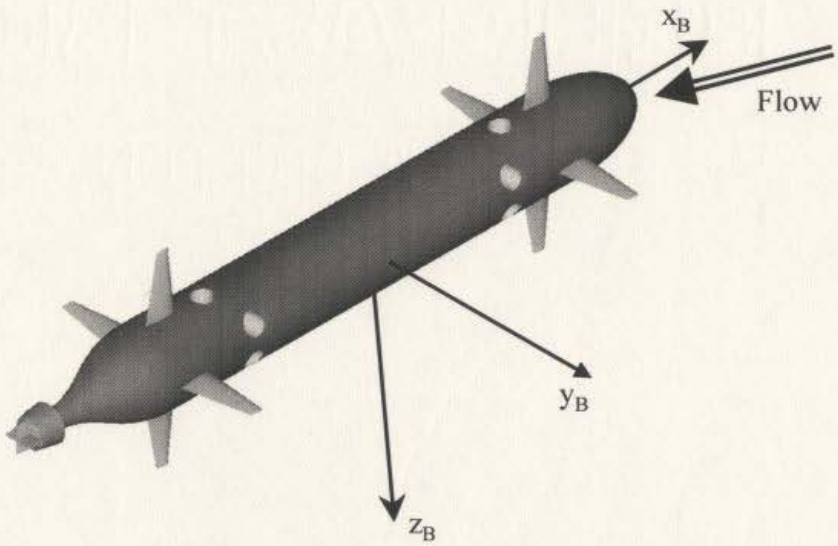

Figure 2-4: Flow with Respect to the Body Frame

drag force on the hull is by definition colinear with the direction of the flow, while the

simplifies the dynamic equations if the origin is at the center of mass (center of gravity).

lift force on the hull is defined to be perpendicular to the direction of the flow. For modeling purposes. it is convenient to define a frame oriented as the flow and fixed at the center of effort of the hull. It is also useful to attach frames to the center of pressure of the control planes to describe the lift and drag forces on them. They are necessary when the hull is not flying directly into the flow or when the control planes are deflected from their zero position. since the lift and drag directions are then not aligned with the body frame.

These reference frames provide a structure within which the hydrodynamic forces and moments that are exerted on the vehicle can be computed. and within which the vehicle motion can be clearly defined. The orientation of each of the frames can be related to the other by a simple rotation or series of rotations. so that they provide a cohesive structure for the model.

Typically. the equations of motion are written in the body-fixed reference frame. where the mass properties (specifically the moments and products of inertia) remain constant with time. Information about the trajectory of the vehicle is only relevant in the inertial frame. since position and orientation of the vehicle in the body-fixed frame are not physically meaningful. There is. therefore. a need for a suitable transformation between the body frame and the inertial frame to facilitate description of the various vectors involved in describing the motion of the vehicle.

2.3.2 Transforming Vector Descriptions

A rotation matrix may be determined using Euler's Theorem on rotation. which says that *any two rotations of a rigid body about axes which pass through the same point are equivalent to a single rotation about some axis through the same point.* It follows from this that any series of rotations about axes passing through the same point can be combined into pairs leading to a single rotation about an equivalent axis through that same point. It is also true that the orientation of the body-fixed reference frame with respect to the inertial reference frame at any given instant of time does not depend on

the path taken to achieve the orientation: the particular number or character of the rotations that make up the path is not important. Thus a transformation from the body-fixed frame to the inertial frame at some given instant of time can be expressed as a single rotation matrix representing the actual orientation of the vehicle with respect to the inertial reference frame. but the transformation may be made up of a series of arbitrary (read convenient) virtual rotations. The description of any vector in one of the frames can be transformed into a description in the other frame via multiplication by a rotation matrix or its inverse.

When the vector $\mathbf{r}$ rotates with the moving frame. B. it can be described in the stationary frame. I. as the product of the rotation matrix. ${}^{I}_{B}\mathbf{R}$. and the description ($\mathbf{r}_B$) of the vector in frame B.

$$\mathbf{r}_I = {}^{I}_{B}\mathbf{R}\mathbf{r}_B \tag{2.3}$$

where ${}^{I}_{B}\mathbf{R}$ is given by Rodriquez' formula

$${}^{I}_{B}\mathbf{R} = \cos\Theta\mathbf{I} + (1 - \cos\Theta)\,\mathbf{k}\mathbf{k}^T + \mathbf{S}(\mathbf{k})\sin\Theta \tag{2.4}$$

The unit vector $\mathbf{k}$ ($\|\mathbf{k}\| = \left(k_x^2 + k_y^2 + k_z^2\right)^{\frac{1}{2}} = 1$) defines the (equivalent) axis about which frame B is rotated. It can be shown that the description of $\mathbf{k}$ is the same in both frames. The matrix $\mathbf{S}(\mathbf{k})$ is a skew-symmetric matrix representing the crossproduct $\mathbf{k} \times \cdot$. On the other hand. when $\mathbf{r}$ remains fixed in the stationary frame. I. it can be described in the moving frame. B. at some instant of time by

$$\mathbf{r}_B = {}^{B}_{I}\mathbf{R}\mathbf{r}_I \tag{2.5}$$

where

$${}^{B}_{I}\mathbf{R} = \cos\Theta\mathbf{I} + (\mathbf{I} - \cos\Theta)\,\mathbf{k}\mathbf{k}^T - \mathbf{S}(\mathbf{k})\sin\Theta \tag{2.6}$$

is the transpose (and inverse) of (2.4).

For example, for a pure rotation about the x-axis by angle o,

$$\mathbf{k} = \begin{bmatrix} 1 & 0 & 0 \end{bmatrix}^T$$

where the vector moves with the moving frame, the description of the vector in the moving frame can be changed to a description in the stationary frame using

$${}^I_B\mathbf{R} = \begin{bmatrix} 1 & 0 & 0 \\ 0 & co & -so \\ 0 & so & co \end{bmatrix}$$

so that

$$\begin{aligned} [r_x]_I &= [r_x]_B \\ [r_y]_I &= [r_y]_B \cos o - [r_z]_B \sin o \\ [r_z]_I &= [r_y]_B \sin o + [r_z]_B \cos o \end{aligned}$$

Technically, a rotation matrix may be developed to map any frame into any other frame, and the notation should include an indication of which frame is the *from* frame and which is the *to* frame, e.g. ${}^I_B\mathbf{R}$ would indicate the mapping from the body-fixed frame, B, to the inertial frame, I. Since the vectors of interest typically move with the body; i.e., the velocity and acceleration, force and moment vectors are determined in the body frame, we will define $\mathbf{R}$ (without indices) as the rotation matrix mapping the decomposition of a given vector in B to a decomposition in I.

$$\mathbf{r}_I = \mathbf{R}\mathbf{r}_B \tag{2.7}$$

Traditionally the rotation matrix is constructed using the aviation standard yaw-pitch-roll sequence [71], since rotations about the body axes are easily described. The body frame is assumed to have been initially coincident with the inertial frame, then

yawed about the common z-axis by an angle, ψ, to the first intermediate frame (1). The body frame is then rotated about the new y-axis (y_1) by a pitch angle, θ, to a second intermediate frame (2). Finally it is rolled about the newest x-axis (x_2) by an angle of ϕ. This leads to

$$\mathbf{R} = \begin{bmatrix} \cos\theta\cos\psi & \sin\phi\sin\theta\cos\psi - \cos\phi\sin\psi & \cos\phi\sin\theta\cos\psi + \sin\phi\sin\psi \\ \cos\theta\sin\psi & \sin\phi\sin\theta\sin\psi + \cos\phi\cos\psi & \cos\phi\sin\theta\sin\psi - \sin\phi\cos\psi \\ -\sin\theta & \sin\phi\cos\theta & \cos\phi\cos\theta \end{bmatrix}$$

Using this traditional method means that the angular velocity vector cannot be transformed between the reference frames by a rotation matrix, since each of the angular rates will be described in a different intermediate frame. An infinitesimal rotation can therefore be written as

$$\Delta n = \begin{bmatrix} \Delta\phi \\ 0 \\ 0 \end{bmatrix} + \begin{bmatrix} 1 & 0 & 0 \\ 0 & \cos\phi & \sin\phi \\ 0 & -\sin\phi & \cos\phi \end{bmatrix} \left(\begin{bmatrix} 0 \\ \Delta\theta \\ 0 \end{bmatrix} + \begin{bmatrix} \cos\theta & 0 & -\sin\theta \\ 0 & 1 & 0 \\ \sin\theta & 0 & \cos\theta \end{bmatrix} \begin{bmatrix} 0 \\ 0 \\ \Delta\psi \end{bmatrix} \right)$$

Dividing by Δt and taking the limit as $\Delta t \longrightarrow 0$

$$\boldsymbol{\nu}_2 = \lim_{\Delta t \to 0} \frac{\Delta n}{\Delta t} = \begin{bmatrix} \dot{\phi} \\ 0 \\ 0 \end{bmatrix} + \begin{bmatrix} 1 & 0 & 0 \\ 0 & \cos\phi & \sin\phi \\ 0 & -\sin\phi & \cos\phi \end{bmatrix} \left(\begin{bmatrix} 0 \\ \dot{\theta} \\ 0 \end{bmatrix} + \begin{bmatrix} \cos\theta & 0 & -\sin\theta \\ 0 & 1 & 0 \\ \sin\theta & 0 & \cos\theta \end{bmatrix} \begin{bmatrix} 0 \\ 0 \\ \dot{\psi} \end{bmatrix} \right)$$

Letting $\nu_2 = \begin{bmatrix} p & q & r \end{bmatrix}$.

$$\begin{bmatrix} p \\ q \\ r \end{bmatrix} = \begin{bmatrix} 1 & 0 & -\sin\theta \\ 0 & \cos\phi & \sin\phi\cos\theta \\ 0 & -\sin\phi & \cos\phi\cos\theta \end{bmatrix} \begin{bmatrix} \dot{\phi} \\ \dot{\theta} \\ \dot{\psi} \end{bmatrix} \tag{2.8}$$

Inverting this gives

$$\begin{bmatrix} \dot{\phi} \\ \dot{\theta} \\ \dot{\psi} \end{bmatrix} = \begin{bmatrix} 1 & \sin\phi\tan\theta & \cos\phi\tan\theta \\ 0 & \cos\phi & -\sin\phi \\ 0 & \sin\phi/\cos\theta & \cos\phi/\cos\theta \end{bmatrix} \begin{bmatrix} p \\ q \\ r \end{bmatrix} \tag{2.9}$$

$$= \mathbf{f}(\phi,\theta)\boldsymbol{\nu}_2 \tag{2.10}$$

which is not equal to the transpose of the transform in equation (2.8).

These results can be combined with the rotation matrices to give a single 6 × 6 transformation matrix. Let $\dot{\boldsymbol{\eta}} = \begin{bmatrix} \dot{\boldsymbol{\eta}}_1^T & \dot{\boldsymbol{\eta}}_2^T \end{bmatrix}^T$, where $\dot{\boldsymbol{\eta}}_1 = \begin{bmatrix} \dot{x} & \dot{y} & \dot{z} \end{bmatrix}^T$ (the velocities along the inertial frame axes) and $\dot{\boldsymbol{\eta}}_2 = \begin{bmatrix} \dot{\phi} & \dot{\theta} & \dot{\psi} \end{bmatrix}^T$ (the angular rates about the inertial axes), and let $\boldsymbol{\nu} = \begin{bmatrix} \boldsymbol{\nu}_1^T & \boldsymbol{\nu}_2^T \end{bmatrix}^T$ where $\boldsymbol{\nu}_1 = \begin{bmatrix} u & v & w \end{bmatrix}^T$ (the velocities along the body-fixed axes) and $\boldsymbol{\nu}_2 = \begin{bmatrix} p & q & r \end{bmatrix}^T$ (the angular rates about the body-fixed axes).

$$\begin{bmatrix} \dot{\boldsymbol{\eta}}_1 \\ \dot{\boldsymbol{\eta}}_2 \end{bmatrix} = \begin{bmatrix} \mathbf{R} & 0 \\ 0 & \mathbf{f}(\phi,\theta) \end{bmatrix} \begin{bmatrix} \boldsymbol{\nu}_1 \\ \boldsymbol{\nu}_2 \end{bmatrix}$$

or, in compact form

$$\dot{\boldsymbol{\eta}} = \mathbf{T}\boldsymbol{\nu}$$

The equations of motion are written in the body frames since the inertial properties of the vehicle are constant in that frame. Also, many of the measured variables are referenced to the vehicle, rather than the environment. The vector quantities involved are easily expressed in either the body frame or the inertial frame.

2.3.3 Equations of Motion

The nonlinear model is based on Newton's 2^{nd} Law. The forces on the vehicle are $\mathbf{F} = m\mathbf{a}$, while the moments are the crossproduct of the force with the moment arm

(the distance from the moment center to the point of application of the force). i.e. $\mathbf{G} = \mathbf{r} \times \mathbf{F}$. Euler expressed both of these in a more consistent notation:

$$\mathbf{F} = \dot{\mathbf{L}} \tag{2.11}$$

that is. the the rate of change of linear momentum. **L**. is equivalent to (the sum of) the forces applied. **F**. and

$$\mathbf{G} = \dot{\mathbf{H}} \tag{2.12}$$

i.e.. the rate of change of angular momentum. **H**. is equivalent to (the sum of) the moments applied. **G**.

Rigid-Body Dynamics

The derivation of the linear and angular momenta equations for a rigid body can be found in any standard textbook on dynamics. such as [72]. The equations written in the body (moving) frame are

$$\mathbf{F} = m\dot{\boldsymbol{\nu}}_1 + \boldsymbol{\nu}_2 \times m\dot{\boldsymbol{\nu}}_1$$

$$\mathbf{G} = \mathbf{I}\dot{\boldsymbol{\nu}}_2 + \boldsymbol{\nu}_2 \times \mathbf{I}\dot{\boldsymbol{\nu}}_2$$

The translational velocity vector is $\boldsymbol{\nu}_1 = \begin{bmatrix} u & v & w \end{bmatrix}^T$. where u. v. and w are the surge (along x_B). sway (along y_B). and heave (along z_B) velocities respectively (refer to Figure 2-3). The angular velocity vector is $\boldsymbol{\nu}_2 = \begin{bmatrix} p & q & r \end{bmatrix}^T$. where p. q. and r are the roll (about x_B). pitch (about y_B). and yaw (about z_B) angular velocities respectively (refer to Figure 2-3). Combining the forces and moments into a single vector equation

$$\begin{bmatrix} \mathbf{F} \\ \mathbf{G} \end{bmatrix} = \begin{bmatrix} m\mathbf{I}_3 & \mathbf{0} \\ \mathbf{0} & \mathbf{I} \end{bmatrix} \begin{bmatrix} \dot{\boldsymbol{\nu}}_1 \\ \dot{\boldsymbol{\nu}}_2 \end{bmatrix} + \begin{bmatrix} \mathbf{S}(\boldsymbol{\nu}_2) & \mathbf{0} \\ \mathbf{0} & \mathbf{S}(\boldsymbol{\nu}_2) \end{bmatrix} \begin{bmatrix} m\mathbf{I}_3 & \mathbf{0} \\ \mathbf{0} & \mathbf{I} \end{bmatrix} \begin{bmatrix} \boldsymbol{\nu}_1 \\ \boldsymbol{\nu}_2 \end{bmatrix}$$

where

$$\mathbf{I}_3 = \begin{bmatrix} 1 & 0 & 0 \\ 0 & 1 & 0 \\ 0 & 0 & 1 \end{bmatrix}$$

and

$$\mathbf{I} = \begin{bmatrix} I_{xx} & -I_{xy} & -I_{xz} \\ -I_{xy} & I_{yy} & -I_{yz} \\ -I_{xz} & -I_{yz} & I_{zz} \end{bmatrix}$$

and $\mathbf{S}(\boldsymbol{\nu}_2)$ is a skew-symmetric matrix representing the crossproduct of $\boldsymbol{\nu}_2$ with the vector acted on by $\mathbf{S}(\boldsymbol{\nu}_2)$, in this case $\boldsymbol{\nu}_1$ or $\boldsymbol{\nu}_2$.

Exciting Forces

For a perfectly rigid body, the quantities defining the rate of change of momentum in each DOF can be determined exactly by algebraic means. The external forces and moments, however, by their nature are somewhat uncertain. These forces and moments constitute six forcing functions (one for each DOF), which includes terms from both viscous effects (viscous damping) and from pressure effects ("added mass" and radiation damping), as well as terms for gravity and buoyancy forces. The magnitude of the gravity and buoyancy forces are fixed, but the moment they form is a function of the orientation of the vehicle relative to the local gravity vector. The viscous forces are functions of the velocity of the vehicle, while the added mass effects are primarily functions of the accelerations of the vehicle. Each set of forces and moments may be analyzed separately, and the results superimposed:

$$\sum \mathbf{F} = \mathbf{F}_S + \mathbf{F}_I + \mathbf{F}_R + \mathbf{F}_C + \mathbf{F}_E$$

where

$\mathbf{F}_S$ Static (hydrostatic) forces - weight and buoyancy

$\mathbf{F}_I$ Ideal fluid forces - "Added Mass"

$\mathbf{F}_R$ Real fluid forces - "Damping"

$\mathbf{F}_C$ Control forces

$\mathbf{F}_E$ Environmental forces - waves, current, etc.

Environmental Forces For the present these forces are assumed to be zero, since the preliminary testing of C-SCOUT will be in calm water. The numerical model has been built to accommodate a module for environmental effects, but the module is not currently used.

Static Forces The static forces of buoyancy and weight always act in the z-direction (negative and positive, respectively) with respect to the earth-fixed reference frame, but are necessarily represented by a system of a force and a moment in the body-fixed reference frame. Exploitation of the similarities of these two forces, that is that the two forces are in opposite directions, leads to the following unified form:

$$\mathbf{F}_S = \mathbf{W} - \mathbf{B}$$

The forces can be written in terms of their x, y, and z components (see Figure 2-5).

$$\begin{aligned} F_{S,x} &= -(W - B)\sin\theta \\ F_{S,y} &= (W - B)\sin\phi\cos\theta \\ F_{S,z} &= (W - B)\cos\phi\cos\theta \end{aligned} \tag{2.13}$$

The moments caused by these forces can be determined by the cross product

$$\mathbf{G} = \mathbf{r} \times \mathbf{F}$$

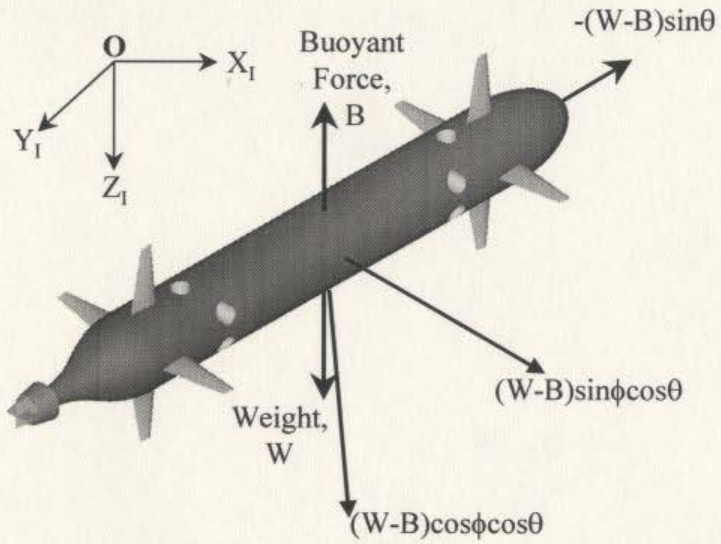

Figure 2-5: Static Forces described in the Body Frame (Traditional Method)

$$\begin{aligned} G_{S,x} &= (y_g W - y_b B)\cos\phi\cos\theta - (z_g W - z_b B)\sin\phi\cos\theta \\ G_{S,y} &= -(z_g W - z_b B)\sin\theta - (x_g W - x_b B)\cos\phi\cos\theta \\ G_{S,z} &= (x_g W - x_b B)\sin\phi\cos\theta + (y_g W - y_b B)\sin\theta \end{aligned} \tag{2.14}$$

Equations (2.14) are written with respect to an arbitrary frame oriented the same as the body frame, but not necessarily coincident with it, therefore x_g, y_g, and z_g (which define the position of the center of mass in that arbitrary frame) may be non-zero.

If the vehicle is neutrally buoyant, the weight is equal to the buoyant force, and there is no net force, i.e., equations (2.13) reduce to zero. Equations (2.14) however do not reduce to zero.

For an AUV with symmetry about the vertical centerplane $y_g = y_b = 0$. Further, the origin of the body-fixed reference frame is typically fixed at the center of gravity,

so $x_g = y_g = z_g = 0$. Given these conditions. 2.14 reduces to

$$\begin{aligned} G_{S,x} &= z_b B \sin\phi \cos\theta \\ G_{S,y} &= z_b B \sin\theta + x_b B \cos\phi \cos\theta \\ G_{S,z} &= -x_b B \sin\phi \cos\theta \end{aligned} \tag{2.15}$$

"Ideal" Forces The ideal forces are those forces associated with potential flow. They are pressure induced forces caused by motion of the body in an inviscid fluid (i.e. a fluid with no viscosity and hence no dissipative shear forces - this is known as an "ideal" fluid). The forces can be written in terms of a matrix of derivatives of acceleration terms

$$\begin{bmatrix} X \\ Y \\ Z \\ K \\ M \\ N \end{bmatrix} = \begin{bmatrix} X_u & X_v & X_w & X_p & X_q & X_r \\ Y_u & Y_v & Y_w & Y_p & Y_q & Y_r \\ Z_u & Z_v & Z_w & Z_p & Z_q & Z_r \\ K_u & K_v & K_w & K_p & K_q & K_r \\ M_u & M_v & M_w & M_p & M_q & M_r \\ N_u & N_v & N_w & N_p & N_q & N_r \end{bmatrix} \begin{bmatrix} \dot{u} \\ \dot{v} \\ \dot{w} \\ \dot{p} \\ \dot{q} \\ \dot{r} \end{bmatrix}$$

Some of the terms are zero, and there is symmetry about the main diagonal [73]. The forces were solved for numerically by a program developed at DREA (Defence Research Establishment Atlantic in Dartmouth, Nova Scotia, Canada) called ESAM (Estimate Submarine Added Masses).

"Real" and Control Forces The real fluid forces are those hydrodynamic forces that result from viscous flow over the body. The control forces result from activation of the control actuator to change the direction and/or speed of the vehicle in one or more DOF. That is, the control is achieved by inducing flow or by redirecting the flow, therefore, it is reasonable to deal with the forces due to control actions at

the same time as other forces due to viscous effects. These forces can be determined experimentally, or analytically via lift and drag equations for the hull and appendages (control planes in the case of C-SCOUT).

The viscous forces are functions of the body geometry, the relative velocity of the body in the flow, the density of the fluid, and a coefficient of proportionality.

$$\mathcal{L} = \frac{\rho}{2} C_{\mathcal{L}} A_{ref} V^2$$

$$\mathcal{D} = \frac{\rho}{2} C_{\mathcal{D}} A_{ref} V^2$$

Various frames and their corresponding rotation matrices are required to express in the body frame the lift and drag forces on the various components.

Lift and drag on the bare hull depend on the velocity relative to the free-stream flow of water (see Figure 2-4). This relationship can be described by angles of attack, α, and sideslip, β. The SNAME (1950) standard defines the angles (see Figure 2-6) in terms of the local velocities:

$$\cos\beta = \frac{(u^2+w^2)^{1/2}}{(u^2+v^2+w^2)^{1/2}} \qquad \sin\beta = \frac{-v}{(u^2+v^2+w^2)^{1/2}}$$

$$\cos\alpha = \frac{u}{(u^2+w^2)^{1/2}} \qquad \sin\alpha = \frac{w}{(u^2+w^2)^{1/2}}$$

An alternative set of angles can be similarly defined:

$$\cos\alpha' = \frac{(u^2+v^2)^{1/2}}{(u^2+v^2+w^2)^{1/2}} \qquad \sin\alpha' = \frac{w}{(u^2+v^2+w^2)^{1/2}}$$

$$\cos\beta' = \frac{u}{(u^2+v^2)^{1/2}} \qquad \sin\beta' = \frac{-v}{(u^2+v^2)^{1/2}}$$

This second set is merely reversal of rotation operations between the Flow axis (or frame) and the body frame. Both these sets will be useful for transforming the descriptions of lift and drag on the control planes into the body frame. Yet a third

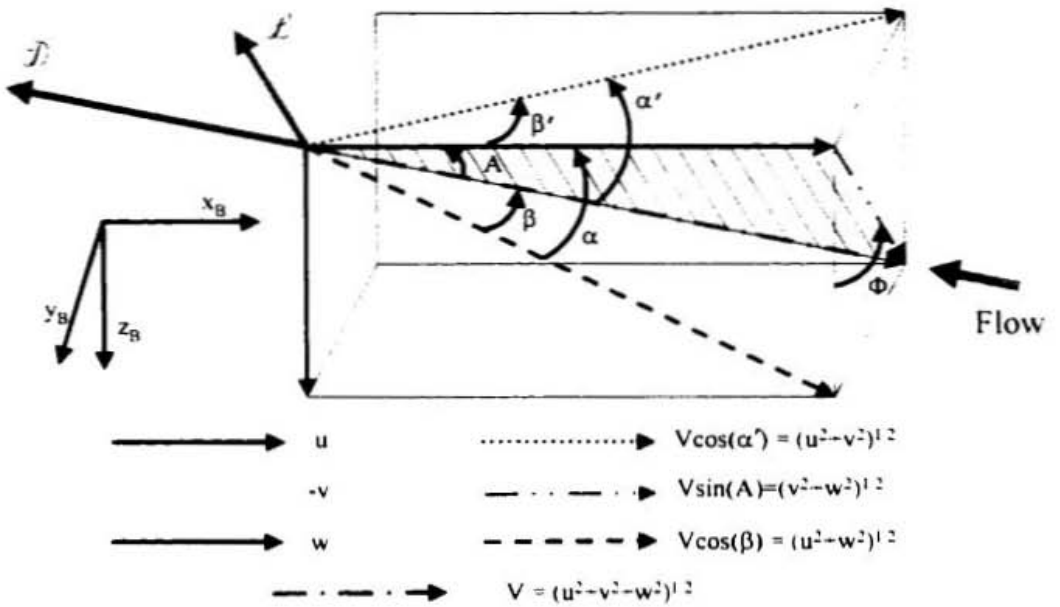

Figure 2-6: Lift, Drag, Angle of Attack, and Angle of Sideslip for a Vehicle Oriented Arbitrarily to the Flow

set can be defined by:

$$\cos A = \frac{u}{(u^2+v^2+w^2)^{1/2}} \qquad \sin A = \frac{(v^2+w^2)^{1/2}}{(u^2+v^2+w^2)^{1/2}}$$

$$\cos \Phi = \frac{w}{(v^2+w^2)^{1/2}} \qquad \sin \Phi = \frac{-v}{(v^2+w^2)^{1/2}}$$

Hull This third set is particularly useful to an axisymmetric (circular cross-section) vehicle, as it gives the angle of attack as a single rotation operation: the angle of sideslip is nonexistent. The roll angle, Φ, allows description of the lift and drag forces in the body-fixed frame, and is necessitated by the presence of fins and gravity-buoyancy considerations. The lift and drag equations for the hull are functions of angle of attack and are therefore easily and logically described in the plane in which

they occur (see Figure 2-7).

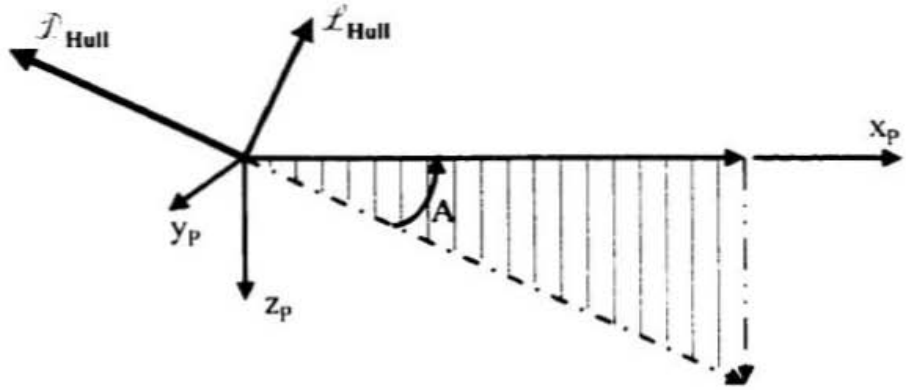

Figure 2-7: Hull Lift and Drag in Their Plane

$$\begin{bmatrix} X_{Hull} \\ Y_{Hull} \\ Z_{Hull} \end{bmatrix}_P = \begin{bmatrix} \cos(\pi + A) & 0 & -\sin(\pi + A) \\ 0 & 1 & 0 \\ \sin(\pi + A) & 0 & \cos(\pi + A) \end{bmatrix} \begin{bmatrix} \mathcal{D}_{Hull} \\ 0 \\ \mathcal{L}_{Hull} \end{bmatrix}$$

The lift and drag forces are

$$\begin{aligned} \mathcal{D}_{Hull} &= \frac{1}{2}\rho C_{D_H} A_{Hull} V_{CE}^2 \\ \mathcal{L}_{Hull} &= \frac{1}{2}\rho C_{L_H} A_{Hull} V_{CE}^2 \end{aligned}$$

In these equations the reference area, A_{Hull}, is the wetted surface area of the hull, and V_{CE} is the magnitude of the velocity at the center of effort

$$V_{CE} = \left(v_{CE}^2(x) + v_{CE}^2(y) + v_{CE}^2(z)\right)^{\frac{1}{2}}$$

and the velocity at the center of effort ($\boldsymbol{\nu}_{CE} = \begin{bmatrix} r_{CE}(x) & r_{CE}(y) & r_{CE}(z) \end{bmatrix}^T$) is

$$\boldsymbol{\nu}_{CE} = \boldsymbol{\nu}_1 + \boldsymbol{\nu}_2 \times \mathbf{r}_{CE} \tag{2.16}$$

where $\boldsymbol{\nu}_1$ is the velocity of the AUV at the origin of the body-fixed reference frame (the center of mass). $\boldsymbol{\nu}_2$ is the angular velocity of the vehicle. and $\mathbf{r}_{CE}$ is the position vector describing the location of the center of effort in the body frame.

The description of the lift and drag forces is then transformed from the lift-drag plane frame (P) to the body-fixed frame (B) via Φ (see Figure 2-8).

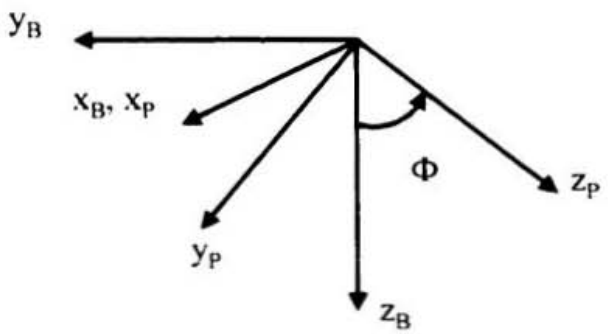

Figure 2-8: Flow vs. Lift-Drag Plane Reference Axes

$$\begin{bmatrix} X_{Hull} \\ Y_{Hull} \\ Z_{Hull} \end{bmatrix}_B = \begin{bmatrix} 1 & 0 & 0 \\ 0 & \cos\Phi & -\sin\Phi \\ 0 & \sin\Phi & \cos\Phi \end{bmatrix} \begin{bmatrix} X_{Hull} \\ Y_{Hull} \\ Z_{Hull} \end{bmatrix}_P$$

Here the matrix represents a rotation of Φ about $x_P = x_B$.

Combining the rotation matrices gives

$$\begin{bmatrix} X_{Hull} \\ Y_{Hull} \\ Z_{Hull} \end{bmatrix}_B = \begin{bmatrix} -\cos A & 0 & \sin A \\ \sin\Phi\sin A & \cos\Phi & \sin\Phi\cos A \\ -\cos\Phi\sin A & \sin\Phi & -\cos\Phi\cos A \end{bmatrix} \begin{bmatrix} \mathcal{D}_{Hull} \\ 0 \\ \mathcal{L}_{Hull} \end{bmatrix}$$

If $\boldsymbol{\nu}_1$, $\boldsymbol{\nu}_2$, and $\mathbf{r}_{CE}$ are known, the angles A and Φ can be readily determined based on knowledge of the velocity at the center of effort:

$$\cos(A) = \frac{v_{CE}(x)}{V_{CE}}$$

$$\cos(\Phi) = \frac{v_{CE}(z)}{\left(v_{CE}^2(y) + v_{CE}^2(z)\right)^{\frac{1}{2}}}$$

This velocity information is directly ascertained from the vehicle velocity at the origin of the body frame via equation (2.16).

Control Planes For the control planes only the flow along the chord, c (see Figure 2-9), is dealt with; the flow along the span, b, is neglected. The effects of the aspect ratio (three-dimensional end effects) are accounted for by using the empirical equation (2.22) for determining the lift on the control plane.

The relevant flow for the horizontal planes (see Figure 2-6) is

$$V_{CP}\cos(\beta) = \left(v_{CP}^2(x) + v_{CP}^2(z)\right)^{\frac{1}{2}}$$

where V_{CP} is the magnitude of the velocity at the center of pressure (CP) of the control plane

$$V_{CP} = \left(v_{CP}^2(x) + v_{CP}^2(y) + v_{CP}^2(z)\right)^{\frac{1}{2}}$$

and the velocity at the center of effort ($\boldsymbol{\nu}_{CP} = \begin{bmatrix} v_{CP}(x) & v_{CP}(y) & v_{CP}(z) \end{bmatrix}^T$) is

$$\boldsymbol{\nu}_{CP} = \boldsymbol{\nu}_1 + \boldsymbol{\nu}_2 \times \mathbf{r}_{CP} \tag{2.17}$$

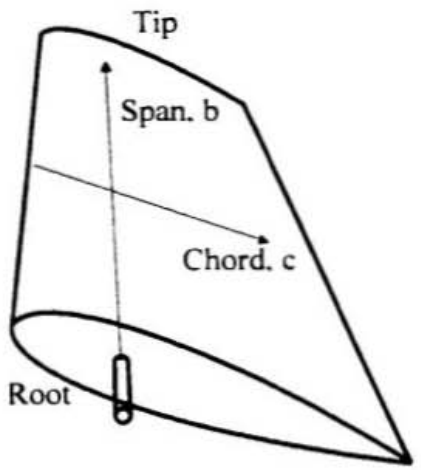

Figure 2-9: Control Plan Nomenclature

The relevant flow for the vertical planes (see Figure 2-6) is

$$V_{CP}\cos(\alpha') = \left(\nu_{CP}^2(x) + \nu_{CP}^2(y)\right)^{\frac{1}{2}}$$

For the horizontal control planes (HCP):

$$\begin{aligned} D_{HCP} &= \frac{1}{2}\rho C_D A_{CP}\left(V_{CP}\cos(\beta)\right)^2 \\ \mathcal{L}_{HCP} &= \frac{1}{2}\rho C_{\mathcal{L}} A_{CP}\left(V_{CP}\cos(\beta)\right)^2 \end{aligned}$$

where the lift and drag coefficients, $C_{\mathcal{L}}$ and C_D, are functions of the deflection of the control plane, δ_{HCP}, added to the angle of attack, α, of the hull. To express the forces in the body frame a rotation about the y_B-axis by $\pi + \alpha$ is required (see Figure 2-10).

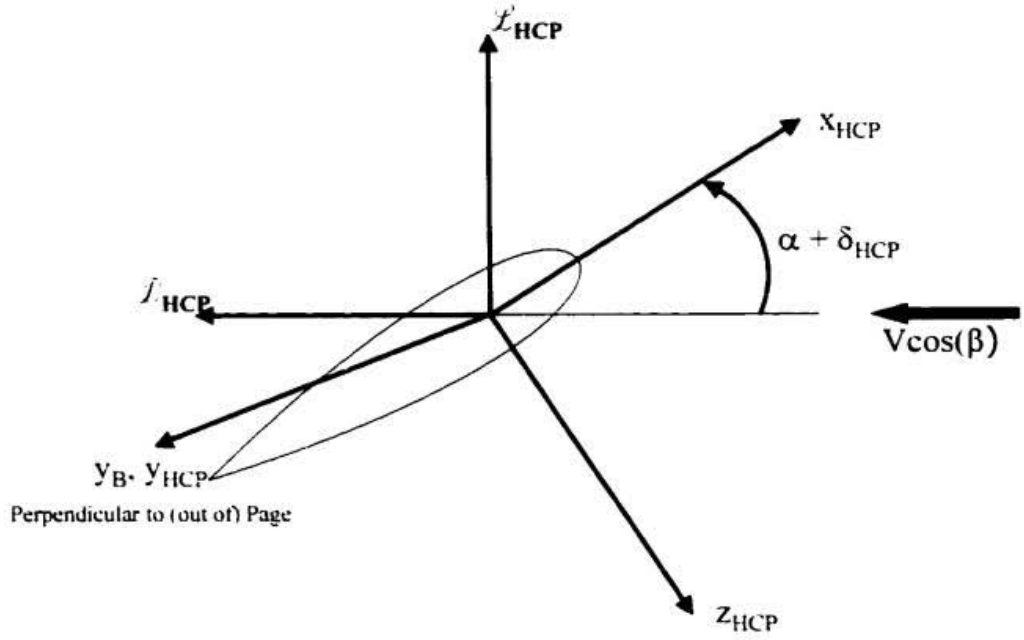

Figure 2-10: Lift and Drag on Horizontal Control Planes

$$\begin{bmatrix} X_{HCP} \\ Y_{HCP} \\ Z_{HCP} \end{bmatrix}_B = \begin{bmatrix} \cos(\pi+\alpha) & 0 & -\sin(\pi+\alpha) \\ 0 & 1 & 0 \\ \sin(\pi+\alpha) & 0 & \cos(\pi+\alpha) \end{bmatrix} \begin{bmatrix} \mathcal{D}_{HCP} \\ 0 \\ \mathcal{L}_{HCP} \end{bmatrix}$$

$$= \begin{bmatrix} -\cos(\alpha) & 0 & \sin(\alpha) \\ 0 & 1 & 0 \\ -\sin(\alpha) & 0 & -\cos(\alpha) \end{bmatrix} \begin{bmatrix} \mathcal{D}_{HCP} \\ 0 \\ \mathcal{L}_{HCP} \end{bmatrix}$$

For the vertical control planes (VCP):

$$\mathcal{D}_{VCP} = \frac{1}{2}\rho C_{\mathcal{D}} A_{CP} \left(V_{CP}\cos(\alpha')\right)^2$$

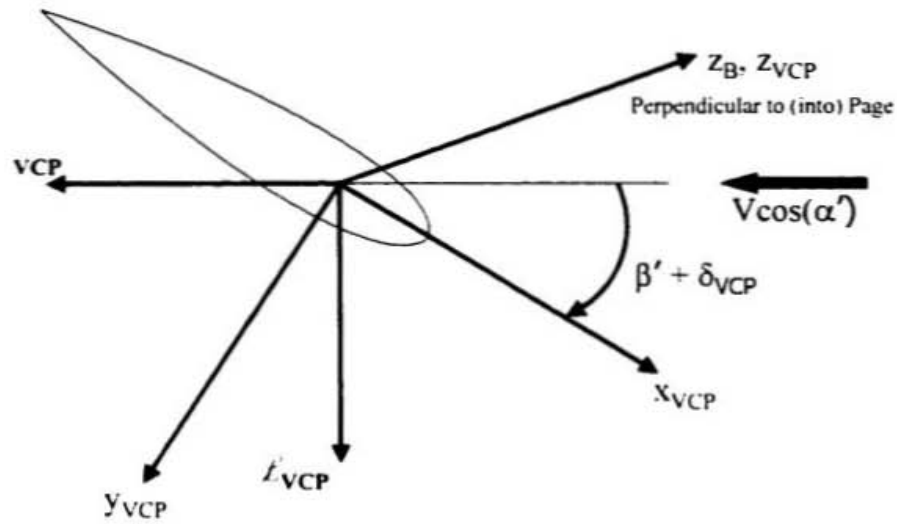

Figure 2-11: Lift and Drag on Vertical Control Planes

$$\mathcal{L}_{VCP} = \frac{1}{2}\rho C_{\mathcal{L}} A_{CP} (V_{CP}\cos(\alpha'))^2$$

where the lift and drag coefficients, $C_{\mathcal{L}}$ and $C_{\mathcal{D}}$, are functions of the deflection of the control plane, δ_{VCP}, added to the angle of attack, β'. To express the forces in the body frame, a rotation about the z_B-axis by $\pi + \beta'$ is required (see Figure 2-11).

$$\begin{bmatrix} X_{VCP} \\ Y_{VCP} \\ Z_{VCP} \end{bmatrix}_B = \begin{bmatrix} \cos(\pi+\beta') & -\sin(\pi+\beta') & 0 \\ \sin(\pi+\beta') & \cos(\pi+\beta') & 0 \\ 0 & 0 & 1 \end{bmatrix} \begin{bmatrix} \mathcal{D}_{VCP} \\ \mathcal{L}_{VCP} \\ 0 \end{bmatrix}$$

$$= \begin{bmatrix} -\cos(\beta') & \sin(\beta') & 0 \\ -\sin(\beta') & -\cos(\beta') & 0 \\ 0 & 0 & 1 \end{bmatrix} \begin{bmatrix} \mathcal{D}_{VCP} \\ \mathcal{L}_{VCP} \\ 0 \end{bmatrix}$$

The values of α, β, α', and β' for each control plane can be determined readily from knowledge of the velocities at the centers of pressures. These velocities are

determined from application of equation (2.17) to each control plane.

Determining the Coefficients and Centers of Force Application Using the above relations, it is relatively easy to calculate the hydrodynamic forces on the hull and planes and express them in the body frame. The only issues to be resolved is the values of the coefficients in the lift and drag equations, and the points of application of the forces.

For the hull, the lift and drag coefficients can be determined from programs such as DATCOM, but in this work they were derived from analytical equations developed by Munk, for airships, Allen & Perkins and Hopkins for guided missiles. Munk used potential flow considerations to develop an expression for the normal force on airships [74].

$$f_N = (k_2 - k_1)\frac{\rho V^2}{2}\sin(2\alpha)\frac{dS}{dx}$$

Ward [75] showed that this force acted at an angle that bisected the angle between the normal line to the flow and the normal line to the vehicle, so that

$$f_N = (k_2 - k_1)\frac{\rho V^2}{2}\sin(2\alpha)\cos(\alpha/2)\frac{dS}{dx}$$

This expression must be integrated over the length of the vehicle to give the normal force on the body, but axial force was ignored in Munk's analysis. Note that, because of the bisection of the angle, $f_C = f_N$.

Allen and Perkins [76] [77] added a viscous term to represent the cross-flow drag on the hull of guided missiles.

$$f_N = (k_2 - k_1)\frac{\rho V^2}{2}\sin(2\alpha)\cos(\alpha/2)\frac{dS_x}{dx} + \eta C_{D_c} 2r\frac{\rho V^2}{2}\sin^2(\alpha)$$

Hopkins [78] derived equations similar to those of Allen and Perkins, but he used

different limits of integration for each of the terms in the equations. He integrated the potential terms from the nose to a point x_0 on the body, and the viscous flow terms from x_0 to the tail. Allen and Perkins had integrated both sets of terms over the whole length of the hull, and added the results. Hopkins also neglected the friction drag term in the lift equation.

$$C_{\mathcal{L}} = (k_2 - k_1)\frac{S_{x_0}}{A_{ref}}\sin(2\alpha)\cos(\alpha/2) + \eta C_{\mathcal{D}_c}\frac{(A_P - A_{P0})}{A_{ref}}\sin^2(\alpha)\cos(\alpha) \qquad (2.18)$$

where

$$S_{x_0} = \pi r_{x_0}^2$$

is the cross-sectional area of the hull at the station x_0: that is, r_{x_0} is the equivalent radius of the hull at x_0 (assuming the vehicle has an approximately circular cross-section: C-SCOUT has a circular cross-section).

$$r_{x_0} = f(x_0)$$

The station x_0 can be determined from [78].

$$\frac{x_0}{L} = 0.378 + 0.527\frac{x_1}{L} \qquad (2.19)$$

where x_1 is the axial station where the rate of change of cross-section with respect to axial distance from the nose first reaches its maximum negative value. In the case of the C-SCOUT, this is the point of inflection on the cubic spline tail section ($x_1 = 2.463$ m for the base vehicle).

The other parameters in equation (2.18) include a reference area, A_{ref}, which could be L^2, or $V^{\frac{2}{3}}$, or some other parameter having the units of area (the present model uses wetted surface area). The crossflow drag coefficient, $C_{\mathcal{D}_c}$, and the parasitic drag, $C_{\mathcal{D}_0}$, are also required, as are the planform area, A_P, and A_{P0}, the planform area up to station x_0. The parameter denoted as η is the drag proportionality factor for taking

into account the end effects of a finite-length cylinder. It is the ratio of the drag coefficient of a circular cylinder of finite length to that of a cylinder of infinite length. The only available data is for negligibly low Mach number (as with C-SCOUT), and a Reynolds number of 88.000 (C-SCOUT values are between 0 and 800.000 based on maximum diameter of the hull and cross-currents of up to 2 m/s). The simulation model used $\eta = 0.65$ from Figure 3 of [78], based on the length-to-diameter ratio of the base configuration of C-SCOUT. The drag proportionality factor is multiplied by C_{D_c}, the crossflow drag coefficient for an infinite length cylinder.

Similarly, equations were developed for drag and pitching moment.

$$C_D = C_{D_0} + (k_2 - k_1)\frac{S_{x_0}}{A_{ref}}\sin(2\alpha)\sin(\alpha/2) + \eta C_{D_c}\frac{(A_P - A_{P0})}{A_{ref}}\sin^3(\alpha) \qquad (2.20)$$

$$\begin{aligned} C_M &= (k_2 - k_1)\left(\frac{V - S_{x_0}(x_0 - x_m)}{A_{ref}L_{ref}}\right)\sin(2\alpha)\cos(\alpha/2) \\ &\quad + \eta C_{D_c}\left(\frac{A_P}{A_{ref}}\left(\frac{x_m - x_p}{L_{ref}}\right) - \frac{A_{P0}}{A_{ref}}\left(\frac{x_m - x_{p0}}{L_{ref}}\right)\right)\sin^2(\alpha) \end{aligned} \qquad (2.21)$$

For the control planes at small angles of attack, the coefficients can be determined from available literature on wing sections (e.g., [79]). At higher angles of attack there is a need for further data.

The coefficient of lift can be calculated based on empirical data [79]

$$C_L = \left[\frac{a_0 a_e}{\cos\Omega\sqrt{\frac{a_0^2}{\cos^4\Omega} + 4 + \frac{57.3 a_0}{\pi}}}\right]\alpha + \frac{C_{D_c}}{a_e}\left(\frac{\alpha}{57.3}\right)^2 \qquad (2.22)$$

where α is the angle of attack of the control plane, in degrees. The effective aspect ratio, a_e, of the control plane is given by

$$a_e = \frac{b^2}{A_{CP}}$$

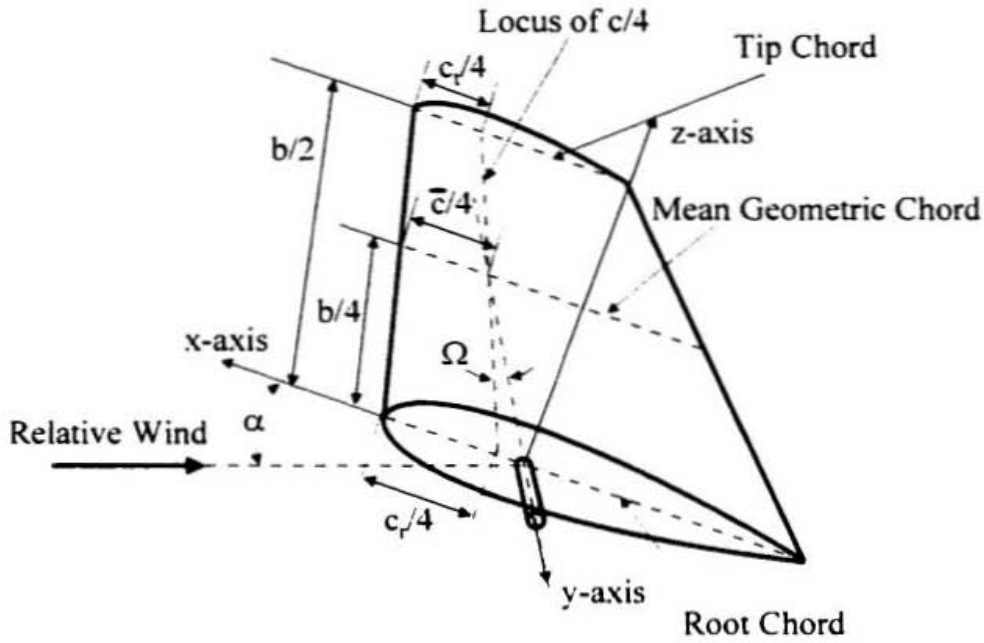

Figure 2-12: Control Plane Geometry

where b is the span (twice the distance from the root of the plane to the tip - see Figure 2-12) of the control plane, and A_{CP} is the planform area. The other parameters are the control plane's crossflow drag coefficient, C_{D_c}, the sweep angle, Ω, and the section lift-curve slope at $\alpha = 0$, a_0. This last parameter is

$$\left(\frac{\partial C_L}{\partial \alpha}\right)_{\alpha=0} = 0.9\left(\frac{2\pi}{57.3}\right)/^{\circ}$$

For the C-SCOUT, the crossflow drag coefficient used is 0.36 from Figure 28 of [79], based on the taper ratio (0.4) and the faired tips of the control planes. The sweep angle is zero, by design. The section lift-slope at zero angle of attack is 0.0736 for α in degrees.

The drag coefficient is

$$C_D = C_{D_0} + \frac{C_L^2}{\pi a_e e} \tag{2.23}$$

where e is Oswald's efficiency factor: a value of 0.9 was used in this model.

The pitching moment coefficient (pitching about the quarter-chord line) can be determined by [79]

$$C_{m_{c/4}} = \left[0.25 - \left(\frac{\partial C_m}{\partial C_L}\right)_{C_L=0}\right]\left(\frac{\partial C_L}{\partial \alpha}\right)_{C_L=0}\alpha - \frac{1}{2}\frac{C_{D_C}}{a_e}\left(\frac{\alpha}{57.3}\right)^2$$

but the pitching moment of the control plane was ignored as being small.

Center of Effort In order to determine the moments applied to the rigid body, the lift and drag forces on each control plane are assumed to act through the respective centers of pressure (CP). Again the location of this point is well established in the literature for small angles (below stall) of attack, but the center moves with higher angles of attack to mid-chord at 90° (although it will continually move with shed vortices). The center of effort (CE) for the hull is a similar point on the hull where the lift and drag forces on the hull are assumed to act. In general, this point may be different in roll, in pitch, or in yaw, but for a body with at least two planes of symmetry about the center of volume, the centers of effort for roll, pitch and yaw do coincide. The CE may be determined by comparing the moment and force coefficients of the particular dimension.

To find the center of effort in pitch, the pitching moment at an arbitrary point can be written

$$M(x) = M(BRC) + Z(BRC) * (-x)$$

where BRC is the Balance Resolving Center, which can be the center of gravity. The center of effort (for pitching moment) is the point at which there is no moment about a beam-wise axis through that point, i.e. $M(x_{CE}) = 0$. Therefore

$$0 = M(BRC) - x_{CE} * Z(BRC)$$

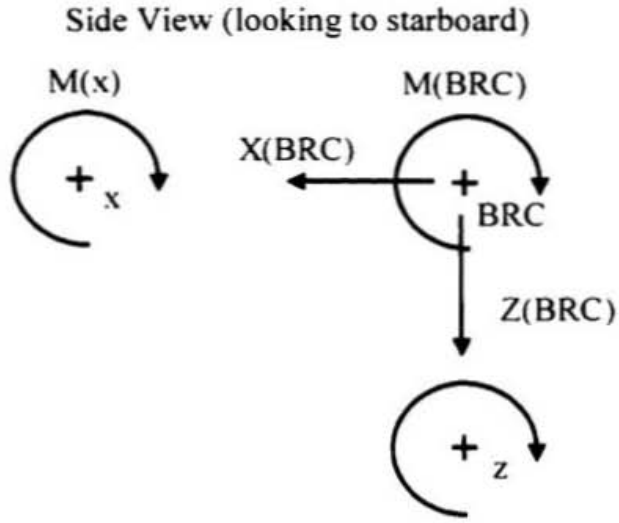

Figure 2-13: Center of Effort in Pitch

or.

$$x_{CE} = \frac{M(BRC)}{Z(BRC)}$$

this ratio can be written in terms of the normal force and moment relations

$$x_{CE} = \frac{(\frac{1}{2})\rho C_m V^2 A_{ref} l}{(\frac{1}{2})\rho C_N V^2 A_{ref}} = \frac{l C_m}{C_N}$$

so that the center of effort is a function of the characteristic length and the ratio of moment and normal force coefficients - in this case the pitching moment and the heave force (normal force). For an axisymmetric body like C-SCOUT. this center is common for roll. pitch. and yaw.

Center of Pressure The center of pressure for each control plane was assumed to be at the quarter-chord point of the section about 42% of the halfspan out from the root chord. The center of pressure can be determined from expressions given by

Whicker and Fehlner [79].

$$CPc = 0.25 - \frac{C_{m_{\overline{c/4}}}}{C_L \cos\alpha + C_D \sin\alpha}$$

$$CPs = \frac{C_L\left(\frac{4}{3\pi}\cdot\frac{b}{2}\right)\cos\alpha + C_D\left(\frac{b}{2}\right)\sin\alpha}{b\left(C_L\cos\alpha + C_D\sin\alpha\right)}$$

Equations of Motion in Matrix Form Once the coefficients and centers are determined, the forces causing the vehicle motion can be summarized succinctly as:

$$\begin{bmatrix} \mathbf{F} \\ \mathbf{G} \end{bmatrix} = \begin{bmatrix} \mathbf{F}_S \\ \mathbf{G}_S \end{bmatrix} + \begin{bmatrix} \mathbf{F}_{\dot{\nu}_1} & \mathbf{F}_{\dot{\nu}_2} \\ \mathbf{G}_{\dot{\nu}_1} & \mathbf{G}_{\dot{\nu}_2} \end{bmatrix} \begin{bmatrix} \triangle\dot{\boldsymbol{\nu}}_1 \\ \triangle\dot{\boldsymbol{\nu}}_2 \end{bmatrix} + \begin{bmatrix} \mathbf{F}_H \\ \mathbf{G}_H \end{bmatrix}$$

where the final vector includes all the nonlinear, viscous-effect terms. The equations of motion can now be written by equating the forcing functions with the rigid-body dynamics.

$$\begin{aligned} &\begin{bmatrix} \mathbf{F}_S \\ \mathbf{G}_S \end{bmatrix} + \begin{bmatrix} \mathbf{F}_{\dot{\nu}_1} & \mathbf{F}_{\dot{\nu}_2} \\ \mathbf{G}_{\dot{\nu}_1} & \mathbf{G}_{\dot{\nu}_2} \end{bmatrix} \begin{bmatrix} \triangle\dot{\boldsymbol{\nu}}_1 \\ \triangle\dot{\boldsymbol{\nu}}_2 \end{bmatrix} + \begin{bmatrix} \mathbf{F}_H \\ \mathbf{G}_H \end{bmatrix} \\ = &\begin{bmatrix} m\mathbf{I}_3 & \mathbf{0} \\ \mathbf{0} & \mathbf{I} \end{bmatrix} \begin{bmatrix} \triangle\dot{\boldsymbol{\nu}}_1 \\ \triangle\dot{\boldsymbol{\nu}}_2 \end{bmatrix} + \begin{bmatrix} \mathbf{S}(m\mathbf{I}_3\boldsymbol{\nu}_{2e}) & -\mathbf{S}(m\mathbf{I}_3\boldsymbol{\nu}_{1e}) \\ \mathbf{0} & \mathbf{S}(\boldsymbol{\nu}_{2e})\mathbf{I} - \mathbf{S}(\mathbf{I}\boldsymbol{\nu}_{2e}) \end{bmatrix} \begin{bmatrix} \triangle\boldsymbol{\nu}_1 \\ \triangle\boldsymbol{\nu}_2 \end{bmatrix} \end{aligned} \tag{2.24}$$

This formulation can be rearranged in terms of the accelerations.

$$\begin{aligned} &\left(\begin{bmatrix} m\mathbf{I}_3 & \mathbf{0} \\ \mathbf{0} & \mathbf{I} \end{bmatrix} - \begin{bmatrix} \mathbf{F}_{\dot{\nu}_1} & \mathbf{F}_{\dot{\nu}_2} \\ \mathbf{G}_{\dot{\nu}_1} & \mathbf{G}_{\dot{\nu}_2} \end{bmatrix} \right) \begin{bmatrix} \triangle\dot{\boldsymbol{\nu}}_1 \\ \triangle\dot{\boldsymbol{\nu}}_2 \end{bmatrix} \\ = &\begin{bmatrix} \mathbf{F}_S \\ \mathbf{G}_S \end{bmatrix} + \begin{bmatrix} \mathbf{F}_H \\ \mathbf{G}_H \end{bmatrix} - \begin{bmatrix} \mathbf{S}(m\mathbf{I}_3\boldsymbol{\nu}_{2e}) & -\mathbf{S}(m\mathbf{I}_3\boldsymbol{\nu}_{1e}) \\ \mathbf{0} & \mathbf{S}(\boldsymbol{\nu}_{2e})\mathbf{I} - \mathbf{S}(\mathbf{I}\boldsymbol{\nu}_{2e}) \end{bmatrix} \begin{bmatrix} \triangle\boldsymbol{\nu}_1 \\ \triangle\boldsymbol{\nu}_2 \end{bmatrix} \end{aligned} \tag{2.25}$$

2.4 Nonlinear Model of a Streamlined AUV

The nonlinear model is implemented in Matlab^{TM}/Simulink^{TM}. At its heart, it is a variable-time-step integrator solving a set of six second-order differential equations.

$$\dot{\boldsymbol{\nu}} = \begin{bmatrix} \dot{\boldsymbol{\nu}}_1 \\ \dot{\boldsymbol{\nu}}_2 \end{bmatrix} = \mathbf{M}_{\mathbf{A}}^{-1} \begin{bmatrix} \mathbf{F} \\ \mathbf{G} \end{bmatrix}$$

The order of the equations is reduced by augmenting the system with six identity equations ($\boldsymbol{\nu}$=$\boldsymbol{\nu}$): i.e., each second-order differential equation is reduced to two first-order differential equations. The system thus has 12 states. Integration of the six higher-order equations leads to the velocities, while integration of the lower-order equations leads to the position and orientation information.

$$\begin{bmatrix} \ddot{\boldsymbol{\eta}} \\ \dot{\boldsymbol{\eta}} \end{bmatrix} = \begin{bmatrix} \mathbf{T} & \dot{\mathbf{T}} \\ \mathbf{0} & \mathbf{T} \end{bmatrix} \begin{bmatrix} \dot{\boldsymbol{\nu}} \\ \boldsymbol{\nu} \end{bmatrix}$$

It is the $\begin{bmatrix} \ddot{\boldsymbol{\eta}} & \dot{\boldsymbol{\eta}} \end{bmatrix}^T$ vector that is integrated to obtain the new values of $\dot{\boldsymbol{\eta}}$ (the velocities in the inertial frame), and $\boldsymbol{\eta}$ (the position and orientation of the vehicle in the inertial frame. The inverse of $\mathbf{T}$ is applied to bring the velocities back into the body-fixed frame.

$$\boldsymbol{\nu} = \mathbf{T}^{-1}\dot{\boldsymbol{\eta}}$$

The velocities are then used to recalculate the forces and moments, and thus the accelerations at the new time step.

The nonlinear model was used to study the sensitivity of the AUV motion response to changes in hydrodynamic parameters (see Chapter 4).

2.5 Linear Model of a Streamlined AUV

In equation (2.2) $\mathbf{X}_{\Xi}$ is the force at equilibrium, which should be zero by definition of equilibrium. Each of the other terms has a coefficient, $X_{\dot{}}$, that is really a derivative term $\frac{dX}{dt}$, therefore they are called either hydrodynamic coefficients or hydrodynamic derivatives. They give the slope (or curvature, etc. if second order and higher order terms are retained in the expansion) of the response of the vehicle to small changes in the parameters about the chosen equilibrium condition. The values are only valid over a limited (but not necessarily small) range near that equilibrium condition.

The coefficients are typically determined from physical model tests. The advantage is that with experimental data, all the interactions between hull and appendages will be included in the data, and the coefficients will take these interactions into account. The disadvantages include the cost of model testing, and the difficulty in extracting the coefficients from the experimental data.

A linear model can be developed from the nonlinear model by perturbing the nonlinear model by a small amount, ϵ, from some given equilibrium state, Ξ, such that the rate of change of force (or moment) with respect to the parameter perturbed may be determined. E.g.,

$$\mathbf{X}_u = \frac{\partial \mathbf{X}}{\partial u}\Delta u \cong \frac{\mathbf{X}_\epsilon - \mathbf{X}_0}{\epsilon}\Delta u$$

This process was followed to obtain the velocity dependent derivatives for the linear model of C-SCOUT. The added masses from ESAM were used for the acceleration dependent derivatives. In matrix form the full set of six linear equations of motion

are

$$\begin{bmatrix} X \\ Y \\ Z \\ K \\ M \\ N \end{bmatrix} = \begin{bmatrix} X_{\dot{u}} & X_{\dot{v}} & X_{\dot{w}} & X_{\dot{p}} & X_{\dot{q}} & X_{\dot{r}} \\ Y_{\dot{u}} & Y_{\dot{v}} & Y_{\dot{w}} & Y_{\dot{p}} & Y_{\dot{q}} & Y_{\dot{r}} \\ Z_{\dot{u}} & Z_{\dot{v}} & Z_{\dot{w}} & Z_{\dot{p}} & Z_{\dot{q}} & Z_{\dot{r}} \\ K_{\dot{u}} & K_{\dot{v}} & K_{\dot{w}} & K_{\dot{p}} & K_{\dot{q}} & K_{\dot{r}} \\ M_{\dot{u}} & M_{\dot{v}} & M_{\dot{w}} & M_{\dot{p}} & M_{\dot{q}} & M_{\dot{r}} \\ N_{\dot{u}} & N_{\dot{v}} & N_{\dot{w}} & N_{\dot{p}} & N_{\dot{q}} & N_{\dot{r}} \end{bmatrix} \begin{bmatrix} \dot{u} \\ \dot{v} \\ \dot{w} \\ \dot{p} \\ \dot{q} \\ \dot{r} \end{bmatrix}$$

$$+ \begin{bmatrix} X_u & X_v & X_w & X_p & X_q & X_r \\ Y_u & Y_v & Y_w & Y_p & Y_q & Y_r \\ Z_u & Z_v & Z_w & Z_p & Z_q & Z_r \\ K_u & K_v & K_w & K_p & K_q & K_r \\ M_u & M_v & M_w & M_p & M_q & M_r \\ N_u & N_v & N_w & N_p & N_q & N_r \end{bmatrix} \begin{bmatrix} u \\ v \\ w \\ p \\ q \\ r \end{bmatrix}$$

$$+ \begin{bmatrix} X_\phi & X_\theta \\ Y_\phi & Y_\theta \\ Z_\phi & Z_\theta \\ K_\phi & K_\theta \\ M_\phi & M_\theta \\ N_\phi & N_\theta \end{bmatrix} \begin{bmatrix} \phi \\ \theta \end{bmatrix} + \begin{bmatrix} X_\delta \\ Y_\delta \\ Z_\delta \\ K_\delta \\ M_\delta \\ N_\delta \end{bmatrix} + \begin{bmatrix} X_\Xi \\ Y_\Xi \\ Z_\Xi \\ K_\Xi \\ M_\Xi \\ N_\Xi \end{bmatrix}$$

where the terms with subscripts ϕ and θ represent the gravity-buoyancy forces, and the vector of (summed) forces with subscript δ is in reality a matrix with a column for each control input.

2.5.1 State-Space Representation

The standard form for a state-space model is:

$$\dot{\mathbf{x}} = \mathbf{A}\mathbf{x} + \mathbf{B}\mathbf{u}$$

$$\mathbf{y} = \mathbf{C}\mathbf{x} + \mathbf{D}\mathbf{u}$$

In order to achieve this format, the gravity-buoyancy effects must be included in the **A** matrix, since they are vital to the correct solution. In order to include them the state vector is augmented

$$\mathbf{x} = \begin{bmatrix} \Delta u & \Delta v & \Delta w & \Delta p & \Delta q & \Delta r & \Delta\phi & \Delta\theta \end{bmatrix}^T$$

and the Newton-Euler Equations are augmented by two kinematic equations to keep the **A** matrix square, facilitating linear analysis.

$$\begin{aligned} \dot{\phi} &= p + q\sin\phi\tan\theta + r\cos\phi\tan\theta \\ \dot{\theta} &= q\cos\phi - r\sin\phi \end{aligned}$$

Now, the (real) mass matrix becomes:

$$\mathbf{M}_A = \begin{bmatrix} \mathbf{M}'_A & \mathbf{0} \\ \mathbf{0} & \mathbf{I}_2 \end{bmatrix}$$

where the original (real) mass matrix is:

$$\mathbf{M}'_A = \begin{bmatrix} m & 0 & 0 & 0 & 0 & 0 \\ 0 & m & 0 & 0 & 0 & 0 \\ 0 & 0 & m & 0 & 0 & 0 \\ 0 & 0 & 0 & I_{xx} & -I_{xy} & -I_{xz} \\ 0 & 0 & 0 & -I_{yx} & I_{yy} & -I_{yz} \\ 0 & 0 & 0 & -I_{zx} & -I_{zy} & I_{zz} \end{bmatrix}$$

and the augmentation consist of a 2×2 identity matrix:

$$\mathbf{I}_2 = \begin{bmatrix} 1 & 0 \\ 0 & 1 \end{bmatrix}$$

Next, the rigid-body cross-coupling terms are augmented to form the 8×8 matrix:

$$\mathbf{S} = \begin{bmatrix} \mathbf{S}' & \mathbf{0} \\ \mathbf{0} & \mathbf{0} \end{bmatrix}$$

with

$$\mathbf{S}' = \begin{bmatrix} \mathbf{S}_{11} & \mathbf{S}_{12} \\ \mathbf{0} & \mathbf{S}_{22} \end{bmatrix}$$

where

$$\mathbf{S}_{11} = m\mathbf{S}(\boldsymbol{\nu}_{2\Xi})$$

$$\mathbf{S}_{12} = -m\mathbf{S}(\boldsymbol{\nu}_{1\Xi})$$

$$\mathbf{S}_{22} = \mathbf{S}(\boldsymbol{\nu}_{2\Xi})\mathbf{I} - \mathbf{S}(\mathbf{I}\boldsymbol{\nu}_{2\Xi})$$

The (virtual) added mass matrix is also augmented to an 8×8 form:

$$\mathbf{F}_{\dot{\eta}} = \begin{bmatrix} \mathbf{F}'_{\dot{\eta}} & \mathbf{0} \\ \mathbf{0} & \mathbf{0} \end{bmatrix}$$

where

$$\mathbf{F}'_{\dot{\eta}} = \begin{bmatrix} X_{\dot{u}} & X_{\dot{v}} & X_{\dot{w}} & X_{\dot{p}} & X_{\dot{q}} & X_{\dot{r}} \\ Y_{\dot{u}} & Y_{\dot{v}} & Y_{\dot{w}} & Y_{\dot{p}} & Y_{\dot{q}} & Y_{\dot{r}} \\ Z_{\dot{u}} & Z_{\dot{v}} & Z_{\dot{w}} & Z_{\dot{p}} & Z_{\dot{q}} & Z_{\dot{r}} \\ K_{\dot{u}} & K_{\dot{v}} & K_{\dot{w}} & K_{\dot{p}} & K_{\dot{q}} & K_{\dot{r}} \\ M_{\dot{u}} & M_{\dot{v}} & M_{\dot{w}} & M_{\dot{p}} & M_{\dot{q}} & M_{\dot{r}} \\ N_{\dot{u}} & N_{\dot{v}} & N_{\dot{w}} & N_{\dot{p}} & N_{\dot{q}} & N_{\dot{r}} \end{bmatrix}$$

The velocity-dependent hydrodynamic derivatives are combined with the kinematic equations to form:

$$\mathbf{F}_\eta = \begin{bmatrix} \mathbf{F}'_\eta & \mathbf{F}_s \\ \mathbf{K}_{pqr} & \mathbf{K}_{o\theta} \end{bmatrix}$$

where the original hydrodynamic derivatives form the upper left block

$$\mathbf{F}'_\eta = \begin{bmatrix} X_u & X_v & X_w & X_p & X_q & X_r \\ Y_u & Y_v & Y_w & Y_p & Y_q & Y_r \\ Z_u & Z_v & Z_w & Z_p & Z_q & Z_r \\ K_u & K_v & K_w & K_p & K_q & K_r \\ M_u & M_v & M_w & M_p & M_q & M_r \\ N_u & N_v & N_w & N_p & N_q & N_r \end{bmatrix}$$

and, assuming the longitudinal and transverse distances between the centers of gravity and buoyancy (x_b and y_b respectively) are zero

$$\mathbf{F}_s = \begin{bmatrix} 0 & -(W - B)\cos\theta_e \\ (W - B)\cos o_e \cos\theta_e & -(W - B)\sin o_e \sin\theta_e \\ -(W - B)\sin o_e \cos\theta_e & -(W - B)\cos o_e \sin\theta_e \\ -z_b B \cos o_e \cos\theta_e & z_b B \sin o_e \sin\theta_e \\ 0 & z_b B \cos\theta_e \\ 0 & 0 \end{bmatrix}$$

Further,

$$\mathbf{K}_{pqr} = \begin{bmatrix} 0 & 0 & 0 & 1 & \sin o_e \tan\theta_e & \cos o_e \tan\theta_e \\ 0 & 0 & 0 & 0 & \cos o_e & 0 \end{bmatrix}$$

and

$$\mathbf{K}_{o\theta} = \begin{bmatrix} q_e \cos o_e \tan\theta_e - r_e \sin o_e \tan\theta_e & q_e \sin o_e \csc^2\theta_e + r_e \cos o_e \csc^2\theta_e \\ -q_e \sin o_e - r_e \cos o_e & -\sin o_e \end{bmatrix}$$

Finally. the control input matrix must also be augmented with a 2×5 zero matrix (in the case of the base configuration of C-SCOUT).

$$\mathbf{U} = \begin{bmatrix} \mathbf{U}' \\ \mathbf{0} \end{bmatrix}$$

$$\mathbf{U}' = \begin{bmatrix} X_{\dot{c}as} & X_{\dot{c}ap} & X_{\dot{c}au} & X_{\dot{c}al} & X_{\dot{c}T} \\ Y_{\dot{c}as} & Y_{\dot{c}ap} & Y_{\dot{c}au} & Y_{\dot{c}al} & Y_{\dot{c}T} \\ Z_{\dot{c}as} & Z_{\dot{c}ap} & Z_{\dot{c}au} & Z_{\dot{c}al} & Z_{\dot{c}T} \\ K_{\dot{c}as} & K_{\dot{c}ap} & K_{\dot{c}au} & K_{\dot{c}al} & K_{\dot{c}T} \\ M_{\dot{c}as} & M_{\dot{c}ap} & M_{\dot{c}au} & M_{\dot{c}al} & M_{\dot{c}T} \\ N_{\dot{c}as} & N_{\dot{c}ap} & N_{\dot{c}au} & N_{\dot{c}al} & N_{\dot{c}T} \end{bmatrix}$$

in the case of the base configuration. so. the Newton-Euler equations can be written

$$\mathbf{F}_{\dot{\eta}}\dot{\mathbf{x}} + \mathbf{F}_{\eta}\mathbf{x} + \mathbf{U}\mathbf{u} = \mathbf{M}_{A}\dot{\mathbf{x}} + \mathbf{S}\mathbf{x}$$

and rearranged in terms of the accelerations for the sake of integration

$$(\mathbf{M}_{A} - \mathbf{F}_{\dot{\eta}})\,\dot{\mathbf{x}} = (\mathbf{F}_{\eta} - \mathbf{S})\,\mathbf{x} + \mathbf{U}\mathbf{u}$$

and put into standard form

$$\dot{\mathbf{x}} = (\mathbf{M}_{A} - \mathbf{F}_{\dot{\eta}})^{-1}\,(\mathbf{F}_{\eta} - \mathbf{S})\,\mathbf{x} + (\mathbf{M}_{\mathbf{A}} - \mathbf{F}_{\dot{\eta}})^{-1}\,\mathbf{U}\mathbf{u}$$

Therefore

$$\begin{aligned} \mathbf{A} &= (\mathbf{M}_{A} - \mathbf{F}_{\dot{\eta}})^{-1}\,(\mathbf{F}_{\eta} - \mathbf{S}) \\ \mathbf{B} &= (\mathbf{M}_{A} - \mathbf{F}_{\dot{\eta}})^{-1}\,\mathbf{U} \end{aligned}$$

The linear model is used for fault condition simulations (see Chapter 5). The equilibrium condition used is straight and level flight at 3 m/s.

Chapter 3

Sensitivity of Added Mass to Vehicle Geometry

Each of the six forcing functions in the equations of motion include terms which represent the extra effort (in terms of "added mass") required to move the body through the fluid. The extra effort is required due to pressure forces exerted by the fluid on the body. The added mass values used in the nonlinear and linear models are assumed to be constant, and are determined off-line by a separate computer program - Estimate Submarine Added Masses (ESAM) developed by George Watt of Canada's Defence Research Establishment Atlantic (DREA) [80]. The assumption of constant added mass implies further assumption that the vehicle is deeply submerged in the water, i.e., it is not operating near the surface, the bottom, or any other boundary.

Because the values of the added mass are dependent on the geometry of the vehicle, and because the modular nature of C-SCOUT facilitates and sometimes necessitates changes in the geometry of the vehicle for different configurations, the values of added mass are expected to change. Therefore it is important to understand how the added mass changes with the variations in geometry, and how sensitive the values are to changes in various geometric parameters.

3.0.2 Notes on Reference Frames

Fixing the Reference Frame

Newton's second law describes the force necessary to accelerate a body.

$$\mathbf{F} = m\mathbf{a}$$

This expression can be rearranged in terms of the mass of the body.

$$m = \frac{\mathbf{F}}{\mathbf{a}}$$

Mass is a scalar quantity and does not require a spatial reference, however force and acceleration are vector quantities, and must be expressed with respect to a reference frame such as the vehicle body frame (B in Figure 2-3). A spatial reference frame is also required to fully describe the distribution of mass and the location of the center of mass. The distribution of mass defines the moments and products of inertia, so they too are frame dependent. A reference frame attached to the vehicle and moving with it allows us to treat the inertial properties as constant over time, since the mass distribution will not change, regardless of the orientation of the vehicle. Placing the origin of the reference frame at the center of mass of the vehicle eliminates the need for using the parallel axis theorem to determine moments and products of inertia. It is also possible to choose an orthogonal axes system (the "principle axes") where the products of inertia are zero. However, the body reference frame is usually chosen such that the motions are easily described, i.e. forward (surge), sideways (sway), and up/down (heave), with rotations about these axis corresponding to roll, pitch and yaw respectively. Therefore the principle axes are not used in our subsequent analysis and there remain nonzero products of inertia.

The Effects of Floodwater

Many vehicles like the C-SCOUT are free-flooding, and part of the mass and inertial properties includes the effect of the entrained water. The water inside the vehicle actually travels with the vehicle and is therefore included with the vehicle component masses to give a "wet" mass. Added mass is concerned with the movement of water external to the hull, and is an entirely different mechanism. Even though there is water internal to the hull, it is the hull geometry alone that affects the external flow and is the generator of added mass effects. Here the term center of mass refers to the center of the "wet" mass, i.e. the center of mass of the vehicle including the entrained floodwater.

The body-fixed reference frame is "attached" to the vehicle at this center of mass. For the base configuration this is 1.284 m from the tip of the nose and 0.011 m below the axis of revolution of the hull. For the full configuration this is 1.550 m from the tip of the nose and 0.011 m below the axis of revolution of the hull. Also the center of buoyancy refers to the center of the volume of water displaced by the external geometry of the hull, as opposed to the center of the volume of water displaced by the vehicle, which could arguably mean only the volume displaced by the vehicle components, and not including the flooded spaces. The center of buoyancy for both configurations is at $x_b = 0$ m, $y_b = 0$ m, and $z_b = -0.011$ m (all with respect to the body-fixed reference frame). The center of buoyancy is 0.011 m above the center of mass, the latter center also being used as the origin of the body-fixed reference frame.

3.1 The Role of Added Mass

3.1.1 Added Mass Properties

When a body accelerates in a fluid, the fluid around the body is disturbed and is also accelerated. The movement of the fluid requires additional force over and above

that necessary to accelerate the body itself. Added mass is the proportionality factor relating the extra force to the acceleration of the body [81]. It is important to note that there is no distinct mass of water travelling with the vehicle: the added mass is a virtual mass only, and is a convenient way of describing the extra force required to push a body through a fluid. The added mass is important in the accurate calculation of vehicle accelerations. The kinetic energy required for the fluid motion is imparted by pressure forces. Since the fluid pressure acts normal to the hull surface, the geometry of the body is fundamental to the effects experienced.

The nature of the hull-fluid interaction also means that the added mass is not a simple scalar, but must account for the accelerations in all six DOF that result from each of the forces and moments. The general form for an added mass matrix has 36 elements to completely describe the ratio of extra force to acceleration in each combination of DOF, and is given as:

$$\begin{bmatrix} X_{\dot{u}} & X_{\dot{v}} & X_{\dot{w}} & X_{\dot{p}} & X_{\dot{q}} & X_{\dot{r}} \\ Y_{\dot{u}} & Y_{\dot{v}} & Y_{\dot{w}} & Y_{\dot{p}} & Y_{\dot{q}} & Y_{\dot{r}} \\ Z_{\dot{u}} & Z_{\dot{v}} & Z_{\dot{w}} & Z_{\dot{p}} & Z_{\dot{q}} & Z_{\dot{r}} \\ K_{\dot{u}} & K_{\dot{v}} & K_{\dot{w}} & K_{\dot{p}} & K_{\dot{q}} & K_{\dot{r}} \\ M_{\dot{u}} & M_{\dot{v}} & M_{\dot{w}} & M_{\dot{p}} & M_{\dot{q}} & M_{\dot{r}} \\ N_{\dot{u}} & N_{\dot{v}} & N_{\dot{w}} & N_{\dot{p}} & N_{\dot{q}} & N_{\dot{r}} \end{bmatrix} \tag{3.1}$$

The elements of the added mass matrix can be considered constant for a deeply submerged vehicle, but may have frequency dependencies near the surface or a boundary. In this study a deeply submerged vehicle is assumed.

For any body there are really only 21 unique elements in the added mass matrix, because it is symmetric about the diagonal, i.e., $X_{\dot{v}} = Y_{\dot{u}}$[1], $X_{\dot{w}} = Z_{\dot{u}}$, etc.[73].

[1]Standard notation for bodies submerged in a fluid (SNAME(1950) [70]) is used throughout this thesis, except in the plots due to some software notational limitations.

Therefore, (3.1) becomes:

$$\begin{bmatrix} X_{\dot{u}} & X_{\dot{v}} & X_{\dot{w}} & X_{\dot{p}} & X_{\dot{q}} & X_{\dot{r}} \\ X_{\dot{v}} & Y_{\dot{v}} & Y_{\dot{w}} & Y_{\dot{p}} & Y_{\dot{q}} & Y_{\dot{r}} \\ X_{\dot{w}} & Y_{\dot{w}} & Z_{\dot{w}} & Z_{\dot{p}} & Z_{\dot{q}} & Z_{\dot{r}} \\ X_{\dot{p}} & Y_{\dot{p}} & Z_{\dot{p}} & K_{\dot{p}} & K_{\dot{q}} & K_{\dot{r}} \\ X_{\dot{q}} & Y_{\dot{q}} & Z_{\dot{q}} & K_{\dot{q}} & M_{\dot{q}} & M_{\dot{r}} \\ X_{\dot{r}} & Y_{\dot{r}} & Z_{\dot{r}} & K_{\dot{r}} & M_{\dot{r}} & N_{\dot{r}} \end{bmatrix} \tag{3.2}$$

Typically, the added mass terms for a body are expressed in the form of non-dimensional coefficients based on the vehicle length, e.g. $X'_{\dot{u}} = X_{\dot{u}}/\rho l^3$ (in accordance with [70]). In general, each coefficient is non-dimensionalized by ρl^n, where the power, n, varies according to the type of coefficient. For the added mass coefficients representing the effect of a force on a linear acceleration ($X'_{\dot{u}}$, $X'_{\dot{v}}$, $X'_{\dot{w}}$, $Y'_{\dot{v}}$, $Y'_{\dot{w}}$, and $Z'_{\dot{w}}$), n is three. The cube of the length represents the volume of the vehicle, which is proportional to the mass of water displaced by the outer hull (∇), i.e. $\nabla = \rho V$ where ρ is the density of the fluid and V is the volume taken up by the hull of the vehicle, and $\rho V \approx \rho l^3$. For coefficients representing the effect of a moment on an angular acceleration ($K'_{\dot{p}}$, $K'_{\dot{q}}$, $K'_{\dot{r}}$, $M'_{\dot{q}}$, $M'_{\dot{r}}$, and $N'_{\dot{r}}$), n is five, as would be expected since $\nabla d^2 \approx \rho l^5$ (d is an arbitrary metric of length). Finally, for the remaining coefficients which represent the effects of a force on an angular acceleration, or the effect of a moment on a linear acceleration ($X'_{\dot{p}}$, $X'_{\dot{q}}$, $X'_{\dot{r}}$, $Y'_{\dot{p}}$, $Y'_{\dot{q}}$, $Y'_{\dot{r}}$, $Z'_{\dot{p}}$, $Z'_{\dot{q}}$, and $Z'_{\dot{r}}$), n is four.

Some of the 21 coefficients are known to be zero for vehicles that have port-starboard symmetry about the x-z plane of the vehicle. These include $X'_{\dot{v}}$, $X'_{\dot{p}}$, $X'_{\dot{r}}$, $Y'_{\dot{w}}$, $Y'_{\dot{q}}$, $Z'_{\dot{p}}$, $Z'_{\dot{r}}$, $K'_{\dot{q}}$ and $M'_{\dot{r}}$. If the vehicle also has top-bottom symmetry about the x-y plane, four more of the coefficients, added mass coefficients $X'_{\dot{w}}$, $X'_{\dot{q}}$, $Y'_{\dot{p}}$, and $K'_{\dot{r}}$ would be zero. In the reference frame used for modeling this vehicle, however, there is no symmetry about the x-y plane, so these four coefficients can have non-zero values. The value of $X'_{\dot{w}}$ is zero, i.e. when this type of vehicle experiences a force

in the surge direction, there is no direct acceleration in the heave direction. Thus, for a typical torpedo-like vehicle such as the C-SCOUT, there are 11 non-zero added mass coefficients: $X'_{\dot{u}}$, $X'_{\dot{q}}$, $Y'_{\dot{v}}$, $Y'_{\dot{p}}$, $Y'_{\dot{r}}$, $Z'_{\dot{w}}$, $Z'_{\dot{q}}$, $K'_{\dot{p}}$, $K'_{\dot{r}}$, $M'_{\dot{q}}$ and $N'_{\dot{r}}$, so the matrix (3.2) reduces to:

$$\begin{bmatrix} X'_{\dot{u}} & 0 & 0 & 0 & X'_{\dot{q}} & 0 \\ 0 & Y'_{\dot{v}} & 0 & Y'_{\dot{p}} & 0 & Y'_{\dot{r}} \\ 0 & 0 & Z'_{\dot{w}} & 0 & Z'_{\dot{q}} & 0 \\ 0 & Y'_{\dot{p}} & 0 & K'_{\dot{p}} & 0 & K'_{\dot{r}} \\ X'_{\dot{q}} & 0 & Z'_{\dot{q}} & 0 & M'_{\dot{q}} & 0 \\ 0 & Y'_{\dot{r}} & 0 & K'_{\dot{r}} & 0 & N'_{\dot{r}} \end{bmatrix} \tag{3.3}$$

Of the eleven, six are along the main diagonal of the matrix, and represent the principle coefficients. That is, if the vehicle is forced in a particular direction (or rotated about a particular axis), one of these six values represents the added mass coefficient (or added-mass-moment-of-inertia coefficient); that is, the ratio of additional force (moment) required to achieve the acceleration in that DOF. The remaining five off-diagonal values represent coupling terms which describe the effects of force in one DOF on the acceleration in another DOF.

Since the reference frame is attached to the center of mass for simpler calculation of the dynamics, $X'_{\dot{q}}$, $Y'_{\dot{p}}$, and $K'_{\dot{r}}$ are typically not zero. The remaining added mass coefficients, $Y'_{\dot{r}}$ and $Z'_{\dot{q}}$, are the result of fore-aft asymmetry in the vehicle.

3.1.2 Added Mass Sensitivity

Sensitivity of the added mass coefficients to variations in geometry can be significant. Therefore, the vehicle behaviour (specifically the transient response to command changes, fault conditions, etc.) will be affected with changes in the vehicle geometry. In particular, variations in the following geometric parameters result in variations in the added mass values:

1. the length-to-diameter ratio, L/D, of the vehicle hull;

2. the location of the control planes along the length of the vehicle - measured as x_{fqca}, the distance from the nose to the quarter-chord axis of the forward control planes, and x_{aqca}, the distance from the nose to the quarter-chord axis of the after control planes; and

3. the size of the control planes.

The only parameter missing from this list is the size of the vehicle. If the shape of the vehicle is not changed, then when the geometry is reduced to a nondimensional form using length as the scaling factor, any sized vehicle will be reduced to the exact same nondimensional model, thus the added mass coefficients will not be affected. The dimensional added masses will vary in magnitude with the scaling factor (the size of the vehicle).

These parameters are direct design variables (i.e., their values are chosen in the design). The values of direct design variables like these greatly influence the values of indirect design variables (such as added mass coefficients, lift and drag coefficients, and centers of pressure), so that obtaining a certain value of the indirect design variable may be the motivating factor in choosing the particular direct design variable. Further, these geometric parameters represent a comprehensive set of the direct design variables for an axi-symmetric vehicle like the C-SCOUT. That is, when the results of systematic variation of each parameter are combined, they will provide a complete picture of the variation in added mass coefficients that can be expected.

3.2 Expected Results

When the above parameters (L/D, control plane location, and control plane size) are varied, the relative geometry of the vehicle (i.e. its shape) changes. Therefore it is expected that the added mass coefficients will change in value as the parameters are

varied. To clearly see the effects of the geometry changes it was necessary to use several different types of hull-fin (control plane) configurations.

3.2.1 Bare Hull L/D

When the length-to-diameter ratio (L/D) is varied by changing the length of the parallel mid-body while keeping the diameter constant, the nose and tail geometries are not affected by the variation, except to be separated by a lesser or greater distance.

The size of the control plane, being constant, does not affect the added mass coefficients, but the relative location of the control planes does, as will be seen in the consideration of the location of the control planes. The effect of the relative location of the control planes will obscure the effects of the variation in the length-to-diameter ratio, therefore only the bare hull was examined for the effects of varying L/D.

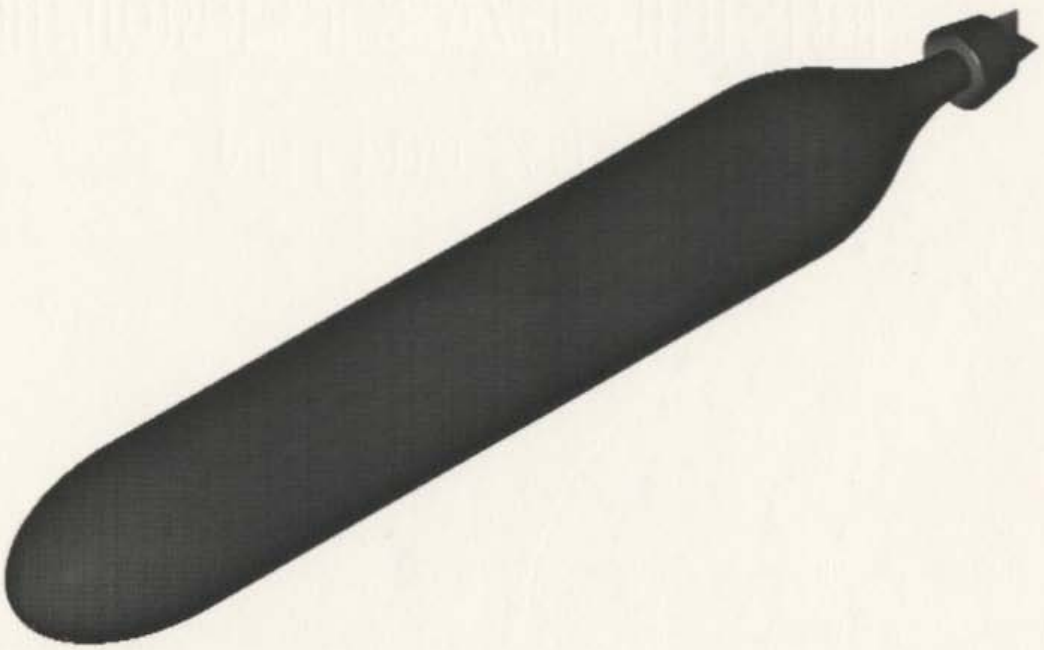

Figure 3-1: C-SCOUT Bare Hull

It is expected that for a neutrally buoyant vehicle, the mass would vary in pro-

portion to the length of the vehicle, when the diameter is being held constant. The displacement of the vehicle, ∇, (i.e. the mass of the volume of water displaced by the outer hull of the vehicle) would also vary with the length by the same factor of proportionality.

Principle translational acceleration coefficients, $X'_{\dot{u}}$, $Y'_{\dot{v}}$, and $Z'_{\dot{w}}$, vary with ∇: the larger the displacement of a body, the more extra force required to move it through the fluid. However, added mass is only affected by motion normal to the hull, and in this study the volume of the hull is only changed along the surge (x-)axis. Thus, $Y'_{\dot{v}}$ and $Z'_{\dot{w}}$ should vary linearly with L/D, because sway and heave motions are perpendicular to the changing length, i.e. these coefficients "see" the change in volume. $X'_{\dot{u}}$ would remain constant since the surge motion is parallel to rather than perpendicular to the changing length dimension, i.e. this coefficient does not "see" the change in volume. It would remain constant, that is, if the reference axes were at the center of buoyancy. The origin of the reference frame is at the vehicle center of mass rather than the center of the displaced volume of fluid (the center of buoyancy): i.e., $z_b \neq 0$, and $X'_{\dot{u}}$ has a dependence on the value of z_b. Although z_b is constant in the absolute sense in its dimensional form, its nondimensional form, z_b/L, varies as L changes. The combination of $z_b \neq 0$ and the variation of z_b/L cause the variation of $X'_{\dot{u}}$ with L/D.

Principle angular acceleration terms, $K'_{\dot{p}}$, $M'_{\dot{q}}$, and $N'_{\dot{r}}$, vary with the product of ∇ and d^2 where d is a metric of length (e.g. a moment arm). This moment arm is parallel to the surge axis for both $M'_{\dot{q}}$ (d normal to the heave axis) and $N'_{\dot{r}}$ (d normal to the sway axis). From this it can be seen that $M'_{\dot{q}}$ and $N'_{\dot{r}}$ should vary with $(L/D)^5$, since both ∇ and d vary linearly with length. The moment arm is normal to the surge axis for $K'_{\dot{p}}$ and is not affected by changes in length, so $K'_{\dot{p}}$ should vary only as ∇, which varies linearly with L/D.

The combined effects of $z_b \neq 0$ and the variance of z_b/L also cause the variation of the two coupling coefficients $X'_{\dot{q}}$ and $Z'_{\dot{q}}$, which represent coupling in the surge-pitch

DOF and the heave-pitch DOF respectively.

In the case of the coupling coefficients $Y'_{\dot{p}}$, $Y'_{\dot{r}}$, and $K'_{\dot{r}}$, which represent sway-roll coupling, sway-yaw coupling, and roll-yaw coupling respectively, a linear variance with L/D is expected.

3.2.2 Control Plane Location

The C-SCOUT is designed with zero angle of sweep on the control planes. It is also designed such that the shaftlines run through the loci of section quarter-chord points for each control plane, i.e. the shaftlines are aligned with the quarter-chord axes (x_{qca}), and are perpendicular to the hull at the parallel mid-body (see Figure 3-2).

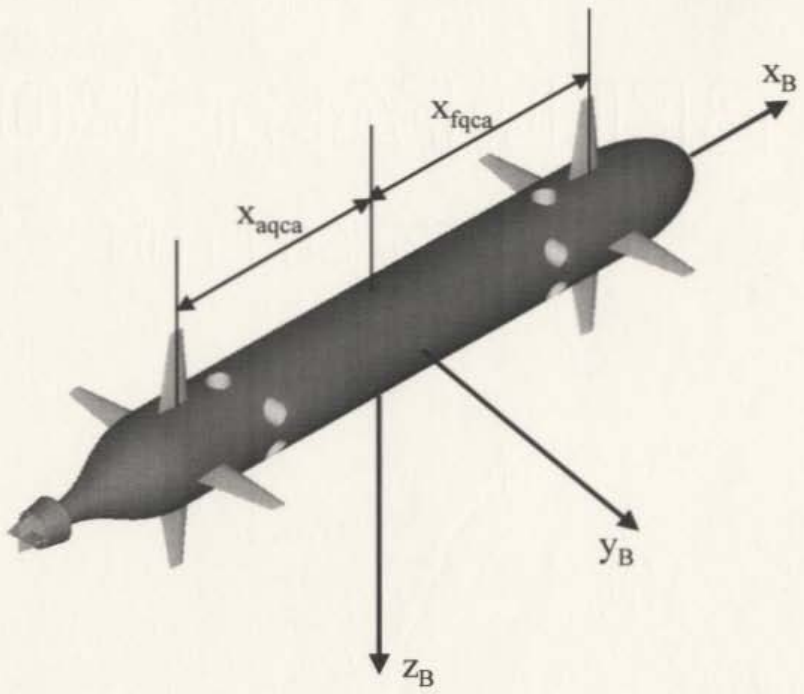

Figure 3-2: Location of Quarter-Chord Axes (Shaftlines) of Control Planes

Those coefficients that are purely concerned with forces and linear accelerations, $X'_{\dot{u}}$, $Y'_{\dot{v}}$, and $Z'_{\dot{w}}$, are not affected by changes in the control plane location. Because

of the radial rather than longitudinal moment arm. $K'_{\dot{p}}$ is also unaffected by changes in location along the surge axis. There is also no change to the relevant moment arm for $Y_{\dot{p}}$, so it too should be unaffected by changes in the location of the control planes along the surge axis.

The coefficients that would be most affected would be those having to do with pitch and yaw X'_q, Y'_r, Z'_q, K'_r, M'_q, and N'_r. Added mass terms $X_{\dot{q}}$, $Y'_{\dot{r}}$, $Z'_{\dot{q}}$, and $K'_{\dot{r}}$ would vary linearly with the change in control plane location. For these coefficients, the moment is affected linearly by the moment arm defined by the location along the x-axis of the control surfaces. In the case of $K'_{\dot{r}}$, the coefficient is nonzero as a result of roll-yaw coupling caused by $z_b \neq 0$, and then subject to the moment arm in yaw. Finally, M'_q and $N'_{\dot{r}}$ variation with the square of the distance along the x-axis is expected, since the two coefficients are representative of angular momentum terms (which are proportional to ∇d^2).

3.2.3 Control Plane Size

The size of the control planes was varied by scaling the volume while maintaining the relative geometry (shape). Since the variations are three-dimensional, it is expected that all of the added mass coefficients would be significantly affected. The amount and type (linear, quadratic....) of variation is not immediately apparent without numerical analysis. In addition, the interference effects of the hull on the control planes are not readily determined without numerical analysis. One could speculate that the variations in added mass coefficients should be proportional to the volume of the control plane, or to a volume-representative parameter such as b^3 (b is the span of the control plane - see Figure 2-12), if the interference effects are relatively small. The added mass contributions of the control planes are only a fraction of that of the hull, so the variations will be less significant than those resulting from changes to hull geometry.

3.3 Numerical Analysis Procedure

The sensitivity of the added mass coefficients to changes in geometry was investigated using a program called Estimate Submarine Added Masses (ESAM) developed by George Watt of Canada's Defence Research Establishment Atlantic (DREA) [80]. This program was developed for use with submarine modeling. It replaces the hull and each appendage with an equivalent ellipsoid. The optimal hull ellipsoid dimensions are chosen by comparison of added mass predictions with those from strip theory. The optimal hull ellipsoid is also used to calculate interference effects of the hull on the appendages. The added mass coefficients for each component are calculated from the exact expressions for ellipsoids[82] and the results summed to give the overall vehicle coefficients. The input to the program is the vehicle geometry. ESAM actually calculates the non-dimensional coefficients based on the vehicle length, e.g. $X'_u = X_u/\rho l^3$ (in accordance with [70]). This program was used with several geometries to generate corresponding added mass coefficients. The results are presented in Figures 3-4 through 3-11. Note that in these figures the notation for the coefficients is slightly different: Xud = X_u, etc. Also note that these plots are for the dimensional forms of added mass, and hence the appropriate units are given on the y-axis of each plot.

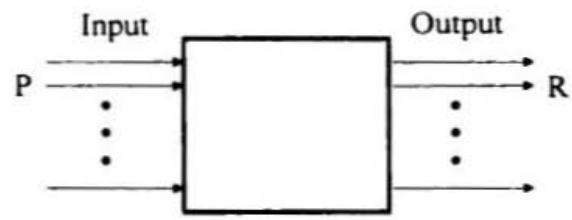

Figure 3-3: Generic Input/Output Block Diagram

The purpose of the sensitivity analysis is to determine the effect of variations in specific geometric parameters on the added mass coefficients. In general, the sensi-

tivity of a given output to a specific input can be calculated by comparing both the output variable, R, and the input parameter, P, to nominal values (refer to Figure 3-3). For each case the sensitivity, S, of the response to the variation in parameter is calculated [54]:

$$S = \frac{(R - R_{nom})/R_{nom}}{(P - P_{nom})/P_{nom}} \tag{3.4}$$

The value of S can be thought of as the percent change in the output variable due to a 1% change in the input parameter: in this case S represents the percent change in the added mass coefficient for a 1% change in the specific geometric parameter. The value of S also provides a measure of how accurately the geometric parameter must be specified in order to minimize its effects on the added mass coefficient.

3.4 Results

3.4.1 Quality of Variation

The mass and inertial properties of C-SCOUT[2] are presented in equation (3.5). They were determined from buoyancy-trim calculations to obtain a neutrally buoyant C-SCOUT, with level static trim.

$$\mathbf{M}_I = \begin{bmatrix} m & 0 & 0 & 0 & 0 & 0 \\ 0 & m & 0 & 0 & 0 & 0 \\ 0 & 0 & m & 0 & 0 & 0 \\ 0 & 0 & 0 & I_{xx} & -I_{xy} & -I_{xz} \\ 0 & 0 & 0 & -I_{xy} & I_{yy} & -I_{yz} \\ 0 & 0 & 0 & -I_{xz} & -I_{yz} & I_{zz} \end{bmatrix}$$

[2]The vehicle data presented here are for the C-SCOUT before it was constructed; i.e., it is the best estimate of the as-built vehicle, and was used to allow the analysis to proceed while the vehicle was being constructed.

$$
= \begin{bmatrix} 314.7 & 0 & 0 & 0 & 0 & 0 \\ 0 & 314.7 & 0 & 0 & 0 & 0 \\ 0 & 0 & 314.7 & 0 & 0 & 0 \\ 0 & 0 & 0 & 0.6 & 0 & -0.8 \\ 0 & 0 & 0 & 0 & 150.3 & 0 \\ 0 & 0 & 0 & -0.8 & 0 & 149.6 \end{bmatrix} \tag{3.5}
$$

For the C-SCOUT vehicle configuration, the values of added mass (via ESAM, and after multiplying by ρl^n) are:

$$
\mathbf{M}_V = \begin{bmatrix} -2.531 & 0 & 0 & 0 & 0.028 & 0 \\ 0 & -164.494 & 0 & -1.796 & 0 & 13.876 \\ 0 & 0 & -164.494 & 0 & -13.876 & 0 \\ 0 & -1.796 & 0 & -3.601 & 0 & 0.142 \\ 0.028 & 0 & -13.876 & 0 & -74.827 & 0 \\ 0 & 13.876 & 0 & 0.142 & 0 & -74.827 \end{bmatrix} \tag{3.6}
$$

where the units for both matrices are

$$
Units: \begin{bmatrix} \mathrm{kg} & \mathrm{kg} & \mathrm{kg} & \mathrm{kg\cdot m} & \mathrm{kg\cdot m} & \mathrm{kg\cdot m} \\ \mathrm{kg} & \mathrm{kg} & \mathrm{kg} & \mathrm{kg\cdot m} & \mathrm{kg\cdot m} & \mathrm{kg\cdot m} \\ \mathrm{kg} & \mathrm{kg} & \mathrm{kg} & \mathrm{kg\cdot m} & \mathrm{kg\cdot m} & \mathrm{kg\cdot m} \\ \mathrm{kg\cdot m} & \mathrm{kg\cdot m} & \mathrm{kg\cdot m} & \mathrm{kg\cdot m^2} & \mathrm{kg\cdot m^2} & \mathrm{kg\cdot m^2} \\ \mathrm{kg\cdot m} & \mathrm{kg\cdot m} & \mathrm{kg\cdot m} & \mathrm{kg\cdot m^2} & \mathrm{kg\cdot m^2} & \mathrm{kg\cdot m^2} \\ \mathrm{kg\cdot m} & \mathrm{kg\cdot m} & \mathrm{kg\cdot m} & \mathrm{kg\cdot m^2} & \mathrm{kg\cdot m^2} & \mathrm{kg\cdot m^2} \end{bmatrix} \tag{3.7}
$$

Length to Diameter

The length-to-diameter ratio (L/D) is varied by changing the length of the parallel mid-body while keeping the diameter constant. This means the nose and tail geometries are not affected by the variation, except to be separated by a lesser or

greater distance. To negate any possible influence of the control planes. their geometry was not included in the ESAM input file. The ratio was varied from $L/D = 3$ to $L/D = 10$.

The plots (see Figure 3-4) show the linear variation of Y_v and Z_w with changing L/D. They also show a nonlinear relationship between X_u and L/D. This latter relationship stems from the choice of reference axis for the ESAM analysis. The origin of the reference frame is at the vehicle center of mass rather than the center of buoyancy. The combination of $z_b \neq 0$ and the variation of z_b / L cause the nonlinear variation of X_u with L/D.

Principle angular acceleration terms. M_q. and N_r. are expected to vary with $(L/D)^3$. The principle angular acceleration term. K_p. is expected to vary linearly with L/D. These relationships are born out by the analysis (see Figure 3-4).

The coupling terms X_q and Z_q. which represent coupling in the surge-pitch DOF and the heave-pitch DOF respectively. like X_u. are in the surge-heave-pitch plane (x-z plane). such that variation in L and z_b/L combine to give the nonlinear variances displayed in the analysis results (see Figure 3-5).

In the case of Y_p. Y_r and K_r. which represent sway-roll coupling. sway-yaw coupling. and roll-yaw coupling respectively. the plots show a linear variance with L/D. These added masses are in the sway-roll-yaw plane. and as such vary with L and z_b/D. the latter of which remains constant for all changes in L/D (i.e. L is varied while D is held constant).

Control Plane Location

The location of the shaftline (quarter-chord axis) for the forward fins was varied from 15% to 40% of the full configuration vehicle length aft of the nose in 5% increments. while the quarter-chord axis for the after fins (x_{aqca}) was fixed at 81.2% of L. The location of the shaftline for the after fins was varied from 60% to 85% of the full configuration vehicle length aft of the nose in 5% increments. while the quarter-chord

axis of the forward fins (x_{fqca}) was fixed at 15.5% of L.

Figures 3-6, 3-7, 3-8 and 3-9 show that the coefficients $X_{\dot{u}}$, $Y_{\dot{v}}$, $Z_{\dot{w}}$, $K_{\dot{p}}$, $X_{\dot{q}}$, and $Y_{\dot{p}}$ are all virtually constant and relatively insensitive to variations along the hull x-axis of the location of the control planes. Note that the last point on the plots for the after control plane variations represents a location where a significant portion of the control plane is over the cubic spline tail section rather than the parallel mid-body, so the values of the added masses at that location do not follow the trend. Added mass terms $Y_{\dot{r}}$, $Z_{\dot{q}}$, and $K_{\dot{r}}$ vary linearly with x_{fqca} or x_{aqca}. For the first two, it can be seen that $Y_{\dot{r}} = -Z_{\dot{q}}$. The reason for the dependence can be more readily seen from the corresponding terms $N_{\dot{v}} = -M_{\dot{w}}$, where it becomes apparent that the moment is affected linearly by the moment arm, x_{fqca} or x_{aqca}. $K_{\dot{r}}$ is a result of roll-yaw coupling caused by $z_b \neq 0$. Again, $K_{\dot{r}}$ is dependent x_{fqca} or x_{aqca} as the moment arm. Finally, $M_{\dot{q}} = N_{\dot{r}}$, and they vary with x^2_{fqca} or x^2_{aqca}, as would be expected of angular momentum terms. Note that the third angular momentum term, $K_{\dot{p}}$, is only affected by moment arms perpendicular to the vehicle x-axis, and is therefore insensitive to variations in x_{fqca} or x_{aqca}.

Control Plane Size

The size of the control planes was varied by scaling the span, b (see Figure 2-12). This really scales the volume, as the geometry of the whole fin is kept in proportion by calculating each of the other dimensions from the span. The size was varied from 50% to 150% of the as-built control plane.

In analyzing the effects of the control plane size, the nominal base hull was used in each case, and the total values of the added mass coefficients, including the hull, control planes and the interference effects were determined via ESAM. However, the bare hull portions of the coefficients were ignored, and only the control plane (complete with interference effects) were examined because the bare hull contributions remained constant.

All of the added masses were significantly affected (See Figures 3-10 and 3-11). as expected. There is a direct relation to the volume of the control plane as parameterized by b^3 (where b is the span of the control planes).

3.4.2 Sensitivity Values

The sensitivity of the added masses to variations in geometry also changes with the amount of variation. The maximum sensitivities of each significant added mass coefficient are listed in Table 3.1 for the nondimensional coefficients. and in Table 3.2 for the same coefficients multiplied by ρl^n).

Table 3.1: Maximum Sensitivity of Added Mass Coefficients to Changes in Geometric Parameters

	Hull	Control Plane		
	L/D	Location		Size
		Fwd	Aft	
X'_u	27.465	0.004	0.011	1.289
Y'_v	4.787	0.000	0.017	0.459
Z'_w	4.787	0.000	0.017	0.459
K'_p	31.297	0.000	0.000	7.985
M'_q	2.417	0.722	0.766	0.692
N'_r	2.417	0.722	0.766	0.692
X'_q	63.772	0.000	0.009	1.287
Y'_p	12.968	0.001	0.008	0.444
Y'_r	12.286	24.130	23.656	4.488
Z'_q	12.286	24.130	23.656	4.488
K'_r	29.810	23.831	23.253	4.631

From Tables 3.1 and 3.2. it can be seen that the dimensional forms of the coefficients have the same sensitivity to variations in control plane parameters as do the nondimensional coefficients. i.e. the sensitivity of each of the added mass coefficients is equivalent to the sensitivity of the corresponding dimensional form. On the other hand. redimensionalizing the added mass coefficients has major effects on the sensitivity of the coefficients to changes in hull geometry. This is a direct result of using the hull length as the dimensionalizing factor. In all cases. it is the sensitivity of the

Table 3.2: Maximum Sensitivity of Dimensional Added Masses to Changes in Geometric Parameters

	Hull	Control Plane		
	L/D	Location		Size
		Fwd	Aft	
$X_{\dot{u}}$ (kg)	0.818	0.004	0.011	1.289
$Y_{\dot{v}}$ (kg)	1.252	0.000	0.017	0.459
$Z_{\dot{w}}$ (kg)	1.252	0.000	0.017	0.459
$K_{\dot{p}}$ (kg · m^2)	1.249	0.000	0.000	7.985
$M_{\dot{q}}$ (kg · m^2)	6.040	0.722	0.766	0.692
$N_{\dot{r}}$ (kg · m^2)	6.040	0.722	0.766	0.692
$X_{\dot{q}}$ (kg · m)	0.819	0.000	0.009	1.287
$Y_{\dot{p}}$ (kg · m)	1.252	0.001	0.008	0.444
$Y_{\dot{r}}$ (kg · m)	1.421	24.130	23.656	4.488
$Z_{\dot{q}}$ (kg · m)	1.421	24.130	23.656	4.488
$K_{\dot{r}}$ (kg · m^2)	1.405	23.831	23.253	4.631

dimensional values that is of importance, since they are the values used in the model, and represent the real effects of added mass.

The length-to-diameter ratio was varied from $L/D = 3$ to $L/D = 10$. Sensitivity was calculated using $L/D = 6.7$ (the as-built ratio) as the nominal value for the base configuration. Table 3.2 suggests that all the added mass coefficients are affected significantly[3] by the changes in L/D, especially the pitch and yaw added mass-momenta of inertia, $M_{\dot{q}}$ and $N_{\dot{r}}$.

The location of the shaftline for the forward fins was varied from 15% to 40% of the full configuration vehicle length aft of the nose in 5% increments, while the quarter-chord axis of the after control planes (x_{aqca}) was fixed at 81.2% of L. The location of the shaftline for the after fins was varied from 60% to 85% of the full configuration vehicle length aft of the nose in 5% increments, while the quarter-chord axis of the forward control planes(x_{fqca}) was fixed at 15.5% of L. Sensitivity to variations was calculated using 15.5% of L for x_{fqca} and 81.2% of L for x_{aqca} (the as-

[3]Unless otherwise stated, the phrases "affected significantly" and "significantly affected" means that the sensitivities are not negligibly small ($<<1$).

built locations) as the nominal position. but the change in the input parameter (the location of the control planes) in equation 3.4 was divided by the length overall rather than the nominal position of the planes. This makes the forward and aft values more comparable. The sensitivity increases with movement of the control planes outward from the center of mass. For changes in the location of the control planes. only Y_r. Z_q. M_q. N_r. and K_r are significantly affected.

The size of the control planes was varied from 50% to 150% of the nominal size. All of the control plane added masses were significantly affected. however Y_v. Z_w. Y_p. M_q. and N_r have maximum sensitivities less than 1: X_u and X_q have maximum sensitivities of about 1: and Y_r. Z_q. K_p. and K_r have maximum sensitivities greater than 1.

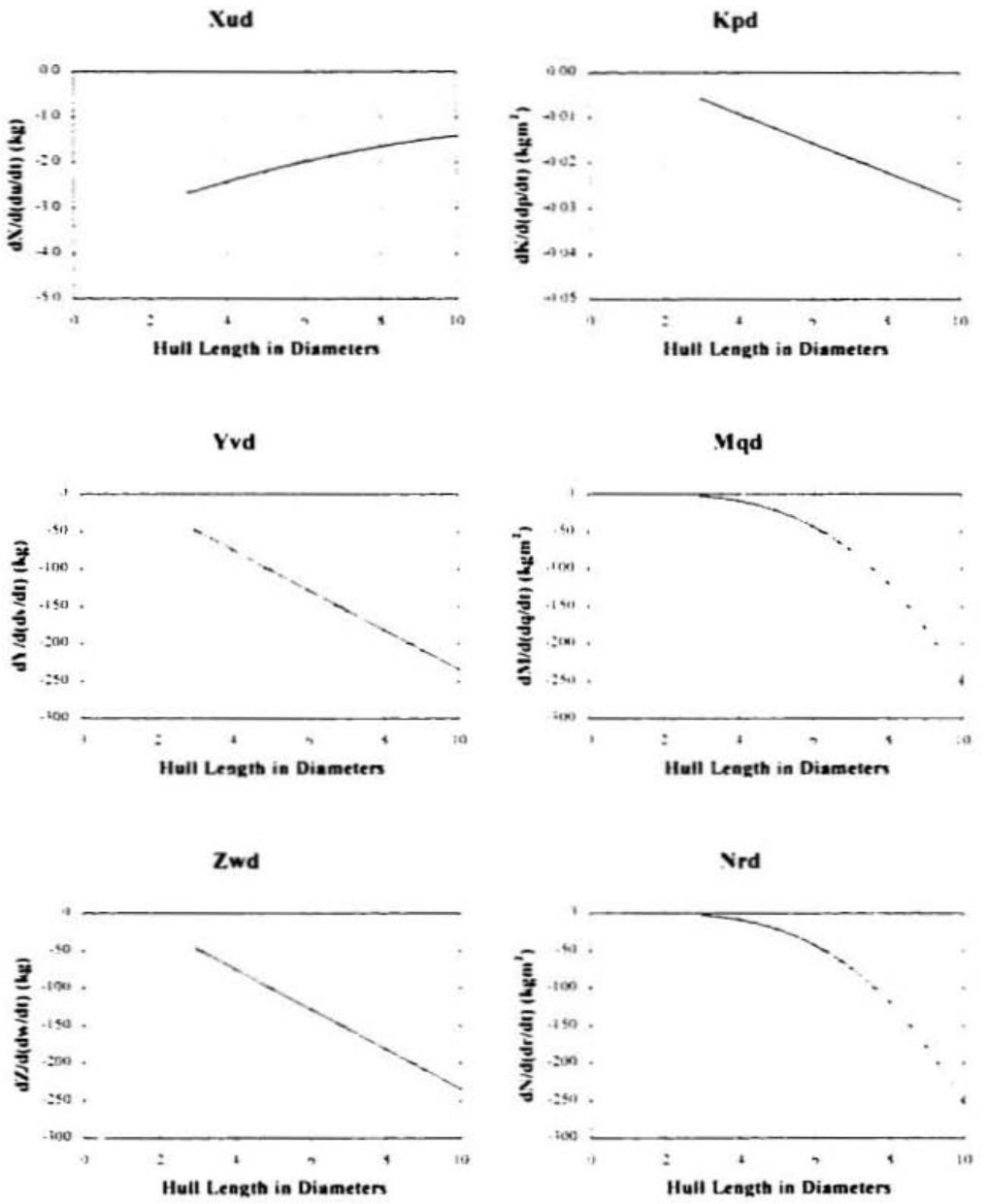

Figure 3-4: Effect of Variation of (Bare Hull) Vehicle Length to Diameter Ratio on the Principle Added Mass Coefficients

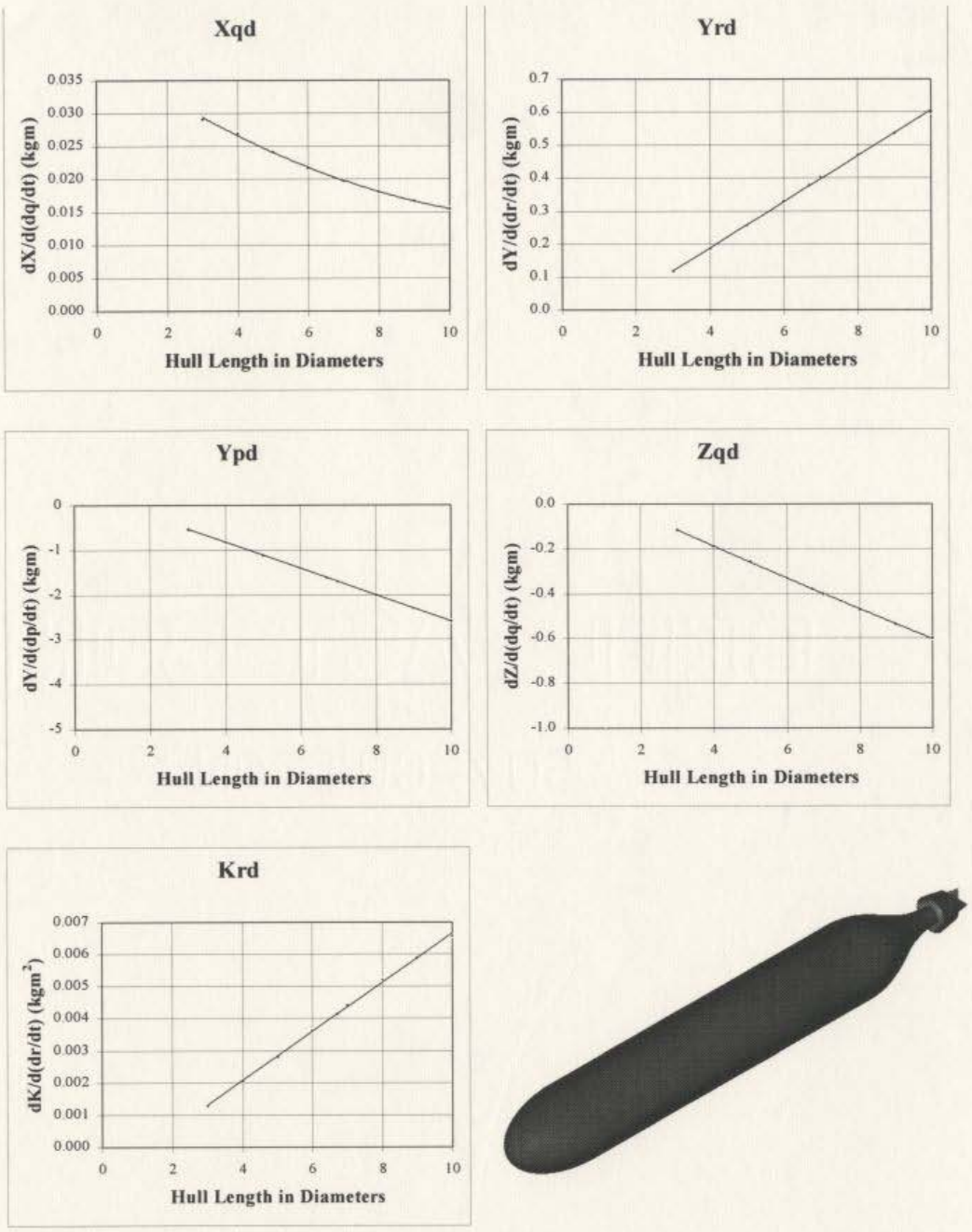

Figure 3-5: Effect of Variation of (Bare Hull) Vehicle Length to Diameter Ratio on the Coupling (Off-Diagonal) Added Mass Coefficients

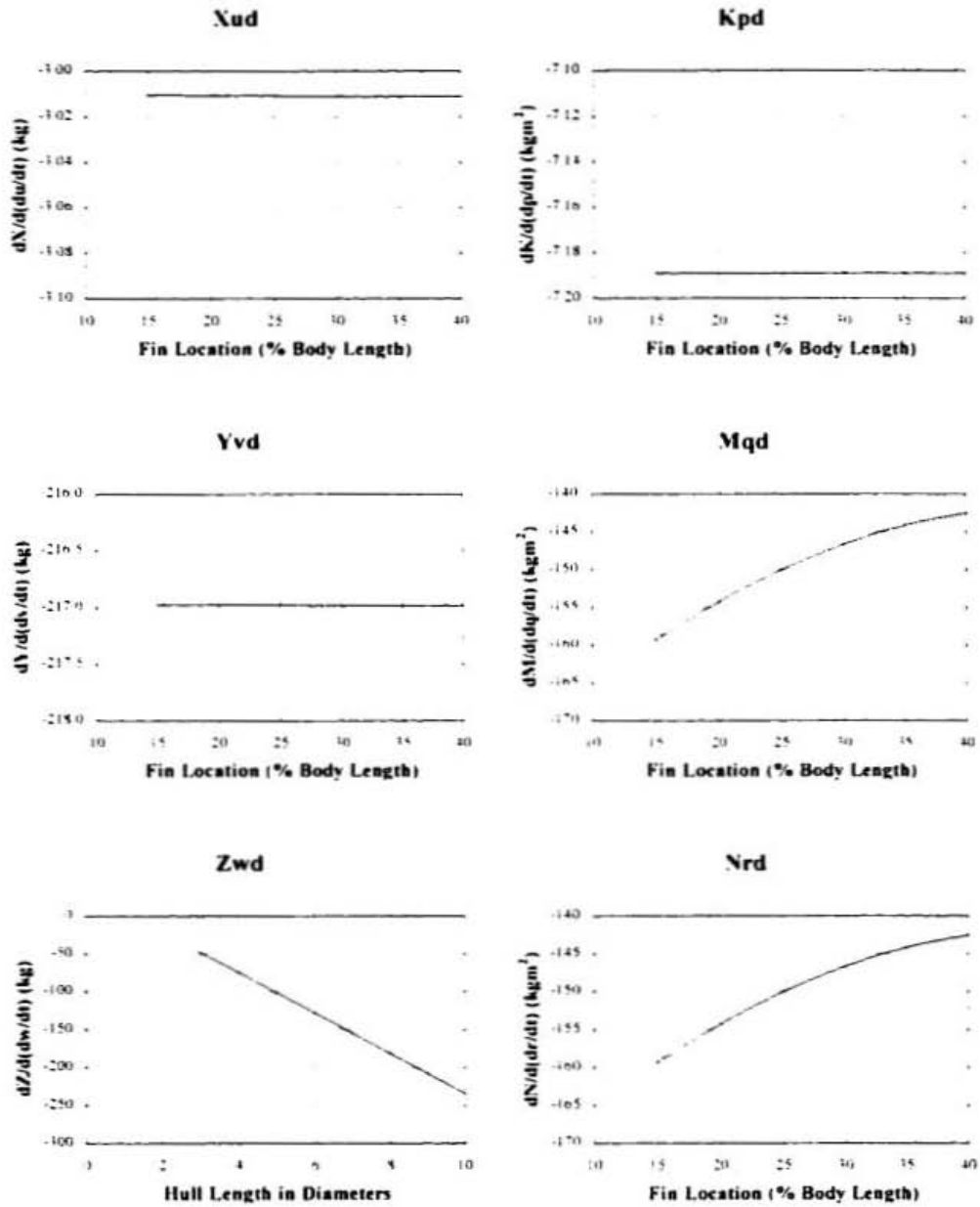

Figure 3-6: Effect of Variation of Forward Control Plane Location on the Principle Added Mass Coefficients

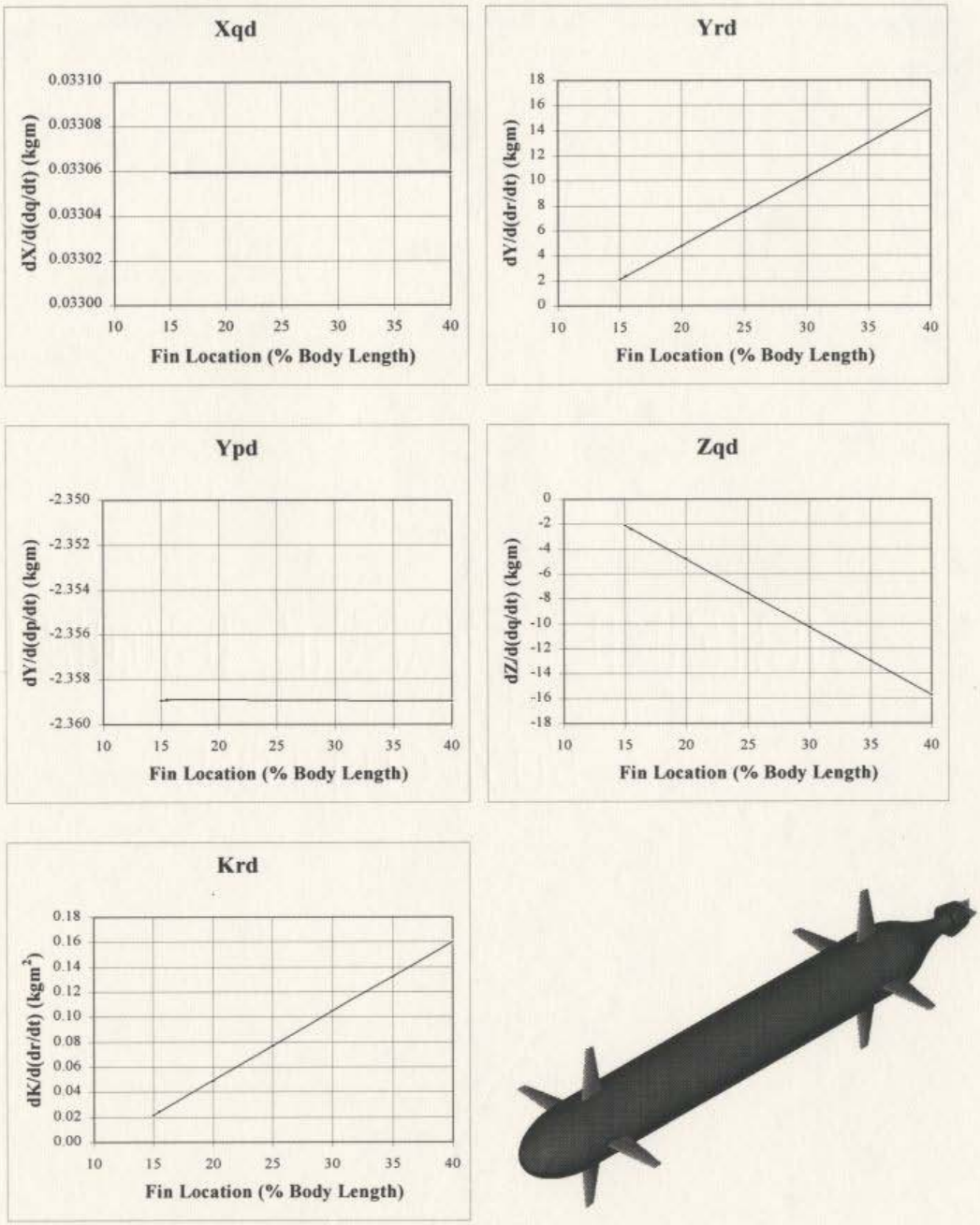

Figure 3-7: Effect of Variation of Forward Control Plane Location on the Coupling (Off-Diagonal) Added Mass Coefficients

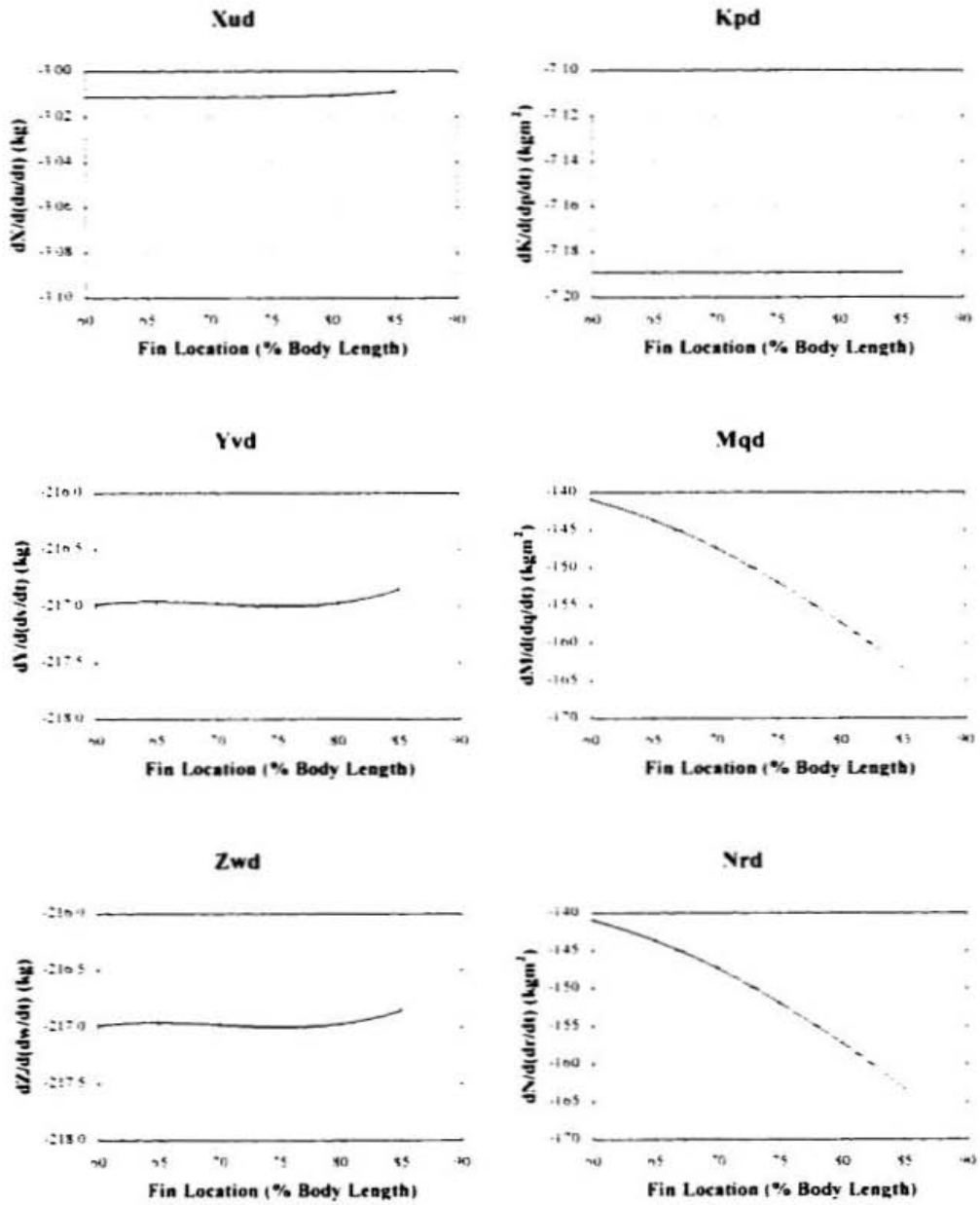

Figure 3-8: Effect of Variation of After Control Plane Location on the Principle Added Mass Coefficients

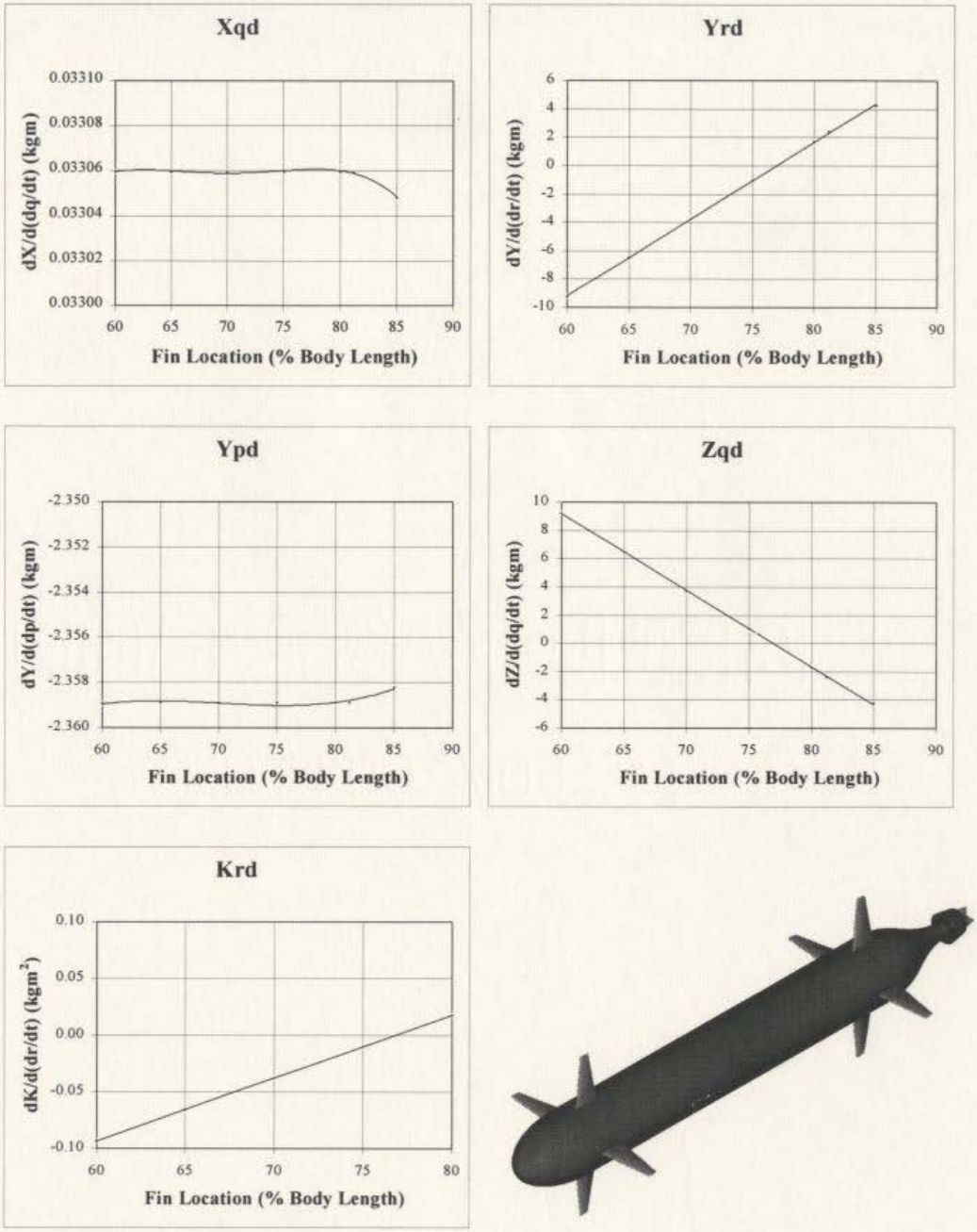

Figure 3-9: Effect of Variation of After Control Plane Location on the Coupling (Off-Diagonal) Added Mass Coefficients

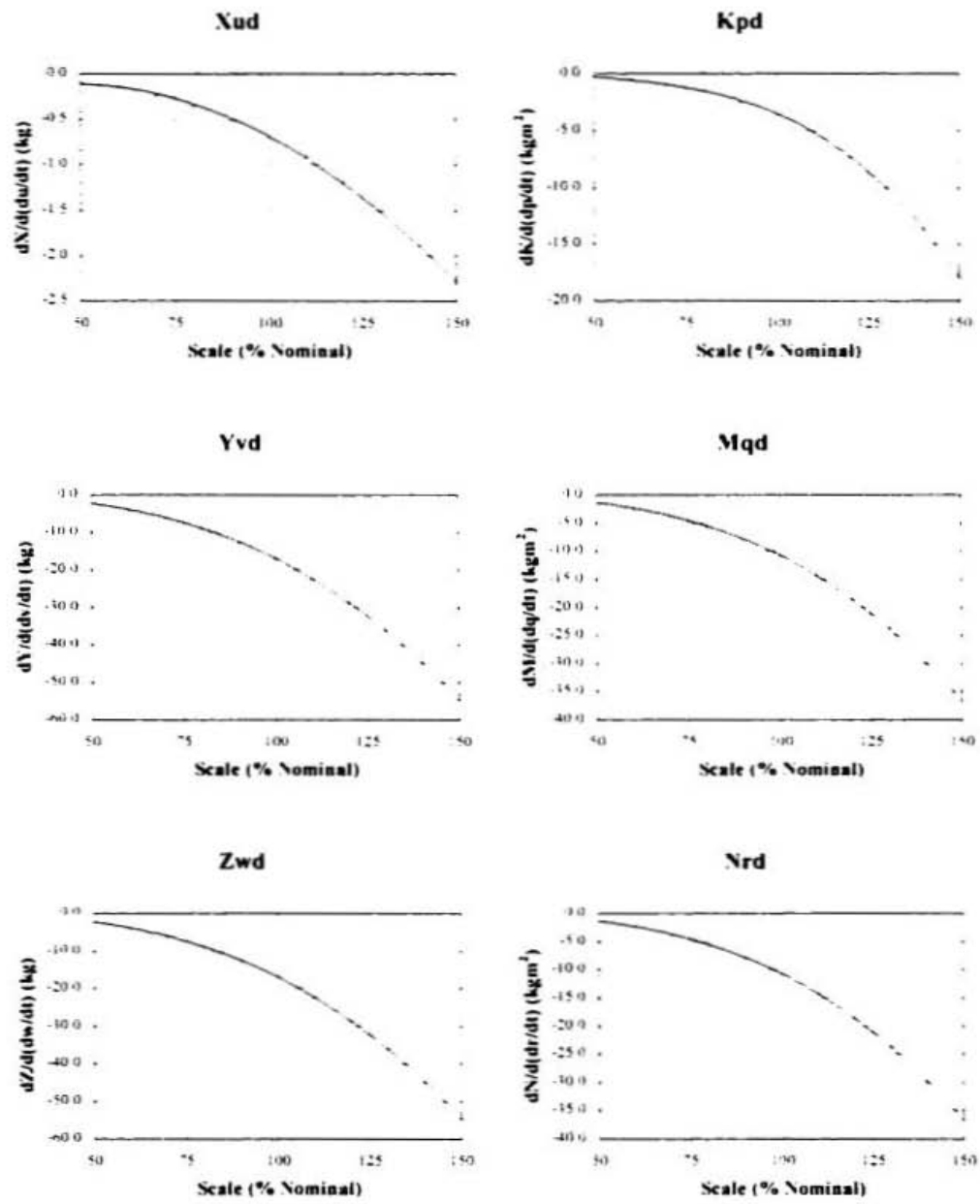

Figure 3-10: Effect of Variation of Control Plane Size on the Principle Added Mass Coefficients of the Control Planes Only

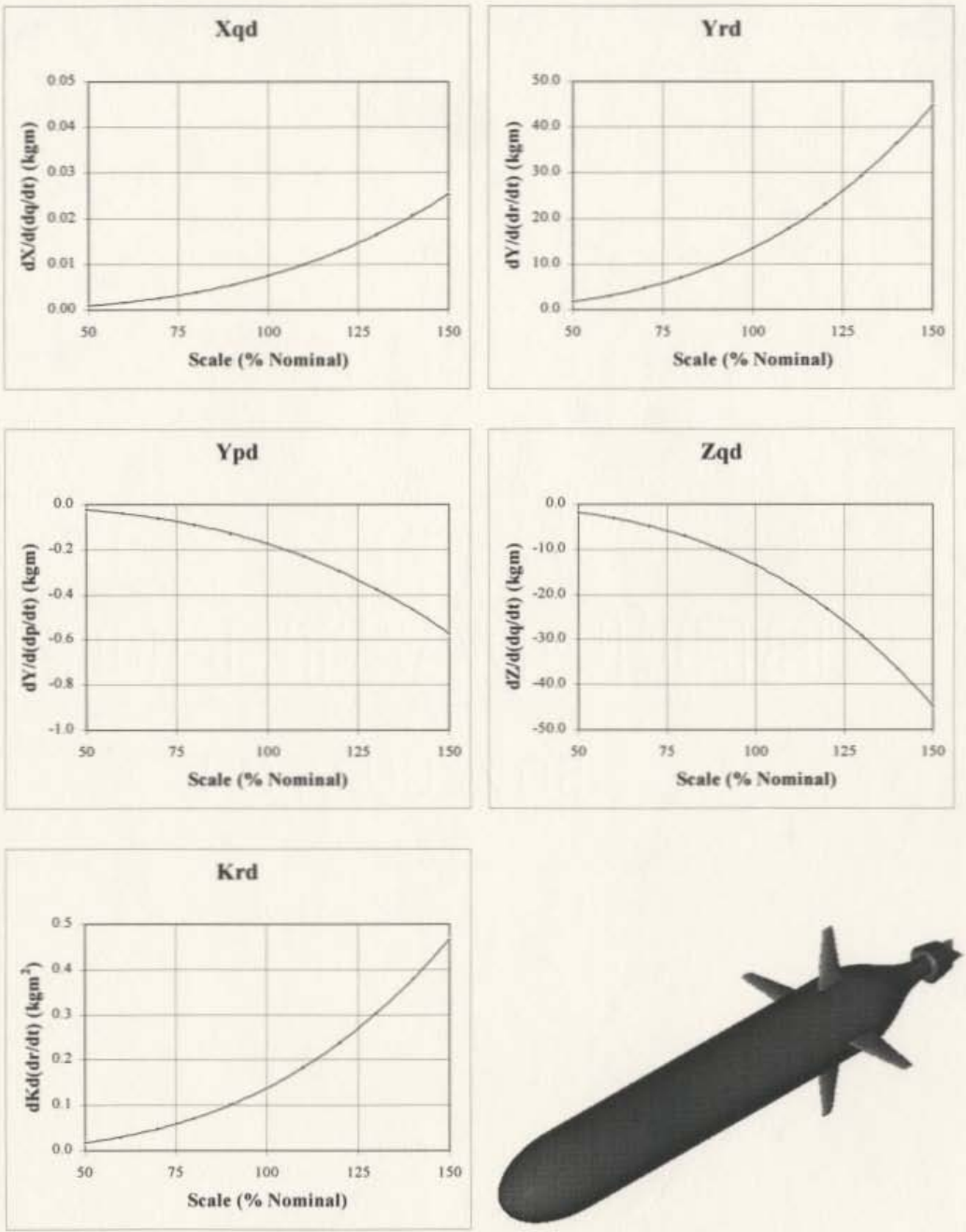

Figure 3-11: Effect of Variation of Control Plane Size on the Coupling (Off-Diagonal) Added Mass Coefficients of the Control Planes Only

Chapter 4

Sensitivity of Vehicle Response to Hydrodynamic Parameters

Each of the six forcing functions include terms from both viscous effects (viscous damping) as well as from pressure effects and gravity and buoyancy forces. The nonlinear computer model used in the simulation uses lift and drag equations to determine the forces on the hull and control planes (fins). The equations are written in terms of coefficients of lift and drag. the density of the water. the geometry of the vehicle (a reference area - wetted surface area is used in this model). and the velocity. There are separate equations for the hull and each control plane. The forces are added together (component-wise in the body-fixed reference frame) to determine the total force on the vehicle.

The moments caused by the lift and drag forces on the fins and hull are determined by a crossproduct involving the forces and the position vector of the center of pressure or center of effort.

The center of pressure (CP) is the point on the control plane where the (fin) lift and (fin) drag are assumed to act. For the wing-section fins. this point is usually very close to the quarter-chord axis ($CPc = c/4$) at some distance along the span from the root chord towards the tip chord. In the case of the C-SCOUT vehicle.

the center of pressure is assumed to be at the quarter-chord point 43% of the half-span ($CPs = 0.429\frac{b}{2}$) out from the root chord. This location is based on formulae presented in [79]. The model uses lift and drag on the control planes at angles of attack below stall. This is justified because the base configuration of C-SCOUT is incapable of hover, and should therefore have dynamics dominated by the effects of forward velocity, i.e., the angles of attack will be low. Lift and drag coefficients for the control planes of small aspect ratio at angles of attack below stall are readily determined from existing literature, such as [79].

The center of effort (CE) is the point along the axis of revolution of the bare hull where the forces of (hull) lift and (hull) drag are assumed to act. In this sense it is very much the center of pressure of the hull, but it will be referred to as the center of effort herein to avoid confusion with the center of pressure of the control planes. The present model has a fixed center of effort on the axis of revolution, forward of the center of buoyancy of the vehicle. There is significant uncertainty associated with the actual location, and the location will move aft along the axis of revolution as the vehicle angle of attack (the angle of the surge axis of the body frame relative to the fluid flow) becomes larger. Therefore, it is important to know what effect any variation of center of effort will have on motion of the vehicle. Lift and drag coefficients for the hull, and the center of effort are determined using methods developed for airships and guided missiles [78].

4.1 The Need for Sensitivity Analysis

Hydrodynamic parameters are typically determined from physical-model testing and there is usually some uncertainty concerning their exact values. However, one of the key elements in the vehicle's effectiveness as a test bed is a fundamental understanding of its maneuverability and of its sensitivity to changes in hydrodynamic parameters. This knowledge of the vehicle will be important when the vehicle is used as a testbed

for other systems. It will facilitate the discernment of behaviours induced by the system under study, by providing a baseline of behaviours inherent to the vehicle itself. This will allow a clearer picture of the effects of the system under test.

Finally, it is important to look at the sensitivity of the vehicle in terms of robustness: how accurately does one have to know the parameters in order to ensure acceptable performance.

4.2 Analysis Procedure

4.2.1 Sensitivity

The purpose of this sensitivity analysis is to determine the effect of variations of specific parameters on the response of the vehicle in some standard maneuvers. For each case the sensitivity of the response measure to the variation in parameter is calculated as in [54] (see equation (3.4)). The value of S can be thought of as the percent change in the measured response variable corresponding to the percentage change in the input parameter.

Here the input parameters can be categorized as:

1. Geometric properties
    (a) Scale
    (b) L/D
    (c) Control plane size
    (d) Control plane location
2. Hydrodynamic properties
    (a) Added mass
    (b) Lift and drag coefficients

(c) Center of effort (CE) of the hull and center of pressure (CP) of the fins (measured with respect to the vehicle center of mass)

These parameters are either direct design variables (i.e., their values are chosen in the design), or they are indirect design variables. The values of the direct design variables greatly influence the values of the indirect design variables, so that obtaining a certain value of the indirect design variable may be the motivating factor in choosing a particular direct design variable. The geometric properties are direct design variables, while the hydrodynamic properties are indirect variables.

The division of the parameters into direct/indirect design variables leads to a more general, two-stage sensitivity analysis. First, the sensitivity of the added mass coefficients to changes in geometry (scale, L/D, control plane size and location) is determined using ESAM. This step was accomplished in Chapter 3 (and reported in [52]). Note that the lift and drag coefficients are "fixed" by selection of the shape of the hull and appendages, as are the centers of pressure and effort - a fundamental set of decisions in the design process. Second, the sensitivity of the vehicle to variations in the added mass coefficients, to lift and drag coefficients, and to location of the centers of effort and pressure is determined by multiple simulations of definitive maneuvers at specific speeds and rudder/elevator angles. This is the subject of the present chapter (and has been reported in [55]).

4.2.2 Definitive Maneuvers

The maneuvers chosen for measuring the response of the vehicle to changes in design parameters are turning circles and horizontal and vertical zigzag maneuvers. These are standard tests performed on ships and submarines and so provide readily understandable criteria for evaluating performance.

To perform the turning circle, the vehicle is commanded to travel with steady forward motion. When this straight and level flight is achieved, the rudder is com-

manded to a particular deflection angle. such that the vehicle enters into a turn (see Figure 4-1[1]). The rudder angle is maintained (as is the commanded forward speed) while the vehicle continues to turn in a circle. There are several measures in the turning circle maneuver which can be used as performance indicators. Here. the radius of the turning circle was chosen as a measure of steady-state response. and the advance was chosen as a measure of the transient response. In terms of the simula-

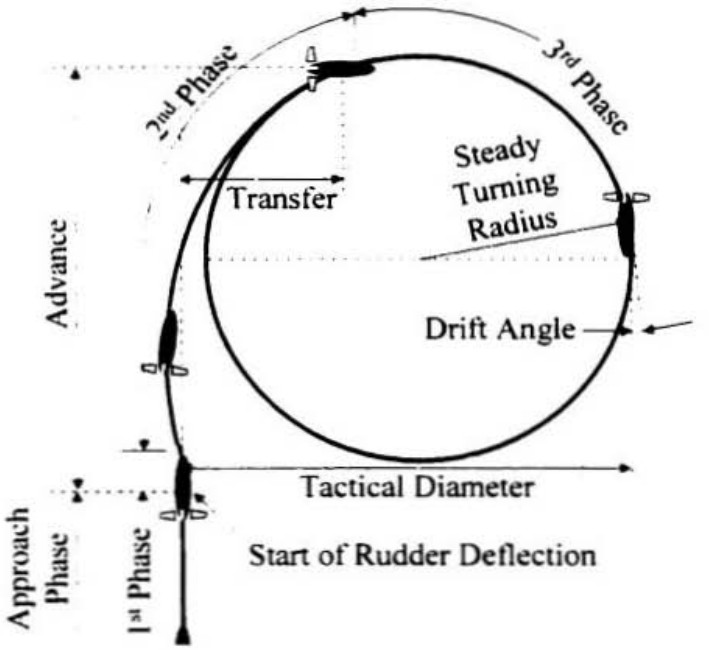

Figure 4-1: Turning Circle

tion. this maneuver was easily implemented by simply setting the upper and lower control planes to the desired angle of deflection at a given time ($10s$). A variable step integrator was used in the Simulink^{TM} model. and each simulation was run for $100s$ to ensure a complete circle was performed even at low speeds.

[1] Ref. Fig.20. C. L. Crane, et al., "Controllability," Chapter IX in Principles of Naval Architecture, vol. III. E. V. Lewis. Ed. The Society of Naval Architects and Marine Engineers. Jersey City. NJ. 1989.

The horizontal (vertical) zigzag also starts with the vehicle travelling in straight and level flight. Then the rudder (elevator) is commanded to a given deflection angle. The rudder (elevator) angle is held until the yaw (pitch) angle of the vehicle reaches a specific value. then the rudder (elevator) is commanded to an equivalent deflection angle on the opposite side (see Figure 4-2[2]). The new deflection angle is held until the vehicle yaw (pitch) angle reaches the specific value. then the first rudder (elevator) deflection angle is again commanded and the cycle is repeated. With the zigzag maneuvers. the parameters measured are the period (τ). the time to reach second execute after the first execute (reach). the overshoot angle (γ_0). and the overshoot width of path (p_0). The first two parameters are measures in time. while the last two are measures in space: each of them may have a different relationship to the variation of the particular coefficient. The zigzag gives a clearer picture of the transient response of the vehicle and a better indication of its controllability than the turning circle does. The zigzag maneuver was more difficult to implement than the turning circle. since the zigzag depends on feedback of the vehicle yaw angle. The vehicle achieves the yaw angle setpoint at a time when the state of the vehicle is changing in a nearly linear manner. i.e. when the variable step integrator is taking large time steps. Consequently. the simulation often oversteps by a significant amount the time when the correct yaw angle is achieved. resulting in what appears to be spurious data for the vehicle response measures. To avoid this. a fixed step integrator was used and the time step adjusted so that when the vehicle achieves the yaw setpoint. it was detected quickly. The results from this integration method are vastly improved from the variable step simulations. but there is still some variation in the data due to not detecting exactly the time at which the vehicle reaches the yaw setpoint. This can have some effect on the trend line analysis.

[2]Ref. Fig.156. C. L. Crane. et al.. "Controllability." Chapter IX in Principles of Naval Architecture. vol. III. E. V. Lewis. Ed. The Society of Naval Architects and Marine Engineers. Jersey City. NJ. 1989.

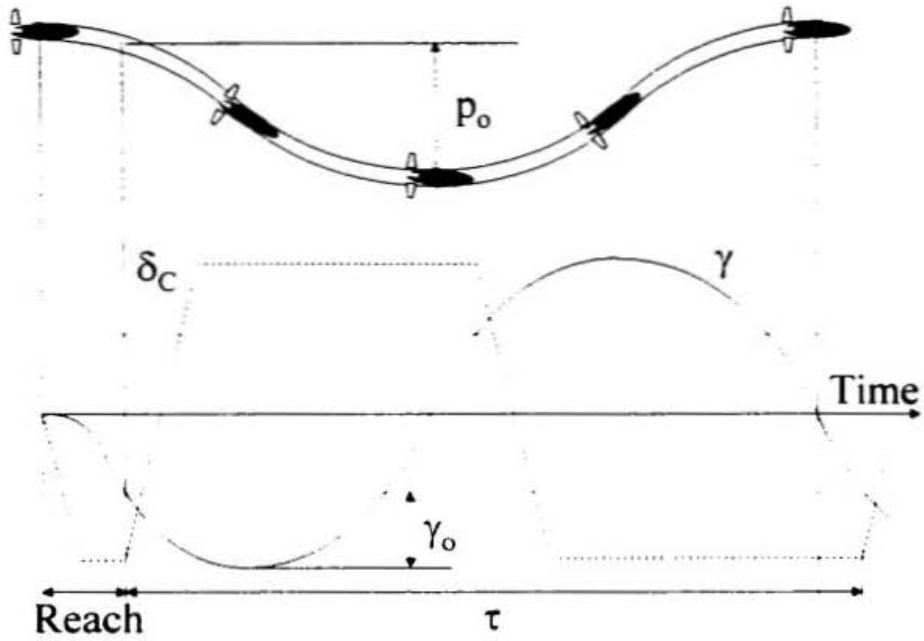

Figure 4-2: Zigzag Maneuver

4.3 Effects of Varying Hydrodynamic Parameters on Vehicle Response

The hydrodynamic parameters varied are the significant (non-zero) added mass coefficients, the lift and drag coefficients for the hull and control planes, and the center of effort of the hull and center of pressure of the control planes. These parameters represent a comprehensive set of variables that influence the behaviour of the AUV. For each of the parameters, a range of simulations at a representative surge (forward) speed and control plane deflection angle were performed.

4.3.1 A Note on the Model

The transit time for the flow over the control plane (mean chord) is the mean chord length divided by the speed of the vehicle: $\bar{c}/u = 0.036\,\mathrm{s}$ at a vehicle speed of $3\,\mathrm{m/s}$. This time is two orders of magnitude less than the shortest period of vehicle motion during zigzags in either plane at $3\,\mathrm{m/s}$. Therefore the quasisteady state modeling approach used here is valid.

The control actuator dynamics are not included in the model. This allows step inputs to the vehicle, resulting in clear indications of vehicle behavior. The reaction time for the control plane is expected much less than the response time of the vehicle, so this simplification is reasonable.

4.3.2 A Note on the Data Analysis and Plots

Note that in some of the figures to be presented later in this analysis, the trend lines do not pass through the data points (diamonds - "Actual" in the plot legends). The trend lines ("Trend" in the plot legends) were determined automatically by a software routine that subjects the data to progressive series of regressions. Each set of data was first averaged. If the data were within 1% of the average, a constant trend line equal to the average was used. If the data were not within 1% of the average, a linear regression was performed. If all the data were not within 1% of the linear trend line, a quadratic regression was performed, and so on until the order of the regression could no longer be supported by the number of data points (the order of the polynomial reached one less than the number of data points). Because of the automatic nature of the software routine, the data points in some cases may show a definite trend which is not reflected by the trend line because the variation in the data is less than 1%. In some cases the 1% tolerance was relaxed to 5% when the order of the polynomial describing the trend line was large (e.g. 5 or 6). This was done because the order of the trend line polynomials may be artificially large due to effects of the integrator (see above). Some of the hydrodynamic parameters (specifically the lift and drag

coefficients for the hull and control planes) are functions of the sine and cosine of their respective angles of attack. In the cases of these parameters the polynomial regression is not a good option.

4.3.3 Added Mass

When a body accelerates in a fluid, the fluid around the body is disturbed and is also accelerated. The movement of the fluid requires additional force over and above that necessary to accelerate the body itself. Added mass is the proportionality factor relating the additional force to the actual acceleration of the body [81]. The value of the added mass is important in the accurate calculation of vehicle accelerations.

The nature of the hull-fluid interaction also means that the added mass is not a simple scalar, but must account for the accelerations in all six DOF that result from each of the forces and moments. The general form for an added mass matrix has 36 elements to completely describe the ratio of additional force to acceleration in each combination of DOF. For any body there are really only 21 unique elements in the added mass matrix, because the matrix is symmetric about the diagonal, i.e., $X_v = Y_u$, $X_w = Z_u$, etc.[73]. For a typical torpedo-like vehicle such as the C-SCOUT, there are 11 non-zero elements: X_u, X_q, Y_v, Y_p, Y_r, Z_w, Z_q, K_p, K_r, M_q and N_r, so the matrix of added mass derivatives is:

$$\begin{bmatrix} X_u & 0 & 0 & 0 & X_q & 0 \\ 0 & Y_v & 0 & Y_p & 0 & Y_r \\ 0 & 0 & Z_w & 0 & Z_q & 0 \\ 0 & Y_p & 0 & K_p & 0 & K_r \\ X_q & 0 & Z_q & 0 & M_q & 0 \\ 0 & Y_r & 0 & K_r & 0 & N_r \end{bmatrix} \tag{4.1}$$

Of the eleven, six are along the main diagonal of the matrix, and represent the principle coefficients. That is, if the vehicle is forced in a particular direction (or

rotated about a particular axis), one of these six values represents the added mass coefficient (or added-mass-moment-of-inertia coefficient): the ratio of additional force (moment) required to achieve the acceleration in that DOF. The remaining five off-diagonal values represent coupling terms which describe the effects of force in one DOF on the acceleration in another DOF.

Since the reference frame is attached to the center of mass for simpler calculation of the dynamics, X_q, Y_p, and K_r are typically not zero. The remaining coupling elements, Y_r and Z_q, are the result of fore-aft asymmetry in the vehicle.

Computer simulations were carried out where each of the significant added masses was varied from 0% to 200% of the nominal values (the values determined by ESAM for the as-designed vehicle). A range of simulations for each of the definitive maneuvers were performed in order to give a comprehensive measure of the vehicle performance.

Turning Circles

The turning circle is a steady-state maneuver: once the vehicle has entered the circle its state of motion remains constant, the only acceleration being an angular acceleration due to the changing direction of the velocity vector. Because of this, the maneuver is expected to be relatively insensitive to variations in added mass values. The only variations in the response measures should be in the transient portion of the maneuver, as the vehicle is moving into the turn from its original straight and level course.

The results of simulations of the turning circle maneuver showed that the radius of turn (for a fixed rudder deflection) was indeed virtually insensitive to variation of any of the added mass elements. Even in the transient portion of the maneuver, only a few of the 11 significant added mass elements affected the vehicle response.

The results did show that there is a very slight increase in the tactical diameter of the vehicle when the added mass in surge (X_u) was increased, however the increase

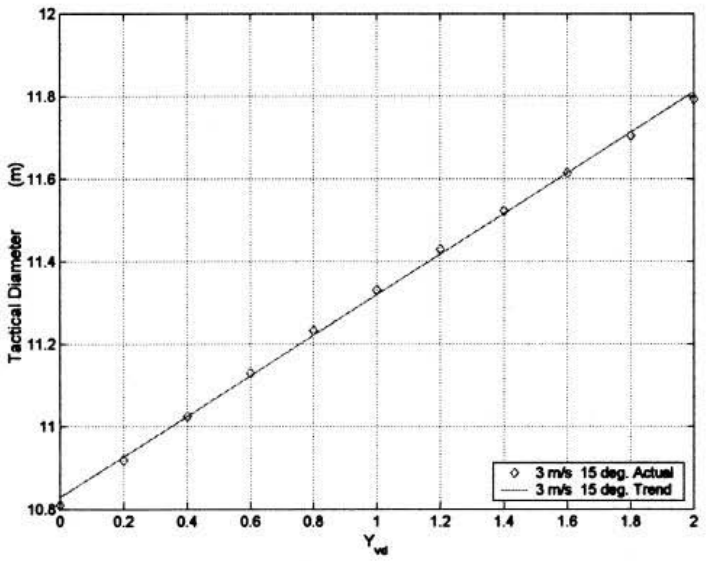

Figure 4-4: Variation of Tactical Diameter with Sway Added Mass, $Y_{\dot{v}}$

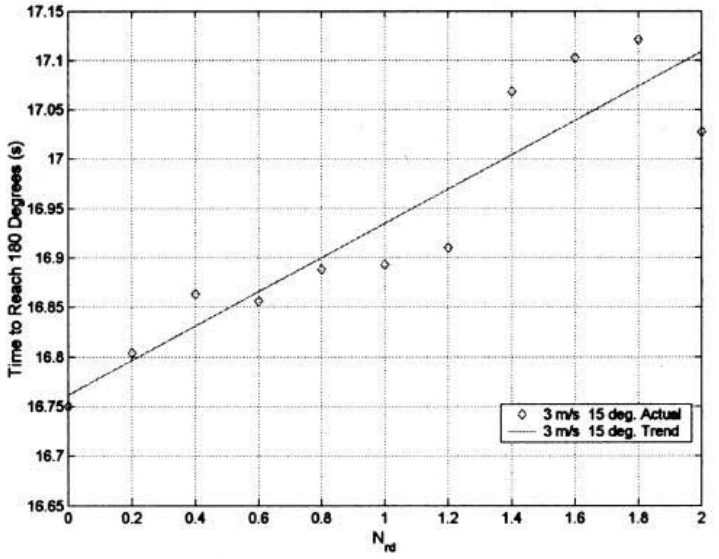

Figure 4-5: Variation of Time to Reach 180° with Yaw Added Mass-Moment of Inertia, $N_{\dot{r}}$

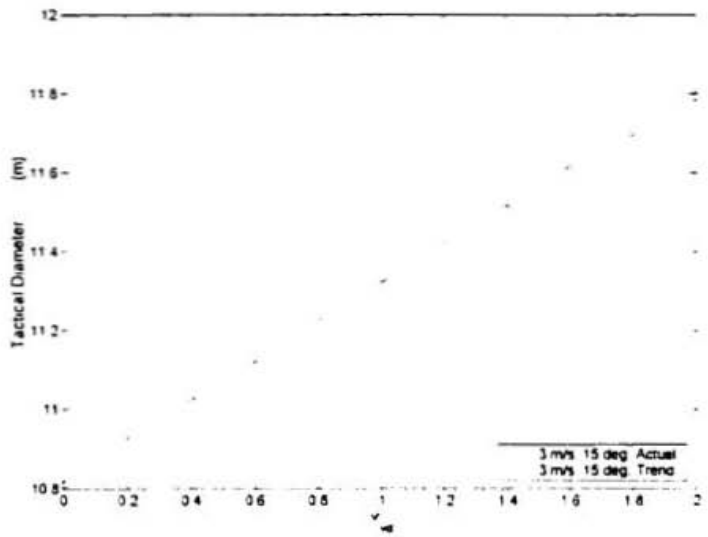

Figure 4-4: Variation of Tactical Diameter with Sway Added Mass, $Y_{\dot{v}}$

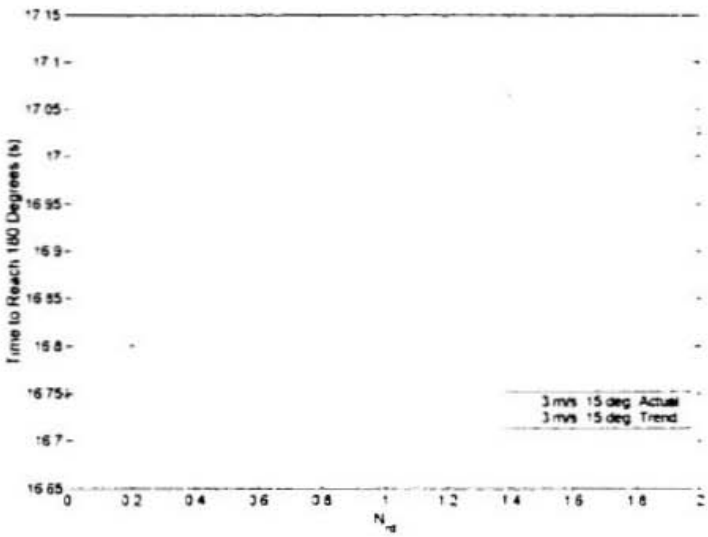

Figure 4-5: Variation of Time to Reach 180° with Yaw Added Mass-Moment of Inertia, $N_{\dot{r}}$

Table 4.1: Maximum Sensitivity of Turning Response Measures to Variations in the Added Mass Coefficients

	Turning Circles			
	Radius of Turn	Advance	Tactical Diameter	Time to Reach 180°
$X_{\dot{u}}$	-0.0001	-0.0015	0.0004	-0.0315
$Y_{\dot{v}}$	-0.0020	0.0237	0.0461	0.0496
$Z_{\dot{w}}$	0.0002	-0.0182	0.0004	-0.0151
$K_{\dot{p}}$	-0.0003	-0.0117	-0.0002	0.0351
$M_{\dot{q}}$	0.0002	-0.0124	0.0004	-0.0260
$N_{\dot{r}}$	0.0007	0.0175	0.0077	0.0260
$X_{\dot{q}}$	0.0005	-0.0190	-0.0002	0.0306
$Y_{\dot{p}}$	-0.0007	0.0174	-0.0020	0.0117
$Y_{\dot{r}}$	-0.0002	0.0237	0.0073	0.0167
$Z_{\dot{q}}$	-0.0002	0.0146	0.0002	0.0311
$K_{\dot{r}}$	0.0006	-0.0137	0.0005	-0.0302

unaffected while the other three measures do show varying degrees of change indicates that the effects of added mass are significant in the transient part of the maneuver (accelerating into the turning circle), but are not significant in the steady turn.

Since the elements represent virtual added inertia, the response measures increase with increase in the added mass element; i.e., as the virtual inertia increases, the vehicle requires more time and space to perform the maneuver (as expected).

The measured responses to turning circles were analyzed using equation (3.4), and the maximum values of S are recorded in Table 4.1 as the measure of sensitivity of that particular response variable to the specific added mass element. Turning circle response is virtually insensitive to variations of added mass coefficients, i.e., the maximum sensitivities determined are all much less then unity.

Zigzags

For zigzag maneuvers, the added masses and added mass-moments of inertia corresponding to the plane of the maneuver are expected to cause variation in the response measures; e.g. increasing $Y_{\dot{v}}$, $N_{\dot{r}}$, and possibly $Y_{\dot{r}}$ causes all the horizontal zigzag re-

sponse measures to increase. These same added masses and added mass-moments of inertia would ideally have no effect on the response measures for vertical zigzags. The added mass elements $Z_{\dot{w}}$, $M_{\dot{q}}$, and Z_q affect the vertical zigzag response in a similar manner, and should not affect the horizontal zigzags. The zigzag maneuver by nature involves constantly varying acceleration in an angular DOF - either yaw in the horizontal plane, or pitch in the vertical plane. Therefore it is reasonable to expect that varying N_r and $M_{\dot{q}}$ will effect the vehicle motion in the applicable plane. The angle of the hull relative to the flow is also changing in a sinusoidal manner in the zigzag maneuver. This means that changes in Y_v will be significant in the horizontal zigzags, and Z_w will be significant in the vertical maneuvers. Variations in the coupling elements Y_r and Z_q may also be influential on the vehicle response.

Increasing the added mass-moments of inertia, N_r and M_q, cause the vehicle to be slower and require more space to accomplish the zigzags, because the vehicle is harder to turn, i.e. it is harder to change its course. Figures 4-7 and 4-8 show that this is indeed the case for N_r, while Figures 4-9 and 4-10 show the same for M_q. The response measures increase linearly as the added mass-moments of inertia increase.

Increasing the added masses, Y_v and Z_w, cause the vehicle to be slowed, but to take less space. The vehicle will not drift as far, and its turning ability is unimpaired. For horizontal zigzags, the temporal measures (period and reach) increase as Y_v increases, but the spatial measures (overshoot angle and width of path) decrease (e.g. see Figures 4-11 and 4-12). For vertical zigzags, the temporal measures also increase linearly as Z_w increases, and the spatial measures decrease (e.g. see Figures 4-13 and 4-14).

Varying Y_r does not affect the response measures significantly in either plane. In the vertical plane maneuvers, there is no asymmetry to cause a sway force or a yaw moment. It is reasonable to expect that the sway-yaw coupling, Y_r, would have an affect on the horizontal zigzags, but the simulations show that the effects are insignificant, causing less than 1% variation in the response measures. This leads

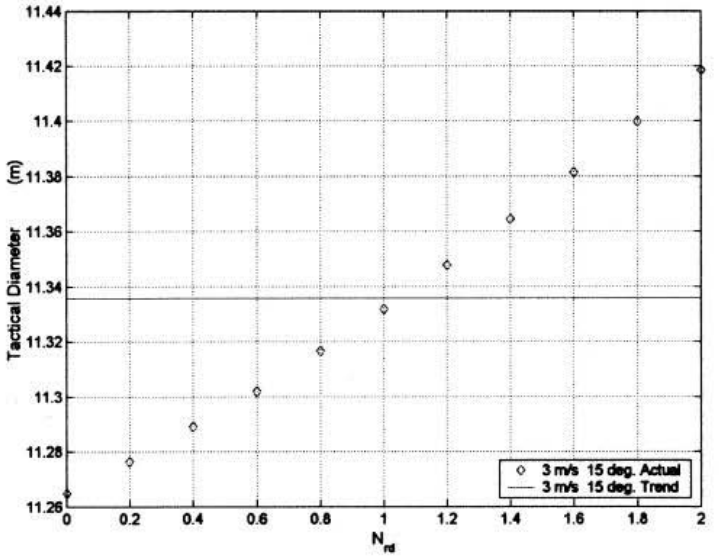

Figure 4-6: Variation of Tactical Diameter with Yaw Added Mass-Moment of Inertia, $N_{\dot{r}}$

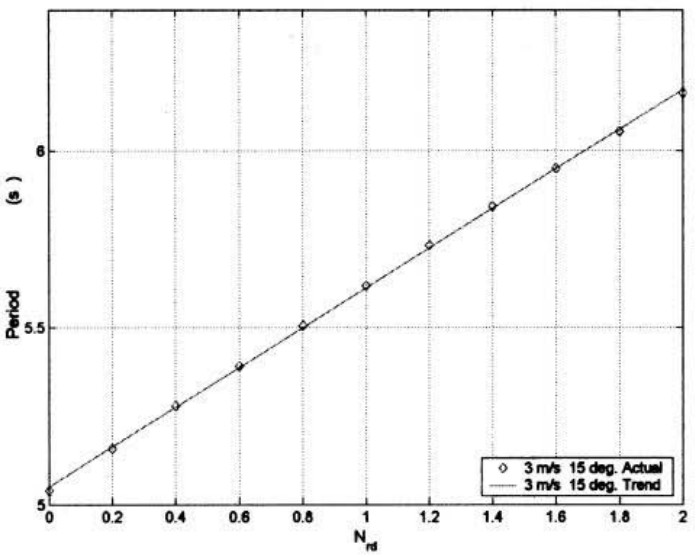

Figure 4-7: Variation of (Horizontal) Zigzag Period with Yaw Added Mass-Moment of Inertia, $N_{\dot{r}}$

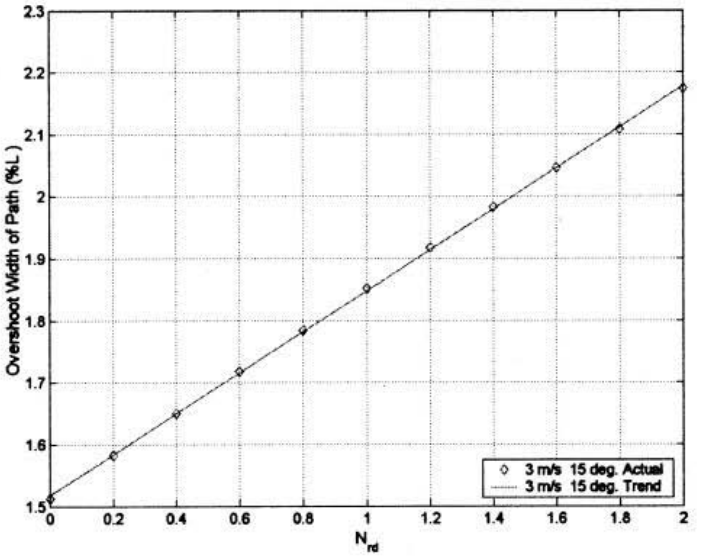

Figure 4-8: Variation of (Horizontal) Zigzag Overshoot Width of Path with Yaw Added Mass-Moment of Inertia, $N_{\dot{r}}$

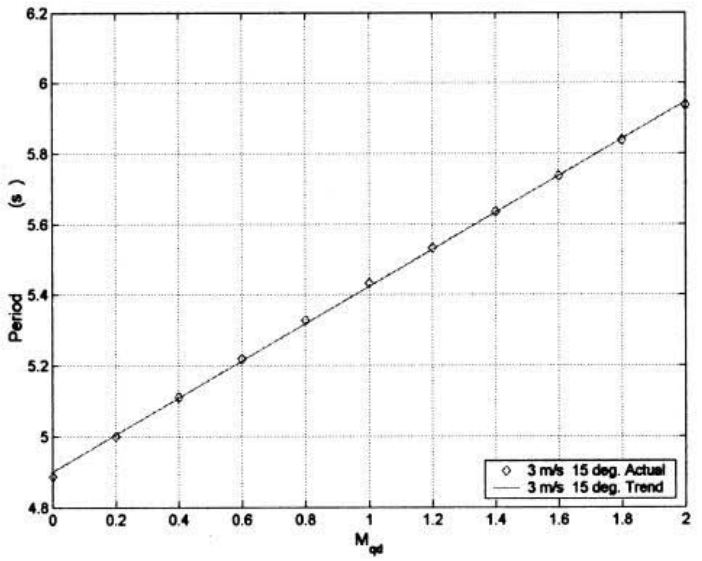

Figure 4-9: Variation of (Vertical) Zigzag Period with Pitch Added Mass-Moment of Inertia, $M_{\dot{q}}$

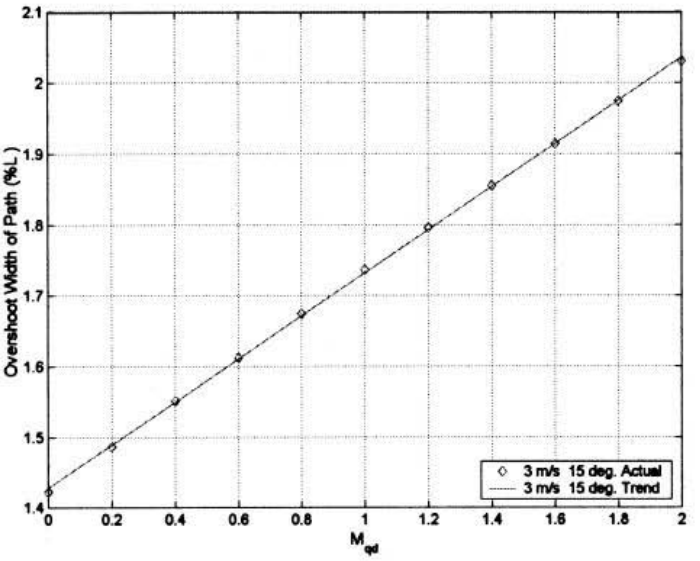

Figure 4-10: Variation of (Vertical) Zigzag Overshoot Width of Path with Pitch Added Mass-Moment of Inertia, $M_{\dot{q}}$

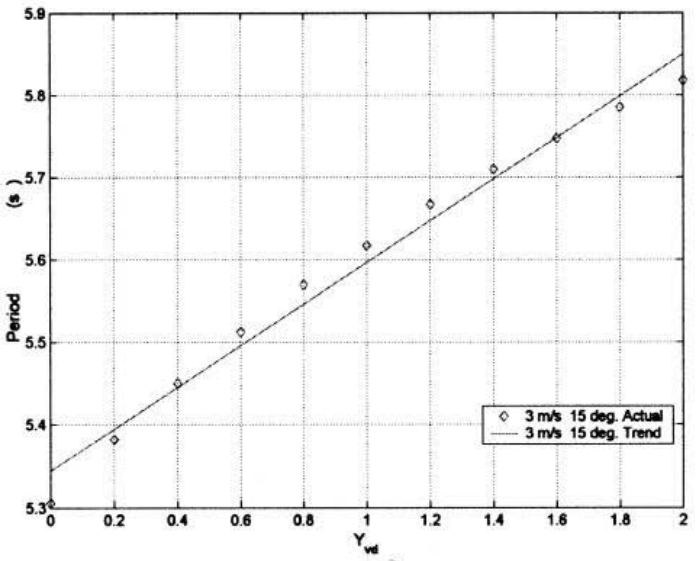

Figure 4-11: Variation of (Horizontal) Zigzag Period with Sway Added Mass, $Y_{\dot{v}}$

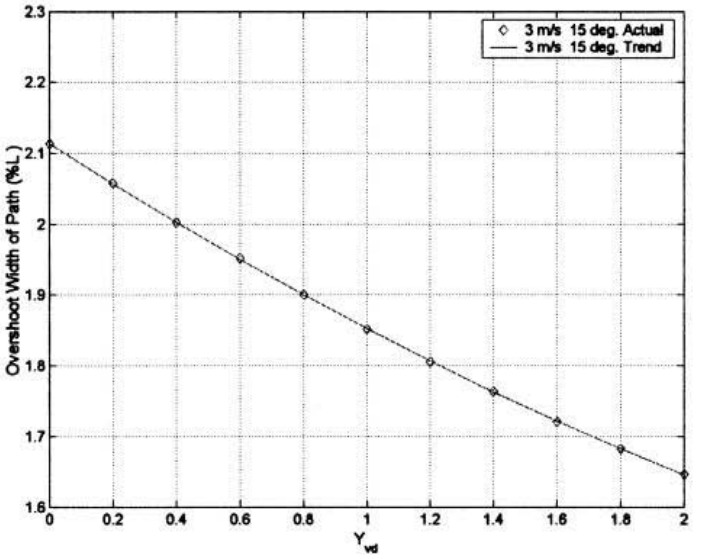

Figure 4-12: Variation of (Horizontal) Zigzag Overshoot Width of Path with Sway Added Mass, $Y_{\dot{v}}$

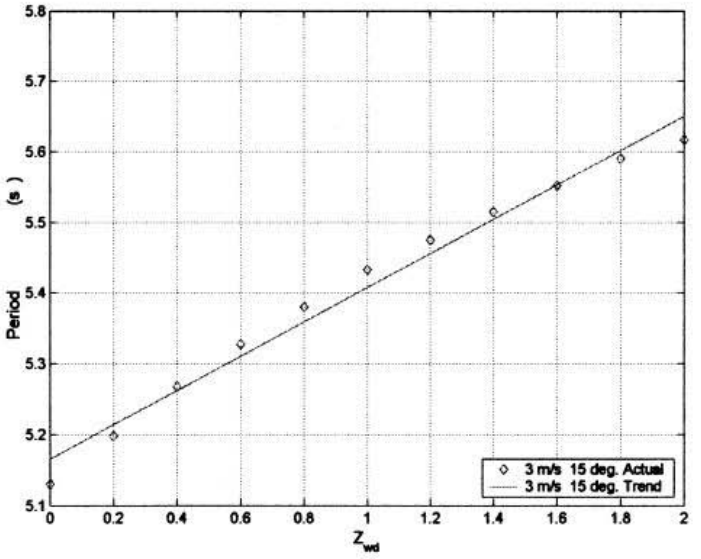

Figure 4-13: Variation of (Vertical) Zigzag Period with Heave Added Mass, $Z_{\dot{w}}$

to the conclusion that the sway added mass, $Y_{\dot{v}}$, and the yaw added mass-moment of inertia, $N_{\dot{r}}$, dominate the response. Both of these latter values are much greater than $Y_{\dot{r}}$. The pitch-heave coupling, $Z_{\dot{q}}$, does affect motion in the vertical plane: all the response measures increase linearly with increasing $Z_{\dot{q}}$. The effects of gravity on the vehicle amplify the importance of $Z_{\dot{q}}$. That is, the moment couple of the gravity-buoyancy forces resists any pitching moment, and is therefore a stabilizing moment in the vertical plane. However, the effect of increasing the heave-pitch coupling added mass is to increase the virtual rotational inertia in the vertical plane, decreasing the effectiveness of the gravity buoyancy couple as a stabilizing moment, and making the vehicle less "stiff", allowing larger motions. Varying $Z_{\dot{q}}$ also has a very slight effect on zigzags in the horizontal plane, causing the spatial measures (overshoot angle and overshoot width-of-path) to increase by a small amount as $Z_{\dot{q}}$ increases. There is a very weak coupling between roll and yaw that, along with the asymmetry about the x-y plane of the vehicle, results in the slight (less than 1%) variation in the spatial measures.

The zigzag response measures (in either the horizontal or the vertical plane) are not significantly sensitive to variations in any of the other coupling terms or the roll added mass-moment of inertia, $K_{\dot{p}}$.

The zigzag maneuver response measures have a greater sensitivity to variations in the added mass coefficients than do the turning circle response measures: zigzag maneuvers provide a better test for transient measures than turning circles do, see Tables 4.2 and 4.3.

For horizontal zigzags, the sway added mass, $Y_{\dot{v}}$, the yaw added mass-moment of inertia, $N_{\dot{r}}$, and the sway-yaw coupling, $Y_{\dot{r}}$, affect the vehicle response, but a large variation of any of these would only change the response by a small amount: e.g. a positive 10% change in C-SCOUT's $N_{\dot{r}}$ would increase the overshoot angle by 3.1%.

For vertical zigzags, the heave added mass, $Z_{\dot{w}}$, the pitch added mass-moment of inertia, $M_{\dot{q}}$, and the heave-pitch coupling, $Z_{\dot{q}}$, affect the vehicle response. Like the

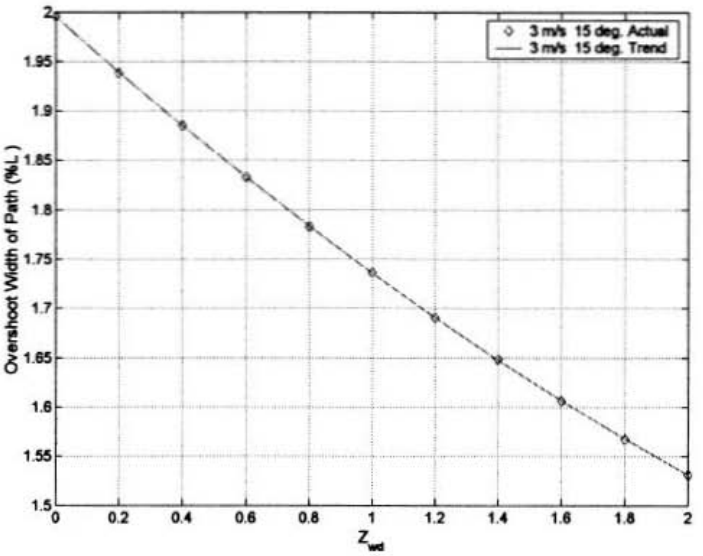

Figure 4-14: Variation of (Vertical) Zigzag Overshoot Width of Path with Heave Added Mass, $Z_{\dot{w}}$

Table 4.2: Maximum Sensitivity of Horizontal Zigzag Response Measures to Variations in the Added Mass Coefficients

	Horizontal Zigzags			
			Overshoot	
	Period	Reach	Angle	Pathwidth
$X_{\dot{u}}$	-0.0022	0.0000	-0.0001	-0.0002
$Y_{\dot{v}}$	0.0556	0.0432	-0.2104	-0.1411
$Z_{\dot{w}}$	0.0000	0.0000	-0.0000	-0.0000
$K_{\dot{p}}$	0.0000	0.0000	0.0000	-0.0000
$M_{\dot{q}}$	0.0000	0.0000	-0.0000	-0.0000
$N_{\dot{r}}$	0.1028	0.0907	0.3098	0.1832
$X_{\dot{q}}$	0.0000	0.0000	0.0000	0.0000
$Y_{\dot{p}}$	0.0000	0.0000	-0.0002	0.0002
$Y_{\dot{r}}$	0.0423	0.0324	0.1027	0.0545
$Z_{\dot{q}}$	0.0000	0.0000	-0.0000	-0.0000
$K_{\dot{r}}$	0.0000	0.0000	0.0001	0.0000

Table 4.3: Maximum Sensitivity of Vertical Zigzag Response Measures to Variations in the Added Mass Coefficients

	Vertical Zigzags			
			Overshoot	
	Period	Reach	Angle	Pathwidth
$X_{\dot{u}}$	-0.0012	0.0000	-0.0001	0.0002
$Y_{\dot{v}}$	0.0000	0.0000	0.0000	0.0000
$Z_{\dot{w}}$	0.0557	0.0428	-0.1699	-0.1494
$K_{\dot{p}}$	0.0000	0.0000	0.0000	0.0000
$M_{\dot{q}}$	0.1003	0.0878	0.2801	0.1808
$N_{\dot{r}}$	0.0000	0.0000	0.0000	0.0000
$X_{\dot{q}}$	0.0000	0.0000	0.0000	-0.0000
$Y_{\dot{p}}$	0.0000	0.0000	0.0000	0.0000
$Y_{\dot{r}}$	0.0000	0.0000	0.0000	0.0000
$Z_{\dot{q}}$	0.0391	0.0321	0.0303	0.0491
$K_{\dot{r}}$	0.0000	0.0000	0.0000	0.0000

horizontal plane elements, the sensitivity of vehicle response to variations in these vertical plane elements are small: e.g. a positive 10% change in C-SCOUT's $M_{\dot{q}}$ would increase the overshoot angle by only 2.8%.

Design Implications

The foregoing results confirm the intuitive design criteria that the added mass properties of the vehicle should be reduced as much as possible. Although they have little effect on the steady state motion they can have an effect on the transient motions. The physical mass and inertial properties of the vehicle are:

$$\mathbf{M}_R = \begin{bmatrix} 314.7 & 0 & 0 & 0 & 0 & 0 \\ 0 & 314.7 & 0 & 0 & 0 & 0 \\ 0 & 0 & 314.7 & 0 & 0 & 0 \\ 0 & 0 & 0 & 2.2 & 0 & 0.8 \\ 0 & 0 & 0 & 0 & 152.2 & 0 \\ 0 & 0 & 0 & 0.8 & 0 & 151.7 \end{bmatrix} \tag{4.2}$$

while the virtual added masses, moments of inertia, and coupling terms are:

$$\mathbf{M}_V = \begin{bmatrix} -2.53 & 0 & 0 & 0 & 0.03 & 0 \\ 0 & -164.49 & 0 & -1.80 & 0 & 13.88 \\ 0 & 0 & -164.49 & 0 & -13.88 & 0 \\ 0 & -1.80 & 0 & -3.60 & 0 & 0.14 \\ 0.03 & 0 & -13.88 & 0 & -74.83 & 0 \\ 0 & 13.88 & 0 & 0.14 & 0 & -74.83 \end{bmatrix} \tag{4.3}$$

The negative signs are because the pressure forces on the hull would tend to retard the vehicle motion. The real mass, $\mathbf{M}_R$, and the virtual added mass, $\mathbf{M}_V$, are originally on opposite sides of the equation: one is a rigid body property, while the other is related to the (pressure) force experienced by the vehicle. When the virtual mass is "subtracted" from the real mass, the net effect is greater apparent mass in most DOF, hence the virtual mass is "added mass".

$$\mathbf{M}_A = \mathbf{M}_R - \mathbf{M}_V = \begin{bmatrix} 317.23 & 0 & 0 & 0 & -0.03 & 0 \\ 0 & 479.19 & 0 & 1.80 & 0 & -13.88 \\ 0 & 0 & 479.19 & 0 & 13.88 & 0 \\ 0 & 1.80 & 0 & 5.80 & 0 & 0.66 \\ -0.03 & 0 & 13.88 & 0 & 227.03 & 0 \\ 0 & -13.88 & 0 & 0.66 & 0 & 226.53 \end{bmatrix} \tag{4.4}$$

Comparing the three matrices (see Table 4.4) it can be seen that the surge added mass derivative makes up only a tiny fraction of the inertial effect in the surge DOF, therefore even doubling it should not affect the vehicle response. This is confirmed by the very low sensitivity values in Tables 4.1, 4.2, and 4.3, and by the simulation data (e.g. Figure 4-3). The small magnitude of the surge derivative is due to the relatively small cross-sectional area of the hull of the AUV.

In comparison, the planform area of the vehicle is much larger, and this is reflected

Table 4.4: Magnitude and Sign Effects of Added Mass Derivatives

	Order of Magnitude			Percent of Apparent Mass		Effective Sign of the Virtual Mass
	Real Mass	Virtual Mass	Apparent Mass	Real	Virtual	
$X_{\dot{u}}$	10^2	10^0	10^2	99.2	0.8	+
$Y_{\dot{v}}$	10^2	10^2	10^2	65.7	34.3	+
$Z_{\dot{w}}$	10^2	10^2	10^2	65.7	34.3	+
$K_{\dot{p}}$	10^0	10^0	10^1	37.9	62.1	+
$M_{\dot{q}}$	10^2	10^2	10^2	67.0	33.0	+
$N_{\dot{r}}$	10^2	10^2	10^2	67.0	33.0	+
$X_{\dot{q}}$	0	10^{-2}	10^{-2}	0.0	100.0	−
$Y_{\dot{p}}$	0	10^0	10^0	0.0	100.0	+
$Y_{\dot{r}}$	0	10^1	10^1	0.0	100.0	−
$Z_{\dot{q}}$	0	10^1	10^1	0.0	100.0	+
$K_{\dot{r}}$	10^0	10^{-1}	10^0	121.6	21.6	−

in the contribution the sway and heave added masses make to the apparent mass[4] of the AUV (34% each in their respective DOF), as well as in the contribution the pitch and yaw added mass-moments of inertia make to the vehicle's apparent mass (33% each in their respective DOF). Because the effects of added mass are associated with vehicle accelerations, even these significant contributions are not of major importance to the steady state motions, and variation of these derivatives does not really affect the response of the vehicle in turning maneuvers (see Table 4.1). The small sensitivity to variation in added mass occurs only in the advance phase of the maneuver where the vehicle transitions from straight ahead into the turn. In the zigzag maneuvers, where the vehicle experiences accelerations throughout the maneuver, the contributions of the added mass derivatives are manifested. For example, varying $N_{\dot{r}}$ by 10% will cause the response measures in the horizontal zigzag to vary by as much as 3.1% (see Table 4.2). Varying $M_{\dot{q}}$ by 10% will cause the response measures in the vertical zigzag to vary by as much as 2.8% (see Table 4.3).

[4]The apparent mass is the sum of the real (physical) mass of the vehicle and the virtual added mass; i.e., what the vehicle mass appears to be in terms of the force necessary to accelerate the vehicle.

The added mass-moment of inertia in the roll DOF, $K_{\dot{p}}$, is actually larger than the real moment of inertia about the surge axis, but even the sum of the two is a small magnitude, and has little effect on the vehicle response in turning circles (see Table 4.1), and next to no effect on the vehicle response in zigzags (see Tables 4.2 and 4.3).

The coupling derivatives, X_q and Y_p, are so small for C-SCOUT as to be of little consequence to the vehicle response.

The Y_r and Z_q coupling derivatives are a result of the fore-aft asymmetry, particularly the control surfaces on the aft end of the parallel mid-body. If there is a sway force pushing the vehicle to the starboard, the fluid force on the control planes will cause a positive yaw moment about the heave axis, in effect decreasing the inertia in yaw, hence the negative sign in Table 4.4. If there is a heave force pushing the vehicle down, the fluid force on the after control planes will cause a negative pitching moment, in effect increasing the inertia in pitch. These two derivatives are not a major influence on the vehicle response in turning circles: e.g. a 100% change in Z_q will only change the advance by about 2% (see Table 4.1). Tables 4.2 and 4.3 show that variation of these derivatives do effect the response of the vehicle in horizontal and vertical zigzag maneuvers.

The K_r coupling derivative is a result of asymmetry about the x-y plane, particularly the uneven offset of the upper and lower control planes relative to the center of mass of the vehicle. The center of pressure of the upper fin is further from the roll axis (which is through the center of gravity according to the chosen body reference frame) than the center of pressure of the lower fin. When the vehicle is subjected to a positive roll moment, the fluid force on the upper fin is greater than that on the lower fin. The net result is a force that causes a positive yaw moment on the vehicle, in effect reducing the yaw inertia. The combined effects of the x-z product of inertia and the roll-yaw coupling added mass-moment of inertia have little effect on the response of the vehicle in turning circle or in zigzags.

In terms of vehicle design, it is useful to reduce the influence of the added mass derivatives as much as possible. This can be accomplished by streamlining the vehicle and reducing the size of the appendages. Reducing the overall size of the vehicle will not reduce the relative contribution of the added mass on the vehicle response, as that contribution will still be in the same proportion to the real mass.

Three of the coupling derivatives actually reduce the inertia of the vehicle, K_r, X_q, and Y_r. The latter of these three can be increased by moving the center of mass forward in the vehicle, but this would mean increasing the Z_q coupling derivative as well, increasing the inertia in heave-pitch. The two former derivatives can be increased by moving the center of gravity down in the vehicle, which would also make the vehicle more stable in roll and pitch. Moving the center of mass down also increases the effect of Y_p meaning the vehicle will roll more with application of a side force. These three derivatives (K_r, X_q, and Y_r) do not form sufficient grounds for moving the center of mass. The design goal should therefore be to reduce all the added mass derivatives.

4.3.4 Lift and Drag Coefficients

Expected Results

The lift and drag coefficients are important during the steady motions, since they are used to calculate the "static" forces of lift and drag. The lift and drag coefficients are empirically derived dimensionless numbers. Lift and drag on the hull are applied at the center of effort (CE), well forward of the center of mass of the vehicle, and thus the lift force produces a moment that tends to destabilize the vehicle. That is, if the vehicle is perturbed from a straight and level path, the lift on the forward-moving hull will cause the vehicle to continue to turn even after the disturbing force is removed. The lift and drag on the (after) fins are applied well aft of the center of mass, at the center of pressure (CP) of each control plane, and, therefore, the lift force on the fins tends to stabilize the vehicle. That is, if the vehicle is perturbed from a straight and level path, the lift on the after control surfaces will cause the vehicle to return to its

original straight and level path. Commanding a change of heading or pitch attitude is accomplished by deflecting the control planes. Changing the angle of deflection of the control planes initially produces a moment on the vehicle, initiating a turn. The lift force on the hull will tend to cause the vehicle to keep turning in that direction. As the turn progresses, the moment caused by the deflected control planes decreases until the moment actually changes sign, i.e. the vehicle has turned past the point where the lift on the fin is zero, and now the fin lift starts to work against the hull lift. The vehicle hull will continue to yaw until the moment caused by the hull lift and the moment caused by the control planes are in dynamic balance. This balance will occur at a specific angle of drift, the angle between the hull and the fluid flow. The hull lift is a function of the drift angle of the vehicle. The control plane lift is a function of the drift angle and the deflection angle of the fins, the sum of these two being the angle of attack of the control plane.

Because the center of effort of the hull lift and drag is well forward of the center of mass of the vehicle, as the lift on the hull increases, it is expected that the vehicle will turn quicker and in a shorter distance. It is also reasonable to expect that the time and space required to reverse the turn will be greater as the hull lift coefficient is increased, unless greater control effort is expended; i.e. the vehicle requires more control authority as the hull lift increases. The temporal measures also increase with the increase in the hull drag coefficient, since drag slows the vehicle down. The increased drag, however, means less distance is required for the turning maneuver, since the vehicle achieves full actuator response in a shorter spatial distance. Hull drag may effect the ability to reverse the turn, causing an increase in the required space for the zigzag maneuver.

Increasing the lift on the control planes is equivalent to increasing the control authority of the vehicle. This causes the vehicle to respond quicker to a turn command and it is easier to reverse the turn, meaning the temporal and spatial requirements are less as the fin lift coefficient increases. Drag on the control planes also tends to slow

the vehicle, increasing the time needed for the maneuvers. The spatial requirements remain virtually constant or decrease slightly with increasing fin drag. However, at small fin-deflection angles, the drag on the fins represents a small proportion of the total drag on the vehicle.

For both the hull and the control planes, the lift and drag coefficients were varied from 60% to 200% of the nominal values. Again, simulations at a representative surge speed and control plane deflection angle, varying each of the coefficients, were performed.

Turning Circles

All the response measures change with variations in the hull lift coefficient. If up to five percent tolerance is allowed for in the trend lines for the simulation results (see Section 4.3.2), the radius of turn (see Figure 4-15) and the tactical diameter vary as the inverse of the square of the hull lift coefficient, while the advance and time to reach 180° vary linearly (again, when five percent tolerance applied) as the inverse of the hull lift coefficient. If only one percent error is allowed in the simulation results, then the order of each of these relationships increases by one (e.g. the radius of turn varies as the inverse of the cube of the hull lift coefficient).

The radius of turn varies inversely (linearly) with the coefficient of drag of the hull (see Figure 4-16), as does the tactical diameter and the advance, while the time to reach 180° varies directly (linearly) as the hull drag coefficient (see Figure 4-17).

The radius of turn varies directly as the fourth root of the fin lift coefficient (within 1% - see Figure 4-18). The tactical diameter varies as the cube root. The time to reach 180° varies as the square root of the fin lift coefficient, and the advance varies linearly with the fin lift coefficient (see Figure 4-19). When the trend line tolerance is allowed to be up to 5%, the radius of turn and the tactical diameter vary as the square root of the fin lift; the time to reach 180° varies linearly; and the advance is constant over the range of variations of $C_{L_{Fins}}$.

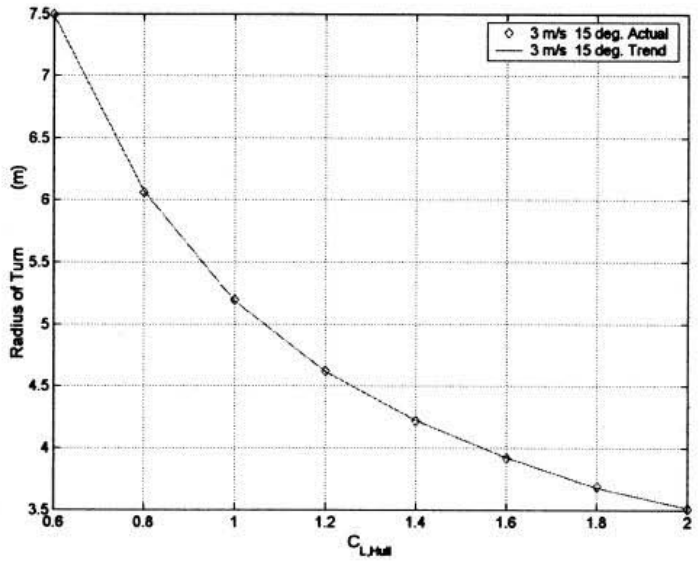

Figure 4-15: Variation of Radius of Turn with Hull Lift Coefficient

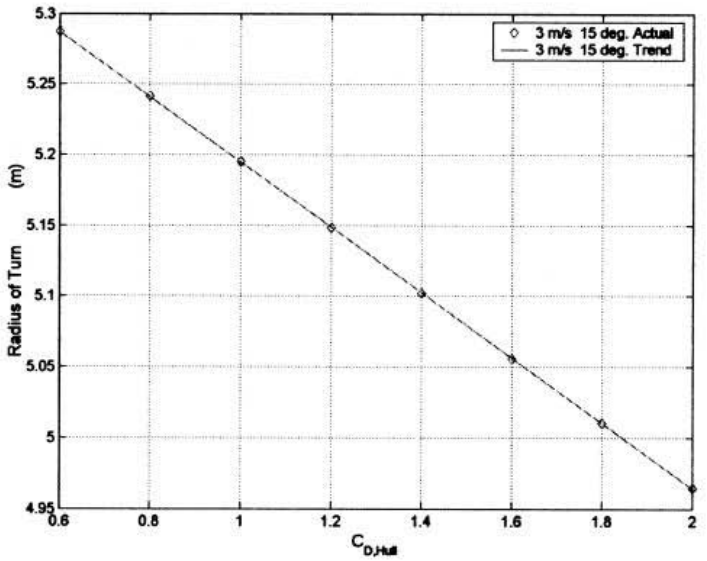

Figure 4-16: Variation of Radius of Turn with Hull Drag Coefficient

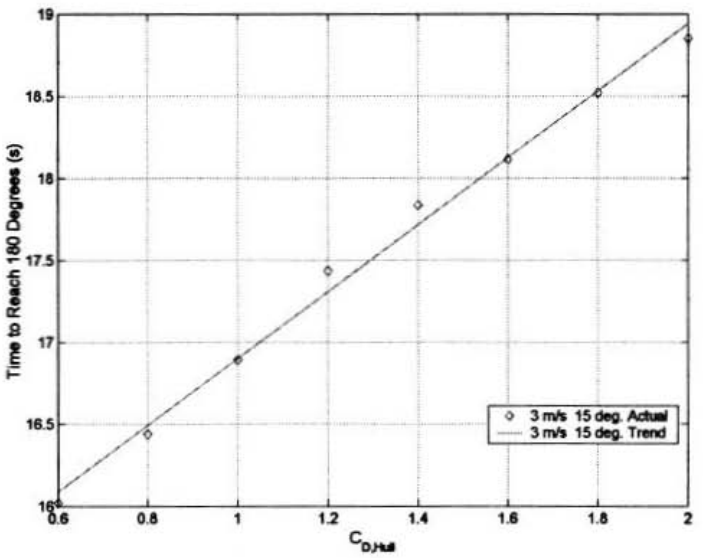

Figure 4-17: Variation of Time to Reach 180° with Hull Drag Coefficient

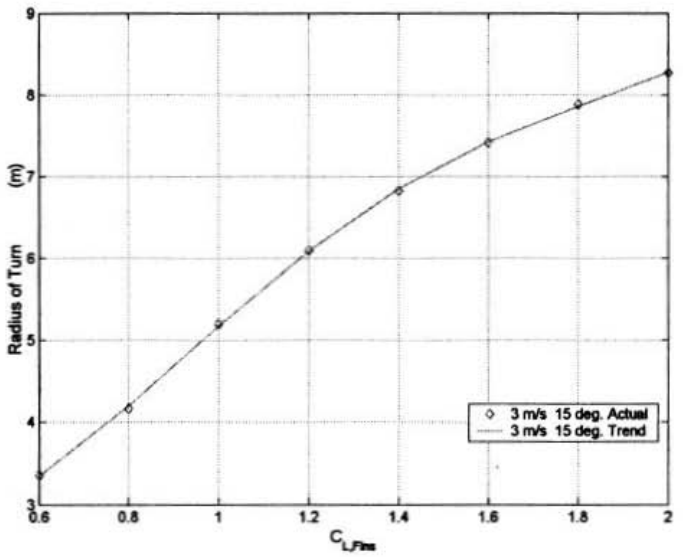

Figure 4-18: Variation of Radius of Turn with Fin Lift Coefficient

Table 4.5: Maximum Sensitivity of Turning Response Measures to Variations in the Lift and Drag Coefficients

	Turning Circles			
	Radius of Turn	Advance	Tactical Diameter	Time to Reach 180°
$C_{L_{Hull}}$	-1.1062	-0.0998	-0.9105	-0.2838
$C_{D_{Hull}}$	-0.0450	-0.1721	-0.0442	0.1607
$C_{L_{Fins}}$	0.9879	0.0251	0.6295	0.1884
$C_{D_{Fins}}$	0.0070	-0.0171	0.0045	0.0508

The radius of turn is not significantly affected by varying the fin drag coefficient, but the advance decreases linearly with increasing fin drag coefficient (see Figure 4-20) and the time to reach 180° increases linearly with increasing fin drag coefficient (see Figure 4-21). Even these two measures are practically constant if 5% tolerance is allowed when calculating the trend line equations.

The responses in turning circles are sensitive to variations in the lift coefficients on the hull and fins, as may be expected since the lift and drag forces are functions of velocity and not acceleration. This is seen in the maximum sensitivity values for radius of turn (see Table 4.5). For both the hull and fins, changes in the lift coefficients affect the response measures more than changes in the drag coefficients do. Increases in the hull lift coefficients tend to cause decreases in the radius of turn and the advance, as is evidenced by the negative sign preceding the maximum sensitivity value. This is a result of the center of effort (the point of application of the hull lift and drag forces) being forward of the center of gravity. An increase in lift on the hull will cause the vehicle to turn more abruptly, since the moment caused by the force is in the direction of the turn. The drag force on the hull, on the other hand, tends to slow down the vehicle, meaning the turn is accomplished in a shorter distance. The lift and drag forces on the fins tend to stabilize the vehicle after the turn is initiated, since these forces are applied at the control plane center of pressure, well aft of the vehicle center of gravity. Therefore, increasing the lift on the fins will cause a larger radius of turn and advance. It is therefore evident that decreasing the

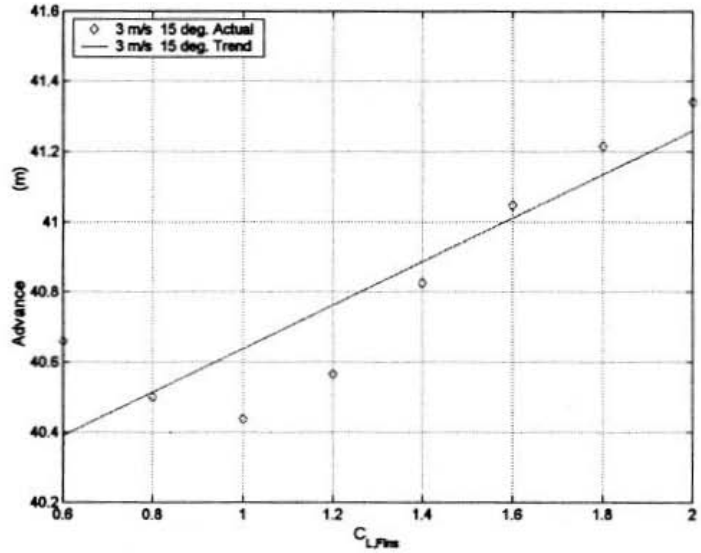

Figure 4-19: Variation of Advance with Fin Lift Coefficient

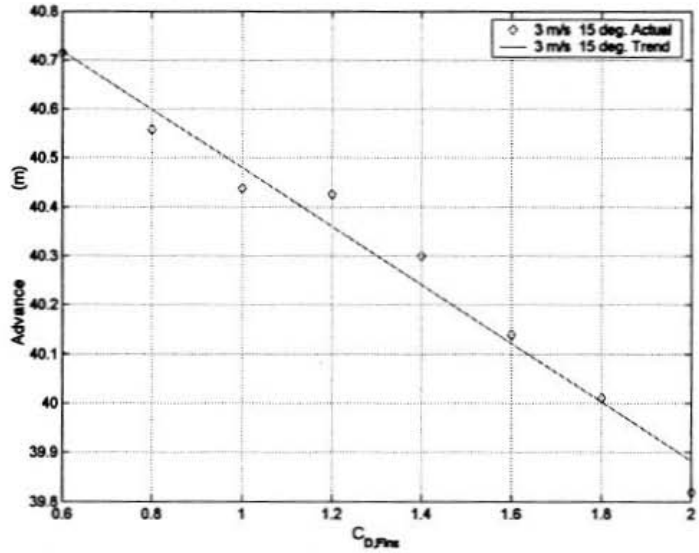

Figure 4-20: Variation of Advance with Fin Drag Coefficient

lift on the fins will cause a smaller radius of turn. However, this must have a limit as zero lift does not mean the vehicle spins on its axis. Rather there is a point when the lift on the fins is no longer effective as an agent for initiating the turn, and the vehicle will not turn at all. Drag on the fins, like drag on the hull, slows the vehicle down, but to a lesser extent. Thus the vehicle advance is reduced but the turning radius is increased with an increase in the drag coefficient. The drag coefficients for both the hull and fins affect the advance more than the radius of turn.

Zigzags

The vehicle response in horizontal zigzags was very similar to that in vertical zigzags, both qualitatively and quantitatively. For maneuvers in both planes, the period of response (τ) varied nonlinearly with variations in the hull lift and the fin lift coefficients, and linearly with variations in the hull drag and fin drag coefficients. For changes in the hull lift coefficient, the period, the overshoot angle and the overshoot width of path increased as the square root of the hull lift coefficient (e.g. see Figure 4-22), while the reach measure decreased linearly with increase in the lift coefficient (see Figure 4-23). The response measures in zigzags generally increase linearly with increasing hull drag (e.g. see Figure 4-24), though the spatial measures of overshoot angle and overshoot width of path reduce to constants when up to 5% tolerance in the trend lines for the simulation data is allowed. This would indicate that the major effect of hull drag is to slow down the vehicle (as expected), but that drag has only a small effect on the actual space required for the maneuver. The obvious result is that the hull should be designed with the minimum drag possible.

When 5% tolerance in the trend lines is allowed, the period varies as the inverse of the cube of the fin lift coefficient, while the reach becomes (inversely) linear. The overshoot width of path varies with the inverse of the fin lift coefficient to the fourth power, and the overshoot angle varies as the inverse of the coefficient to the fifth power. These high order polynomials may be artefacts of the integration, showing

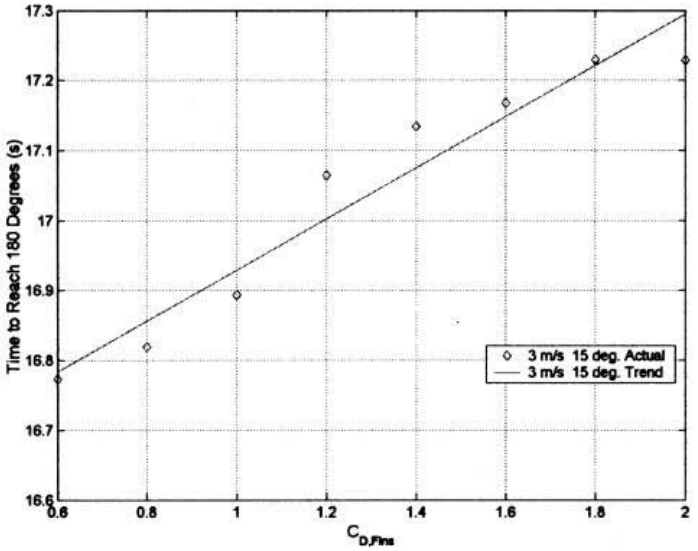

Figure 4-21: Variation of Time to Reach 180° with Fin Drag Coefficient

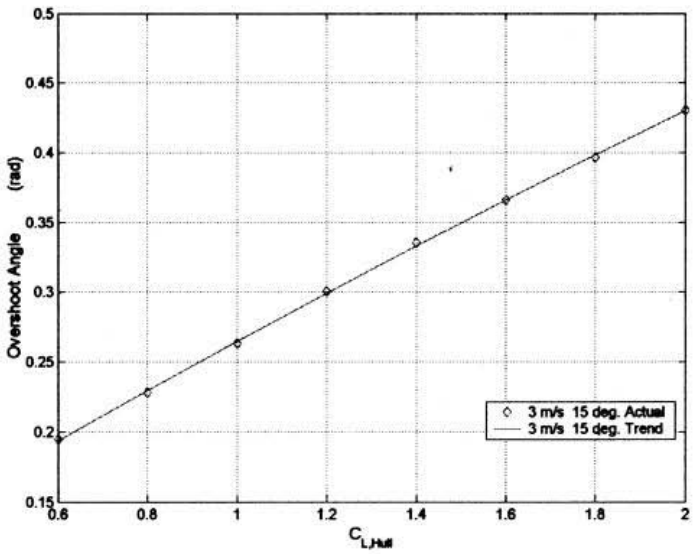

Figure 4-22: Variation of (Horizontal) Zigzag Overshoot Angle with Hull Lift Coefficient

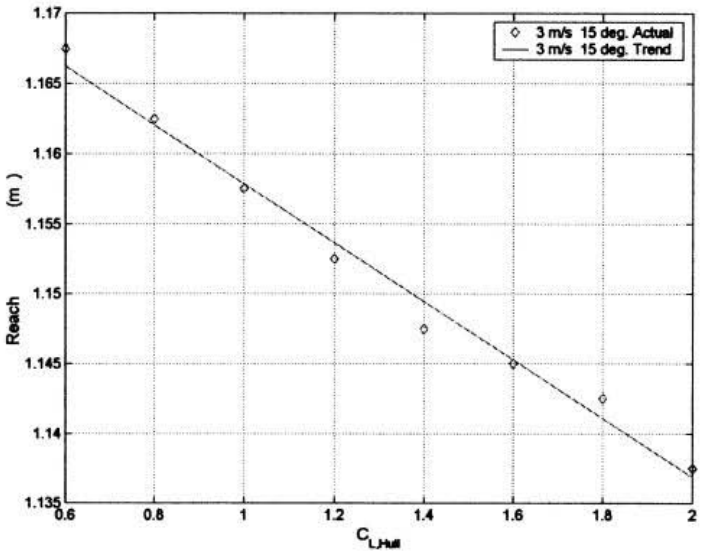

Figure 4-23: Variation of (Horizontal) Zigzag Reach with Hull Lift Coefficient

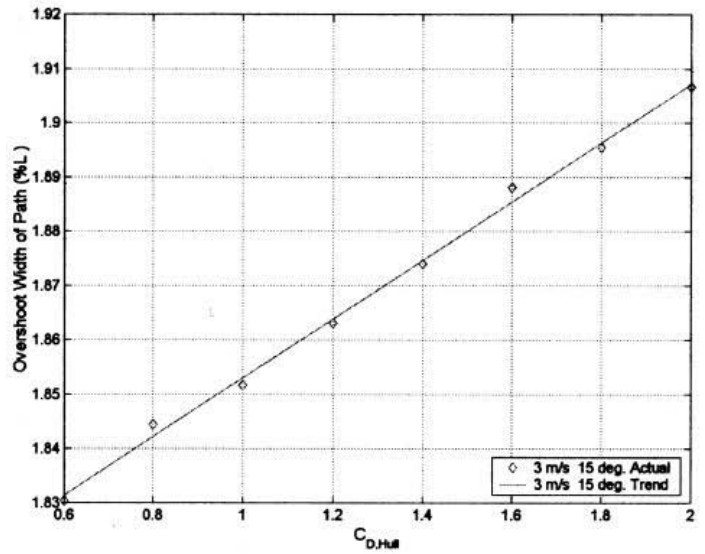

Figure 4-24: Variation of (Horizontal) Zigzag Overshoot Width of Path with Hull Drag Coefficient

Table 4.6: Maximum Sensitivity of Horizontal Zigzag Response Measures to Variations in the Lift and Drag Coefficients

	Horizontal Zigzags			
			Overshoot	
	Period	Reach	Angle	Pathwidth
$C_{\mathcal{L}_{Hull}}$	0.2158	-0.0216	0.7104	0.4896
$C_{\mathcal{D}_{Hull}}$	0.3861	0.3456	0.1221	0.0328
$C_{\mathcal{L}_{Fins}}$	-1.4976	-0.4374	-3.4213	-2.4767
$C_{\mathcal{D}_{Fins}}$	0.0467	0.0432	-0.0397	-0.0087

Table 4.7: Maximum Sensitivity of Vertical Zigzag Response Measures to Variations in the Lift and Drag Coefficients

	Vertical Zigzags			
			Overshoot	
	Period	Reach	Angle	Pathwidth
$C_{\mathcal{L}_{Hull}}$	0.2151	-0.0268	0.6813	0.5079
$C_{\mathcal{D}_{Hull}}$	0.3670	0.3480	0.0304	-0.0175
$C_{\mathcal{L}_{Fins}}$	-1.2540	-0.4443	-3.0019	-1.8472
$C_{\mathcal{D}_{Fins}}$	0.0414	0.0428	-0.0291	-0.0101

up as uncertainty in the results, rather than actual trends in the data. Both the overshoot measures appear to be approximately inversely proportional to the square of the lift coefficient when the data is viewed by eye (see Figure 4-25 for example). The period (Figure 4-26) and the reach increase linearly as the fin drag coefficient is increased, while the overshoot angle tends to decrease with increasing $C_{\mathcal{D}_{Fins}}$, and the overshoot width of path is not significantly affected.

The maximum sensitivity values for the horizontal zigzag maneuvers and the vertical zigzag maneuvers are very similar, differing only in the signs of some of the values near zero (see Tables 4.6 and 4.7). The values of maximum sensitivity indicate that it is important to know the lift coefficients accurately, since a 10% variation in $C_{\mathcal{L}_{Hull}}$ can mean an 7.1% change in the overshoot angle (Table 4.6) and a 5.1% change in the overshoot width of path (Table 4.7). This is even more evident in the case of the fin lift coefficient, $C_{\mathcal{L}_{Fins}}$, where a 10% increase can result in a 24.8% decrease in the overshoot width of path and a 34.2% change in the overshoot angle (Table 4.6).

The hull drag coefficient must also be known with some accuracy. while the fin drag coefficient can be much more approximate.

Design Implications

In steady state maneuvers such as the turning circle. it is beneficial if the hull lift is large as this produces a tighter turn. Increased hull drag also reduces the radius of turn. but at the expense of time (and energy expended) to complete the maneuver. In turning circles. the less the lift on the after control fins. the tighter the turn. Like the hull. only on a smaller scale. increasing the drag of the control planes will tighten the turn at the expense of time and energy. The contradictory nature of these relations for the fins suggests that there is an optimal size for the control surface. The optimal size would also be a function of the hull lift and drag characteristics and the placement of the control planes on the hull.

In zigzag maneuvers. increasing the hull lift causes greater overshoots. and generally poorer performance. Increasing the hull drag increases the time taken to accomplish the maneuver. but has little (less than 1%) effect on the overshoot angle and width of path. Increasing the fin lift reduces the time and space required for the maneuver. Increasing the fin drag increases the time required. but has little effect on the spatial requirements. It should be noted that lift and drag are related so that increasing one generally means increasing the other. Clearly. the design must seek the optimal balance between the lift and drag on the fin that will allow the vehicle to meet its performance criteria while minimizing the energy expended in doing so.

4.3.5 Center of Effort (Hull) and Center of Pressure (Control Planes)

The center of pressure (CP) of the control plane is the point at which the lift and drag forces acting on the plane are assumed to act. For angles of attack below stall. this point is typically located very near the $c/4$ (quarter-chord) point of the section

of the control plane (for NACA 00XX symmetric sections). The C-SCOUT control planes are designed such that the locus of $c/4$ points along the span of each plane is perpendicular to the hull. Variation of the location of the center of pressure along the chord and the span is included in the study for completeness.

The center of effort (CE) of the hull is the assumed point of application of the hull lift and drag forces, and is varied along x-axis. "Center of effort" rather than "center of pressure" is used for the hull to make it easier to determine which component, the hull or a control plane, is being addressed. The location of the center of effort is not easily determined, as it is dependent on dynamics of the fluid flow. The location will move aftward along the axis of rotation of the hull as the angle of attack of the hull increases. In addition, the point of transition from laminar to turbulent flow is important, and vortex shedding and after-body separation are also significant factors in determining the location of the center of effort. Variation of the location is an important issue for accurate modeling of underwater vehicles using lift and drag equations. In the model used in the present study, the center of effort is fixed at the nose of the vehicle since the vehicle motion is dominated by the forward (surge) velocity, such that the effective angle of attack between the hull and the fluid flow is small.

Expected Results

As the location of the CE increases (CE moves forward), there is a greater moment arm (about the center of mass) applied to the hull lift force. This will result in a greater drift angle, β, in turns and an increased need for control authority (the effort needed to achieve commanded states), meaning that it will be harder to reverse a turn. There should be little effect on the drag of the vehicle.

Variation of CP outward along the span of the control plane should have no significant effect on the vehicle response. Variation aftward along the chord, however, will effectively mean a slight increase in the moment arm for the fin lift force, resulting

in greater control authority. This will make it easier to reverse a turn, and the vehicle should respond more quickly and in a shorter distance. It will also result in a smaller drift angle in steady turns. These same effects could be more readily achieved by moving the whole control plane aft along the vehicle.

Turning Circles

The radius of turn decreases with an increase of the distance from the center of mass to the center of effort, but that there is a minimum at about the nominal location of CE, which is at the nose of the vehicle. When the center of effort is located beyond the nose of the vehicle, the radius of turn increases again (see Figure 4-27). The variations of the advance and time to reach 180° increase nonlinearly as the distance from the center of mass to the CE increases (e.g. see Figure 4-28).

As the center of pressure of the control plane moves aft along the chord, there is a change in the moment arm along the longitudinal axis of the vehicle, so there should be some effect of the variation on the response measures. In turning circle maneuvers, the radius of turn, the advance, and the time to reach 180° all increase with movement aft of the center of pressure (e.g. see Figure 4-29). It is expected that they should increase, since movement of the center of pressure aft tends to increase the stability of the vehicle (makes β smaller), making turns harder to accomplish.

Changes in the location of the center of pressure for the control planes appear to have little effect on the turning circle response measures. A 10% shift in the location of the center of effort, however, can cause as much as a 5.4% change in the radius of turn. Therefore, it is important to know where the center of effort is (see Table 4.8).

Zigzags

The effect of a larger CE in the zigzag maneuvers will be to increase the period of the maneuver, and to increase the reach, the overshoot angle, and the overshoot

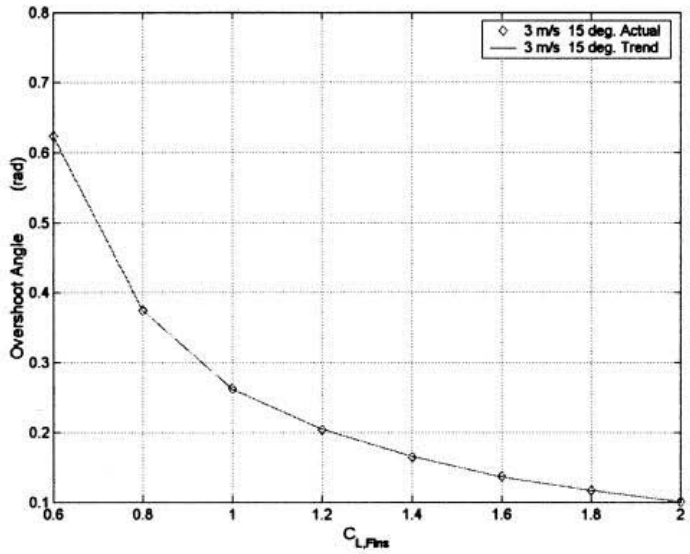

Figure 4-25: Variation of (Horizontal) Zigzag Overshoot Angle with Fin Lift Coefficient

Table 4.8: Maximum Sensitivity of Turning Response Measures to Variations in the Location of the Center of Effort (Hull) and Center of Pressure (Fins)

	Turning Circles			
	Radius of Turn	Advance	Tactical Diameter	Time to Reach 180°
CE_{Hull}	-0.5429	0.1034	-0.3823	0.1611
CPs_{Fins}	0.0059	0.0116	-0.0004	-0.0234
CPc_{Fins}	0.0666	0.0142	0.0512	0.0280

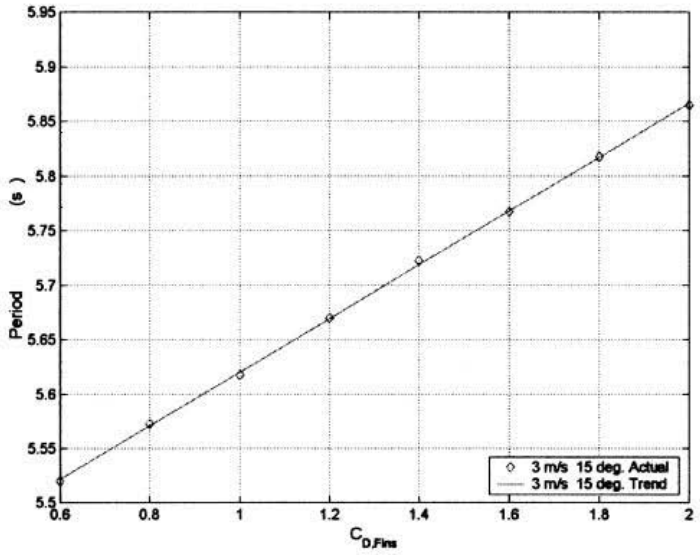

Figure 4-26: Variation of (Horizontal) Zigzag Period with Fin Drag Coefficient

width of path. Plots of response parameters in zigzag maneuvers versus the variation in the location of the CE show that the response in the horizontal plane is very similar to the response in the vertical plane (compare Figures 4-30 and 4-31). In both cases the period, the reach, and the overshoot width of path do indeed increase with increasing distance from the center of mass to CE, but the overshoot angle decreases with increasing distance to CE. The period increases linearly (see Figure 4-32) as the center of effort moves forward. The reach and the overshoot width of path increase nonlinearly as CE moves forward (e.g. Figure 4-31). The overshoot angle generally decreases as the location of CE is moved forward as can be seen in Figure 4-33 (the odd shape to the trend line may be an artifact of the integrator used in the simulation).

As the center of pressure of the control plane moves outward along the span, there is no change in the moment arm along the longitudinal axis of the vehicle, since the control planes were designed such that the quarter-chord axis of the control planes are

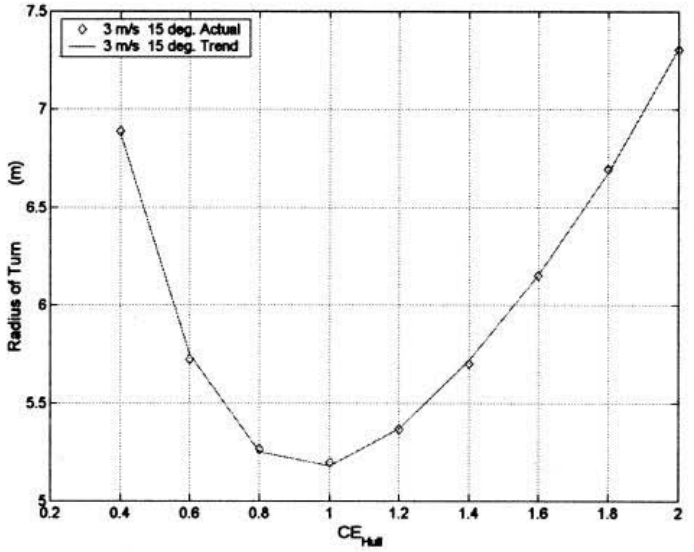

Figure 4-27: Variation of Radius of Turn with Length-Wise Variation of Hull Center of Effort

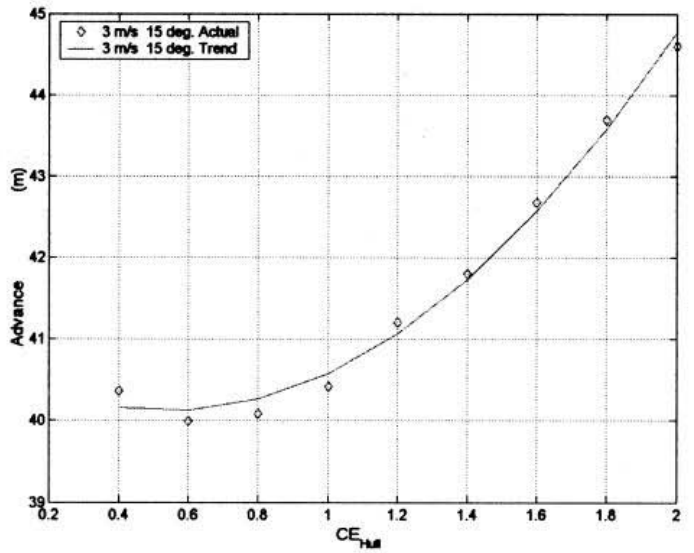

Figure 4-28: Variation of Advance with Length-Wise Variation of Hull Center of Effort

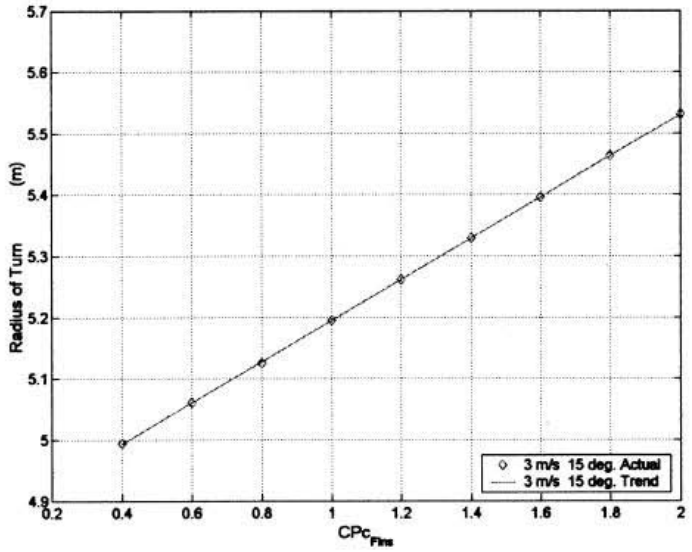

Figure 4-29: Variation of Radius of Turn with Chord-Wise Variation of Fin Center of Pressure

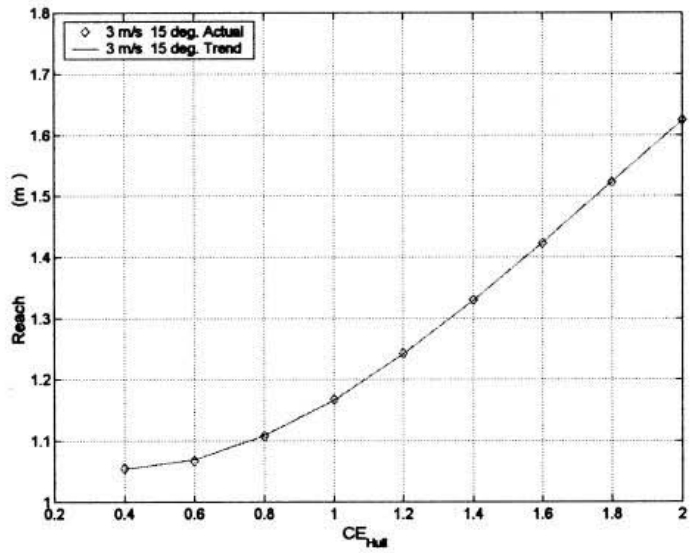

Figure 4-30: Variation of (Vertical) Zigzag Reach with Length-Wise Variation of Hull Center of Effort, CE_{Hull}

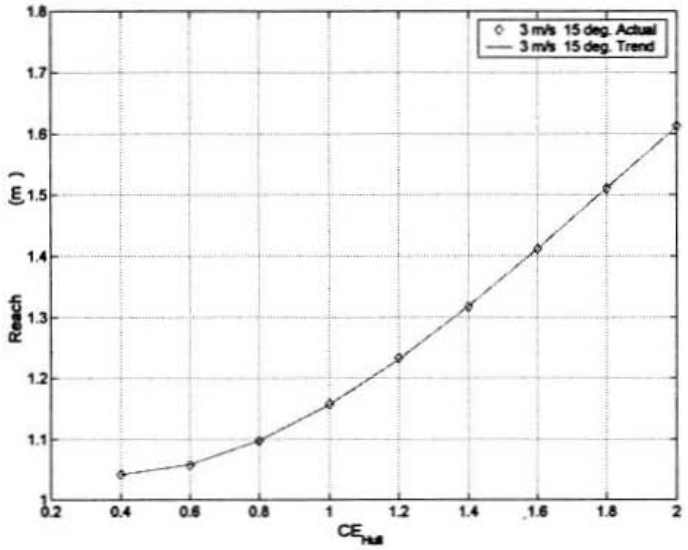

Figure 4-31: Variation of (Horizontal) Zigzag Reach with Length-Wise Variation of Hull Center of Effort, CE_{Hull}

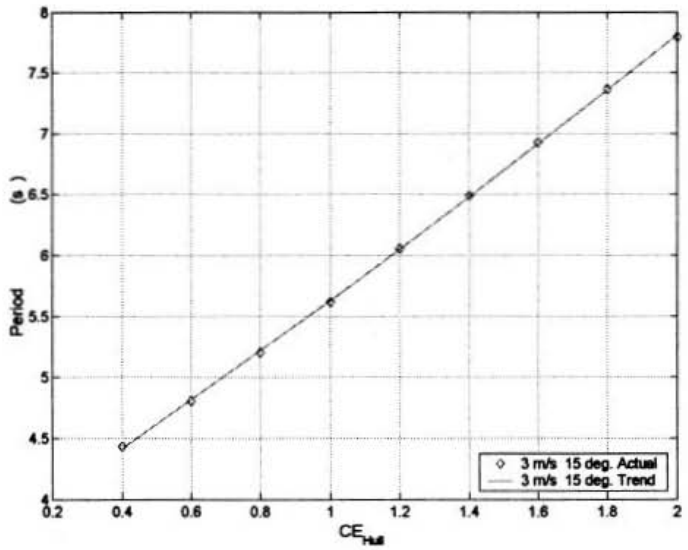

Figure 4-32: Variation of (Horizontal) Zigzag Period with Length-Wise Variation of Hull Center of Effort

perpendicular to the hull. This suggests that there should be almost no change in the vehicle response in turning circles or zigzag maneuvers for variation of the location of CP along the span. Analysis showed this to be true.

The aftward movement of CP along the chord makes it easier to reverse a turn, and therefore, the zigzag response measures should all decrease. This is shown in the simulation results, where all but the reach decrease (e.g. see Figure 4-34), the reach remains constant (within 1%).

The sensitivity of the vehicle response measures to changes in the locations of the centers of effort and pressure are shown Tables 4.9 and 4.10. Again, the response

Table 4.9: Maximum Sensitivity of Horizontal Zigzag Response Measures to Variations in the Location of the Center of Effort (Hull) and Center of Pressure (Fins)

	Horizontal Zigzags			
			Overshoot	
	Period	Reach	Angle	Pathwidth
CE_{Hull}	0.3894	0.3931	-0.3077	0.5526
CPs_{Fins}	-0.0045	0.0000	-0.0006	-0.0011
CPc_{Fins}	-0.0356	-0.0108	-0.1481	-0.0706

Table 4.10: Maximum Sensitivity of Vertical Zigzag Response Measures to Variations in the Location of the Center of Effort (Hull) and Center of Pressure (Fins)

	Vertical Zigzags			
			Overshoot	
	Period	Reach	Angle	Pathwidth
CE_{Hull}	0.4078	0.3919	-0.2662	0.5982
CPs_{Fins}	0.0000	0.0000	-0.0004	-0.0003
CPc_{Fins}	-0.0299	-0.0107	-0.1110	-0.0627

measures are relatively insensitive to variations in the location of the center of pressure of the control planes, but sensitive to variations in the location of the center of effort of the hull.

Design Implications

When the center of effort is moved aft of the nose, the measures of vehicle response in a turn increase. The same measures increase as the center of effort is "moved" forward of the vehicle nose, indicating that the optimal place for the center of effort is at the nose. It is not possible to ensure that the optimum location can be maintained throughout the motion of the vehicle through the fluid, since the center of effort is dependent on the flow conditions. Increasing the distance from the center of mass to the center of effort (moving it forward) will lead to increased period, reach, and overshoot width of path, but decreased overshoot angle. This indicates a need to move the center of effort closer to the center of mass, but again, the center of effort is a function of the flow around the vehicle, and there is no clear design variable that can ensure optimal location of CE over the whole range of vehicle motions.

The effect of moving the location of the control plane center of pressure aft is to increase the response measures, in the same manner as increasing the fin lift did. This means that for a given fin shape (with a specific lift coefficient), the effect of lift force can be made larger by moving the fin aftward on the hull. Moving the control plane center of pressure aft along the chord of the plane will reduce the measures of vehicle response in zigzag maneuvers. This is again similar to the case for increasing the lift on the control plane.

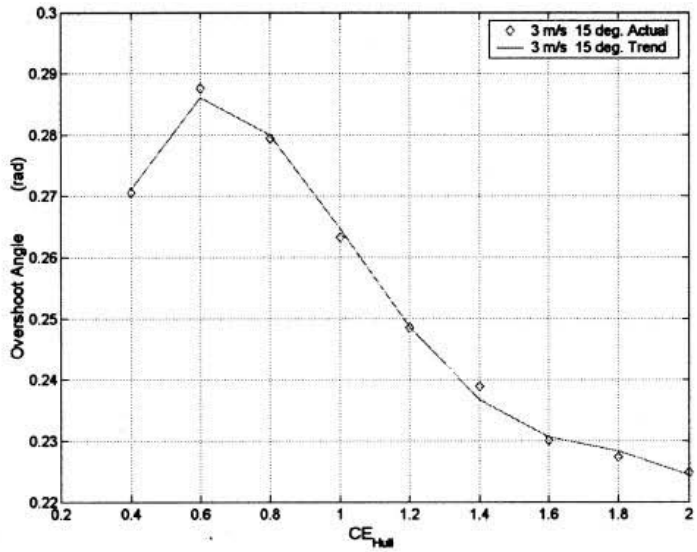

Figure 4-33: Variation of (Horizontal) Zigzag Overshoot Angle with Length-Wise Variation of Hull Center of Effort, CE_{Hull}

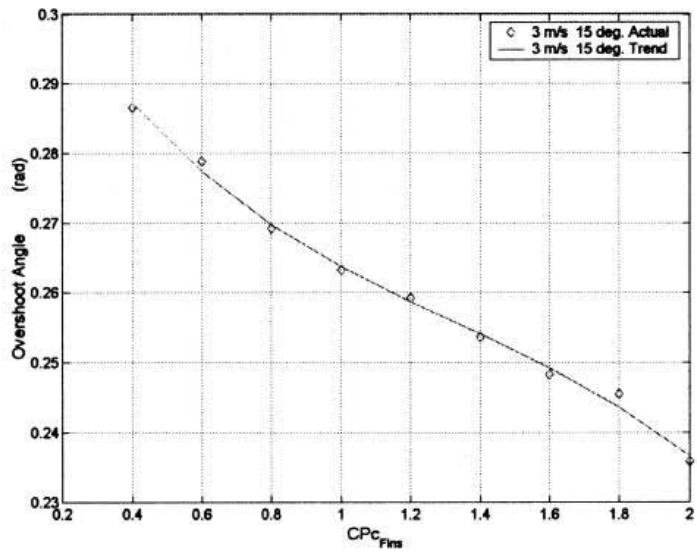

Figure 4-34: Variation of (Horizontal) Zigzag Overshoot Angle with Chord-Wise Variation of Fin Center of Pressure

Chapter 5

Vehicle Response with Control Plane Faults

Control planes have a two-fold role in vehicle dynamics. First, the lift and drag forces on the (after) fins are applied well aft of the center of mass, at the center of pressure (CP) of each control plane, and, therefore, the lift force on the fins tends to stabilize the vehicle. That is, if the vehicle is perturbed from a straight and level path, the lift on the after control surfaces will cause the vehicle to return to its original straight and level path (see Figure 5-1). If the vehicle has forward fins, the CP of the forward fins

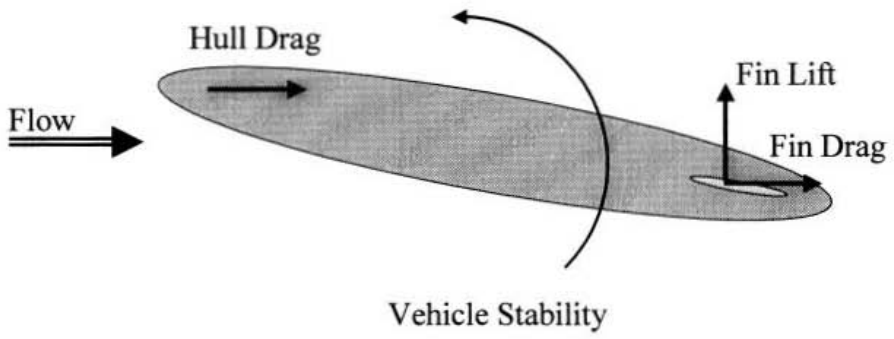

Figure 5-1: Effects of Aft-Mounted Control Planes on Vehicle Stability

will tend to destabilize the vehicle, but they will facilitate greater maneuverability.

Second, the fins are used to initiate a turn, or a dive. Commanding a change of heading or pitch attitude is accomplished by deflecting the control planes. Changing the angle of deflection of the control planes initially produces a moment on the vehicle, initiating a turn (see Figure 5-2b). Since lift and drag forces on the hull are applied at the center of effort (CE), well forward of the center of mass of the vehicle, the lift force produces a moment that tends to destabilize the vehicle. That is, if the vehicle is perturbed from a straight and level path, the lift and drag forces on the forward-moving hull will cause the vehicle to continue to turn even after the disturbing force is removed. Therefore, once the turn is initiated by the control plane, the lift force on the hull will tend to cause the vehicle to keep turning in that direction (see Figure 5-2c). As the turn increases, the angle of attack of the deflected control planes decreases (because the angle of attack of the control plane is decreasing as the angle of attack of the hull is increasing) until it actually changes sign, i.e. the vehicle has turned past the point where the lift force on the fin is zero (Figure 5-2c), and now the fin lift force starts to work against the hull lift force. The vehicle hull will continue to yaw until the moment caused by the hull lift and the moment caused by the control planes are in dynamic balance (Figure 5-2d). This balance will occur at a specific angle of drift, the angle between the hull and the fluid flow. The hull lift force is a function of the drift angle of the vehicle. The control plane lift force is a function of the drift angle and the deflection angle of the fins, the sum of these two being the angle of attack of the control plane.

Stability and maneuverability are conflicting requirements for any vehicle. For a vehicle to hold a stable course, it must be able to reject any kind of force that would cause it to deviate from that course. On the other hand, for a vehicle to be maneuverable, it must be able to change course quickly. One of the key elements of control plane design (size, shape, and location) is to find an applicable balance between these two requirements. The measure of the ability of the control planes

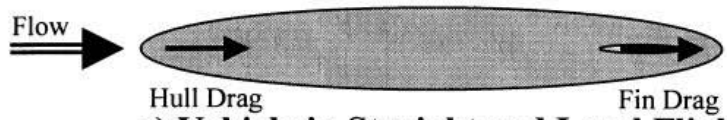

a) Vehicle in Straight and Level Flight

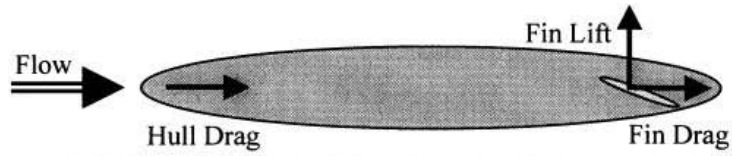

b) Turn Initiated By Control Plane Deflection

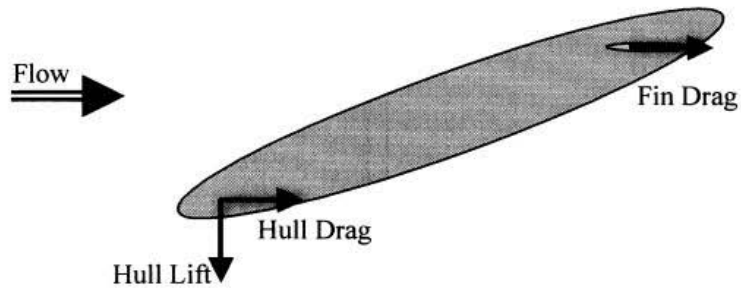

c) Turn Propagated By Lift Force on Hull

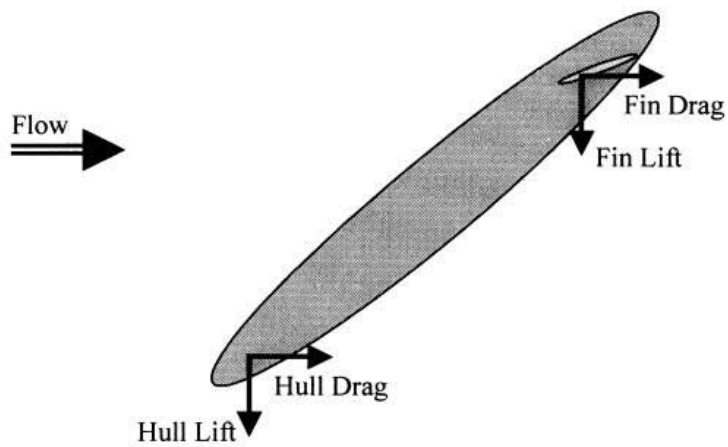

d) Steady Turn: Dynamic Balance Between Lift Forces on Hull and Fins

Figure 5-2: Progression of a Turn

to affect change in the vehicle direction is referred to as the control authority of the control plane. The fins taken together (with the propulsor) form the total control authority for the base configuration of C-SCOUT. If the ability of one or more of the control planes to take up the commanded deflection angle is impaired. the process of diving or turning may be adversely affected. The control authority of that fin. and indeed the vehicle. is reduced.

5.1 Physics of Fault-Free Vehicle Motion

To understand the effects of control plane fault conditions. it is necessary to review the behaviour of the vehicle in its "healthy" state. To examine the nominal ("healthy") state and the fault conditions. three maneuvers common to normal operation will be simulated. These simulations were performed using a linear model of the base configuration of C-SCOUT (Figure 5-3).

5.1.1 Hold Course

To hold course. the vehicle must maintain depth and heading in the face of any environmental disturbance. This is a regulator problem. Any controller that is robust to actuator faults such as jams and control plane losses must be able to hold course even when the faults are present. There should be no roll in this type of motion unless there is a disturbance.

5.1.2 Dive

Diving is a maneuver in the x-z plane of the vehicle. Since the vehicle is symmetric about this plane. there is no cross-coupling into other DOF: i.e.. no induced roll. yaw. or sway. The motions involved are surge. heave and pitch only.

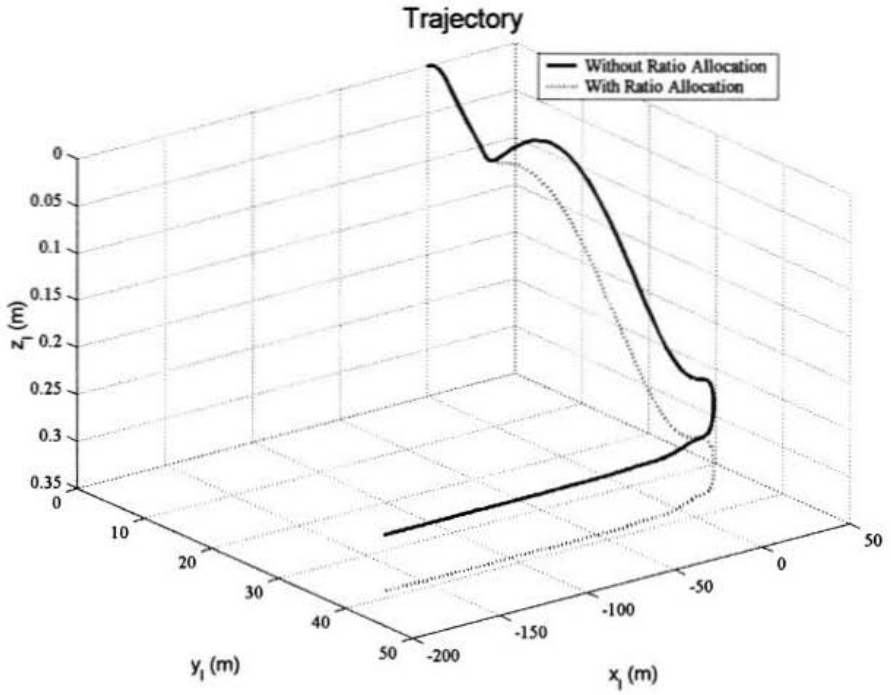

Figure 5-4: Comparison of Vehicle Response in a Turn With and Without Rudder Ratio Compensation

5.2 Physics of Vehicle Motion During (Actuator) Fault Condition

Fault conditions that can occur in operation run from power loss to programming errors to mechanical difficulties. This study is focused on hardware rather than software problems, though there is much overlap in the effects of various fault conditions. Hardware faults include such things as degradation or loss of propulsion, which would have major impact on the motion of vehicles like the base configuration of C-SCOUT, since these type of vehicles are entirely dependent on the propulsor not only for attaining motion, but for facilitating directional control as well. Other major faults involve the jamming of control planes, which may occur due to an electrical or me-

(actuators for control in the horizontal plane) can also be used to cause roll or to compensate for roll induced by other forces acting on the AUV. Although roll is not desirable, when the vertical fins are used, they tend to cause a roll moment because of the asymmetry about the horizontal (x-y) plane, i.e. the distance from the center of mass to the center of pressure of the upper control plane is greater than the distance from the center of mass to the center of pressure of the lower control plane. When a turn is the desired maneuver, the hydrodynamic forces in the horizontal plane induce a roll moment on the vehicle, leading to a pitch and depth excursion.

If roll can be eliminated, or at least, minimized, there should be a forced decoupling between horizontal and vertical maneuvers, such that there is no change in depth when the desired motion is a turn. Further, since a fault condition on any single control plane is likely to induce a roll motion, controlling the roll motion may be key to ensuring reliable motion characteristics even when such faults occur.

The asymmetry about the horizontal (x-y) plane suggests that it may be possible to pre-compensate (a form of feed-forward) for this roll effect by using the ratio of moment arms to the upper and lower fin centers of pressure to allocate the rudder deflections. However when this kind of compensation is implemented, the vehicle responded with a greater depth excursion in a turn: i.e. the roll is prevented but there is a greater change in depth (see Figure 5-4). To negate the roll induced by the asymmetry of the vertical control planes about the surge axis (the x-axis of the body-fixed reference frame), a greater lift force is required on the lower control plane, which has the shorter moment arm. The increase in depth excursion is a result of the increased drag force on the lower control plane as it deflects more in order to produce a greater lift force.

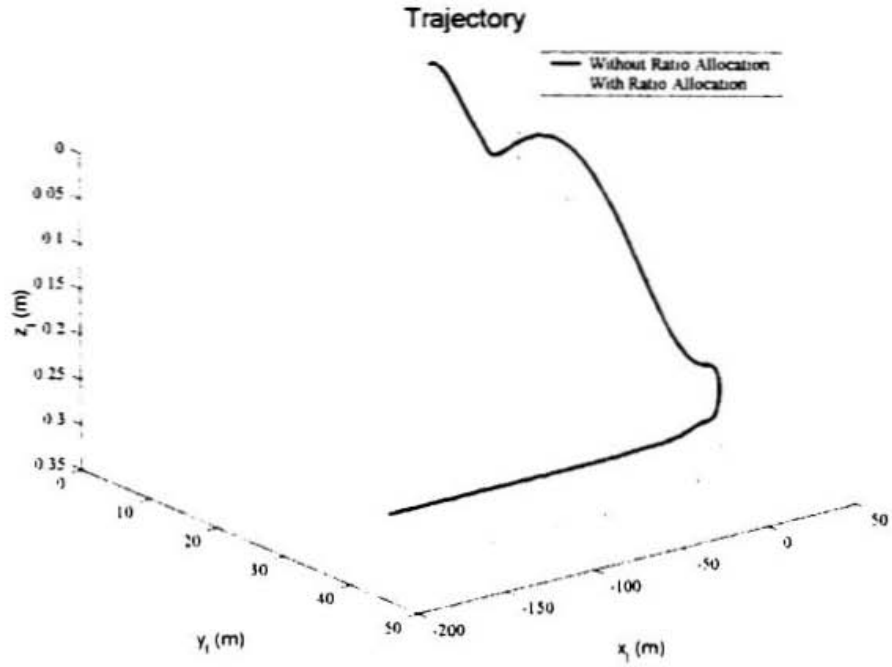

Figure 5-4: Comparison of Vehicle Response in a Turn With and Without Rudder Ratio Compensation

5.2 Physics of Vehicle Motion During (Actuator) Fault Condition

Fault conditions that can occur in operation run from power loss to programming errors to mechanical difficulties. This study is focused on hardware rather than software problems. though there is much overlap in the effects of various fault conditions. Hardware faults include such things as degradation or loss of propulsion. which would have major impact on the motion of vehicles like the base configuration of C-SCOUT. since these type of vehicles are entirely dependent on the propulsor not only for attaining motion. but for facilitating directional control as well. Other major faults involve the jamming of control planes. which may occur due to an electrical or me-

chanical defect. or due to operational hazards such as being fouled with seaweed. etc. It is even possible to loose a control plane if it gets snagged. or is involved with an impact with some other body. (The C-SCOUT control planes are designed with a shear pin such that any significant collision will result in the fin breaking off. rather than in structural damage to the hull and its contents.) There are many other types of fault conditions possible during the course of operation of an AUV. but this study is limited to jammed and missing control planes.

5.2.1 Catastrophic Failures

Propulsor inoperative

This fault is one of the more likely fault conditions. since it is a single point failure. If the propulsor is inoperative. the vehicle will be unable to achieve controlled forward motion. Since the directional control of the vehicle (via control planes) is dependent on the flow of water over the control planes. no forward motion means no directional control. The vehicle is "dead in the water". If the propulsor operation is merely degraded. the control authority of the control planes will be reduced by the square of the vehicle speed. because the control authority is a function of the lift and drag forces on the control planes. and each of these is directly proportional to the square of the velocity of fluid flow.

All four control planes missing

The probability of this fault condition occurring is very low. If all four control planes are missing. there is no directional control. and no stabilizing force on the vehicle. The vehicle is rendered useless.

All four control planes jammed

The probability of all the fins jamming due to mechanical damage is very low, however electronic or controller faults could cause such a loss of control authority. As with four missing fins, there would be no directional control available. In addition, the vehicle trajectory would be fixed by the angles of control planes.

Three control planes missing, fourth jammed; three control planes jammed, fourth missing; two control planes missing, remaining two jammed

The probability of these conditions occurring is very low, since each of these conditions implies several faults occurring simultaneously.

Three of the four control planes missing

Again, the probability of a multi-point failure like this is low. It is expected that the remaining control plane would induce complex coupling of roll-pitch-yaw, making directional control virtually impossible, and course stability highly questionable.

Three of the four control planes jammed

The probability of this fault occurring due to mechanical problems is low, however electronic or controller faults could cause such a loss of control authority. Depending on the angles at which the control planes are jammed, there could be possible complex coupling of roll-pitch-yaw, making directional control virtually impossible. In some very special circumstances there may be enough control authority in the one healthy fin to accomplish some control objectives, but this is expected to be highly unreliable.

Two control planes missing, one jammed; two control planes jammed, one missing

Again, the probability of any of these conditions occurring is low. It is expected that these fault conditions would mean complex coupling of roll-pitch-yaw, with directional

control virtually impossible, and course stability questionable.

5.2.2 Recoverable Failures: Multi-Point

Two control planes missing

The probability here is somewhat low, since it requires a multi-point failure. If the condition does occur, it is more likely that two adjacent fins (e.g. port and upper) rather than that two opposite fins (e.g. port and starboard) would be missing. This assumes that the loss is the result of a collision or snagging incident. In dealing with multi-point failures, no combination should be ignored. It is expected that there would be some degradation of the directional control of the vehicle, however it is possible that at least some subgroup of control (and mission) objectives can be accomplished.

Two control planes jammed

As for two missing planes, the probability is somewhat low, unless there is an electronic or software problem. Stability and maneuverability are expected to be affected by the particulars of the jam conditions. It is expected that there would be some degradation of the directional control of the vehicle, however it is possible that at least some subgroup of control (and mission) objectives can be accomplished.

One control plane missing, one jammed

The probability is somewhat low, since it would likely mean two separate but simultaneous faults. It is very possible that some directional control is available, though full control may not be possible. It is expected that a subgroup of the original objectives may be accomplished.

5.2.3 Recoverable Failures: Single-Point

One control plane missing

This condition is a more probable fault, since it represents a single-point failure rather than a multi-point failure. It may be that full control is still possible, while maintaining course stability.

One control plane jammed

Again, this fault is more probable than multiple fin failures. Full control may still be possible. Course stability should be achievable.

5.3 Vehicle Behaviours

Does there exist a single controller that will provide adequate control of the vehicle without regard to the control plane status: i.e. a single robust controller for fault-free operation that will also provide acceptable performance when one of the control planes is jammed or missing? To help answer this question, a series of simulations using the linear model of C-SCOUT (operating at a steady forward speed of 3 m/s) were performed. The series included various fault conditions.

5.3.1 Simulation Procedure

The series of simulations included three basic maneuvers common to AUV missions: holding course, diving (in this case a 100 m descent), and turning (here a starboard turn through 180 °). The vehicle was assumed to be in the fault condition at the start of the simulation, and the dive and turn maneuvers were initiated well after the start of the run. Note that in all the plots that follow, the starting position of the vehicle is (0, 0) in both the horizontal (x-y) and vertical (x-z) planes. All the simulations used the linear model of the C-SCOUT with the dynamics corresponding to straight and

level flight at 3 m / s.

Hold (Course)

For the vehicle to hold its course (and speed), all rates except the surge velocity (i.e., forward speed) should be zero. In terms of the velocity parameters described in the body frame, this means

$$v = w = p = q = r = 0$$

and u is a constant. In terms of the velocity parameters described in the inertial frame, it means

$$\dot{z} = \dot{\phi} = \dot{\theta} = \dot{\psi} = z = 0$$

The values of $\dot{x}$ and $\dot{y}$ are constant, therefore x and y will vary linearly with time, however the heading angle, ψ, will be constant. There may be some small angle of roll (ϕ) and/or pitch (θ) to balance some external force or moment, but these angles should not result in changes to the heading or depth.

Dive 100 m

At the end of the dive maneuver, the depth, z, should have a new, constant value ($z_0 + 100\,\mathrm{m}$). Otherwise the vehicle velocity and position variables should be as described under Hold (Course). In the simulations, z_0 is zero even though the vehicle is assumed to be deeply submerged even at the start, though strictly speaking, the 100 m dive represents a Δz from the nominal depth, $z_0 \neq 0$.

Turn Through 180°

At the end of the turn, the heading, ψ, should have a new, constant value ($\psi_0 + 180^\circ$). Otherwise the vehicle velocity and position variables should be as described under Hold (Course). In the simulations, ψ_0 is zero.

Roll Compensation and Depth Control Gain

The simulations were performed using closed-loop (proportional) control for the heading, depth, and roll. The individual control plane deflections (after starboard, after port, after upper, and after lower, respectively) were commanded as follows:

$$\begin{aligned}
\delta_{as} &= k_z\left(z_{setpoint} - z_{actual}\right) + k_{\phi_a} k_{\phi_e}\left(\phi_{setpoint} - \phi_{actual}\right) \\
\delta_{ap} &= k_z\left(z_{setpoint} - z_{actual}\right) - k_{\phi a} k_{\phi r}\left(\phi_{setpoint} - \phi_{actual}\right) \\
\delta_{au} &= k_v\left(v_{setpoint} - v_{actual}\right) - k_{\phi a} k_{\phi r}\left(\phi_{setpoint} - \phi_{actual}\right) \\
\delta_{al} &= k_v\left(v_{setpoint} - v_{actual}\right) + k_{\phi a} k_{\phi r}\left(\phi_{setpoint} - \phi_{actual}\right)
\end{aligned} \tag{5.1}$$

For the horizontal control planes a positive deflection means trailing edge down, while for the vertical control planes, a positive deflection means trailing edge to port. In either case, a positive deflection of the control plane pair will result in a negative moment on the vehicle - negative pitch (nose down) for the horizontal pair, and negative yaw (nose to port) for the vertical pair.

For each of the three maneuvers a simulation was performed for four modes of roll compensation:

- N - without active roll compensation (i.e. only the passive roll stability effects) - no active compensation. Passive roll stability is provided by the vertical distance between the center of buoyancy (the buoyant force acting through the center of the volume from which water is displaced - see Figure 5-5) and the center of mass (or gravity, where the weight of the vehicle acts). When the vehicle is upright, the forces of buoyancy and weight have a common line of action, but opposite directions, and for a neutrally buoyant vehicle, they cancel each other. When the vehicle rolls, the lines of action of these two forces are no longer colinear, and a righting moment is produced which will tend to return the vehicle back to the upright position (see Figure 5-5). The lack of active roll compensation was implemented by setting k_{ϕ_a} to zero in equations (5.1).

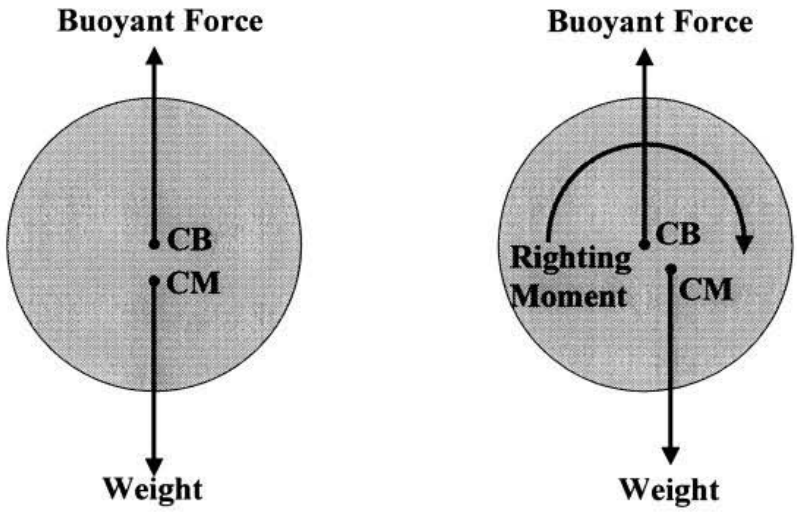

Figure 5-5: Passive Stability

- E - active roll compensation via **e**levators (starboard and port "horizontal" control planes). Here a differential deflection of the horizontal control planes will actively force the vehicle back to the upright position; e.g., a positive deflection of the port plane and a negative deflection of the starboard plane will generate a positive roll moment on the vehicle. This form of active roll compensation was accomplished by setting k_{ϕ_a} to unity and k_{ϕ_r} to zero in equations (5.1).

- R - active roll compensation via **r**udders (upper and lower "vertical" control planes). The R-type active roll compensation was implemented by setting k_{ϕ_a} to unity and k_{ϕ_e} to zero in equations (5.1).

- A - active roll compensation via **a**ll control planes. Here the roll compensation was performed by setting both k_{ϕ_r} and k_{ϕ_e} to unity in equations (5.1).

In each case where k_{ϕ_a}, k_{ϕ_r} and k_{ϕ_e} were not being used as a filter mechanism (i.e. set to unity or zero), the gain value was the same, 0.0148.

In addition, each of these cases was further simulated at two values of depth

controller gain. In the vertical plane, the gravity-buoyancy couple acts as a restoring moment, making the vehicle response very similar to a first-order system, where the magnitude of the controller gain can cause the system to exhibit an overdamped (no overshoots) response or an underdamped (overshoots present) response in depth. The former response was achieved by setting the depth controller gain, $k_z = 0.01$, while the latter response was accomplished with a depth controller gain of 0.07.

5.3.2 Nominal (No-Fault) Behaviour

All maneuvers were achieved. In the cases of holding course (see Figure 5-6) and diving 100 m (see Figure 5-8), no roll was induced, therefore there were no parasitic motions even without active roll compensation. The vehicle response under all modes of roll compensation is identical during course holding. Note the slight descent of the vehicle as it settles into a nonzero pitch attitude that will result in level flight. As well, the vehicle response under all modes of roll compensation is identical during the diving maneuver. In the turn through 180°, a roll angle was induced on the vehicle and a change in depth occurred. Using the rudders to affect roll compensation did reduce the roll angle, but increased the depth excursion (see Figure 5-10 where the vehicle starts off moving in the positive x-direction then almost immediately turns through 180° and continues on in the negative x-direction). Roll compensation via the elevators or via all control planes working together reduced both the roll angle and the depth change. However, with no active roll compensation, the depth excursion is less than 1% of the distance travelled. Therefore, compensation is not really required for the healthy vehicle even in turns.

The vehicle response with the underdamped ($k_z = 0.07$) depth controller was very similar to the vehicle response with the overdamped ($k_z = 0.01$) depth controller, except that the depth was better controlled (less steady state error), as expected (see Figures 5-7, 5-9 and 5-11). Note that the higher gain does mean overshoots are present in the transient response.

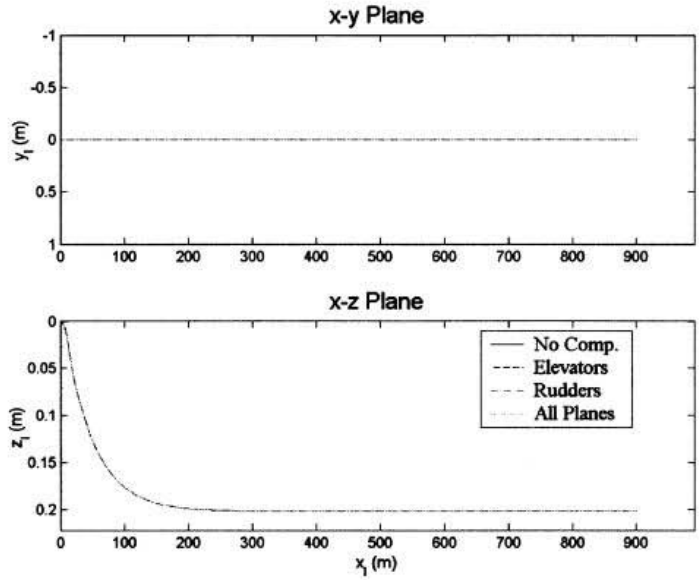

Figure 5-6: Comparison of Vehicle Response in Course Holding with and without Active Roll Compensation ($k_z = 0.01$)

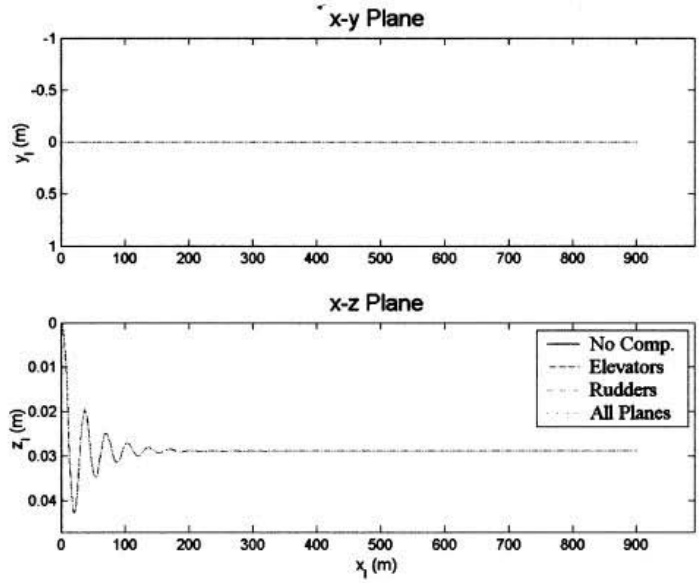

Figure 5-7: Comparison of Vehicle Response in Course Holding with and without Active Roll Compensation ($k_z = 0.07$)

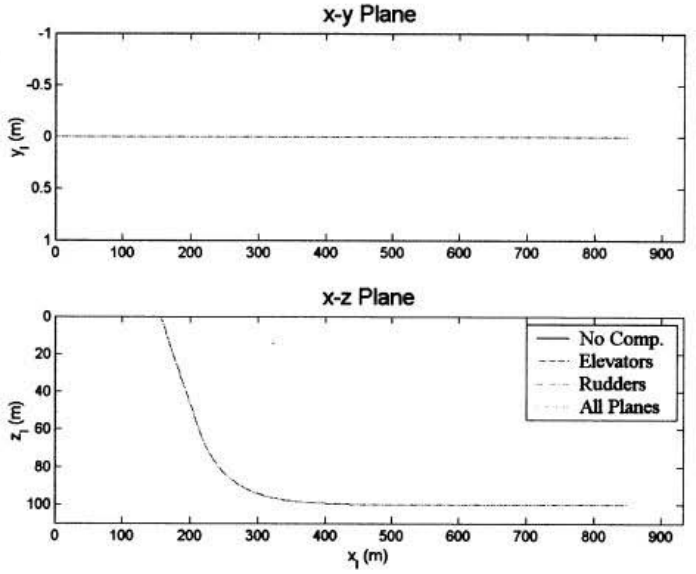

Figure 5-8: Comparison of Vehicle Response in a 100 m Dive with and without Active Roll Compensation ($k_z = 0.01$)

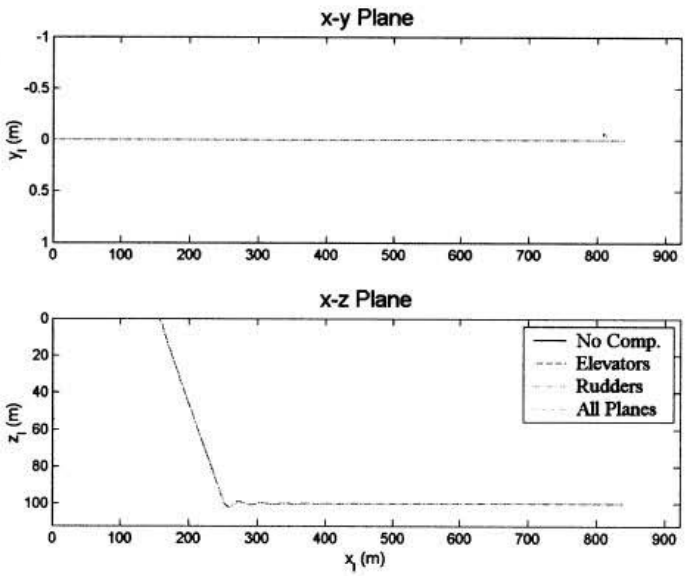

Figure 5-9: Comparison of Vehicle Response in a 100 m Dive with and without Active Roll Compensation ($k_z = 0.07$)

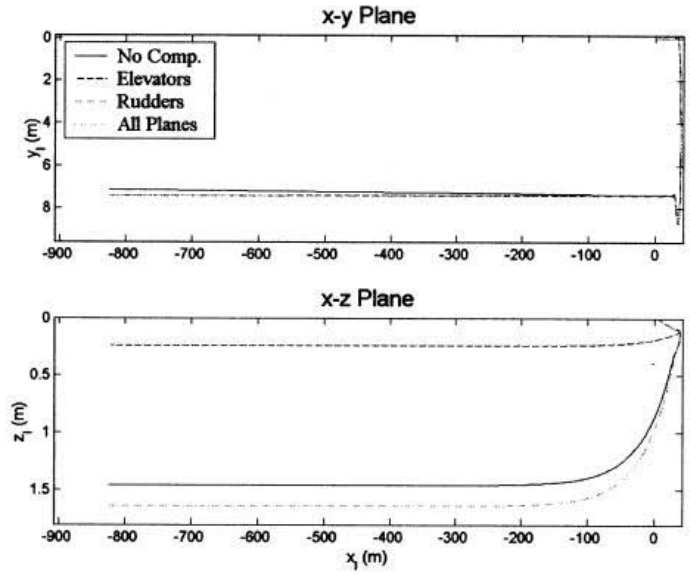

Figure 5-10: Comparison of Vehicle Response in a 180° Turn with and without Active Roll Compensation ($k_z = 0.01$)

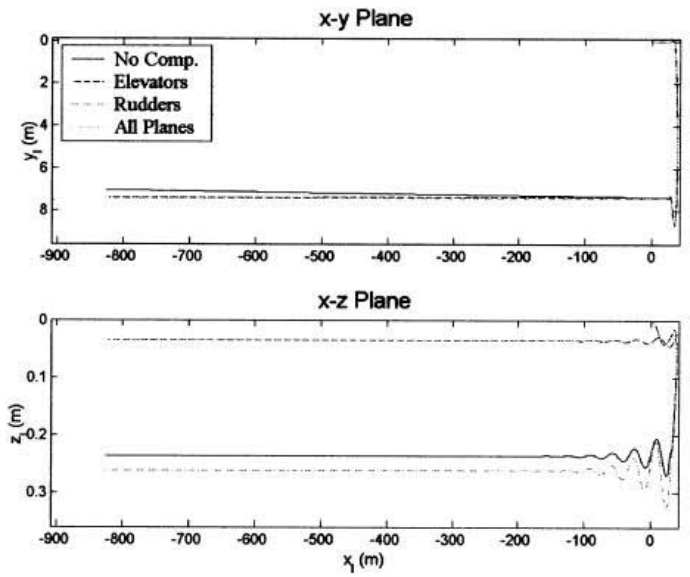

Figure 5-11: Comparison of Vehicle Response in a 180° Turn with and without Active Roll Compensation ($k_z = 0.07$)

5.3.3 Jammed Fin Faults

Holding Course with Jammed Horizontal Control Planes

At large angles of jam on the horizontal (port or starboard) control planes the vehicle response with roll compensation via elevators. E. is unacceptable. due to the large depth excursion (e.g. see Figure 5-12). To control the roll. the other horizontal plane would have to match the angle of jam. and the net result would be a change in depth for which the depth controller is not able to adequately compensate. In addition the compensation via elevators induces a large heading error. Compensation via the rudders. R. or via all control planes. A. improves the vehicle response in heading (over the response of the vehicle without active roll compensation. N). but the error in depth for N is equal to that for R. and less than that for A. Therefore the best overall control in this instance includes active roll compensation via the rudders. R. but the response is only slightly better than that for A or N. The depth excursion is greater when the depth controller gain is lower (compare Figures 5-12 and 5-13). The heading error is not significantly affected. except for control with roll compensation via the elevators (E). which is still unacceptable due to the depth excursion induced. The response for R is still marginally better than the response for A and N. The sign of the angle of jam determines whether the vehicle will rise or descend (compare Figures 5-12 and 5-14): it also determines the direction of the induced heading error in all cases except E. where the controller is unable to recover from the initial heading error. While the error in depth for N is still equal to that for R. and less than that for A. as in the case of the starboard control plane jammed at a negative angle of deflection. when the control plane is jammed at a positive angle of deflection. the drift in heading is worse for R and A than it is for N. This suggests that the initial heading error plays a significant role in determining which is the best method of compensation (N in this latter case). The magnitude of the depth excursion also decreases with a reduction in the angle of jam (see Figure 5-15).

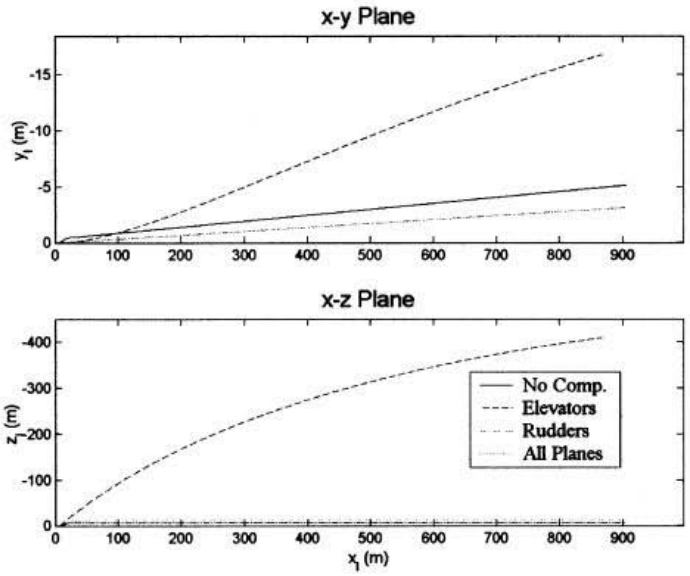

Figure 5-12: Comparison of Vehicle Response in Course Holding when the Starboard Control Plane is Jammed at -25° ($k_z = 0.07$)

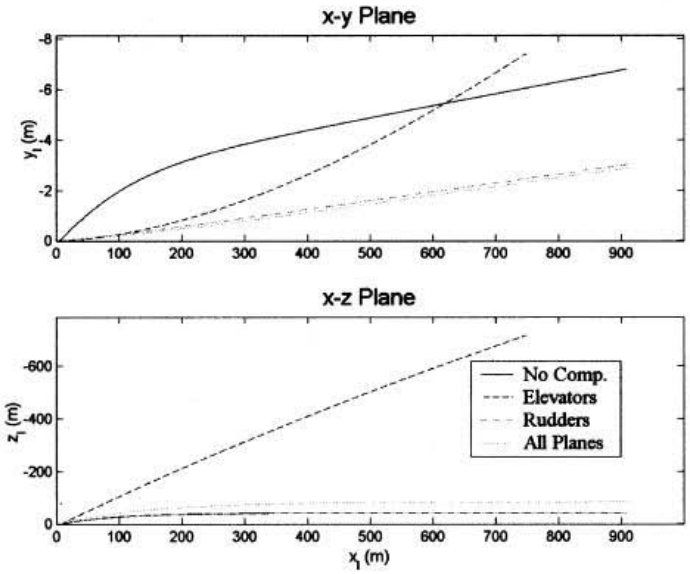

Figure 5-13: Comparison of Vehicle Response in Course Holding when the Starboard Control Plane is Jammed at -25° ($k_z = 0.01$)

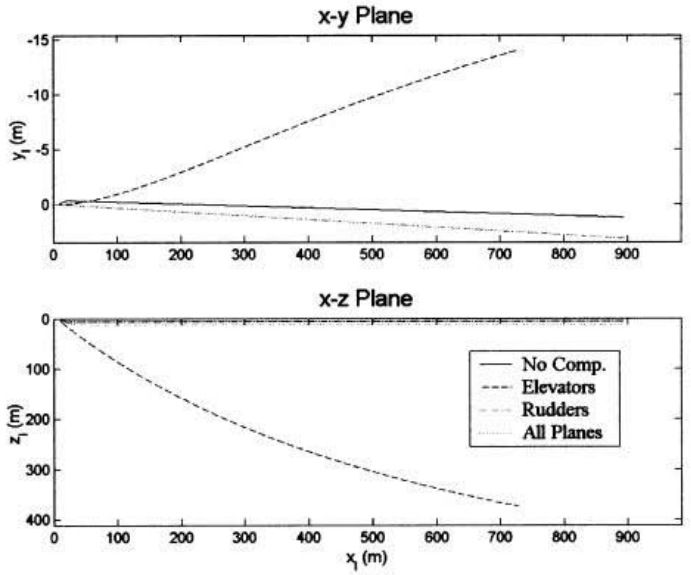

Figure 5-14: Comparison of Vehicle Response in Course Holding when the Starboard Control Plane is Jammed at 25° ($k_z = 0.07$)

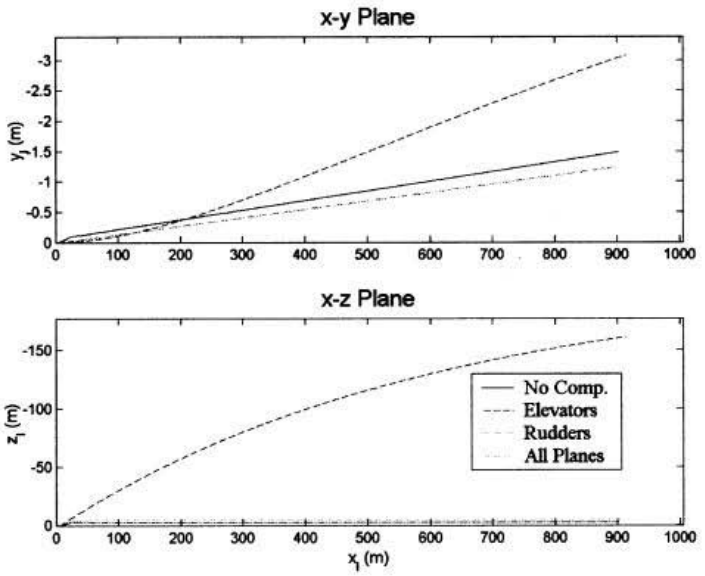

Figure 5-15: Comparison of Vehicle Response in Course Holding when the Starboard Control Plane is Jammed at -10° ($k_z = 0.07$)

as does the heading error. For a given sign of the angle of jam, the relative merit of the various compensation methods remains unchanged. A jam on the opposite side control plane changes the direction of heading error induced (compare Figures 5-12 and 5-16), otherwise the vehicle response is basically the same.

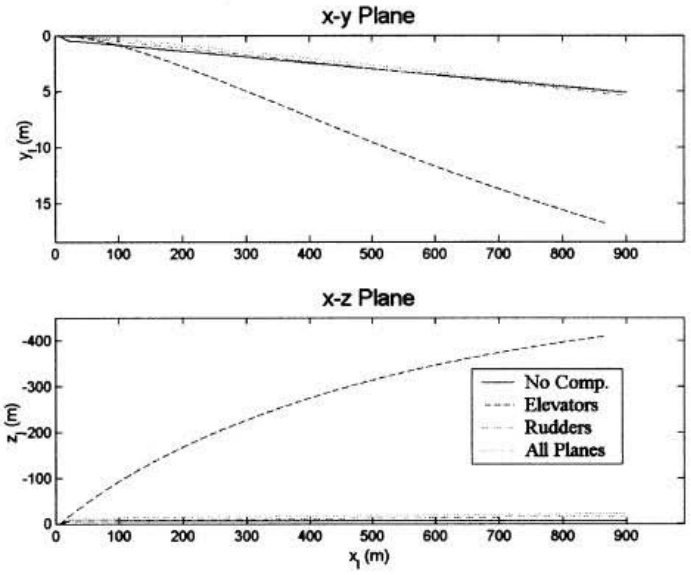

Figure 5-16: Comparison of Vehicle Response in Course Holding when the Port Control Plane is Jammed at -25° ($k_z = 0.07$)

Holding Course with Jammed Vertical Control Planes

When the jam involves the upper control plane, it is the vehicle response with roll compensation via rudders, R, that is unacceptable (see Figure 5-17) because of the large heading error induced by the matching of the lower control plane deflection to the upper jam angle in order to reduce the roll of the vehicle. Compensation methods E and A improve the heading error that occurs with N, but they are very slightly greater in depth error. Even in the face of slightly worse response in depth, the best overall control is provided by E, since the heading error is very nearly zero. Again, the

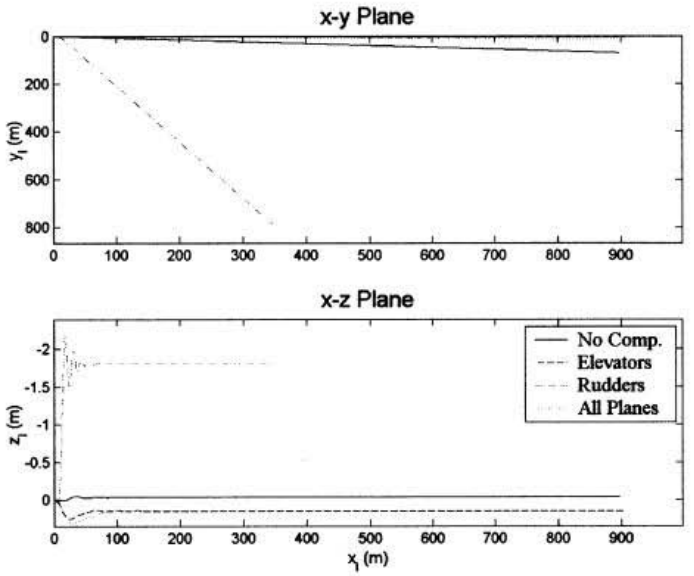

Figure 5-17: Comparison of Vehicle Response in Course Holding when the Upper Control Plane is Jammed at -25° ($k_z = 0.07$)

depth excursion is greater for the depth controller with the lower gain, however, the heading error is the same in both cases (compare Figures 5-17 and 5-18). When the angle of jam is zero, the vehicle holds course pretty much as the undisturbed nominal (fault-free) vehicle does (compare Figures 5-7 and 5-19). The major effect of the sign of the angle of jam is to change the direction of heading error (compare Figures 5-17 and 5-20). When holding course, the vehicle response is severely degraded, even when A is used, if the lower control plane is jammed at large deflection angles (see Figure 5-21, where it can be seen that the best vehicle response is achieved when N is used). At lower angles of jam, however, the vehicle response for the lower plane jams and the upper plane jams, is similar.

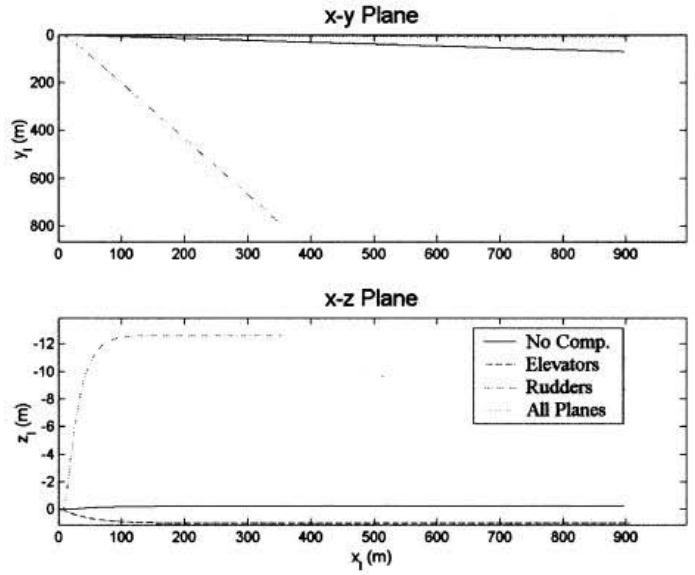

Figure 5-18: Comparison of Vehicle Response in Course Holding when the Upper Control Plane is Jammed at -25° ($k_z = 0.01$)

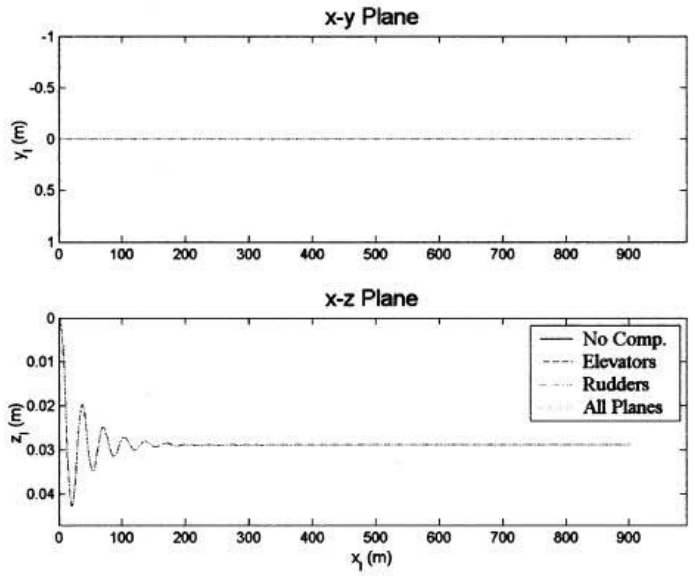

Figure 5-19: Comparison of Vehicle Response in Course Holding when the Upper Control Plane is Jammed at 0° ($k_z = 0.07$)

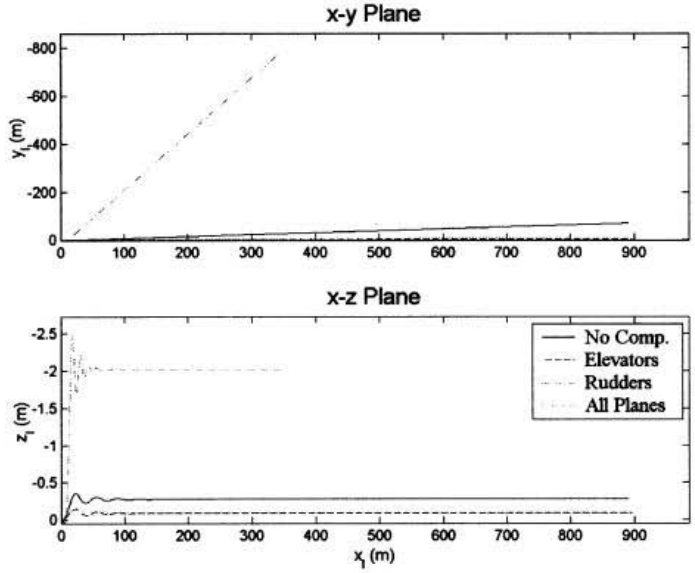

Figure 5-20: Comparison of Vehicle Response in Course Holding when the Upper Control Plane is Jammed at 25° ($k_z = 0.07$)

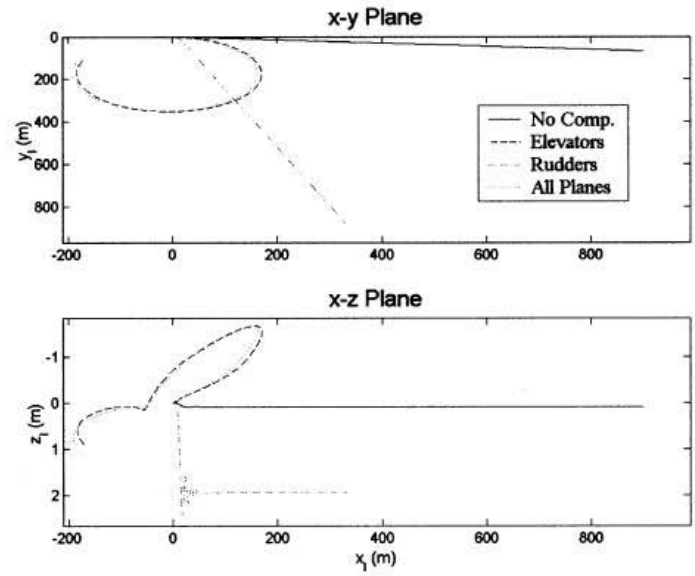

Figure 5-21: Comparison of Vehicle Response in Course Holding when the Lower Control Plane is Jammed at -25° ($k_z = 0.07$)

Diving 100 m with Jammed Horizontal Control Planes

None of the compensation methods were effective in the dive maneuver at high negative angles of horizontal control plane jam. The dive was not achieved with or without active roll compensation (see Figure 5-22). At lower jam angles the dive was achieved,

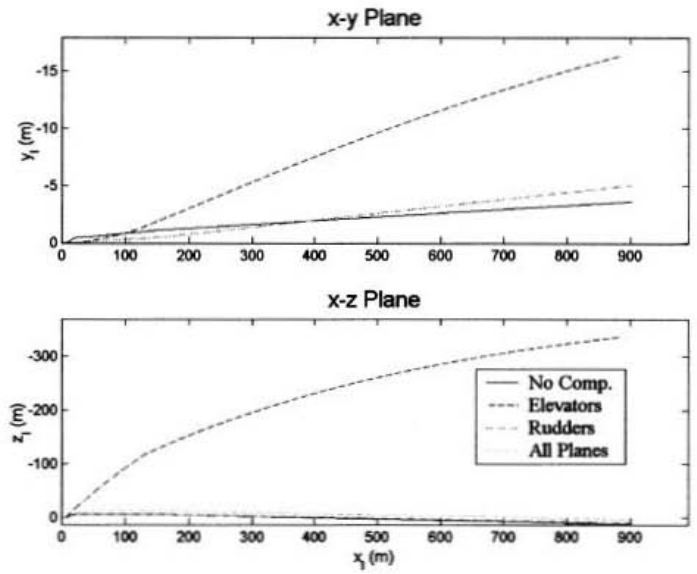

Figure 5-22: Comparison of Vehicle Response in a 100 m Dive when the Starboard Control Plane is Jammed at -25° ($k_z = 0.07$)

except when the roll compensation via elevators was implemented (see Figure 5-23). Compensation via the rudders, R, or via all control planes, A, improves the vehicle response in heading (over the response of the vehicle without active roll compensation, N), but the error in depth for N is equal to that for R, and less than that for A. Therefore the best overall control in this instance is that using R, but the response is only slightly better than that for A, while N has a significant offset in sway. Again, the higher gain depth controller reduced the steady state error in depth (compare Figures 5-23 and 5-24). The heading errors are comparable with either gain for the depth controller. At a jam angle of 0°, the control authority of the one remaining

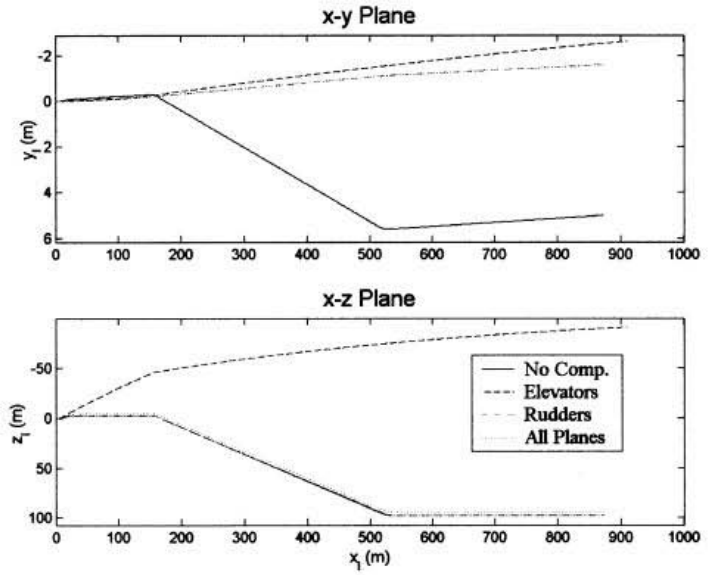

Figure 5-23: Comparison of Vehicle Response in a 100 m Dive when the Starboard Control Plane is Jammed at -10° ($k_z = 0.07$)

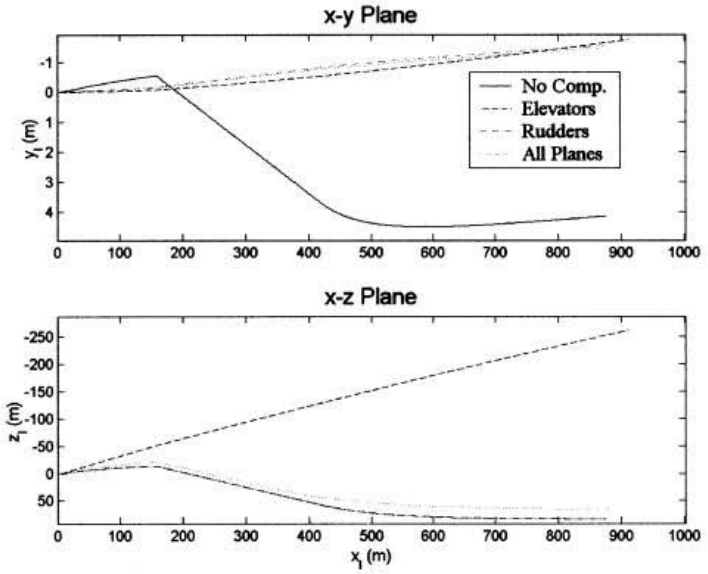

Figure 5-24: Comparison of Vehicle Response in a 100 m Dive when the Starboard Control Plane is Jammed at -10° ($k_z = 0.01$)

horizontal control plane is still insufficient to achieve the commanded depth change in a reasonable amount of time if the horizontal control plane is used (alone. i.e. E) for roll compensation as well as depth control (see Figure 5-25). Control with R or A does result in the vehicle accomplishing the dive with less error in track than does the control without roll compensation. When the angle of jam is 25 °. the controller with E is unable to stop the descent (see Figure 5-26): i.e.. the remaining horizontal fin has insufficient control authority. The best control is with N. since the vehicle response shows the least depth error and the least drift in heading. The vehicle response is very similar whether it is the port control plane or the starboard that is experiencing the jam condition. except that the direction of the heading error changes.

Diving 100 m with Jammed Vertical Control Planes

For jams to the upper control plane. the vehicle response in a dive maneuver is unacceptable when the controller uses R (see Figure 5-27) because of the large heading error induced by the matching of the lower control plane deflection to the upper control plane jam angle. In fact. only N results in the vehicle achieving the dive without a huge heading error. When the depth controller gain is lower. vehicle response for N is still the only one acceptable for this maneuver (see Figure 5-28). The vehicle response when the jam angle is 0 ° is like that of the fault-free vehicle (compare Figures 5-9 and 5-29). The response for the vehicle with the lower control plane in a jam condition is worse for E. R. and A at large angles of jam than that of the vehicle with an upper control plane jammed (compare Figures 5-27 and 5-30): for N the heading error is worse for the lower plane. while the depth error is the same as that of the upper plane jammed at the equivalent angle of deflection. At lower angles of jam. however. the vehicle response is similar whether the upper or the lower control plane is jammed. The sign of the jam angle for either the upper or lower control plane affects the direction of the heading error induced.

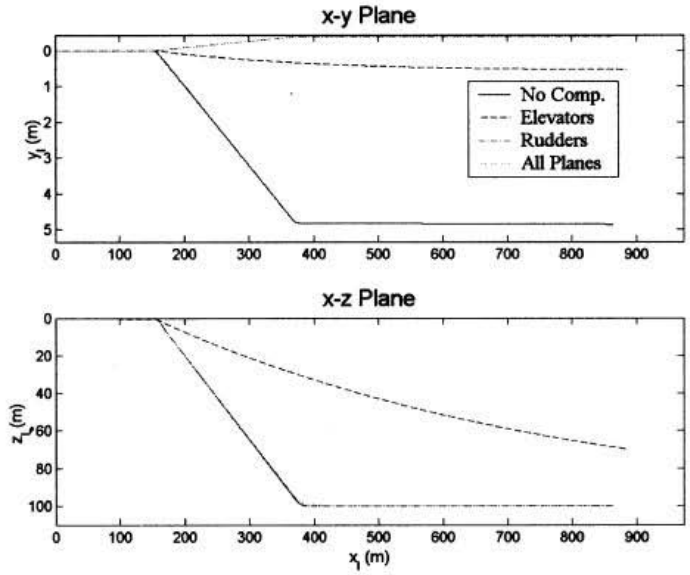

Figure 5-25: Comparison of Vehicle Response in a 100 m Dive when the Starboard Control Plane is Jammed at 0° ($k_z = 0.07$)

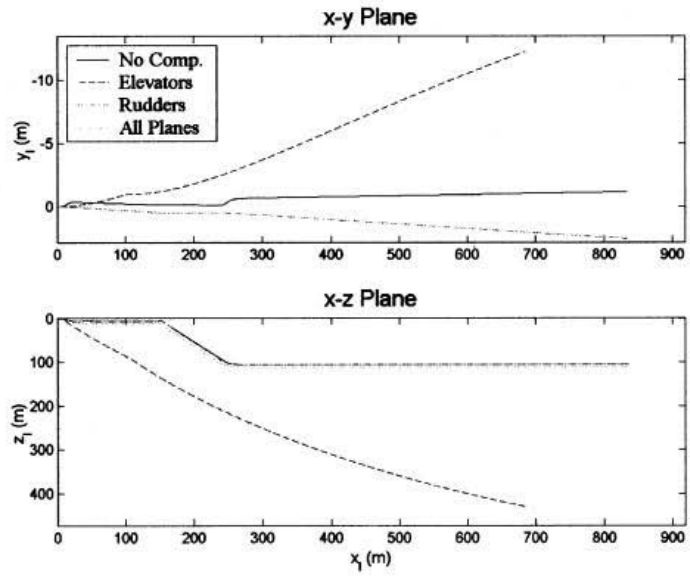

Figure 5-26: Comparison of Vehicle Response in a 100 m Dive when the Starboard Control Plane is Jammed at 25° ($k_z = 0.07$)

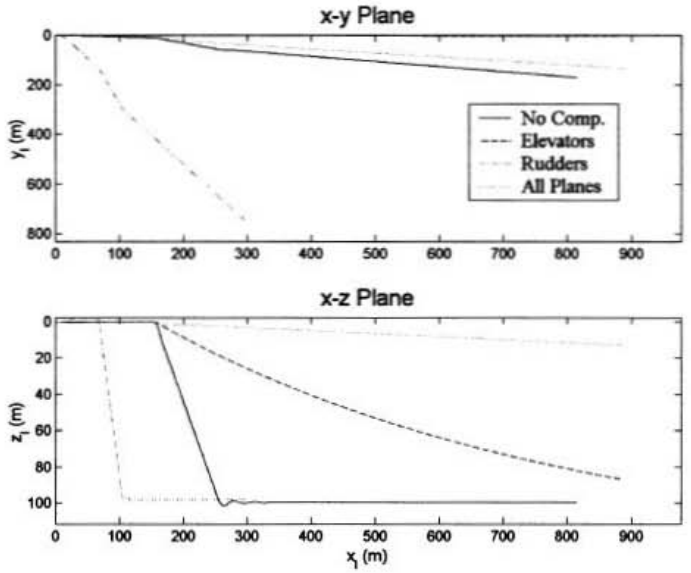

Figure 5-27: Comparison of Vehicle Response in a 100 m Dive when the Upper Control Plane is Jammed at -25° ($k_z = 0.07$)

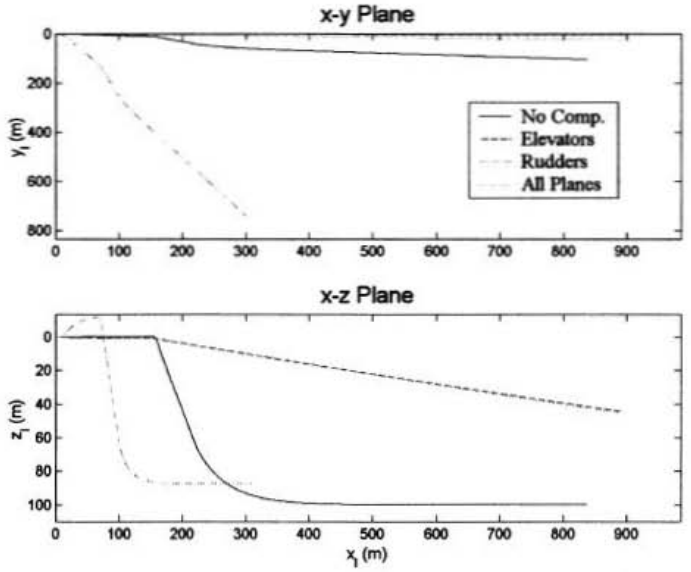

Figure 5-28: Comparison of Vehicle Response in a 100 m Dive when the Upper Control Plane is Jammed at -25° ($k_z = 0.01$)

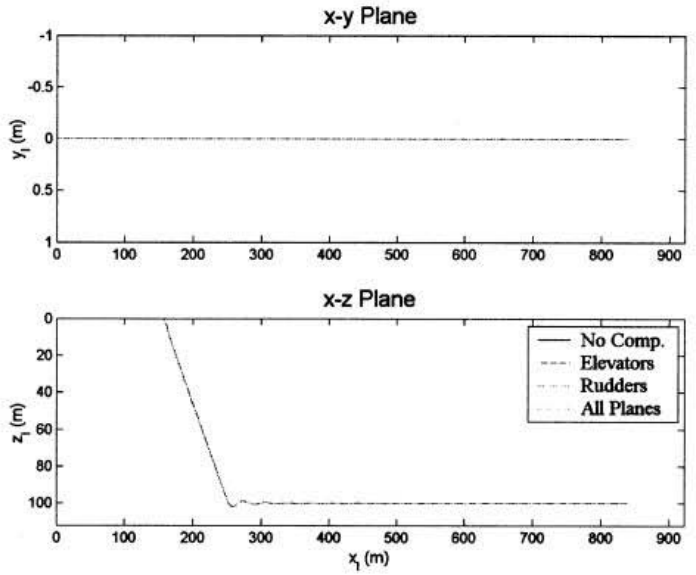

Figure 5-29: Comparison of Vehicle Response in a 100 m Dive when the Upper Control Plane is Jammed at 0° ($k_z = 0.07$)

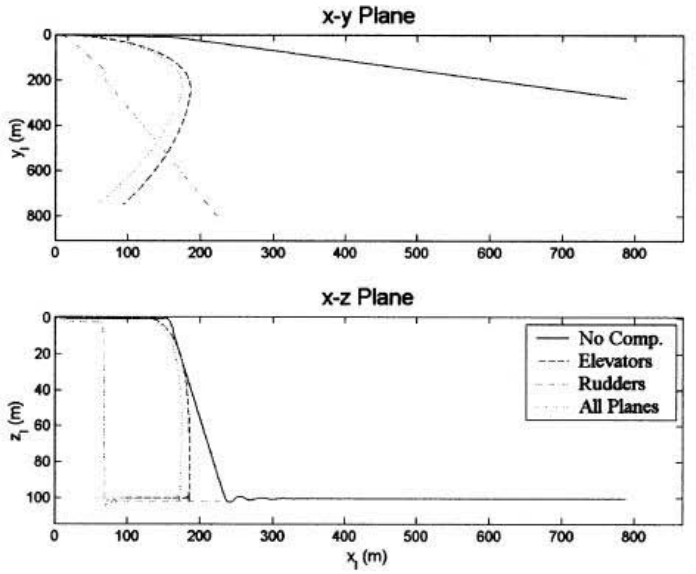

Figure 5-30: Comparison of Vehicle Response in a 100 m Dive when the Lower Control Plane is Jammed at -25° ($k_z = 0.07$)

Symmetry of Maneuvers and Symmetry of Fault Conditions

Both dives and holding course are maneuvers in the x-z plane of the inertial reference frame. Assuming the vehicle starts (and ends) the maneuver in straight and level flight (i.e., the body-fixed heave axis is parallel to the inertial z-axis), this plane is also the plane of symmetry of a vehicle like C-SCOUT. Vehicle response is expected to reflect this symmetry. Since the vehicle is not symmetric about the x-y plane of the body-fixed reference axes (even when the body-fixed heave axis is parallel to the inertial z-axis), the vehicle response is not expected be symmetric in the horizontal plane. The fault condition simulations show that, for holding course and diving maneuvers, the following are true:

- Symmetry condition 1: vehicle response with a jammed starboard control plane is similar to vehicle response with a jammed port control plane for any given angle of jam, the major difference being the direction of heading error induced;
- Symmetry condition 2: vehicle response with the upper (or lower) control plane jammed at a positive deflection angle is similar to vehicle response with the upper (or lower) control plane jammed at the same magnitude of negative deflection angle, with the direction of induced heading error again the major difference;
- Asymmetry condition 1: vehicle response with a jammed upper control plane is not necessarily similar to vehicle response with a jammed lower control plane for comparable angles of jam; and
- Asymmetry condition 2: vehicle response with the starboard (or port) control plane jammed at a positive deflection angle is not necessarily similar to vehicle response with the starboard (or port) control plane jammed at the same magnitude of negative deflection angle.

The turning maneuver, on the other hand is not in the plane of symmetry, and while the asymmetry conditions hold, the two symmetry conditions do not necessarily apply: there may be significant differences in response between the port and starboard jam conditions. In the case investigated here (a 180° turn to starboard), the starboard fin is inboard, while the port fin is outboard. The reverse occurs for a turn to port, and the responses outlined below for each of these fins would be reversed; i.e. the responses for a jammed starboard fin during a turn to starboard should be similar to the vehicle response when the port control plane is jammed (at the same angle) during a turn to port, since each is the inboard control plane in their respective maneuvers. The same asymmetry is applicable to the sign of upper or lower control plane deflection angles. For example, the vehicle response in a turn to a particular side at a given rudder deflection angle, for a positive angle of jam on the upper control plane will not be similar to the response in a turn to the same side when the upper control plane is jammed at an equivalent (in magnitude) negative deflection angle. However, the response to the upper fin positive-deflection-angle jam during a turn to starboard should be similar to the equivalent upper fin negative-deflection-angle jam during a turn to port.

Turning 180° with Jammed Horizontal Control Planes

Vehicle response in a turn using E is unacceptable when inboard fin (starboard in this case) is jammed at $-25°$, since the vehicle does not achieve the turn. Vehicle response in a turn using A is also unacceptable, since large heading and depth errors are induced. The response for control with R is best, since it reduces the drift in depth that occurs when N is used (see Figure 5-31). When the starboard control plane is jammed at $25°$, the depth increases rather than decreases for control with N, and the magnitude of the excursion is greater (compare Figures 5-31 and 5-32). Control with R is still superior to that with N, since the drift in depth is reduced with R. When the outboard (port in this case) control plane is jammed at $-25°$, the best response

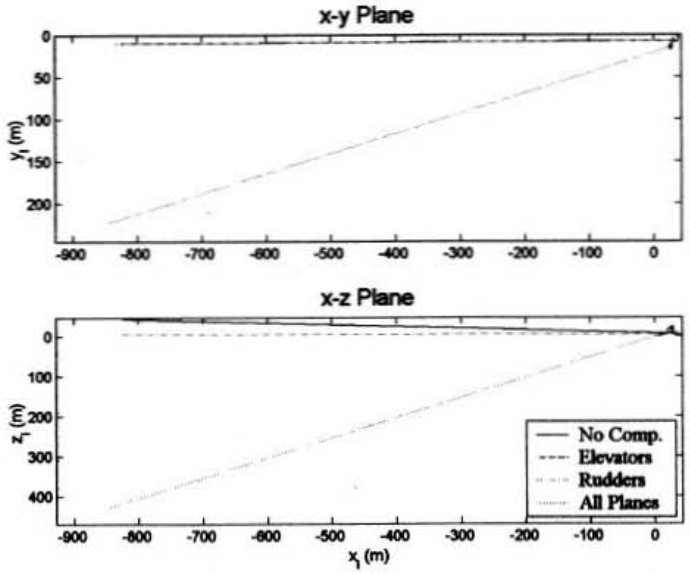

Figure 5-31: Comparison of Vehicle Response in a 180° Turn when the Starboard Control Plane is Jammed at -25° ($k_z = 0.07$)

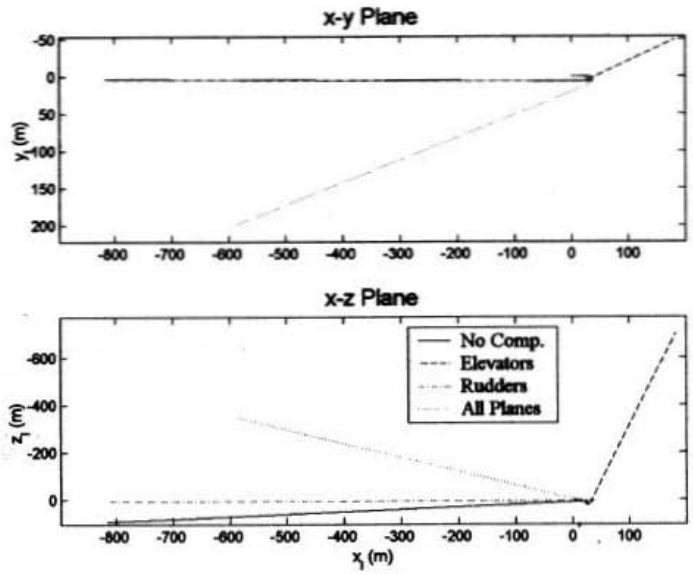

Figure 5-32: Comparison of Vehicle Response in a 180° Turn when the Starboard Control Plane is Jammed at 25° ($k_z = 0.07$)

is provided by the controller using A for roll compensation. while R tends to turn the vehicle more than desired and to induce a drift in depth (compare Figures 5-31 and 5-33). When the outboard control plane is jammed at 25°. the control with A still reduces the depth error. but the heading error is greater than that for N. Control with R is unacceptable for large-angle jams on the outboard control plane. while it is preferred for large-angle jams on the inboard control plane. When the lower gain is used for the depth controller. the vehicle response is generally poorer (larger depth excursions and greater heading error) in turns with an inboard control plane jammed (e.g. compare Figures 5-32 and 5-35). however the response for positive jams on the port (outboard) control plane is improved when A is used along with the lower gain for the depth controller (compare Figures 5-34 and 5-36). The vehicle response for jams at zero degrees for either control plane are similar (compare Figures 5-37 and 5-38). as might be expected since nominally both fins would be near zero deflection in a turn. anyway. Again. E causes more problems than it solves.

Turning 180° with Jammed Vertical Control Planes

When the upper control plane is jammed at −25°. the vehicle will turn past 180° if no roll compensation is used (see Figure 5-39). Active roll compensation via the elevators or all (remaining) control planes will help the vehicle achieve the correct amount of turn. while keeping the depth excursion small. Similar behaviour results when either depth controller gain is used. but the higher gain depth controller reduces the depth excursion (compare Figures 5-39 and 5-40). When the upper control plane is jammed at 25°. the vehicle will not achieve 180° if no roll compensation is used (see Figure 5-41). Again. active roll compensation via E or A will help the vehicle achieve the correct amount of turn. while keeping the depth excursion small. When the lower control plane is jammed at −25°. the vehicle will again turn past 180° if N is used. but in this case. neither E or A will not help the vehicle achieve the correct amount of turn in a reasonable time (see Figure 5-42). When the lower fin jams at

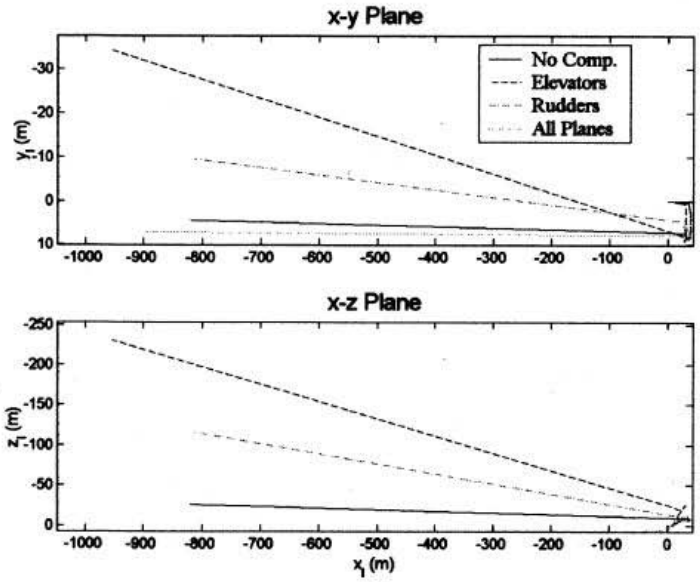

Figure 5-33: Comparison of Vehicle Response in a 180° Turn when the Port Control Plane is Jammed at -25° ($k_z = 0.07$)

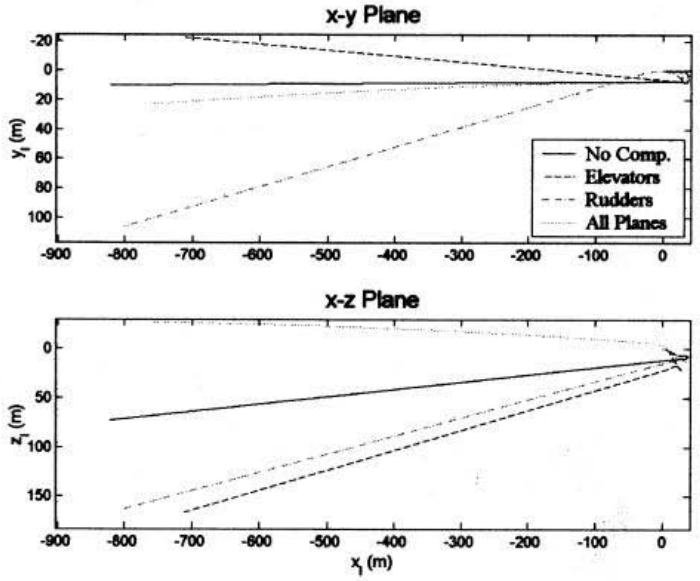

Figure 5-34: Comparison of Vehicle Response in a 180° Turn when the Port Control Plane is Jammed at 25° ($k_z = 0.07$)

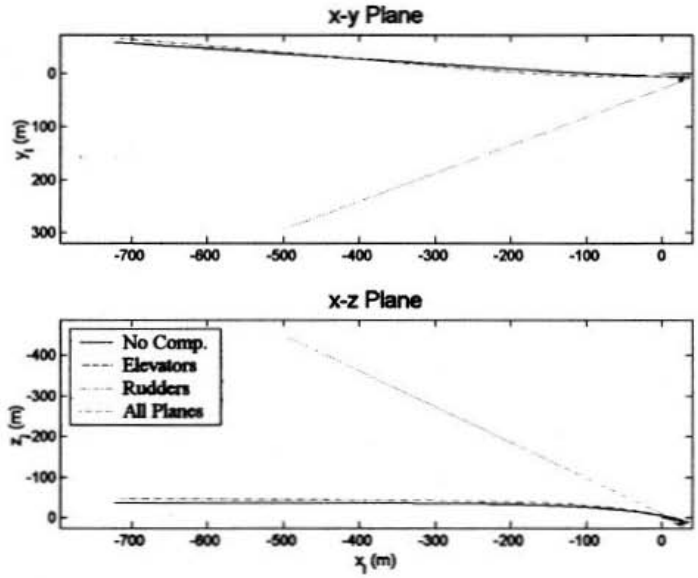

Figure 5-35: Comparison of Vehicle Response in a 180° Turn when the Starboard Control Plane is Jammed at 25° ($k_z = 0.01$)

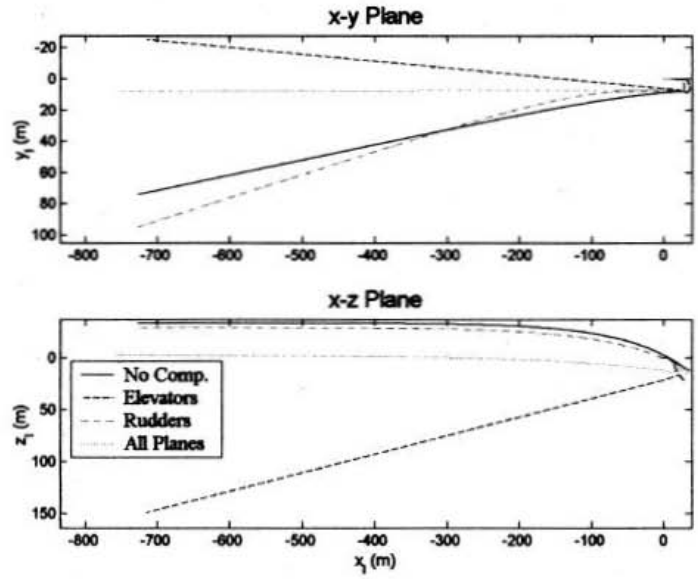

Figure 5-36: Comparison of Vehicle Response in a 180° Turn when the Port Control Plane is Jammed at 25° ($k_z = 0.01$)

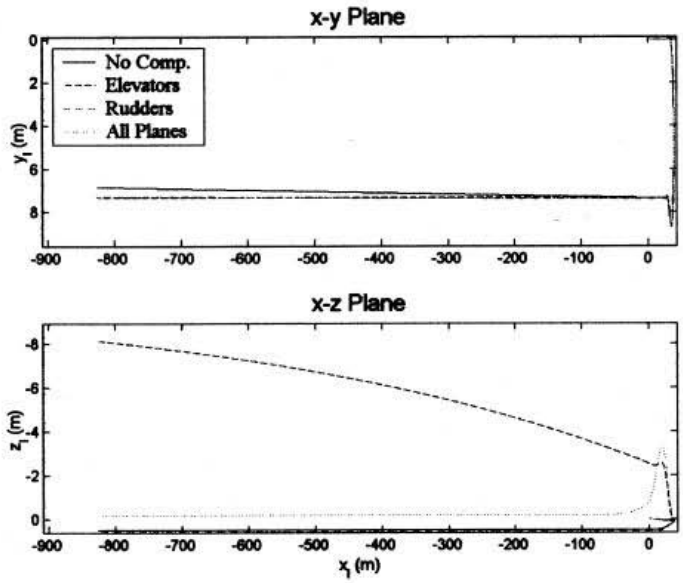

Figure 5-37: Comparison of Vehicle Response in a 180° Turn when the Starboard Control Plane is Jammed at 0° ($k_z = 0.07$)

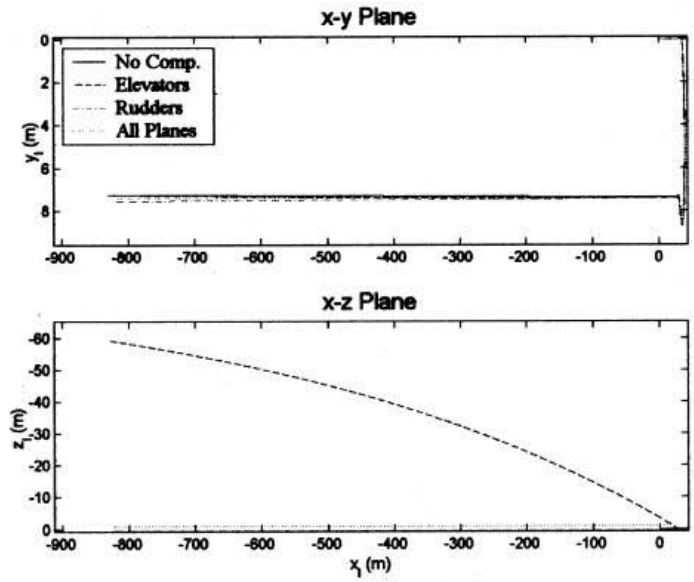

Figure 5-38: Comparison of Vehicle Response in a 180° Turn when the Port Control Plane is Jammed at 0° ($k_z = 0.07$)

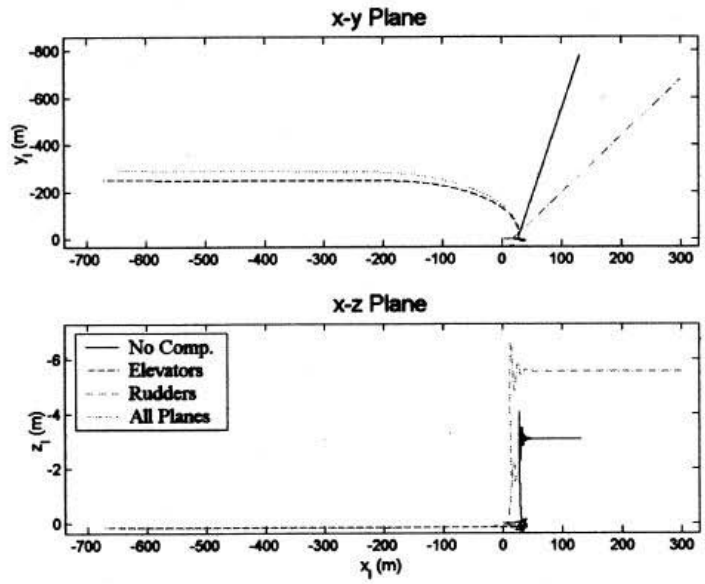

Figure 5-39: Comparison of Vehicle Response in a 180° Turn when the Upper Control Plane is Jammed at -25° ($k_z = 0.07$)

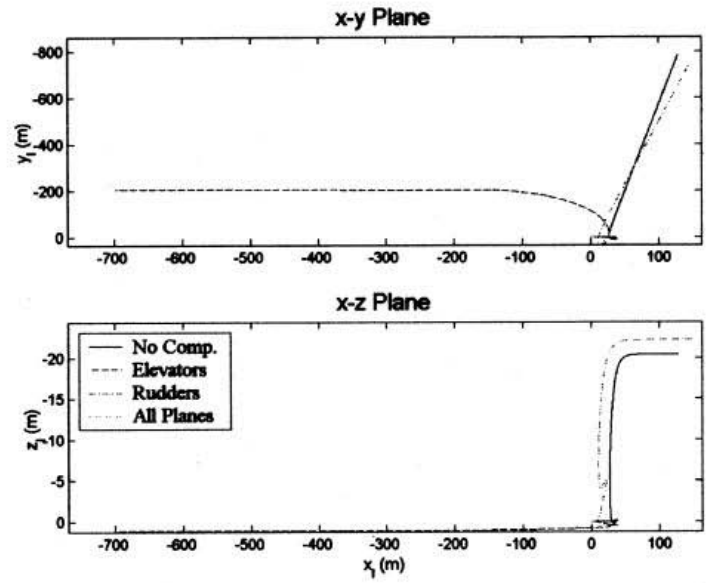

Figure 5-40: Comparison of Vehicle Response in a 180° Turn when the Upper Control Plane is Jammed at -25° ($k_z = 0.01$)

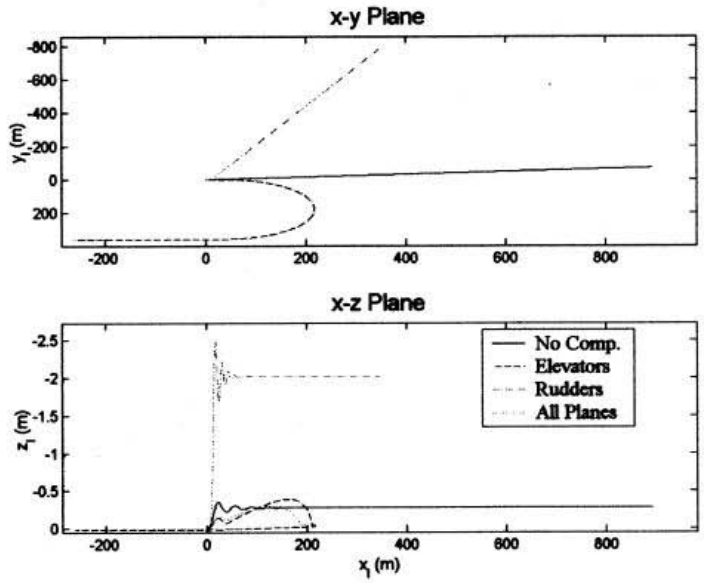

Figure 5-41: Comparison of Vehicle Response in a 180° Turn when the Upper Control Plane is Jammed at 25° ($k_z = 0.07$)

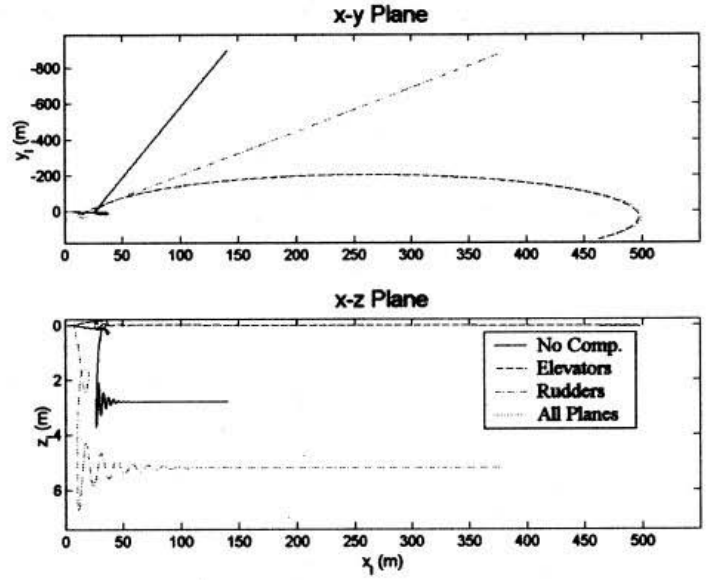

Figure 5-42: Comparison of Vehicle Response in a 180° Turn when the Lower Control Plane is Jammed at -25° ($k_z = 0.07$)

25°, the vehicle response is not acceptable even with active roll compensation, since the vehicle will not achieve 180° if N is used, and it turns past 180° if E or A is used (see Figure 5-43). The controller with no active roll compensation gives a reasonable response if the upper control plane is jammed at zero degrees (see Figure 5-44). The vehicle response with the lower control plane jammed at zero degrees is similar to that with the upper control plane jammed at zero. In fact, the responses for jams at $\pm 10°$ are similar for the upper and lower control planes; it is only at the higher angles of jam that there are significant differences in the vehicle response.

General Comments on Jammed Control Planes

Using the elevators alone was ineffective when the jammed plane is one of the horizontal planes. The same was true of the rudders when the jammed plane is one of the vertical planes. The vehicle response (in terms of depth and heading error) when active roll compensation via all planes, A, is incorporated is sometimes worse than the response of the vehicle without active roll compensation, N, but these errors may be corrected by supplementing the present proportional controller with integral action.

The vehicle response with the underdamped depth controller ($k_z = 0.07$) was similar to the vehicle response with the overdamped depth controller ($k_z = 0.01$), except that the depth was better controlled (less steady state error), as expected. In turns, this improved depth control also induced a reduction in heading error.

5.3.4 Missing Control Planes

Holding Course with Missing Horizontal Control Planes

For the cases of port or starboard control plane missing, active roll compensation does not significantly improve the vehicle response for holding course when the overdamped (lower gain) depth controller is used (see Figure 5-45). The errors in heading and depth are small even when N is used. The control with E induces a drift in depth

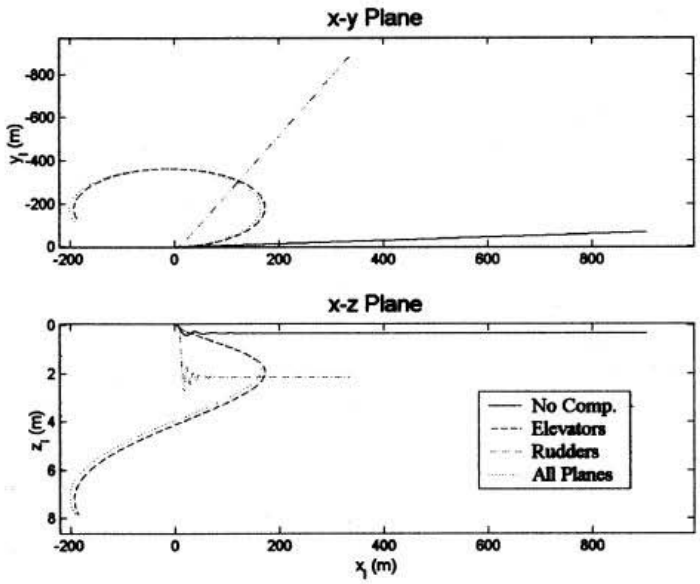

Figure 5-43: Comparison of Vehicle Response in a 180° Turn when the Lower Control Plane is Jammed at 25° ($k_z = 0.07$)

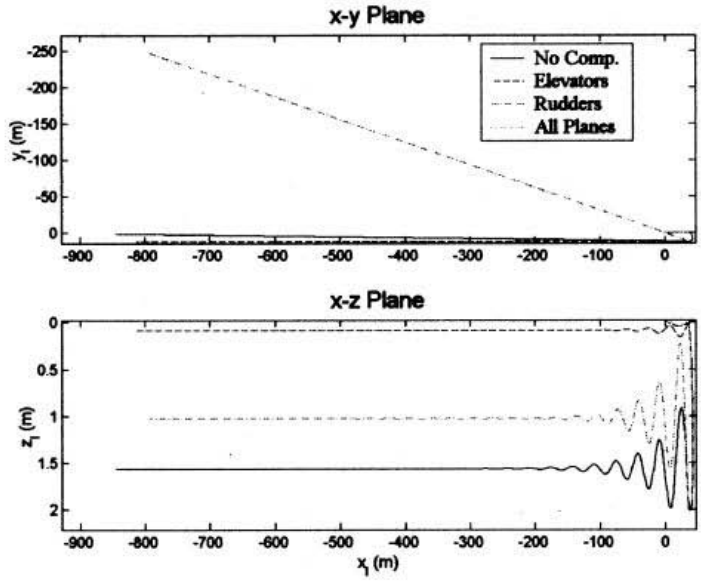

Figure 5-44: Comparison of Vehicle Response in a 180° Turn when the Upper Control Plane is Jammed at 0° ($k_z = 0.07$)

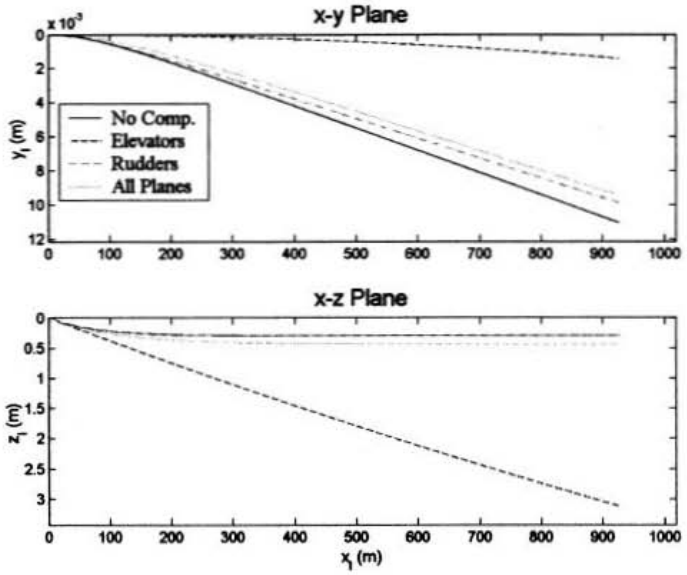

Figure 5-45: Comparison of Vehicle Response in Holding Course when the Starboard Control Plane is Missing ($k_z = 0.01$)

that would make the vehicle response less acceptable. The response for the vehicle when the port control plane is missing is essentially the same except that the heading error is in the opposite direction. When the underdamped (higher gain) controller is used, the vehicle response becomes unstable in all cases except for control with E (see Figure 5-46). Only active roll compensation via the elevators provides stable control, but the vehicle is unable to maintain depth, though the error is small for holding course.

Holding Course with Missing Vertical Control Planes

When either the upper or the lower control plane is missing, there is no induced roll and the vehicle has the same response while holding course with or without active roll compensation (see Figure 5-47). The vehicle response is very similar to that of the nominal (healthy) vehicle (compare Figure 5-47 with Figure 5-6). This result assumes

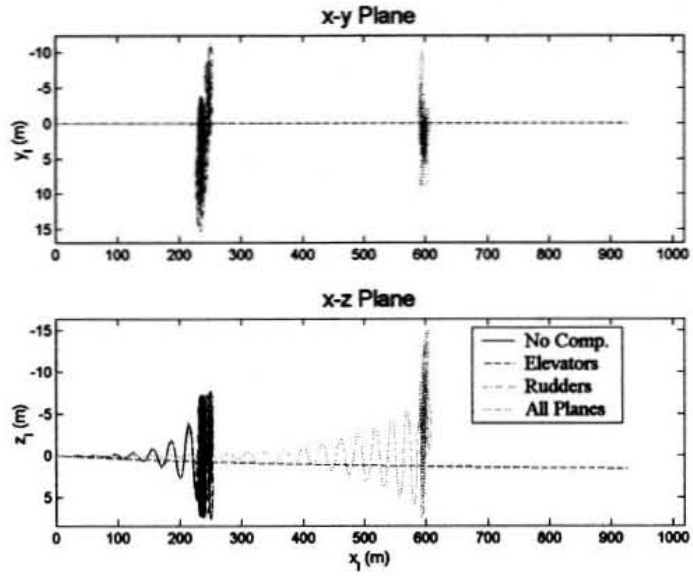

Figure 5-46: Comparison of Vehicle Response in Holding Course when the Starboard Control Plane is Missing ($k_z = 0.07$)

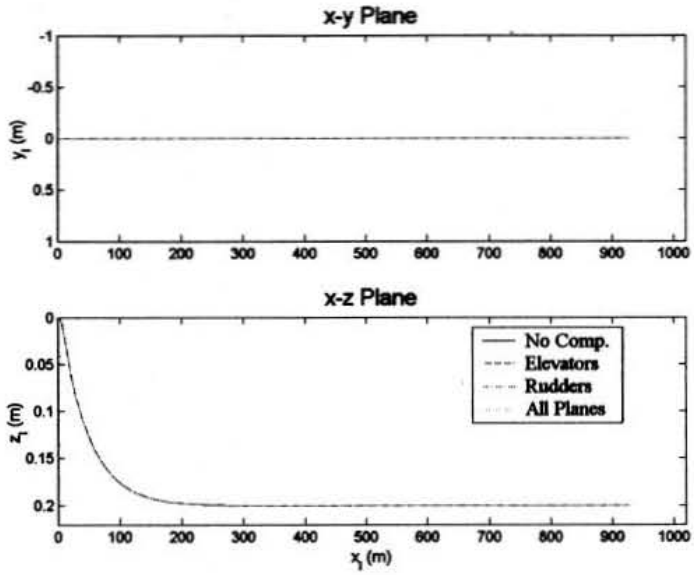

Figure 5-47: Comparison of Vehicle Response in Holding Course when the Upper Control Plane is Missing ($k_z = 0.01$)

that whatever the cause of the missing control plane, the vehicle remains symmetrical about the x-z plane; this is somewhat unlikely in the context of a real mission.

Diving 100 m with Missing Horizontal Control Planes

When either of the horizontal planes is missing, R or A gives better vehicle response in dive than control without active roll compensation, since they reduce the heading error (sway offset - see Figure 5-48). Roll compensation via E is, understandably, inadequate. This is true when the overdamped ($k_z = 0.01$) depth controller is used, however, when the underdamped ($k_z = 0.07$) depth controller is used, the vehicle response is not acceptable for any of the cases (see Figure 5-49). Roll compensation via E provides the best response, but it is still insufficient to achieve the dive in a reasonable time.

Diving 100 m with Missing Vertical Control Planes

The vehicle response in dive is very similar to that of the nominal (healthy) vehicle (compare Figure 5-50 with Figure 5-8). When either the upper or the lower control plane is missing, there is no induced roll and the vehicle has the same response with or without active roll compensation.

Turning 180° with Missing Horizontal Control Planes

For the overdamped depth controller, the vehicle response in turns with R was best, but it was only slightly better (less heading error) than the response with N (see Figure 5-51). For the underdamped depth controller, only active roll compensation via the elevators was able to adequately accomplish the turn, but even this controller was unable to maintain the depth (see Figure 5-52). The response in a turn with the port control plane missing is similar to that with the starboard plane missing (compare Figure 5-51 and Figure 5-53). Again, the response with R is slightly better than the response with N.

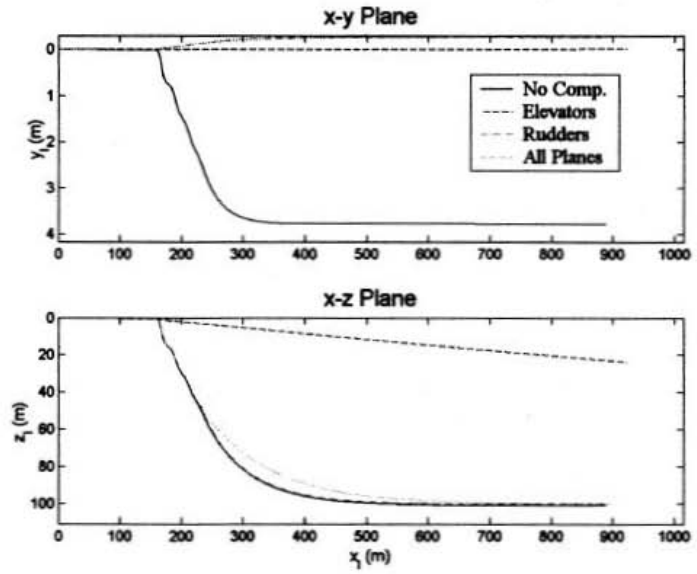

Figure 5-48: Comparison of Vehicle Response in a 100 m Dive when the Starboard Control Plane is Missing ($k_z = 0.01$)

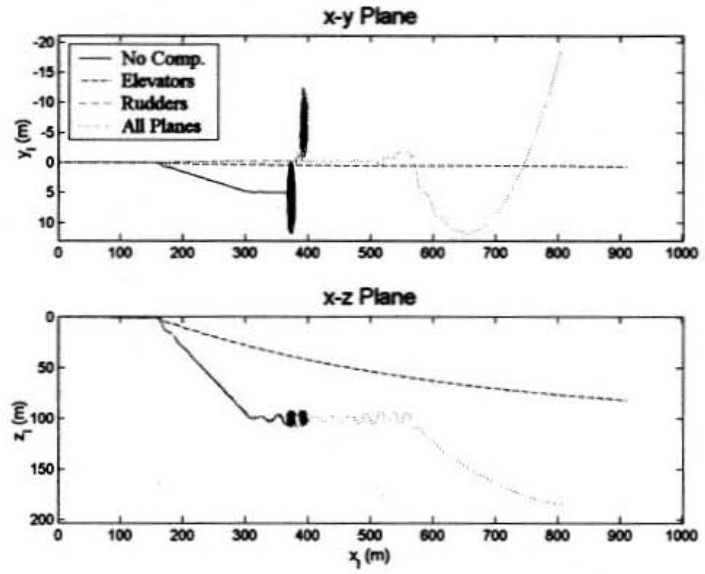

Figure 5-49: Comparison of Vehicle Response in a 100 m Dive when the Starboard Control Plane is Missing ($k_z = 0.07$)

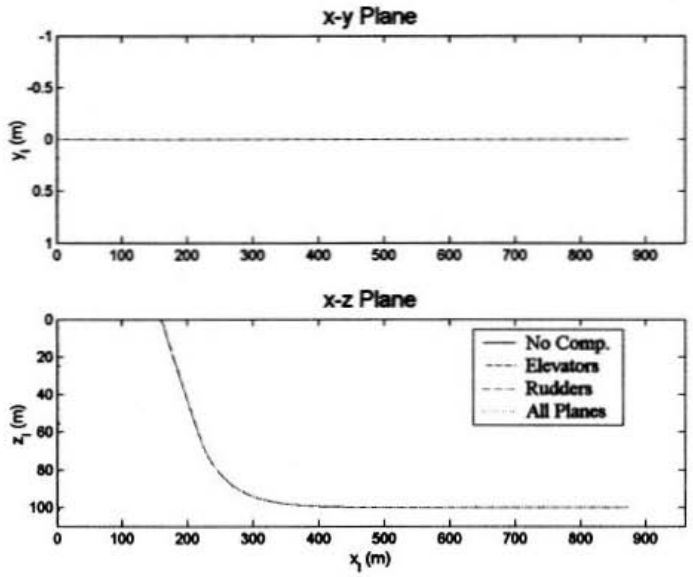

Figure 5-50: Comparison of Vehicle Response in a 100 m Dive when the Upper Control Plane is Missing ($k_z = 0.01$)

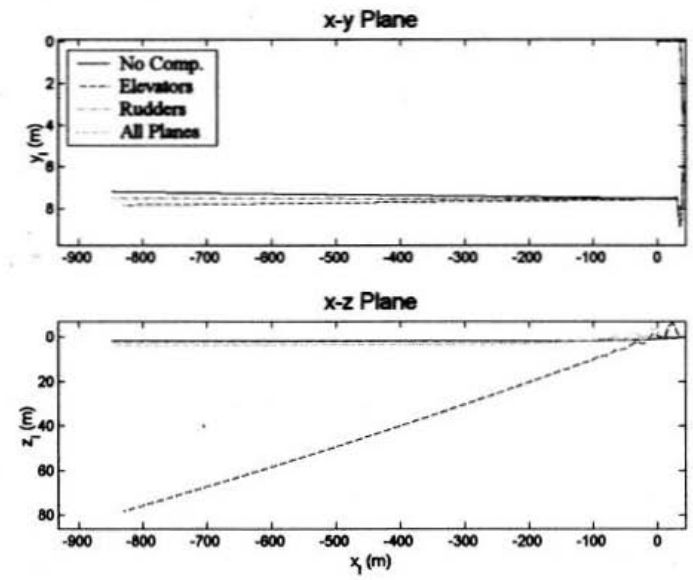

Figure 5-51: Comparison of Vehicle Response in a 180° Turn when the Starboard Control Plane is Missing ($k_z = 0.01$)

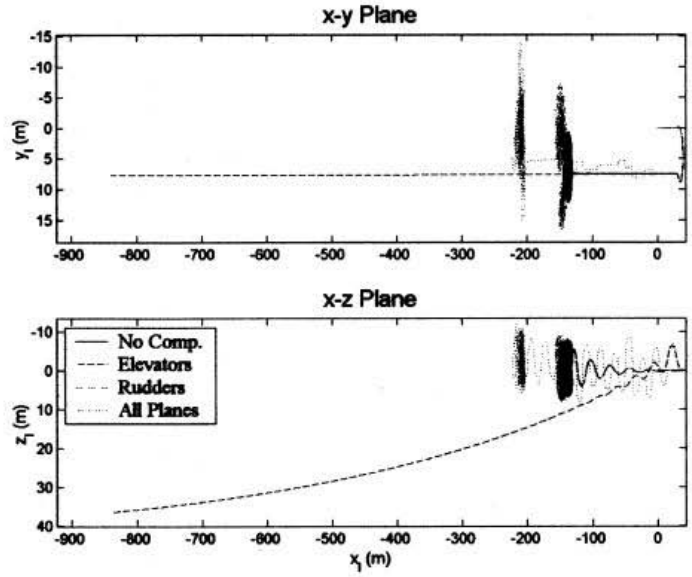

Figure 5-52: Comparison of Vehicle Response in a 180° Turn when the Starboard Control Plane is Missing ($k_z = 0.07$)

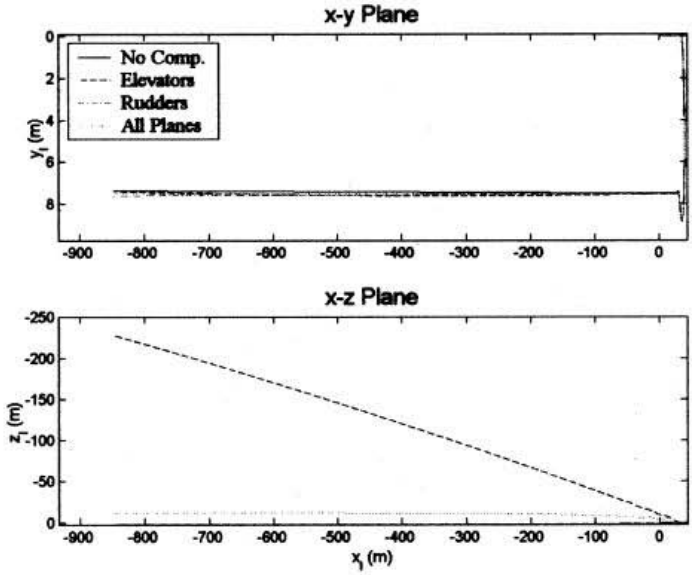

Figure 5-53: Comparison of Vehicle Response in a 180° Turn when the Port Control Plane is Missing ($k_z = 0.01$)

Turning 180° with Missing Vertical Control Planes

In the cases of the vertical control planes missing during turns, the integrator was unable to resolve the model, and no data is available.

5.4 Operational Envelopes

5.4.1 Safety Context

Submarines[83]

Manned submarines can have two basic hazards: flooding and depth excursions such as may be caused by a jammed control plane. In both cases, the recovery procedure involves ascending.

In the case of flooding, the submarine must surface to allow the crew to escape; there is little hope of keeping the submarine from sinking eventually (unless the flooding can be stopped quickly enough), because, even at the surface, submarines have very little reserve buoyancy. "Recovery" from flooding involves blowing the main ballast tanks, invoking whatever buoyancy is still available. To supplement the hydrostatic force of buoyancy, hydrodynamic lift forces can be generated by increasing speed and setting the dive planes to cause the submarine to ascend. Clearly, the faster the submarine is travelling, the more rapidly it will ascend when the control planes are used. This indicates that, at greater depths, there is a minimum safe operating speed that will allow recovery from a flood situation at that depth.

On the other hand, depth excursions due to control plane jams are more dangerous at higher speeds, since the submarine will dive deeper in a given time period. Therefore the recovery procedure will involve reducing speed. For some submarines, setting the rudders hard over will assist in slowing down the submarine. The ascent will be assisted if the unjammed fins are set to pitch the submarine upwards. (Submarines often have a set of dive planes forward on the hull or on the sail, in

addition to the after planes. If one of the control planes jams, it may be necessary to set the corresponding plane on the other side of the submarine to the same angle to avoid roll, but the other set of dive planes can be used to counteract the dive.) The possibility of a jammed control plane suggests that there is a maximum safe operating speed at depth. Further, if it is assumed that the control plane will jam at the angle it was set to, the possibility of a depth excursion due to a jammed plane also suggests that there should be restrictions on the control plane deflection angles when operating near the maximum depth for the submarine. This suggests that there exists an "operational envelope" for submarines: a range of safe operating speeds and control plane deflection angles.

AUV

In the case of an AUV, the risk to human occupants does not exist, but it is desirable to be able to recover the vehicle. Vehicles like the C-SCOUT have an Emergency Response System (ERS) of one form or another. C-SCOUT's ERS will include a releasable ballast. C-SCOUT is also free-flooding except for the pressure vessel and the control plane actuator motor housings. If the pressure vessel floods, the electronics will shut down and the ERS will automatically release the ballast, bringing the vehicle to the surface rapidly. (This recovery method is not really suitable for manned submarines since the rate of ascent would be rapid, and the slamming of the vehicle after it breaches the surface would be dangerous for a large structure and its occupants.)

If one of the actuator motor housings floods, the control plane would most likely jam.

The baseline C-SCOUT has only one set of horizontal control planes. Recovery from a jammed horizontal plane should involve reduction in speed to avoid large depth excursions. Restrictions on speed and deflection angles may also be appropriate.

5.4.2 Performance Context

The idea of operational envelopes can be utilized for performance criteria as well as safety considerations. In Tables 5.1 through 5.6. N. E. R. and A are as defined above. The lower case letters represent the individual control planes which jam: s for starboard, p for port, u for upper, and l for lower. The two columns represent the two possible cases of roll relevance. Either the roll is important, such as when holding course on a swath scanning mission, or the roll is unimportant, such as when turning around at the end of a particular track. The values in the tables represent the approximate (hence the tilde, ~) range of safe deflection angles: i.e., if the control planes jammed at these angles, the maneuver would still be achievable within the above limits. Note that ~0 means the deflection angles should be limited to near zero, and NR (no range) indicates the response was not acceptable even at a jam of zero degrees.

The control planes are used in pairs in this work: e.g., the upper and lower control planes are used together as a rudder to affect turns. The italics indicate that particular control plane has a less restrictive operating range, but it has been assigned the restrictions that apply to its counterpart: i.e., each pair of control planes is restricted by the most limited range of the individual control planes that make up the pair. For example, in Table 5.1, the safe operating range for the upper control plane is ~[-25.25], however, since it is used in conjunction with the lower control plane which has a safe operating range of ~[-10.10], the upper control plane is also limited to *~[-10.10]*, and the fact that this range is imposed on it by the lower control plane constraint is indicated by italics.

As an example, Table 5.2 shows the safe operating range of control plane deflection angle for each control surface, for each roll compensation method, for holding course with a depth controller gain of 0.07. When roll is important (i.e. it must be kept within $\pm 1^\circ$ of zero, the information in the table indicates that for the controller without roll compensation (N), all the fins must operate near zero degrees of deflec-

tion angle to avoid compromising one of the following two (arbitrary) conditions: (a) $z_{err} < 1$ m. and (b) $\psi_{err} < 0.01$ rad. When the roll angle can exceed the above limit. the information in the table indicates that for N. the port and starboard (horizontal) control planes may operate within a range of $\pm 25^\circ$ of deflection angle. but the upper and lower (vertical) control planes may only operate within a range of $\pm 10^\circ$ of deflection angle without danger of compromising either one of the two conditions.

Figures 5-54 through 5-59 show envelopes of acceptable operation: they are graphical displays of the information in Tables 5.1 through 5.6. for each compensation method when the depth controller gain is 0.07. For example. Figure 5-54 is a graphical representation of the information contained in the first four rows of Table 5.1 for the controller without active roll compensation. used to hold course when the specific fins experience a jam condition. The roll compensation method used is indicated by the letter (N. E. R. or A) in the upper left corner of the figure. and the depth controller gain is noted along with the maneuver type above the coloured block. The heading across the top indicates the angle of jam for the particular control plane. The control planes are listed down the left side.

The coloured block is a matrix of jammed plane conditions. and the colour of a particular element of the matrix indicates the acceptability of the vehicle response in the specified maneuver with the particular control plane jammed at the given angle. The yellow (lightest gray) and shaded yellow (next lightest gray) areas show the response of the vehicle is acceptable in depth ($z_{err} < 1$ m). and heading ($\psi_{err} <$ 0.01 rad). The shaded blue (dark gray) and blue (next darkest gray) areas indicate the vehicle response is not acceptable in depth and heading. The shading indicates where the roll requirement ($\phi < 0.01743$ rad) is not met.

For example. Figure 5-54. only the upper and lower control planes at $\pm 25^\circ$ are blue. indicating a compromise of the above criteria. Therefore if roll is not important. the horizontal control planes may operate within a range of $\pm 25^\circ$. and the vertical control planes may operate within a range of $\pm 10^\circ$. However. all the control planes

are shaded at $\pm 10^\circ$ and $\pm 25^\circ$, indicating that when the roll angle must be limited, all the control planes should operate near 0° of deflection (which is not practical).

The best situation would see the entire block as yellow (lightest gray). These figures represent the performance envelopes at a speed of 3 m/s. For a more complete picture of the operational performance limits, a similar analysis at other vehicle speeds must be added.

5.4.3 Simulation Results

Based on the information in Tables 5.1 and 5.2, it is recommended that the higher depth control gain (0.07) be used when holding course, since the operating ranges for horizontal control planes are broader for the N, R, and A controllers when roll is not important, and the operating ranges are broader for the R and A controllers when roll must be controlled to within one degree. The higher gain in effect increases the control authority of the horizontal control planes, leading to faster response and tighter depth control.

With a depth controller gain of 0.07, if vehicle roll angle is not an important issue, no active roll compensation is necessary. The operational envelope will be unrestricted (up to the maximum $\pm 25^\circ$) for the horizontal (starboard/port) planes, and restricted to about $\pm 10^\circ$ for the vertical (upper/lower) control planes (see Figure 5-54). If roll is important, it can be kept within $\pm 1^\circ$ using active roll compensation via all the (remaining) control planes. In terms of the operational envelope, the cost of controlling the roll is that the horizontal planes are now restricted to about $\pm 10^\circ$ too (see Figure 5-55).

Tables 5.3 and 5.4 show that the depth controller gain of 0.07 gives better results (though perhaps only marginally), since the safe operating range for the controller without active roll compensation (N) is increased from ˜[0.10] to ˜[10.10].

With the depth controller gain set to 0.07, and if roll angle is not important, then no active roll compensation is required. The operational envelope (see Figure

Table 5.1: Range of Safe Control Plane Deflections for Vehicle Holding Course Based on Jammed Control Planes ($k_z = 0.01$)

Hold ($k_z = 0.01$)		Roll Important	Roll Unimportant
N	s	˜0	˜0
	p	˜0	˜0
	u	˜0	˜[-10.10]
	l	˜0	˜[-10.10]
E	s	˜0	˜0
	p	˜0	˜0
	u	*˜[-10.10]*	*˜[-10.10]*
	l	˜[-10.10]	˜[-10.10]
R	s	˜0	˜0
	p	˜0	˜0
	u	˜0	˜0
	l	˜0	˜0
A	s	˜0	˜0
	p	˜0	˜0
	u	˜[-10.10]	˜[-10.10]
	l	˜[-10.10]	˜[-10.10]

Table 5.2: Range of Safe Control Plane Deflections for Vehicle Holding Course Based on Jammed Control Planes ($k_z = 0.07$)

Hold ($k_z = 0.07$)		Roll Important	Roll Unimportant
N	s	˜0	˜[-25.25]
	p	˜0	˜[-25.25]
	u	˜0	˜[-10.10]
	l	˜0	˜[-10.10]
E	s	˜0	˜0
	p	˜0	˜0
	u	*˜[-10.10]*	*˜[-10.10]*
	l	˜[-10.10]	˜[-10.10]
R	s	*˜[-10.10]*	*˜[-10.10]*
	p	˜[-10.10]	˜[-10.10]
	u	˜0	˜0
	l	˜0	˜0
A	s	˜[-10.10]	˜[-10.10]
	p	˜[-10.10]	˜[-10.10]
	u	˜[-10.10]	˜[-10.10]
	l	˜[-10.10]	˜[-10.10]

Table 5.3: Range of Safe Control Plane Deflections for Vehicle Diving 100 m Based on Jammed Control Planes ($k_z = 0.01$)

Dive ($k_z = 0.01$)		**Roll Important**	**Roll Unimportant**
N	s	˜0	˜0
	p	˜0	˜0
	u	˜0	˜[0.10]
	l	˜0	˜*[0.10]*
E	s	NR	NR
	p	NR	NR
	u	˜[10.10]	˜[10.10]
	l	˜[10.10]	˜[10.10]
R	s	˜0	˜0
	p	˜0	˜0
	u	˜0	˜0
	l	˜0	˜0
A	s	˜0	˜0
	p	˜0	˜0
	u	˜[-10.10]	˜[-10.10]
	l	˜[-10.10]	˜[-10.10]

Table 5.4: Range of Safe Control Plane Deflections for Vehicle Diving 100 m Based on Jammed Control Planes ($k_z = 0.07$)

Dive ($k_z = 0.07$)		**Roll Important**	**Roll Unimportant**
N	s	˜0	˜0
	p	˜0	˜0
	u	˜0	˜[10.10]
	l	˜0	˜[10.10]
E	s	NR	NR
	p	NR	NR
	u	˜[10.10]	˜[10.10]
	l	˜[10.10]	˜[10.10]
R	s	˜0	˜0
	p	˜0	˜0
	u	˜0	˜0
	l	˜0	˜0
A	s	˜0	˜0
	p	˜0	˜0
	u	˜[-10.10]	˜[-10.10]
	l	˜[-10.10]	˜[-10.10]

Table 5.5: Range of Safe Control Plane Deflections for Vehicle Turning 180 Degrees Based on Jammed Control Planes ($k_z = 0.01$)

Turn ($k_z = 0.01$)		**Roll Important**	**Roll Unimportant**
N	s	NR	~0
	p	NR	~0
	u	NR	~[0.10]
	l	NR	~[0.10]
E	s	NR	NR
	p	NR	NR
	u	*~[-10.10]*	*~[-10.10]*
	l	~[-10.10]	~[-10.10]
R	s	~0	~0
	p	~0	~0
	u	NR	NR
	l	NR	NR
A	s	~0	~0
	p	*~0*	*~0*
	u	~[-10.10]	~[-10.10]
	l	~[-10.10]	~[-10.10]

Table 5.6: Range of Safe Control Plane Deflections for Vehicle Turning 180 Degrees Based on Jammed Control Planes ($k_z = 0.07$)

Turn ($k_z = 0.07$)		**Roll Important**	**Roll Unimportant**
N	s	NR	~[0.10]
	p	NR	~[0.10]
	u	NR	~[0.10]
	l	NR	~[0.10]
E	s	*NR*	*NR*
	p	NR	NR
	u	*~[-10.10]*	*~[-10.10]*
	l	~[-10.10]	~[-10.10]
R	s	*~[-10.10]*	*~[-10.10]*
	p	~[-10.10]	~[-10.10]
	u	NR	NR
	l	NR	NR
A	s	~0	~0
	p	*~0*	*~0*
	u	~[-10.10]	~[-10.10]
	l	~[-10.10]	~[-10.10]

5-56) would indicate that horizontal control planes should be restricted to angles near zero. but this would not allow the maneuver to be achieved in reasonable time. therefore. the envelope should be expanded to at least $\pm 10^\circ$ and some degradation of performance expected if one of the horizontal planes does jam at an angle not near zero. If the roll angle must be kept within one degree of zero. active roll compensation using all the remaining unjammed control surfaces is best. The operational envelope (Figure 5-57) would also indicate that horizontal control planes should be restricted to angles near zero. but this should be expanded to at least $\pm 10^\circ$ and some degradation of performance expected if one of the horizontal planes does jam at an angle not near zero.

Comparison of Tables 5.5 and 5.6 indicates that the depth controller with a gain of 0.07 still provides better performance. since it broadens the safe operating range of the port and starboard control planes both when no active roll compensation is used. and when roll compensation via rudders is used.

As with holding course and diving. when the higher gain depth controller is implemented. and if roll is not important. then there is no need for active roll compensation and vehicle response is better without it (Figure 5-58).

On the other hand. if roll is important. the active roll compensation via all planes improves the vehicle performance (Figure 5-59). since the vehicle without active roll compensation is unable to maintain the desired roll angle even if the jam is near zero (see Figure 5-58).

5.5 AUV Fault Self-Diagnosis Maneuvers

The idea of the "self-diagnostic" vehicle maneuver is to use the behaviour of the vehicle during a commanded maneuver to determine whether there is a jammed or missing control plane. The condition would be detected by measuring an asymmetry in the hydrodynamic loads on the vehicle or fin. that would indicate the type of fin

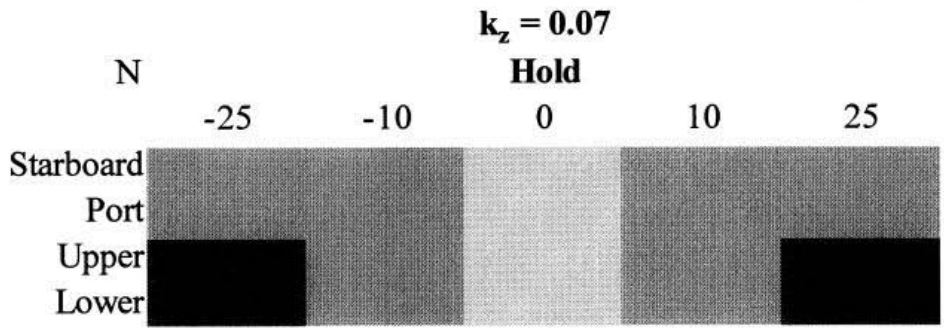

Figure 5-54: Operational Envelope Based on Control Plane Jams for the AUV Holding Course (Depth Controller Gain of 0.07; No Active Roll Compensation)

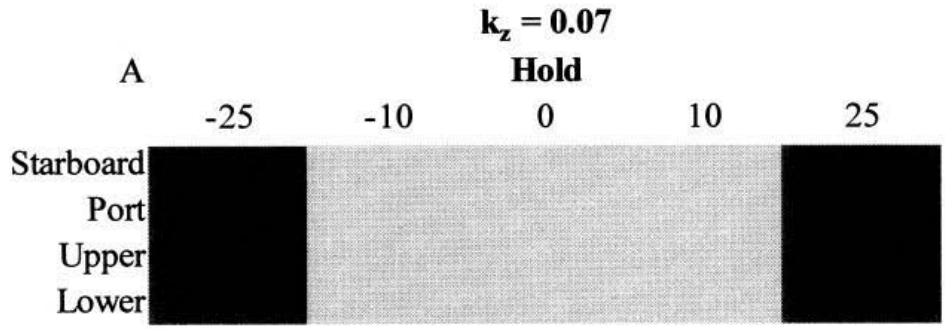

Figure 5-55: Operational Envelope Based on Control Plane Jams for the AUV Holding Course (Depth Controller Gain of 0.07; Active Roll Compensation via All Control Planes)

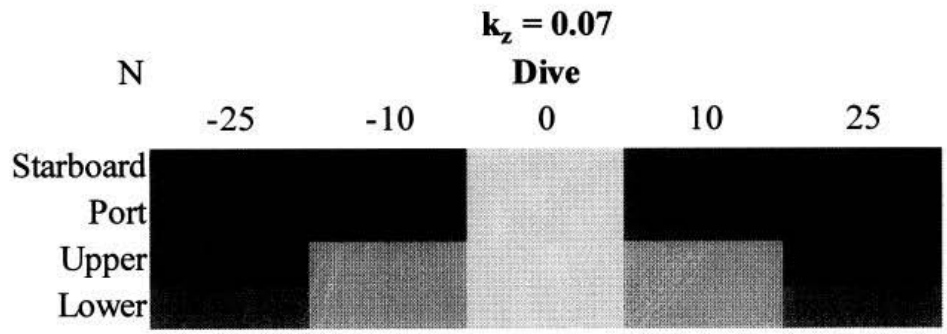

Figure 5-56: Operational Envelope Based on Control Plane Jams for the AUV Diving 100m (Depth Controller Gain of 0.07; No Active Roll Compensation)

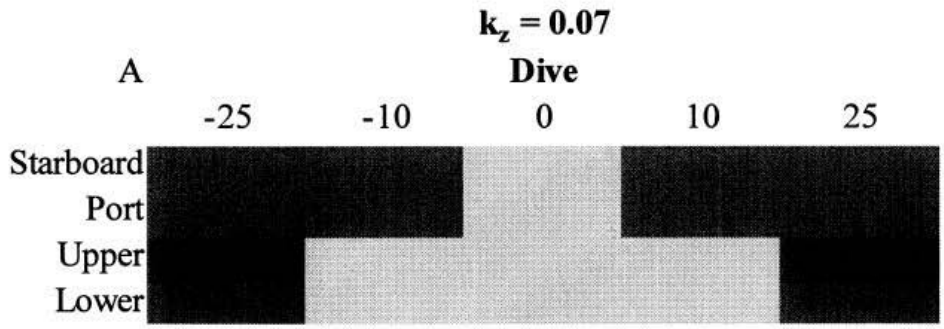

Figure 5-57: Operational Envelope Based on Control Plane Jams for the AUV Diving 100m (Depth Controller Gain of 0.07; Active Roll Compensation via All Control Planes)

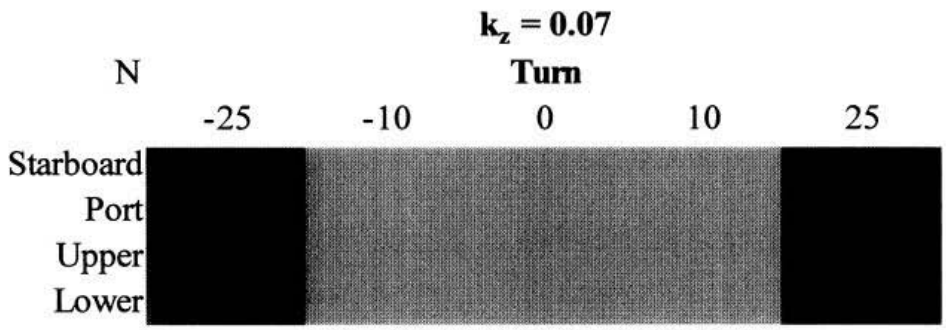

Figure 5-58: Operational Envelope Based on Control Plane Jams for the AUV Turning Through 180° (Depth Controller Gain of 0.07; No Active Roll Compensation)

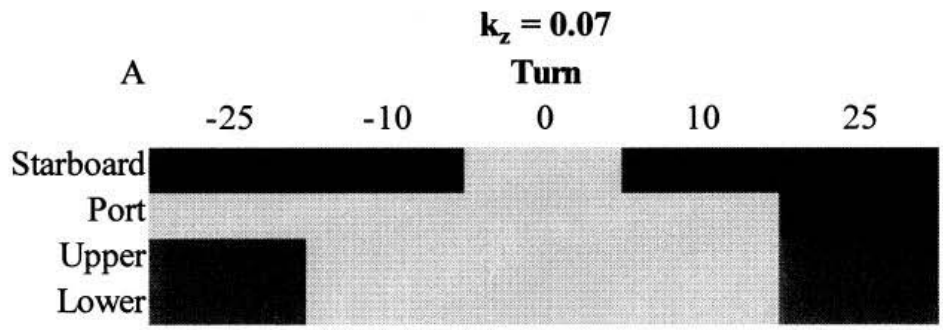

Figure 5-59: Operational Envelope Based on Control Plane Jams for the AUV Turning Through 180° (Depth Controller Gain of 0.07; Active Roll Compensation via All Control Planes)

fault e.g. free-swivelling, gone, jammed at non-zero angle.

Simple diagnostic tests of a single fin actuator can show whether the shaft is moving or not, and whether it is moving the correct amount (as commanded by the software), so in this way the fin actuator servo motor and control software can be checked. Without a shaft torque sensor, all that can be accomplished by this diagnostic is to determine whether the shaft rotates or not, but not whether the fin is still attached to the shaft. To look at hydrodynamic loads on the control plane, we would need a shaft torque sensor. This sensor would verify whether the fin is still attached to the shaft or not. If the fin is still on that shaft but does not turn when the shaft turns then the fin should be self-aligning to the local flow direction so there should be some detectable drag force, but no lift force or pitching moment can be generated. If the fin is fixed to the shaft but the shaft is jammed in a position such that the fin is at zero angle of attack to the local flow direction, then there should be some detectable drag, but no lift or pitching moment. If the fin is fixed to the shaft but the shaft is jammed at a non-zero angle of attack to the local flow, then there should be some detectable lift, drag and pitching moment. The ideal situation would be to have the actuator housing mounted on a three-component balance so that the fin lift, drag and pitching moment can be measured, for each fin. This is not usually practical for an operational AUV.

Knowledge of how the vehicle behaves during fault conditions can be used to provide the information about the nature of the fault condition, assuming an inertial navigation unit or some external tracking device provides trajectory data. Some vehicle maneuvers can be devised that allow the vehicle to deduce whether (i) the fin is still on the actuator shaft, (ii) the fin is gone, (iii) the actuator shaft (or fin) is jammed at zero angle, or (iv) the actuator shaft (or fin) is jammed at some non-zero angle.

When a fault condition occurs, and the vehicle trajectory is affected, the control system should detect the deviation in track. It can then institute a maneuver or

series of maneuvers to ascertain the nature of the fault. Knowing the nature of the fault, the control system is able to classify the expected effects of the fault, and make decisions concerning the viability of the task at hand (or even the mission), and about which fault recovery procedures to implement. This assumes the behaviour in the fault condition is significantly different than nominal behaviour, but if it isn't there is no need for fault recovery procedures.

For example, if the fault condition is a jammed control plane, once the control system detects a fault, and determines which fin is stuck, it may find a deflection angle for the opposing fin that brings the vehicle behaviour (response) back to being "symmetrical" (although degraded), e.g. dives without turning. Then the angle of jam of the defective fin can then be deduced from the angle at which you need to set the opposing fin in order to regain "symmetrical behaviour".

Chapter 6

Conclusions

This work has entailed two sensitivity studies to look at design choices that influence vehicle behaviour, and a simulation study to examine vehicle behaviour in the presence of control plane fault conditions. They were carried out to increase knowledge about the physics of vehicle response, so that better control could be obtained, especially with a view to extending the nominal (fault-free) ability of an AUV to carry out a mission or a task, even with a control plane fault.

Sensitivity analyses provide a better understanding of the behaviour of the C-SCOUT. The results for C-SCOUT are qualitatively valid for vehicles of the same general type, because it is typical of many vehicles active in the world today. Further, the procedure itself is applicable in general to any vehicle geometry. Quantifying the sensitivity for a typical vehicle like C-SCOUT is one step in understanding the fundamental behaviour of AUV in general.

The sensitivity of added mass values to changes in geometry is important for modular vehicles, where changes to vehicle configuration may be desired during operation (e.g. swapping out payload packages). This work has provided a systematic study of the sensitivity of added mass to variations in vehicle geometry. To the authors knowledge, this kind of study has not been reported before.

Added mass and other hydrodynamic parameters can have varying degrees of

effects on the vehicle response. The parameter values result from choices made during design. and it is therefore important to understand the nature of the effect of the parameters on vehicle response. and how sensitive the vehicle is to changes in the parameters. Also. since the parameters are typically determined from physical model testing and there is usually some uncertainty concerning their exact values. it is important to look at the sensitivity of the vehicle in terms of how significant the uncertainty is. Although a study of this nature has been done using a nonlinear model before [54]. this work has provide new data. based on a different modelling approach.

In order to increase reliability of AUV. it is also useful to look at vehicle behaviour under conditions beyond the scope of nominal. fault-free control: under conditions such as control plane jams and loss of a control plane. Rather than aborting a mission because of such a failure. knowledge of the expected vehicle behaviour can enable the controller to replan the mission so as to complete some or all of the mission objectives. This study is new in aim and scope.

6.1 Sensitivity of Added Mass Coefficients to Variations in Geometry

A numerical study has been made of the effect of variations of geometry on added mass coefficients for a typical axisymmetric. streamlined AUV. The results are summarized in Table 6.1. In the study. the length-to-diameter ratio of the hull was varied from a value of 3 to a value of 10. using a hull with no appendages. Next. the location of the forward control planes was varied from 15% to 40% of the (full configuration) vehicle length. aft of the nose: and the location of the after control planes was varied from 60% to 85% of the vehicle length. aft of the nose. Finally. the size of the control planes was varied from 50% to 200% of the nominal size. Here. the base configuration hull was used. and the hull-fin interactions included in the data. but the contribution

of the hull to the vehicle added mass coefficients was ignored when investigating the effects of varying the size of the control planes.

Reference frames are necessary to describe the forces and moments acting on a vehicle, and hence the accelerations it experiences. To simplify the dynamics equations, a reference frame is fixed to the center of mass (gravity) of the vehicle body. The x_B-axis of the body-fixed reference frame is pointed towards the nose of the vehicle, the y_B-axis points directly to starboard, and the z_B-axis is directed toward the bottom of the vehicle. The six basic motions (degrees of freedom, or DOF) are: translation along the x_B-axis (called surge), translation along the y_B-axis (sway), translation along the z_B-axis (heave), rotation about the x_B-axis (roll), rotation about the y_B-axis (pitch), and rotation about the z_B-axis (yaw). Each of the translation motions has an associated added mass, and each of the rotational motions has an associated added mass-moment of inertia. In addition, there are added mass coupling coefficients that represent interactions between the different motions.

Table 6.1: Variance of Added Mass Coefficients with Geometric Parameters

	Hull	Control Plane	
	L/D	Location	Size
X_u	$(L/D)^{-2}$	*Const.*	b^3
Y_v	L/D	*Const.*	b^3
Z_w	L/D	*Const.*	b^3
K_p	L/D	*Const.*	b^3
M_q	$(L/D)^{-3}$	x_{qca}^2	b^3
N_r	$(L/D)^{-3}$	x_{qca}^2	b^3
X_q	$(L/D)^{-2}$	*Const.*	b^3
Y_p	L/D	*Const.*	b^3
Y_r	L/D	x_{qca}	b^3
Z_q	L/D	x_{qca}	b^3
K_r	L/D	x_{qca}	b^3

For changes in the length-to-diameter ratio (L/D) ratio (made in the parallel mid-body to preserve the nose and tail geometry), examination of the hull without appendages showed that the sway added mass Y_v, the heave added mass Z_w, the roll

added mass-moment of inertia $K_{\dot{p}}$, and the added mass coupling coefficients $Y_{\dot{p}}$, $Y_{\dot{r}}$, and $K_{\dot{r}}$ all vary linearly with changing L/D, while the surge added mass $X_{\dot{u}}$, and the added mass coupling coefficients X_q, and Z_q vary roughly as the square of this ratio due to the variation of the center of buoyancy expressed by the variation of z_b/L with L/D. Finally, the pitch added mass-moment of inertia $M_{\dot{q}}$ and the yaw added mass-moment of inertia $N_{\dot{r}}$ vary with $(L/D)^3$. As the L/D ratio increases, it is the mass-moments of inertia about the axes normal to the longitudinal centerline of the hull that are most affected.

For changes in the location of the control planes, added masses vary with x_{qca}^n (x_{qca} being the distance along the surge axis to the quarter-chord axis of the control planes), where $n = 0$ for $X_{\dot{u}}$, $Y_{\dot{v}}$, $Z_{\dot{w}}$, $K_{\dot{p}}$, X_q, and $Y_{\dot{p}}$; $n = 1$ for $Y_{\dot{r}}$, Z_q, and $K_{\dot{r}}$; and $n = 2$ for $M_{\dot{q}}$ and $N_{\dot{r}}$. It is the mass-moments of inertia about the axes normal to the length of the hull that are again most affected by this variation of the vehicle geometry

For changes to the size of the control planes, where the shape of the plane is preserved, the added mass coefficients vary roughly with the cube of the scaling parameter (here the span, b, i.e.,they vary as b^3). Varying the size of the control planes affects all the added mass coefficients in more or less the same manner.

The study illustrated the effects of variation of geometry on the added mass of a given vehicle. The next study showed how the added mass (and other hydrodynamic parameters) affect vehicle motion. Together, these studies provide the vehicle designer with valuable data about several design choices. The data can be applied to a given set of constraints, enabling the designer to make informed decisions.

6.2 Sensitivity of Vehicle Response to Hydrodynamic Parameters

In addition to added mass, there are other hydrodynamic parameters of import for determining vehicle motion behaviour. In the nonlinear model of C-SCOUT, based as it is on lift and drag equations, these other parameters are the lift and drag coefficients for the hull and control planes, and the locations of the centers of pressure for the hull (center of effort) and control planes. Each of these parameters was included in the sensitivity study.

6.2.1 Variation of Added Mass

Changes to the magnitudes of added mass have no effect on the vehicle response except during transient conditions. The steady state motions are dominated by the effects of the lift and drag forces. In turning circles the added masses affect only the advance of the vehicle into the turn, and those response measures that include this portion of the maneuver (the advance, the tactical diameter, and the time to reach 180°). Even then, only a few of the added mass elements cause significant changes in the vehicle response when they are varied. The overall effect of varying these elements caused relatively minor variations in the response measures. The worst case variation of a turning circle response measure is less than 6% for a 100% change in the sway added mass, $Y_{\dot{v}}$.

For horizontal zigzags, varying the sway added mass, $Y_{\dot{v}}$, and the yaw added mass-moment of inertia, $N_{\dot{r}}$, did have noticeable effects on the vehicle response: e.g. a 10% change in $N_{\dot{r}}$ results in a 2.6% change in the overshoot angle. In the vertical plane it was the variation of the heave added mass, $Z_{\dot{w}}$, and the pitch added mass-moment of inertia, $M_{\dot{q}}$, that were significant (e.g. a 10% change in $M_{\dot{q}}$ results in a 2.9% change in the overshoot angle). Although changing the roll added mass-moment of inertia, $K_{\dot{r}}$, does not cause any significant change in the vehicle response, it is clear

that the other principle coefficients must be known with reasonable accuracy to have a good model of the vehicle, since varying the principle added mass derivatives can significantly change the vehicle response in transient maneuvers. Varying the heave-pitch coupling element, Z_q, also results in changing the response of the vehicle, but none of the other coupling coefficients cause the same magnitude of effects.

Even though the vehicle is symmetric about the x-z plane, but not about the chosen x-y plane (the center of mass is below the longitudinal axis of rotation), the response in horizontal zigzags is very similar to the response in vertical zigzags.

It is useful to design the vehicle so as to reduce the influence of the added mass derivatives as much as possible (to reduce the apparent inertia of the vehicle) by streamlining the vehicle and reducing the size of the appendages. Reducing the overall size of the vehicle will not reduce the relative contribution of the added mass on the vehicle response, as that contribution will still be in the same proportion to the real mass. An increase in each of the coupling derivatives, K_r, X_q, and Y_r, will actually reduce the inertia of the vehicle, but they cannot be increased without increasing other derivatives which would increase the apparent inertia of the vehicle. The design goal should therefore be to reduce all the added mass derivatives, including K_r, X_q, and Y_r.

6.2.2 Variation of Lift and Drag Coefficients

The turning circle response measures vary nonlinearly with variations in both the hull lift coefficient and the fin lift coefficient. The measures vary as the inverse of the square of $C_{\mathcal{L}_{Hull}}$ and directly as the square root of $C_{\mathcal{L}_{Fins}}$.

The response measures in turning circles remain constant or vary linearly with changes to the drag coefficients - either hull drag or fin drag. The effect of drag is mostly to increase the time of response. Variations in the hull drag coefficient have a greater affect on the time required for the turn than do variations in the control plane drag coefficient, because the hull is the largest component of the vehicle in the

flow. The effect of varying the fin drag is relatively small in comparison, even with four fins.

Response measures for zigzag maneuvers are very similar whether the zigzag is in the horizontal plane or in the vertical plane, even though there are some effects due to the gravity and buoyancy forces and the couple they produce. Increasing the hull lift force results in an increase in the period of the zigzag and in the overshoot angle and width of path, each of these varying as the square root of the hull lift coefficient. The reach (time to reach a heading 90° from the original heading) is unaffected by changes in the hull lift. Increasing the fin lift coefficient reduces each of the measures: they vary as the inverse of the fin lift coefficient squared.

Both $C_{D_{Hull}}$ and $C_{D_{Fins}}$ slow the vehicle down further as they are increased in value. In addition, increasing the hull drag increases the spatial requirements for the maneuvers. Increasing the fin drag coefficient, however, decreases the spatial requirements.

Increasing the hull lift force causes the vehicle to turn more sharply, but it makes it more difficult to recover from the turn. This is consistent with the destabilizing influence of a side force applied forward of the center of mass. Increasing the hull drag slows the vehicle down, tending to reduce the spatial requirements for the maneuver at the expense of requiring more time, and, consequentially, more energy. Hull lift and drag forces are functions of the size and shape of the hull, which may be chosen based on other criteria, such as mission or payload requirements. Some effort must be made in the design of the vehicle to reduce the drag as much as possible. This will also reduce the lift force on the hull, and therefore the (control) effort required to cause the vehicle to turn and to recover from a turn.

Increasing the drag on the control planes has the same effect as increasing the hull drag: the vehicle is slower and requires more energy to complete the maneuver. Increasing the lift of the after fins increases the stability of the vehicle, reducing the turning ability (increasing the radius of turn), but increasing the ability of the

vehicle to initiate and recover from turns: i.e. more fin lift translates into more control authority. The downside of increasing the fin lift is that it means an accompanying increase in fin drag. The design must seek the optimal balance between the lift and drag on the fin that will allow the vehicle to meet its performance criteria while minimizing the energy expended in doing so. However, the primary criterion for the control plane is that it must have sufficient control authority to meet the performance goals.

6.2.3 Variation of Centers of Effort and Pressure

When the center of effort of the hull is moved aft of the nose (closer to the center of mass), the measures of vehicle response in a turn increase. The same measures increase as the center of effort is moved forward of the vehicle nose, indicating that the optimal place for the center of effort is at the nose. Moving the center of effort of the hull forward, away from the vehicle center of mass, will lead to increased overshoot width of path (but decreased overshoot angle). This result indicates a need to move the center of effort closer to the center of mass in order to decrease the overshoot width of path, and, in so doing, the overall width of path of the vehicle. Thus, the vehicle response in transient conditions (as indicated by the response in zigzag maneuvers) contradicts the response in steady conditions (as indicated by the vehicle response in turning circles). In either case, however, the center of effort is a function of the flow around the vehicle, and there is no clear design variable that can ensure optimal location of CE over the whole range of vehicle motions.

Variation of the location of the center of pressure of the control plane along the span of the control plane (perpendicular to the hull for C-SCOUT) has virtually no effect on the response of the vehicle in any of the maneuvers studied. Moving the location of the center of pressure aft along the chord of the control plane generally causes an increase in the values of the response measures in turning circles and a reduction of the response measures in zigzag maneuvers. This is consistent with the

concept of increased control authority with increased moment arm to the center of pressure. The effect of moving the location of the control plane center of pressure is much the same as the effect produced by increasing the fin lift. This means that for a given fin shape (with a specific lift coefficient), the effect of lift force can be made larger by moving the fin aftward on the hull.

6.3 Vehicle Controllability in the Face of Control Plane Fault Conditions

For holding course, the higher depth control gain (0.07) should be used. If vehicle roll is not an important issue, no active roll compensation is necessary. The operational envelope will be unrestricted (up to the maximum $\pm 25^\circ$) for the horizontal (starboard/port) planes, and restricted to less than about $\pm 10^\circ$ for the vertical (upper/lower) control planes. If roll is important, it can be kept within $\pm 1^\circ$ using active roll compensation via all the (remaining) control planes. In terms of the operational envelope, the cost of controlling the roll is that the horizontal planes are now restricted to less than about $\pm 10^\circ$ too.

When diving, the best gain for the depth controller is 0.07. Again, if roll angle is not important, then no active roll compensation is required. The operational envelope would indicate that horizontal control planes should be restricted to angles near zero, but this would not allow the maneuver to be achieved in reasonable time, therefore, the envelope should be expanded to at least $\pm 10^\circ$ and some degradation of performance expected if one of the horizontal planes jams at an angle not near zero. If the roll angle must be kept within one degree of zero, active roll compensation using all the remaining unjammed control surfaces is best. The operational envelope is the same as that of the vehicle without active roll compensation when roll is not an issue. The same arguments apply.

The depth controller with a gain of 0.07 still provides better performance (a re-

duction in depth error. and even in heading error) for turns. As with holding course and diving. if roll is not important. then there is no need for active roll compensation and vehicle response is better without it. On the other hand. if roll is important. the active roll compensation via all planes improves the vehicle performance. since the vehicle without active roll compensation is unable to maintain the desired roll angle even if the jam is near zero.

In general. the depth controller gain should be kept as high as possible without inducing instability into the system: in this study the value of 0.07 was a reasonable value. The higher value of gain for the depth controller ensures smaller unwanted depth excursions. and can lead to smaller heading errors when the heave or pitch motions are coupled into the yaw by a non-zero roll angle. To guarantee adequate performance even with jammed control planes. the port and starboard control planes should be restricted to angles near zero. Since this is too restrictive. especially in maneuvers involving diving. the operational envelope for the horizontal planes can be expanded to $\pm 10^{\circ}$. but some degradation of performance can be expected if one of the horizontal planes jams at an angle not near zero. The operational envelope for the upper and lower control planes is $\pm 10^{\circ}$ to provide guarantees of acceptable performance even with jammed planes. The choice of active roll compensation depends on how important the roll angle is to the maneuver: use all the remaining planes to compensate for the effects of the jammed plane if roll must be limited. otherwise no roll compensation is necessary or of benefit.

Chapter 7

Recommendations for Future Work

The work presented here represents the first steps in gaining a systematic, fundamental understanding of vehicle behaviours. This knowledge will provide a foundation for further analysis of behaviours in various planned (e.g. commanded changes) and unplanned (e.g. actuator faults) conditions the vehicle will experience over the course of its active lifetime. Future work should include activity in the following areas.

7.1 Further Simulations

The computer model should be used to increase knowledge of AUV behaviour:

1. increased data points for sensitivity studies and fault condition simulations;
2. investigate multipoint failures.

7.2 Hydrodynamics

Experimental work is necessary, including:

1. computer model validation via PMM, MDTF, Cavitation Tunnel, and free-swimming model tests;

2. validate simulation studies:

3. investigate behaviour of hull (PMM. Tow Tank tests. Cavitation Tunnel with scale model). control planes (Cavitation Tunnel) at large angles of attack:

4. effects of variations of hull length. hull cross-section. fin size. fin location. fin configuration (inverted Y. high-lift devices. rolling trailing edge). fin type. through-body thruster placement. number of through-body thrusters.

7.3 Model Improvements

The hydrodynamics-based computer model should be improved upon by:

1. increasing accuracy by determining applicable parameters (inertial properties. hydrodynamic coefficients) through physical model testing:

2. include environmental effects - may require changing some constant coefficients (e.g. added masses) to time varying coefficients to allow simulation of motion while submerged but near the free surface and other boundaries such as the bottom (important for simulation of bottom profiling missions):

3. inclusion of through-body thrusters:

4. include algorithms for vehicle behaviour at high angles of attack:

5. integration with a mission planner: environment simulation.

In addition. the model may be used to simulate missions for pre-screening control scripts. and for post mission analysis where required.

7.4 Control

1. look into the combination of controllers necessary for robust control. and how to switch between them

2. hover-cruise: forward-reverse controller switching:

3. investigate applications to multi-vehicle operations.

7.5 The C-SCOUT

C-SCOUT needs to be completed and tested in ROV mode. On completion of that task, C-SCOUT needs to be brought up to operational status, including:

1. integration of navigation instruments:

2. integration of acoustic communication equipment:

3. implementation of software and hardware necessary for autonomous operation, particularly:

   (a) mission level control:

   (b) obstacle detection and avoidance equipment.

The vehicle usefulness could be enhanced by:

1. investigation of best energy storage system:

2. redesign for increased depth:

3. consideration of payload requirements for particular, relevant missions.

Bibliography

[1] NRC(US). *Undersea Vehicles and National Needs.* National Academy Press. Washington. DC. 1996. Report compiled by the Committee on Undersea Vehicles and National Needs of the Marine Board of the Commission on Engineering and Technical Systems of the National Research Council (US).

[2] B. P. Sukhov. "Underwater profiling of icebergs using submersibles." in *Proceedings Oceans '78.* Piscataway. N.J. 1978. pp. 225–230. IEEE.

[3] Bruce Robison. "Deep ocean science." in *Proceedings International Symposium on Unmanned Untethered Submersible Technology.* Durham. NH. 1983. pp. 220–222. University of New Hampshire.

[4] Vanessa Pennell. Christopher D. Williams. Neil Bose. Brian Veitch. Kelly Hawboldt. Timothy L. Curtis. Douglas E. Perrault. Siu O'Young. Mukhtasor. Rehan Sadiq. Tahir Husain. James Ferguson. Greg Eaton. and Peter Reedeker. "Innovative approaches to environmental effects monitoring using an autonomous underwater vehicle." in *International Workshop on Underwater Robotics for Sea Exploitation and Environmental Monitoring.* Rio de Janeiro. Brazil. October 2001. International Advanced Robitics Programme.

[5] Michael Krabach. "Potential AUV applications to nuclear power plant inspection." in *Proceedings International Symposium on Unmanned Untethered Submersible Technology.* Durham. NH. 1983. pp. 226–230. University of New Hampshire.

[6] Frank Wang. "Offshore oil and gas field development and applications of underwater autonomous vehicles." in *Proceedings International Symposium on Unmanned Untethered Submersible Technology*. Durham. NH. 1983. pp. 231-241. Univesity of New Hampshire.

[7] Brian Thomas. "Potential applications of autonomous underwater vehicles." in *Proceedings International Symposium on Unmanned Untethered Submersible Technology*. Durham. NH. 1983. pp. 223-225. University of New Hampshire.

[8] Clifford Funnell. Ed.. *Jane's Underwater Technology*. Jane's Information Group Limited. Coulsdon. Surrey. UK. 3rd edition. 2000-2001.

[9] Peter Maas. *The Terrible Hours*. Harper Collins. New York. NY. 1999.

[10] Norman Estabrook. Bruce Jones. Drew Michel. Andrew Resnick. Robert H. Rogers. Mark Olsson. and Kim Saunders. "State of technology report from the advanced marine technology division." *MTS Journal*. vol. 29. no. 4. pp. 47-56. Winter 1995.

[11] Brian Schostak. "AUV applications within E&P." in *Proceedings 2000 Offshore Technology Conference*. Houston. TX. 2000. p. OTC 12000. OTC Program Committee.

[12] Anders Bjerrum. "Survey AUVs are low risk technology." in *Proceedings 2000 Offshore Technology Conference*. Houston. TX. 2000. p. OTC 11999. OTC Program Committee.

[13] Gwyn Griffiths. K. G. Birch. N. W. Millard. S. D. McPhail. P. Stevenson. M. Peabody. J. R. Perrett. A. T. Webb. M. Squires. and A. Harris. "Oceanographic surveys with a 50 hour endurance autonomous underwater vehicle." in *Proceedings 2000 Offshore Technology Conference*. Houston. TX. 2000. p. OTC 12003. OTC Program Committee.

[14] Jay G. Northcutt, Art A. Kleiner, and Thomas S. Chnace. "A high-resolution survey AUV." in *Proceedings 2000 Offshore Technology Conference*. Houston, TX. 2000. p. OTC 12004. OTC Program Committee.

[15] Bob Barton. "AUVs:"we're seeing things we couldn't see before"." *International Ocean Systems*. vol. 6, no. 1, pp. 6–10. January/February 2002.

[16] Robert Corell. "Summary of technology review (artificial intelligence)." in *Proceedings Unmanned Underwater Submersible Technology*. Durham, NH. 1981. pp. 94–96. University of New Hampshire.

[17] James Ferguson and Gary Bane. "Future directions in the development of military autonomous underwater vehicles." in *Proceedings of the DREP/RRMC Military Robotics Applications Workshop*. Victoria, BC. 1987. pp. 188–195. DREP, Department of National Defence.

[18] Ken Collins. "Cost-effective AUVs for today's offshore industry." in *Proceedings Underwater Intervention (UI '93)*. New Orleans, LA. 1993. pp. 199–207. Marine Technology Society, and The Association of Diving Contractors.

[19] Gwyn Griffiths. "Autosub: A versatile autonomous underwater vehicle." *Hydro International*. pp. 32–35. May/June 1998.

[20] Junku Yuh. "Modeling and control of underwater robotic vehicles." *IEEE Transactions on Systems, Man, and Cybernetics*. vol. 20, no. 6, pp. 1475–1483. November/December 1990.

[21] Bjorn Jalving and Nils Storkersen. "The control system of an autonomous underwater vehicle." in *Proceedings of the 1994 IEEE Conference on Control Applications*. Piscataway, NJ. 1994. pp. 851–856. IEEE.

[22] Anthony J. Healy. "Model-based maneuvering controls for autonomous underwater vehicles." *Transactions of ASME: Journal of Dynamic Systems. Measurement. and Control.* vol. 114. pp. 614–622. December 1992.

[23] A. Chellabi and Meyer Nahon. "Feedback linearization control of underwater vehicles." in *Proceedings Oceans '93.* Victoria. BC. 1993. pp. I:410–I:421. IEEE.

[24] Thor I. Fossen and Ola-Erik Fjellstad. "Robust adaptive control of underwater vehicles: A comparative study." in *IFAC Workshop on Control Applications in Marine Systems (CAMS '95).* 1995. IFAC.

[25] Thor I. Fossen and Svein I. Sagatun. "Adaptive control of nonlinear underwater robotic systems." in *Proceedings of the 1991 IEEE International Conference on Robotics and Automation.* Piscataway. NJ. 1991. pp. 1687–1694. IEEE.

[26] Kevin R. Goheen and E. Richard Jefferys. "Multivariable self-tuning autopilots for autonomous and remotely operated underwater vehicles." *IEEE Journal of Oceanic Engineering.* vol. 15. no. 3. pp. 144–151. July 1990.

[27] Junku Yuh. Joel S. Fox. and R. Lakshmi. "Control and optical sensing in underwater robotic vehicles." in *Proceedings Oceans '90.* Washington. DC. 1990. pp. 88–93. IEEE.

[28] Junku Yuh. "Control of underwater robotic vehicles." in *Proceedings of the 1993 IEEE/RSJ International Conference on Intelligent Robots and Systems.* Piscataway. NJ. 1993. pp. 517–521. IEEE.

[29] Dana R. Yoerger and Jean-Jacques Slotine. "Robust trajectory control of underwater vehicles." *IEEE Journal of Oceanic Engineering.* vol. OE-10. no. 4. pp. 462–470. October 1985.

[30] Frank Dougherty. Tom Sherman. Gary Woolweaver. and Gib Lovell. "An autonomous underwater vehicle (AUV) flight control system using sliding mode control." in *Proceedings Oceans '88*. Baltimore. MD. 1988. pp. 1265–1270. IEEE.

[31] Roberto Cristi. Fotis A. Papoulias. and Anthony J. Healey. "Adaptive sliding mode control of autonomous underwater vehicles in the dive plane." *IEEE Journal of Oceanic Engineering*. vol. 15. no. 3. pp. 152–160. July 1990.

[32] Junku Yuh. "A neural net controller for underwater robotic vehicles." *IEEE Journal of Oceanic Engineering*. vol. 15. no. 3. pp. 161–166. July 1990.

[33] O. J. Sordalen. M. Dalsmo. and O. Egeland. "An exponentially convergent law for nonholonomic underwater vehicle." in *Proceedings IEEE International Conference on Robotics and Automation*. Piscataway. NJ. 1993. pp. 790–795. IEEE.

[34] Yoshihiko Nakamura and Shrikant Savant. "Nonholonomic motion control of an autonomous underwater vehicle." in *IEEE/RSJ International Workshop on Intelligent Robots and Systems (IROS '91)*. Piscataway. NJ. 1991. pp. 1254–1259. IEEE.

[35] Yu K. Alekseev. V. V. Kostenko. and A. Ye. Shumsky. "Use of identification and fault diagnostic methods for underwater robotics." in *Proceedings Oceans '94*. Brest. France. 1994. pp. 489–494. IEEE.

[36] Anthony J. Healey. "A neural network approach to failure diagnostics for underwater vehicles." in *Proceedings of the 1992 Symposium on Autonomous Underwater Vehicle Technology*. Washington. DC. 1992. pp. 131–134. IEEE.

[37] Anthony J. Healey. "Towards an automatic health monitor for autonomous underwater vehicles using parameter identification." in *Proceedings of the American Control Conference*. 1993. pp. 585–589. IFAC.

[38] Rafael R. Rodríguez and Gerald J. Dobeck. "Guidance and control system of the large scale vehicle." in *Proceedings of the 6th International Symposium on Unmanned Untethered Submersible Technology.* Durham. NH. 1989. pp. 434–451. University of New Hampshire.

[39] David Barnett. Stephen McClaran. Eric Nelson. Make McDermott. and Glen Williams. "Architecture of the texas A&M autonomous underwater vehicle controller." in *Proceedings of the 1996 Symposium on Autonomous Underwater Vehicle Technology.* Monterey. CA. 1996. pp. 231–237. IEEE.

[40] David W. Payton. David Keirsey. Dan M. Kimble. Jimmy Krozel. and J. Kenneth Rosenblatt. "Do whatever works: A robust approach to fault-tolerant autonomous control." *Journal of Applied Intelligence.* vol. 2. pp. 225–250. 1992.

[41] Naomi Ehrich Leonard. *Averaging and Motion Control of Systems on Lie Groups.* Ph.D. thesis. University of Maryland. 1994.

[42] Naomi Ehrich Leonard. "Compensating for actuator failures: Dynamics and control of underactuated underwater vehicles." in *Proceedings of the 9th International Symposium on Unmanned Untethered Submersible Technology.* Durham. NH. 1995. pp. 168–177. University of New Hampshire.

[43] Naomi Ehrich Leonard. "Control synthesis and adaptation for an underactuated autonomous underwater vehicle." *IEEE Journal of Oceanic Engineering.* vol. 20. no. 3. pp. 211–220. July 1995.

[44] Douglas Edward Perrault. *Fault Tolerant Control of Autonomous Underwater Vehicles.* M. A. Sc.. University of Victoria. 1998.

[45] J. D. Lambert. "The effect of changes in the stability derivatives on the dynamic behaviour of a torpedo." Technical Report R&M 3143. Admiralty Research Laboratory of the Aeronautical Research Council. UK Ministry of Aviation. March 1956.

[46] Morton Gertler and Grant R. Hagen. "Standard equations of motion for submarine simulation." Report 2510. David Taylor Model Basin (DTMB). Bethesda. MD. June 1967.

[47] J. Feldman. "DTNSRDC revised standard submarine equations of motion." Report DTNSRDC/SPD-0393-09. David W. Taylor Naval Ship Research and Development Center (DTNSRDC). Bethesda. MD. June 1979.

[48] Douglas E. Humphreys and Kenneth W. Watkinson. "Methods for estimating vehicle transfer functions requiring only the geometric and inertia characteristics." in *Oceans '72*. Piscatawy. NJ. 1972. pp. 220–223. IEEE.

[49] Meyer Nahon. "Determination of undersea vehicle hydrodynamic derivatives using the USAF DATCOM." in *Proceedings Oceans '93*. Victoria. B.C.. October 1993. pp. II283–II288. IEEE.

[50] Douglas E. Humphreys. "Development of the equations of motion and transfer functions for underwater vehicles." Technical Report NCSL-287-76. Naval Coastal Systems Laboratory. Panama City. FL. July 1976.

[51] Thor I. Fossen and Ola-Erik Fjellstad. "Nonlinear modelling of marine vehicles in 6 degrees of freedom." *International Journal of Mathematical Modelling of Systems*. vol. 1. no. 1. pp. 1–11. 1995.

[52] Douglas Perrault. Neil Bose. Siu O'Young. and Christopher D. Williams. "Sensitivity of AUV added mass coefficients to variations in hull and control plane geometry." *Ocean Engineering*. Submitted for publication.

[53] Douglas E. Humphreys and Kenneth W. Watkinson. "Prediction of acceleration hydrodynamic coefficients for underwater vehicles from geometric parameters." Technical Report NCSL-TR-327-78. Naval Coastal Systems Laboratory. Panama City. FL. February 1978.

[54] Debabrata Sen. "A study on sensitivity of maneuverability performance on the hydrodynamic coefficients for submerged bodies." *Journal of Ship Research*. vol. 44. no. 3. pp. 186–196. September 2000.

[55] Douglas Perrault. Niel Bose. Siu O'Young. and Christopher D. Williams. "Sensitivity of AUV motion response to variations in hydrodynamic parameters." *Ocean Engineering*. Submitted for Publication.

[56] Timothy Curtis. "Hull. powering and control surface design for the autonomous underwater vehicle C-SCOUT." Report LM-1999-01. Institute for Marine Dynamics. National Research Council of Canada. St. John's. NF. 1999.

[57] Renee Boileau. "Hull structure design for the autonomous underwater vehicle C-SCOUT." Report LM-1999-03. Institute for Marine Dynamics. National Research Council of Canada. St. John's. NF. 1999.

[58] Lucas Gray. "Construction of the C-SCOUT AUV." Report LM-1999-21. Institute for Marine Dynamics. National Research Council of Canada. St. John's. NF. 1999.

[59] Lucas Gray. "C-SCOUT progress: Summer 2000." Report LM-2000-14. Institute for Marine Dynamics. National Research Council of Canada. St. John's. NF. 2000.

[60] Meggan Vickerd. "Fabrication of C-SCOUT Jr.." Report LM-2001-16. Institute for Marine Dynamics. National Research Council of Canada. St. John's. NF. 2001.

[61] Timothy Curtis. Christopher Williams Douglas Perrault. and Neil Bose. "C-SCOUT: A general-purpose AUV for systems research." in *Proceedings of the 2000 International Symposium on Underwater Technology (UT00)*. Tokyo. Japan. May 2000. pp. 73–77. IEEE.

[62] Timothy Curtis, Douglas Perrault, Lloyd Smith, Neil Bose, and Christopher D. Williams. "A tool for ocean research." in *Newfoundland Electrical and Computer Engineering Conference (NECEC)*. St. John's, NF, November 2000. IEEE.

[63] Timothy L. Curtis, Douglas Perrault, Christopher D. Williams, and Neil Bose. "Baseline configuration of the C-SCOUT autonomous underwater vehicle." in *18th Canadian Congress of Applied Mechanics*. A. Swamidas, M. R. Haddara, and R. Seshadri, Eds., St. John's, NF, June 2001, pp. 251–252. Memorial University of Newfoundland.

[64] Timothy L. Curtis, Douglas Perrault, Christopher D. Williams, and Neil Bose. "Maneuvering of the C-SCOUT AUV." in *Proceedings of the 26th American Towing Tank Conference ATTC*. Glen Cove, NY, July 2001.

[65] Lloyd Smith, Steven Taylor, Bryan Delaney, Suzanne Toope, Neil Bose, and Siu O'Young. "An unmanned autonomous vehicle control system using off-the-shelf electronics." in *18th Canadian Congress of Applied Mechanics*. A. Swamidas, M.R. Haddara, and R. Seshadri, Eds., St. John's, NF, June 2001, pp. 255–256. Memorial University of Newfoundland.

[66] Timothy Curtis. *The Design, Construction, Outfitting, and Preliminary Testing of the C-SCOUT Autonomous Underwater Vehicle (AUV)*. M. Eng., Memorial University of Newfoundland, 2001.

[67] Doug Perrault. *User's Manual for AUV Motion Simulator*. Ocean Egineering Research Centre, Faculty of Engineering and Applied Science, Memorial University of Newfoundland, 2002.

[68] Douglas E. Humphreys. "Dynamics and hydrodynamics of ocean vehicles." in *Oceans '81*. Piscataway, NJ, 1981, pp. 88–91. IEEE.

[69] Meyer Nahon. "A simplified model for autonomous underwater vehicles." in *Proceedings of the 1996 IEEE Symposium on Autonomous Underwater Vehicle Technology (AUV '96)*. Monterey, CA. June 1996. pp. 373–379. IEEE.

[70] SNAME. "Nomenclature for treating the motion of a submerged body through a fluid." Technical and Research Bulletin 1-5. Hydrodynamics Subcommittee of the Technical and Research Committee. Society of Naval Architects and Marine Engineers. April 1950.

[71] Thor I. Fossen. *Guidance and Control of Ocean Vehicles*. John Wiley and Sons. West Sussex. UK. 1994.

[72] R.C. Hibbeler. *Engineering Mechanics - Dynamics*. Prentice-Hall. Englewood Cliffs. NJ. 7th edition. 1995.

[73] Frederick H. Imlay. "The complete expressions for "added mass" of a rigid body moving in an ideal fluid." Report 1528. David Taylor Model Basin (DTMB). Bethesda. MD. July 1961.

[74] Max M. Munk. "The aerodynamic forces on airship hulls." Report Report No. 184. National Advisory Committee on Aeronautics (NACA). 1924.

[75] G. N. Ward. "Supersonic flow past slender pointed bodies." *The Quarterly Journal of Mechanics and Applied Mathematics*. vol. 2. no. Part 1. pp. 75–97. March 1949.

[76] H. Julian Allen and Edward W. Perkins. "A study of effects of viscosity on flow over slender inclined bodies of revolution." Report Report 1048. National Advisory Committee for Aeronautics (NACA). 1951.

[77] H. Jullian Allen and Edward W. Perkins. "Characteristics of flow over inclined bodies of revolution." Research Memorandum RM A50L07. National Advisory Committee on Aeronautics (NACA). March 1951.

[78] Edward J. Hopkins. "A semiempirical method for calculating the pitching moment of bodies of revolution at low mach numbers." Research Memorandum RM A51C14. National Advisory Committee for Aeronautics (NACA). May 1951.

[79] L. Folger Whicker and Leo F. Fehlner. "Free-stream characteristics of a family of low-aspect-ratio. all-movable control surfaces for application to ship design." Report 933. David Taylor Model Basin (DTMB). Bethesda. MD. December 1958.

[80] George D. Watt. "Estimates for the added mass of a multi-component. deeply submerged vehicle Part I: Theory and program description." Technical Memorandum TM 88/213. Defence Research Establishment Atlantic (DREA). Dartmouth. NS. October 1988.

[81] Targut Sarpkaya and Michael Isaacson. *Mechanics of Wave Forces on Offshore Structures*. Van Nostrand Reinhold Company. New York. 1981.

[82] Sir Horace Lamb. *Hydrodynamics*. Cambridge University Press. Cambridge. UK. 1932.

[83] Roy Burcher and Louis Rydill. *Concepts in Submarine Design*. Cambridge University Press. Cambrige. UK. 1994.

[84] Donald L. Paster. "Importance of hydrodynamic considerations for underwater vehicle design." in *Oceans '86*. Washington. DC. 1986. pp. 1413–1422. IEEE.

[85] Edward V. Lewis. Ed.. *Principles of Naval Architecture*. vol. III. The Society of Naval Architects and Marine Engineers. Jersey City. NJ. second edition. 1989.

[86] E. Eugene Allmendinger. Ed.. *Submersible Vehicle Systems Design*. The Society of Naval Architects and Marine Engineers (SNAME). Jersey City. NJ. 1990.

CENTRE FOR NFLD. STUDIES
JUL 18 1978
MEMORIAL UNIVERSITY
OF NEWFOUNDLAND